AN ABSTRACT OF THE DISSERTATION OF

Mark T. Ford for the degree of Doctor of Philosophy in Geology presented on December 14, 2011.

Title: Rhyolitic Magmatism of the High Lava Plains and Adjacent Northwest Basin and Range, Oregon: Implications for the Evolution of Continental Crust.

Abstract approved:

_____

Anita L. Grunder Robert A. Duncan

Understanding continental crust formation and modification is a fundamental and longstanding geologic problem. Influx of mantle-derived basaltic magma and partial melting of the crust are two ways to drive crustal differentiation. This process results in a low density upper crust and denser, more refractory lower crust, creating significant and vastly different geochemical reservoirs over time. The High Lava Plains (HLP) and Northwestern Basin and Range (NWBR) in central and eastern Oregon provide an excellent example of intraplate volcanism where we can examine the beginnings of segregation of a relatively young, recently accreted crust.

The origins of continental magmatism and its relationship to plate tectonics, especially away from the continental margins, are only slowly becoming revealed. The western United States is the most volcanically active part of North America during Cenozoic time, and this activity includes the enigmatic volcanism of the HLP and NWBR. Rhyolitic volcanism in the HLP and NWBR is age-progressive but in a direction that is nearly perpendicular to North American Plate motion. Despite being erupted

through a similar crust and with a similar composition of mafic input, the HLP province is strongly bimodal (basalt-rhyolite) while the NWBR province exhibits a continuum of compositions. High silica rhyolites are commonplace in the HLP, with approximately a 1:1 ratio of rhyolite to basalt, even though the crust is comprised of mafic accreted terranes.

Asthenospheric flow, mantle melting and crustal extension coupled with southwesterly North American plate motion explain the age-progressive volcanism of the HLP and NWBR. Differential asthenopheric counterflow and mantle upwelling created by the down-going Cascadia slab, coupled with transtensional stresses related to the rotation of the North American plate and Basin and Range extension, decreasing to the north, can produce the observed variations in rhyolite compositions and volumes in the two adjacent provinces. These differences are caused by fundamentally different petrogenetic processes that take place in the crust.

In the HLP, an increase in mantle-derived magma flux into the lower crust has created low silica rhyolite via partial melt that separated, coalesced and rose buoyantly. This low silica rhyolite may erupt, solidify in the upper crust, or differentiate by fractional crystallization to produce high-iron, high-silica rhyolite containing an anhydrous phase assemblage. In the NWBR, a smaller flux of basaltic magma, coupled with greater transtension resulted in small crustal processing zones where fractional crystallization coupled with magma mixing and recharge created a wide range of compositions. Partial melting to form rhyolites was limited. These rhyolites have lower iron, and hydrous phases (biotite, amphibole) are common. These processes modify the crust in different ways, leaving a stratified crust in the HLP but a less modified crust in the NWBR. Recent geophysical and isotopic studies bear out these differences and allow for a unified, internally consistent model for both provinces, one that relies only on partial melt generation driven by current plate movements and do not require a mantle plume contribution.

The bimodal volcanism of the HLP is a direct consequence of the processes that cause the gravitational differentiation of the continental crust into upper and lower units. The model for the HLP is generally applicable to other localities that have predominantly

mafic crust and a similar balance of crustal transtension and mantle-derived basaltic flux. One such place is Iceland, which has strongly bimodal (basalt – rhyolite) volcanism. In areas where silicic crust has become substantially more mafic due to a high flux of intraplated basalts, such as in the bimodal Snake River Plain, the model is also applicable.

Rhyolitic Magmatism of the High Lava Plains and Adjacent Northwest Basin and Range, Oregon: Implications for the Evolution of Continental Crust

by

Mark T. Ford

A DISSERTATION

Submitted to

Oregon State University

in partial fulfillment of
the requirement for the
degree of

Doctor of Philosophy

Presented December 14, 2011
Commencement June 2012

Doctor of Philosophy dissertation of Mark T. Ford presented on December 14, 2011.

APPROVED:

_____

Co-Major Professor, representing Geology

_____

Co-Major Professor, representing Geology

_____

Chair of the Department of Geosciences

_____

Dean of the Graduate School

I understand that my dissertation will become part of the permanent collection of Oregon State University libraries. My signature below authorizes release of my dissertation to any reader upon request.

_____

Mark T. Ford, Author

ACKNOWLEDGEMENTS

The author expresses sincere appreciation to all members of my committee: Anita Grunder, Bob Duncan, Adam Kent, Dave Graham and my GCR, Richard Peterson. I would like to single out Anita for offering me the opportunity to continue my studies here at Oregon State University and funding a great deal of it. The High Lava Plains of Oregon was where I wanted to study, and I'm very thankful that I was given the chance to work on this wonderful geologic puzzle. I'd also like to give my sincere thanks to Bob for his great efforts in helping advance not only the syntax of this work but also the merit. Without his hard work and support, I may have never finished this dissertation. Adam and Dave were also of great assistance in advancing the scholarship of the work and driving me to do a better job. This thesis is based upon work supported by the National Science Foundation under Grant No. 0506869, thanks NSF!

Many others have helped out along the way. I had some very capable field assistants, Barry Walker and Nathan Watson, who not only provided some feedback on the field geology of the high desert but also kept me from talking to myself too much while in the great wide open. Russell Rosenberg helped a great deal with his very competent sample preparation that I had full confidence in; I cannot give a higher accolade than that. John Huard (Oregon State University) was an irreplaceable cog in the Ar-Ar geochronology wheel. Ilya Bindeman (University of Oregon) was integral in the oxygen isotope work and provided great insight into the results. Rick Conrey (Washington State University) was essential in obtaining the highest quality whole rock composition data and helping me through the sometimes convoluted world of geochemical error analysis. I could go on for many paragraphs on my admiration for Rick Carlson (Department of Terrestrial Magnetism, Washington DC). He was a tremendous surrogate advisor, always willing to answer my many questions, and he would respond with unmatched speed, clarity and depth when I looked for solutions via email. He is truly remarkable.

Then there are the people that helped to shape my thinking and my person while at Oregon State. There are certainly too many to list but a few deserve special mention.

Darrick Boschmann and Layne Bennett were not only good friends but provided irreplaceable help with GIS and the construction of some of the very nice maps in this work. They should be commended for the patience they had when working with me on such issues. Matt Loewen has been a great sounding board for ideas and a great pal. Erin (Whitham) Lieuallen has been a dear friend, a part-time editor and has provided about half of my wardrobe over the years. I'd like to thank my partners in HLP work for great conversations, including Mike Iademarco, Justin Milliard, Darrick Boschmann and Ashley Bromley. There are so many that have provided wonderful scientific banter and friendship over the years and I include only a partial list here, Mike Iademarco, Ashley #1 (Hatfield), Ashley #2 (Bromley), Denise Giles, "one l" Alison (Koleszar), "two l" Allison (Weinsteiger), Justin "the Duck" Milliard, Lucian Farmer, Jeremiah Oxford, BJ Walker, the "Climate Guys", numerous other VIPERs and so many others. Thank you.

I would also like to thank some of the people that have helped to make me the person I am today, and I cherish their love and support. This would include Jason and Walt Strawser and others from the "Coon Hollow Gang," the entire Lynch family, Dick and Ellen Luce and the Clearing Corriedale Sheep and Wool Co., and many others from the Sexton Hollow. This includes some of my dear friends I made while at Idaho State including Kate Pickett, Dan Narsavage, Arron Pope and Duane DeVecchio.

Finally, I'd like to thank my family for their life-long support. I still cannot believe the encouragement I received from my parents. As a lad, when I told my parents that I wanted to study geology, I expected a response like, "Rocks! What the heck are you going to get by studying rocks?" But instead, they backed me all the way. I'm sorry that they were not able to see me complete this educational goal and I miss them.

TABLE OF CONTENTS

TABLE OF CONTENTS (Continued)

TABLE OF CONTENTS (Continued)

LIST OF FIGURES

LIST OF FIGURES (Continued)

LIST OF FIGURES (Continued)

Figure Page

LIST OF TABLES

LIST OF APPENDICES

CHAPTER 1:

Bimodal Volcanism in the High Lava Plains and Northwestern Basin and Range: Reconciling Geochemical and Geophysical Findings and the Relationship of Crustal Modification to Bimodal Volcanism

CRUSTAL GROWTH AND MODIFICATION:

The mechanisms of continental crust growth and modification are a longstanding focus of geologic study (e.g. Taylor and McLennan, 1995; Raia and Spera, 1997; Annen et al., 2006). Both geophysical and geochemical arguments favor mantle derived basaltic magmas playing a significant role in this growth and modification (e.g. McCurry and Rodgers, 2009; Peng and Humphreys, 1998; Hildreth and Moorbath, 1988; Trehu et al., 1994; Peccerillo et al., 2003; Jonasson, 2007). In the High Lava Plains (HLP) and Northwestern Basin and Range (NWBR) in central and eastern Oregon (Figure 1), we have an excellent example of bimodal (basalt – rhyolite) volcanism in an intracontinental setting. Based on the work presented here, we link the formation of this bimodal province with the modification of juvenile crust (accreted terranes), bringing to bear geochronology, major and trace element and isotope geochemistry, petrogenetic models for rhyolite formation, and recent geophysical modeling of crustal structure (Cox, 2011).

The age-progressive trend of rhyolitic volcanism in the HLP – NWBR is counter to what one might expect based on North American plate motion over quasi-stationary mantle upwelling. Some authors (e.g. Jordan et al., 2004; Camp and Ross, 2004; Draper, 1991) advocate for a northwestward migration of a plume head to explain this age trend. New geochronology via $^{40}Ar/^{39}Ar$ dating (Chapter 2) indicates that the NWBR volcanism is linked in its migration to the northwest with volcanism from the HLP. The lack of a mantle plume-derived He isotopic signature in the HLP basalts (Graham et al., 2009), and complexities in modeling plume head dynamics (cf. Jordan et al., 2004) are additional evidence against a plume head model. Notably, mantle flow vectors created by resolving North American plate motion with shear wave anisotropies indicating strong asthenopheric flow (Long et al., 2009) caused by the Cascadia Slab steepening and rollback (Druken et al., 2011) closely match the magnitude and direction of the HLP age-progressive volcanism (Chapter 2). Furthermore, the generation of partial melts created by shear flow in the mantle can drive volcanism in the bimodal HLP, as well as create both the subtle changes in chemistry between the HLP and NWBR rhyolites and the disparity between volumes of the provinces (Chapter 4).

Bimodal volcanism in the HLP is a result of a greater flux of basalt from the mantle, and is more than what is required to drive the largely RAFC-derived (recharge, assimilation and fractional crystallization) continuum of compositions seen in the NWBR. It is, however, substantially less than that required to produce MASH (melting, assimilation, storage and homogenization - Hildreth and Moorbath, 1988, 1991) processes that form arc volcanics. Limited extension caused by transtension in the HLP does not allow many basaltic magmas easy and direct passage through the crust and many stall or slowdown in the lower crust, although some can still traverse the crust. This "Goldilocks" condition of flux and tectonics in the HLP results in some partial melting of the older accreted terranes and recently intraplated basalts. This produces low silica rhyolites that have isotopic signatures which fall along mixing lines between basalts and marine sediments, reflecting a small amount of older crustal contamination (Chapter 3). A larger flux would result in crustal-scale MASH-like processing, while a lower flux or an increase in lithospheric extension would yield AFC-like volcanism, such as that seen in the NWBR. This process is not isolated to just the HLP in this back-arc and can be extended to other bimodal systems (Chapter 4).

The flux of mantle-derived basaltic magmas into the lower crust, coupled with removal of the more easily melted portion of the pre-existing crust leaves a denser residuum and a more refractory and dense lower crust. We refer to this process as "basaltification" (Figure 2). As this process continues and more mantle-derived magma is added through time, the lower crust (density of ~ 2.9 g/cc) increases in thickness. The rhyolitic liquids generated by partial melting buoyantly rise, and may either erupt or become stalled in the uppermost crust where they can differentiate to high silica rhyolites. This leaves behind a crystalline residuum (density of ~ 2.5 g/cc), that is well imaged by geophysical studies (Figure 2). Only rarely do mafic and silicic magmas mingle, resulting in intermediate compositions that show pervasive disequilibrium textures. In a few places, the magmatic flux and attendant partial melt might be vigorous enough to produce a zone of basaltic underplating at the base of the crust (Figure 2) (Fyfe, 1993).

In the NWBR, where crustal extension is greater but the mantle-derived melt flux is less than in the HLP, evidence of widespread crustal anatexis is lacking (Chapter 3).

However, major and trace element geochemical and textural evidence indicate that MASH-like processes are significant. This flux to the lower crust is a result of the mantle thermal regime. Due to the greater amounts of extension in the NWBR, basaltic magmas can more easily traverse the crust and are therefore less likely to stall, interact, and partially melt the host crust. We see evidence of this in the density models constrained by seismic refraction data (Cox, 2011) as well, where the mid to lower crust is less dense than that in the HLP and there is no evidence of a zone of underplating. The NWBR is more suitably described with a "mini-MASH" model, where small, discrete pods of recently emplaced basalt undergo RAFC processes to form the range volcanic rock compositions (Chapter 2 and 4). In contrast to the HLP and NWBR back-arc settings, the Cascades arc has a very high flux of basaltic magmas, which results in substantial partial melt, a large MASH zone, and significant underplating (Hildreth and Moorbath, 1988).

BIMODAL VOLCANISM AND ITS CAUSES:

The production of silicic rocks in the bimodal HLP is a direct result of partial melting of mafic crust and fractionated basaltic magmas that intrude and solidify in the lower crust. These silicic partial melts likely range from 69 – 74 wt. % SiO_2, depending on the degree of melting (cf. Sisson et al., 2005) and while some of these erupt to the surface, some also differentiate via fractional crystallization to produce medium to high silica rhyolites (likely > 73 wt. % SiO_2). Extensive fractionation (50 % or more) of low silica rhyolite to high silica rhyolite can obscure the petrogenetic pathway of the rhyolite (cf. Streck and Grunder, 2008). Without the knowledge derived from in-depth investigations of each individual silicic center, we cannot exclude the possibility that there could be some centers that do not fit the general model we present for the HLP (and NWBR). As the HLP is a zone of transtension, occasionally, basaltic magmas also can erupt to the surface, resulting in a bimodal, basalt - rhyolite volcanism.

Bimodal volcanism occurs in many other parts of the world, usually in areas that have a mafic crust. In Appendix 5, we provide a brief overview of bimodal volcanism from the Snake River Plain (SRP) and Iceland as analogs to the HLP, but bimodal volcanism also occurs in some ocean arcs (e.g. Tamura, et al., 2009), and even at oceanic

hot spots, large igneous provinces and plateaus (e.g. Shamberger and Hammer, 2006; Geist et al., 1995; Frey et al., 2000). In many of these locations, like in the HLP, the crust is very mafic to start with and isotopic constraints generally limit rhyolite formation to partial melting of a mafic protolith or fractional crystallization of mafic magmas, or a combination of these two mechanisms. In all of these cases except the SRP, basalt interaction with a silicic crust with elevated $^{87}Sr/^{86}Sr$ and low $^{143}Nd/^{144}Nd$ isotopic ratios is precluded or believed to be of minor significance either because 1) there is no "continental crust" in the area, or 2) the basaltic magmas largely re-ingest crustal areas that have "mantle-like" isotopic signatures. That is, of course, due to the fact that such locations are either places with oceanic crust or places where the crust has undergone basaltification. In all such cases, the formation of bimodal assemblages heralds the distillation of the mafic crust into a more silicic upper and more mafic lower crust.

The SRP and some continental rifting environments (e.g. Peccerillo et al., 2003; Rooney et al., 2007) are slightly different but show general similarities. Where continental rifting occurs, the basaltic magmas are unable to interact with the crust to a large degree and rhyolites are likely formed by fractional crystallization; they do not have strong crustal isotopic signatures and are often strongly peralkaline (Peccerillo et al., 2003). In the SRP, the mafic mantle input reaches neutral buoyancy (generally defined as where upward driving or buoyant forces match resisting forces) in the silicic upper crust where it produces a hybridized MASH zone of a diorite composition. This hybrid crust then partially melts to produce parental rhyolitic liquids with the proper isotopic ratios and these then fractionally crystalize to produce the high-silica rhyolites of the voluminous SRP ignimbrites (McCurry and Rodgers, 2009). This produces "basaltification" in the upper crust, resulting in a mid-crustal sill complex (Peng and Humphreys, 1998). This process is similar to what we propose for the HLP, except that our basaltification occurs in the lower crust and if hybridizing takes place, it is with mafic accreted terranes (further detailed in Chapter 4).

IMPLICATIONS OF THIS WORK:

We develop an internally consistent model (Figure 2) that is capable of producing a bimodal basalt - rhyolite assemblage in the HLP. The geometry of the downgoing slab produces a mantle flow regime conducive to focused, age-progressive volcanism as seen in the HLP. The same model explains the lower volume, more Great Basin-like suite (cf. Christiansen and McCurry, 2008) from the NWBR, based on lower mantle flux and greater crustal extension, but with a similar age-progressive pattern. The model satisfies many observations including: 1) creating a more dense lower crust, 2) creating a silicic crystal residuum in the upper-most crust, 3) explaining the dearth of intermediate compositions in the HLP, 4) creating a bimodal assemblage in the HLP, 5) explaining the isotopic signature of the rhyolites from both provinces, 6) explaining the increase in FeO* at a given silica content at any long-lived center or over the HLP province as a whole, 7) explaining the geophysically-imaged underplated crust in areas with the greatest flux, 8) potentially adding enough mass to create basinal sag in the Harney Basin, 9) eliminating the need for a plume source of any kind for the HLP volcanism, 10) explaining the existence of one late rhyolite (Iron Mountain) that does not fit the age-progressive sweep of volcanism in the HLP, and 11) production of voluminous ignimbrites in the HLP but not in the NWBR.

Additionally, this model, in which the lower crust becomes more mafic and refractory through time (i.e. basaltification), is applicable to many other bimodal systems, especially those characterized by initially mafic crust. These include the age-progressive ignimbrites of the SRP, some of the Quaternary (non-age-progressive) domes of the SRP, many of the rhyolites in Iceland and potentially other areas such as thickened oceanic plateaus or oceanic hot spots. The model displays the distillation process that begins the stratification of juvenile crust into crust with distinctive upper and lower seismic reflectors, densities and crustal isotopic and chemical signatures.

REFERENCES:

Annen, C., Blundy, J. D. and Sparks, R. S. J., 2006, The genesis of intermediate and silicic magmas in deep crustal hot zones: J. of Petrology, v. 47, p. 505-539.

Camp, V. E. and Ross, M. E, 2004, Mantle dynamics and genesis of mafic magmatism in the intermontane Pacific Northwest, J. of Geophysical Research, v. 109, B08204, doi:10.1029/2003JB002838.

Christiansen, E. H. and McCurry, M., 2008, Contrasting origins of Cenozoic silicic volcanic rocks from the western Cordillera of the United States: Bulletin of Volcanology, v. 70, no. 3, p. 251-267.

Cox, C., 2011, A Controlled- Source Seismic and Gravity Study of the High Lava Plains (HLP): University of Oklahoma MS Thesis, 110 p.

Dicken, S. N., 1950, Oregon Geography: First Preliminary Edition: Ann Arbor, MI, Edwards Brothers, 104 p.

Draper, D. S., 1991, Late Cenozoic bimodal magmatism in the northern Basin and Range Province of southeastern Oregon: J. of Volcanology and Geophysical Research, v. 47, p. 299-328.

Druken, K. A., Long, M. D. and Kincaid, C., 2011, Patterns in seismic anisotropy driven by rollback subduction beneath the High Lava Plains: Geophysical Research Letters, v. 38, L13310, p. 1-6.

Frey F.A., Coffin M.F., Wallace P.J., Weis D., Zhao X., Wise S.W., Jr., Wahnert V., Teagle D.A.H., Saccocia P.J., Reusch D.N., Pringle M.S., Nicolaysen K.E., Neal C.R., Müller D.R., Moore C.L., Mahoney J.J., Keszthelyi L., Inokuchi H., Duncan R.A., Delius H., Damuth J.E., Damasceno D., Coxall H.K., Borre M.K., Boehm F., Barling J., Arndt N.T. and Antretter M., 2000, Origin and Evolution of a Submarine Large Igneous Province: The Kerguelen Plateau and Broken Ridge, Southern Indian Ocean: Earth and Planetary Science Letters, v. 176, p. 73-89.

Fyfe, W. S., 1993, Hot spots, magma underplating, and modification of continental crust: Canadian J. of Earth Sciences, v. 30, p. 908-913.

Geist, D., Howard, K. A. and Larson, P., 1995, The generation of oceanic rhyolites by crystal fractionation – The basalt-rhyolite association at Volcan Alcedo, Galapagos Archipelago: J. of Petrology, v. 36, p. 965-982.

Graham, D. W., Reid, M. R., Jordan, B. T., Grunder, A. L., Leeman, W. P., and Lupton, J. E.,2009, Mantle source provinces beneath the Northwestern USA delimited by helium isotopes in young basalts: J. of Volcanology and Geothermal Research, v. 188, p. 128-140.

Hildreth, W., and Moorbath, S., 1988, Crustal contributions to arc magmatism in the Andes of central Chile: Contributions to Mineralogy and Petrology, v. 98, p. 455-489.

Hildreth, W., and Moorbath, S., 1991, Reply to comment on "Crustal contributions to arc magmatism in the Andes of central Chile" by W. Hildreth and S. Moorbath: Contributions to Mineralogy and Petrology, v. 108, p. 247-252.

Jonasson, K., 2007, Silicic volcanism in Iceland: Composition and distribution within the active volcanic zones: J. of Geodynamics, v. 43, p. 101-117.

Jordan, B. T., Grunder, A. L., Duncan, R. A., and Deino, A. L., 2004, Geochronology of age-progressive volcanism of the Oregon High Lava Plains: Implications for the plume interpretation of Yellowstone: J of Geophysical Research, v. 109, issue B10, p. 1-19.

Long, M. D., Gao, H., Klaus, A., Wagner, L. S., Fouch, M. J., James, D. E., and Humphreys, E., 2009, Shear wave splitting and the pattern of mantle flow beneath eastern Oregon: Earth and Planetary Science Letters, v. 288, p. 359-369.

MacLeod, N. S., Sherrod, D. R., Chitwood, L. A. and Jensen, R. A., 1995, Geologic Map of Newberry Volcano, Deschutes, Klamath, and Lake Counties: Oregon, USGS Miscellaneous Investigations Series Map I-2455, scale 1:62,500 and 1:24,00.

McCurry, M. and Rodgers, D. W., 2009, Mass transfer along the Yellowstone hotspot track I: petrologic constraints on the volume of mantle-derived magma: J. of Volcanology and Geothermal Research, v. 188, p. 86-98.

Peccerillo, A., Barberio, M. R., Yirgu, G., Ayalew, D., Barberi, M. and Wu, T. W., 2003, Relationships between mafic and acid peralkaline magmatism in continental rift settings: a petrological, geochemical and isotopic study of the Gedemsa volcano, central Ethiopian Rift: J. of Petrology v. 44, p. 2003–2032.

Peng, X, and Humphreys, E. D., 1998, Crustal velocity structure across the eastern Snake River Plain and the Yellowstone swell: J. of Geophysical Research, v. 103, p. 7171-7186.

Raia, F and Spera, F. J., 1997, Simulations of crustal anatexis: Implications for the growth on differentiation of continental crust: J. of Geophysical Research, v. 102, p. 22629-22648.

Rooney, T., Furman, T., Bastow, I., Ayalew, D. and Yirgu, G., 2007, Lithospheric modification during crustal extension in the Main Ethiopian Rift: J. of Geophysical Research v. 112, p. B10201.

Shamberger, P. J. and Hammer, J. E., 2006, Leucocratic and gabbroic xenoliths from Hualalai Volcano, Hawaii: J. of Petrology, v. 47, p. 1785-1808.

Sisson, T.W. and Grove, T. L., 1993. Experimental investigations of the role of H2O in calc-alkaline differentiation and subduction zone magmatism: Contributions to Mineralogy and Petrology, v. 113, p. 143-166.

Streck, M. J. and Grunder, A. L., 2008, Phenocryst-poor rhyolites of bimodal, tholeiitic provinces: the Rattlesnake Tuff and implications for mush extraction models: Bulletin of Volcanology, v. 70, p. 385-401.

Tamura, Y., Gill, J. B., Tollstruo, D., Kawabayta, H., Shukuno, H., Chang, Q., Miyazaki, T., Takahashi, T., Hirahara, Y., Kodaira, S., Ishizuka, O., Suzuki, T., Kido, Y., Fiske, R. S. and Tatsumi, Y., 2009, Silicic magmas in the Izu-Bonin oceanic arc and implications for crustal evolution: J. of Petrology, v. 50, p. 685-723.

Taylor, S. R. and McLennan, S. M., 1995, The geochemical evolution of the continental crust: Reviews in Geophysics, v. 33, p. 241-265.

Trehu, A. M., Asudeh, T. M., Brocher, T. M., Luetgert, J. H., Mooney, J. L., Nabelek, J. L. and Nakamura, Y., 1994, Crustal structure of the Cascadia forearc: Science, v. 266, p. 237 – 243.

Walker, G.W., and MacLeod, N.S., 1991, Geologic map of Oregon: U. S. Geological Survey, scale 1:500,000.

FIGURES:

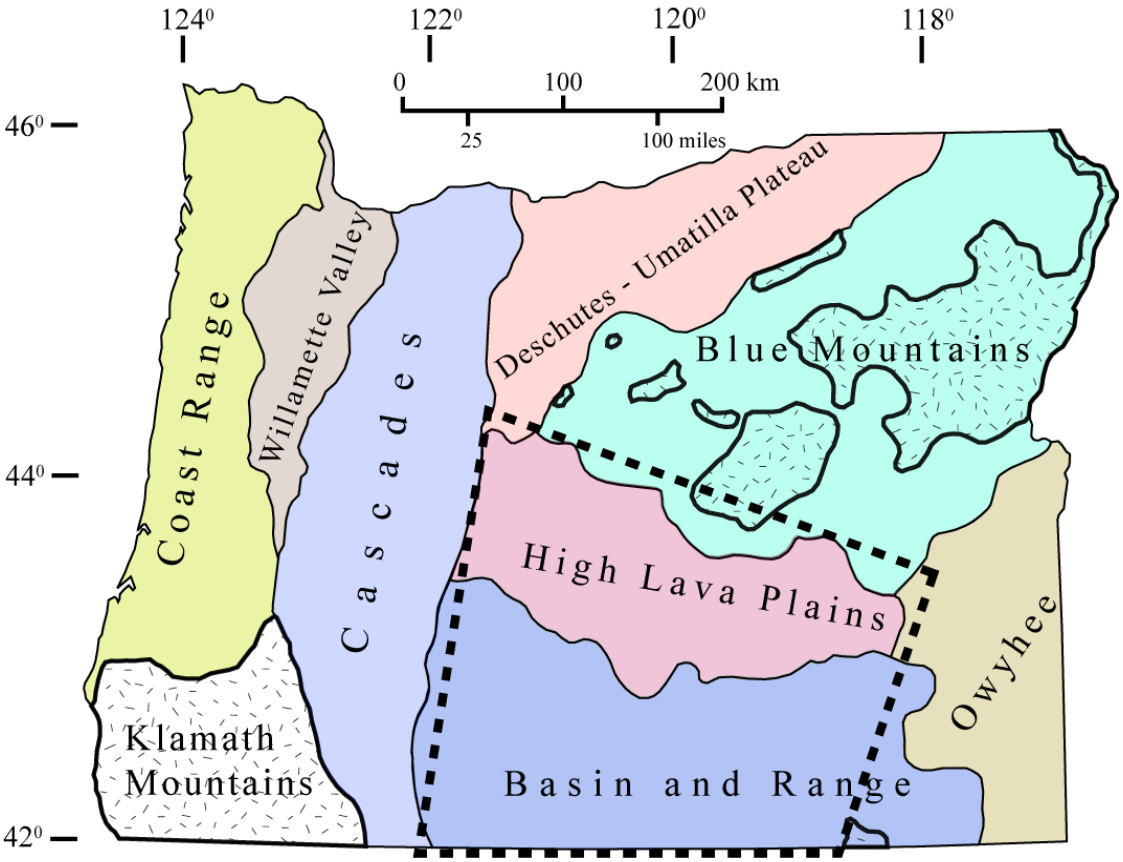

Figure 1: Physiographic provinces of Oregon and study area, outlined by dashed box. The approximate extent of pre-Tertiary outcrops are given in a stipple pattern (adapted after Dicken, 1950 and MacLeod, et al., 1995; Walker and MacLeod, 1991).

Figure 2: Generalized petrogenetic cartoon model for the HLP. Model shows intraplated basaltic magmas in the lower crust, partial melting of lower crustal amphibolite or recently intraplated basaltic plutons to form low silica rhyolites and fractionation in upper crustal chambers to make high silica rhyolites. The model in the Harney Basin area shows a highly diagrammatized Rattlesnake Tuff formation. Small curved lines with arrows indicate assimilation of a few percent of crustal rocks which may lead to more radiogenic $^{207}Pb/^{204}Pb$ or $^{87}Sr/^{86}Sr$ isotope ratios (see text for discussion). Intermediate rocks are mixes of basaltic andesite (or rarely basalt) and rhyolite. The crust – mantle boundary is at ~ 35 km, as imaged by geophysical studies.

Figure 2:

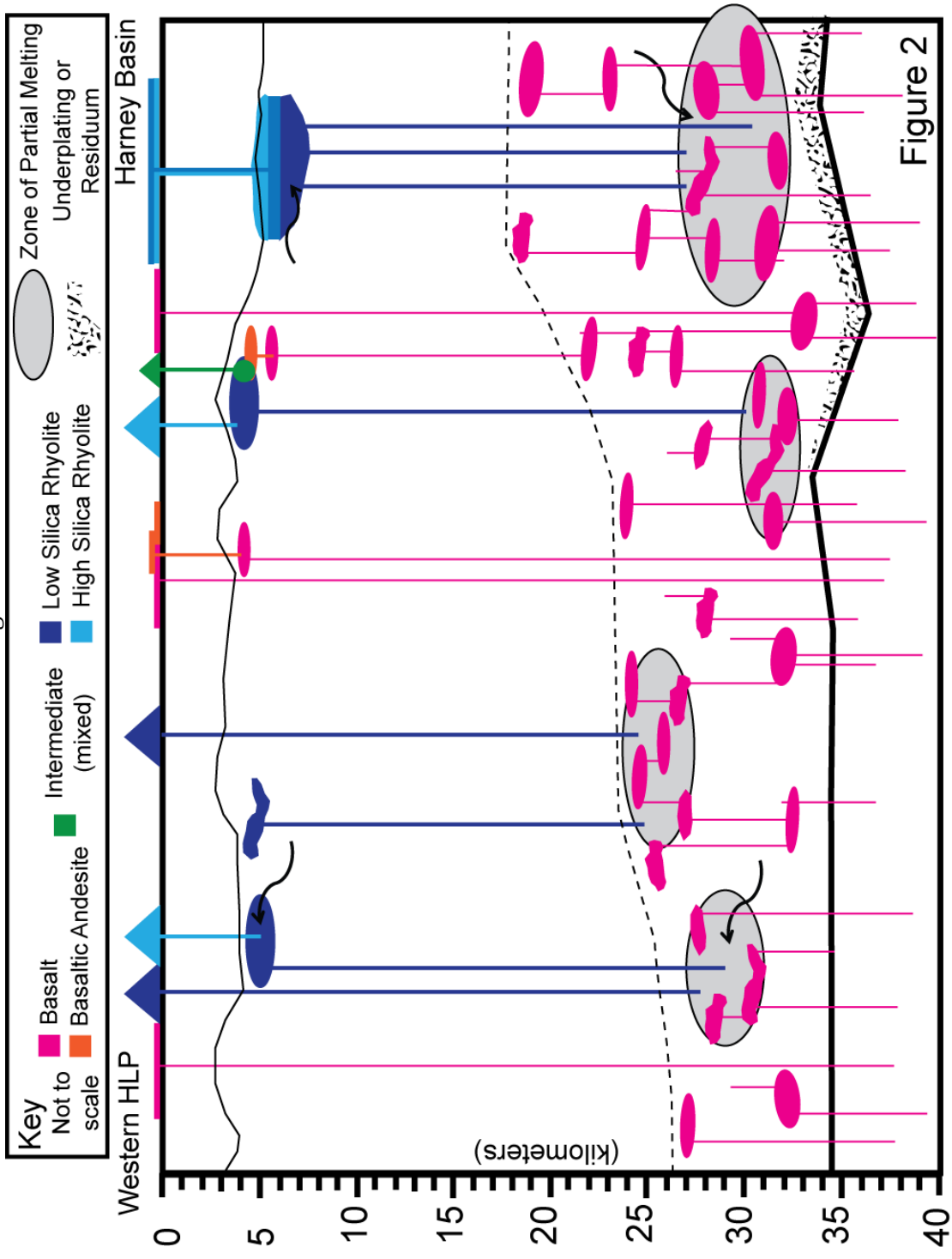
Key
Not to scale
Basalt
Basaltic Andesite
Intermediate (mixed)
Low Silica Rhyolite
High Silica Rhyolite
Zone of Partial Melting
Underplating or Residuum
Western HLP
Harney Basin
(kilometers)
0
5
10
15
20
25
30
35
40
Figure 2

CHAPTER 2:

Bimodal Volcanism of the High Lava Plains and Northwestern Basin and Range of Oregon: Diverse Silicic Magmatic Outcomes as a Result of Crustal Evolution

ABSTRACT:

The High Lava Plains (HLP) and northwestern-most Basin and Range (NWBR) Province is a Cenozoic bimodal basalt - rhyolite province in south-central Oregon and is an excellent example of magmatism in an intraplate continental setting. Here, we use new geochronological and geochemical constraints to link the two suites into a single, age-progressive volcanic trend which moves WNW at ~ 33 km/Ma. The timing of basalt and rhyolite eruptions is decoupled and some rhyolites are relegated to the subsurface due to crustal densification and resultant basin subsidence. We identify three distinguishable types of rhyolites including 1) an anhydrous, hedenbergite ± fayalite bearing, very Fe-rich type, which can be peralkaline, found in the HLP, 2) an augite, commonly paired orthopyroxene ± a hydrous phase, moderate to high Fe type and 3) a hydrous hornblende ± biotite low Fe type. The HLP rhyolites are typically higher in FeO* at a given SiO_2 than the NWBR rhyolites and are higher in high field strength elements (HFSE) and rare earth elements (REE). The differences and variability in rhyolite composition are not reflected by similar ranges in the basalt composition. The HLP suite is more similar to tholeiitic suites like Iceland whereas the NWBR is more similar to calc-alkaline suite like the Cascades volcanic arc. Low silica rhyolites of the HLP are likely produced by partial melts of mafic crust and these then evolve to high silica rhyolites mainly by fractional crystallization. The NWBR rhyolites, in contrast, are likely produced by assimilation – fractional crystallization (AFC) processes. Intermediate compositions from the HLP are usually mixes of mafic and silicic end members whereas the NWBR are not. A high flux of basaltic magmas to the HLP resulted in a denser lower crust due to intraplated basalts and residuum from partial melting and progressively greater degrees of partial melts produced the high-Fe compositions of the HLP rhyolites. The trend of HLP – NWBR volcanism is consistent with westward asthenopheric flow produced by the rollback of the Cascadia slab coupled with southwestward North American Plate motion.

INTRODUCTION:

The origin of silicic magmatism in bimodal basalt - rhyolite settings is a longstanding problem in igneous petrogenesis. This volcanism represents the surface expression of deep-seated modification of continental crust during interacting tectonic and magmatic processes (Bachmann and Bergantz, 2004; Barnes et al., 1996; Jonasson, 1994; Hildreth, 1981; Bowen, 1928; many others). Extensive work on mid-ocean ridges and subduction zones has led to well-developed paradigms that are relatively well defined regarding the processes involved in magma generation, and the resultant changes to the crust (e.g. Rubin, et al., 2001; Parman and Grove, 2004; Bachmann et al., 2007; many others). In comparison, there has been less work done on within-plate continental systems, especially regarding the development of silicic components. Multiple petrogenetic models exist for many systems, resulting in divergent mechanisms for magmatism and the formation and modification of continental crust (cf. Snake River Plain, Idaho: Christiansen and McCurry, 2008; Bonnichsen et al., 2008; Icelandic Rhyolites: Furman et al., 1992; Jonasson, 1994; Ethiopian Rift: Peccerillo et al., 2003; Rooney et al., 2007). Consequently, the need exists for more detailed studies of intraplate bimodal volcanic fields, with an emphasis on the composition and timing of silicic volcanism and the relationship between silicic and mafic magmas, and the relationship between magmatism and crustal formation and modification.

The focus of this work is on Late Cenozoic, basalt - rhyolite volcanism in the southeastern quarter of Oregon (Figure 1) which, in conjunction with the Columbia River Basalts, Steens Basalts and Yellowstone – Snake River Plain (SRP) track (Figure 2), is part of the largest Cenozoic volcanic province in the world (Smith and Luedke, 1984). This widespread sequence of volcanic rocks contains a number archetypal examples of anorogenic, or A-type, (after Loiselle and Wones, 1979) intraplate bimodal volcanism, such as the large volume ignimbrites related to the Yellowstone system (Christiansen and McCurry, 2008), and post-hotspot rhyolite domes of the eastern Snake River Plain (McCurry et al., 2008). We see some of these characteristics in the rhyolites of this work; namely, high FeO*, low MgO, Sr, Eu rocks containing anhydrous phenocryst assemblages. Our study area encompasses approximately 50,000 km^2 and includes both

the physiographic High Lava Plains (HLP) region (Fenneman, 1916; Dicken, 1950) and the northwestern-most Basin and Range Province (NWBR) within Oregon (Figure 1). The HLP extends from east of the Cascades in the vicinity of the massive shield of Newberry Volcano (MacLeod et al., 1995), eastward to the Owyhee Plateau through central Oregon. The NWBR range extends across southern Oregon, from the Cascades to the Owyhee Plateau, but in this study, our focus does not extend eastward of Steens Mountain. The Cascades, contemporaneous subduction-related volcanic rocks, lie just to the west of the HLP and NWBR.

In this work, we report 118 new whole rock major and trace element compositions and 19 new $^{40}Ar/^{39}Ar$ incremental heating ages and examine the spatial-temporal relationship of the rhyolites. In combination with existing studies, our new data enables us to define compositional sub-groups within the rhyolitic sequences and to examine the spatial distribution of these groups. This work also expands on the work of Jordan et al. (2004) by linking the HLP and NWBR rhyolite volcanism east-west age progressive trends and by extending this progression to the California-Oregon border. We provide the first comprehensive, quantitative volume estimates for volcanics in this bimodal province which has erupted nearly equal volumes of basalt – basaltic andesite and rhyolite over the past 12 Ma. We show that the rhyolites from the HLP province are compositionally more similar to the tholeiitic suites (Snake River Plain and Iceland) and the NWBR are more similar to the calk-alkaline Cascades suite. These comparisons provide a first order understanding of the origins of these rocks, as either orogenic, anorogenic, or a combination of the two, and help elucidate tectono-magmatic relationships in this intracontinental setting. Our data also constrain petrogenetic models for rhyolite formation, and allow us to examine how bimodal magmatism has modified the crust over the past ~ 12 Ma. We suggest that volcanism focused in one area over time results in a more refractory crust, principally adding mass via intraplated basalts and removal of less dense crustal components by partial melts (the parental low silica rhyolite), and this impacts the character of any subsequent rhyolitic volcanism. We coin the term “basaltification” for this process of creating a more refractory, more dense crust over time.

The High Lava Plains and Northwest Basin and Range:

Physiographic and Tectonic Background:

This section first examines the physiographic nature and tectonics of the HLP – NWBR and then introduces the petrology, petrography, eruption style and geochronology of the volcanic rocks. The boundary between the HLP and Basin and Range physiographic provinces is somewhat arbitrary, with features of both provinces represented in the other. Major physiographic divisions of the United States (cf. USGS: A Tapestry of Time and Terrain: Vigil et al., 2000) were first described in 1916 and have changed very little since that time (Fenneman, 1916; Vigil, et al., 2000). Large range-bounding normal faults of the Basin and Range gradually decrease in topographic and structural offset northward into the HLP. Flat-lying lava flows and a generally more muted topography is representative of the HLP but extend southward into the NWBR. Both provinces contain some internal drainages (Fenneman, 1916). This division, especially the boundary of internal drainages, dates to the description of the Great Basin boundaries in the reconnaissance work by Russell (1884). We extend this subtle but longstanding physiographic separation to the igneous rocks of the region, separating them into those from the HLP and those from the NWBR.

The physiographic HLP (Figs. 1 and 2) generally outlines a late Miocene and younger volcanic province that is approximately 90 km wide and 275 km long extending across eastern and central Oregon. It is bounded on the east by the Owyhee Plateau, on the west by the predominantly calc-alkaline Cascades volcanic arc, to the south by the extending Basin and Range (NWBR) and to the north by the relatively unextended, accreted terranes of the Blue Mountain Region physiographic province.

The central HLP is cut obliquely by the Brother's Fault Zone (BFZ). The BFZ is characterized by small, northwest-striking normal faults with offsets generally less than 10 m (Lawrence, 1976, Figure 3). While Lawrence (1976) proposed a right-lateral strike-slip zone as the kinematic link between the BFZ and northwestern most Basin and Range tectonic activity, more recent models (Meigs, et al., 2009; Trench, 2008) suggest there is

also an element of independent transtension within the BFZ as a result of the clockwise rotation of the Oregon fore-arc (coastal) block (Wells et al., 1998) and include the possibility of magmatic weakening of the crust. Oligocene through middle Miocene rhyolitic volcanism is also sparsely exposed within the HLP (Jordan et al., 2004; McKee and Walker, 1976; MacLeod et al., 1976) (Figure 4a, b).

The NWBR (Figure 1) is that part of the Great Basin within Oregon, spanning between the Cascades and the Owyhee Plateau, and this work pertains to that portion of the NWBR west of Steens Mountain. The NWBR is cut by middle Miocene and younger normal faults (Basin and Range style, Pezzopane and Weldon, 1993) with scarps as high as 2000 m (e.g. Steens Mountain, Abert Rim). Compared to the HLP there are more exposures of the older (greater than 12 Ma) volcanic rocks in the NWBR due to the greater structural relief (cf. Scarberry, 2007) (Figure 4a, b).

Petrology, Petrography, Eruption Style and Geochronology:

The volcanic rocks younger than 12 Ma in the HLP and NWBR make up a basalt - rhyolite bimodal province that consists generally of widespread, thin basalt lava flows and rhyolitic ash-flow tuffs, intercalated with tuffaceous sediments. The basalts are dominantly low-K high-alumina olivine tholeiites (HAOT), with the most primitive resembling mid-ocean ridge basalts (Hart et al., 1984). Approximately a third of the analyses on mafic rocks (less than 57 wt. % SiO_2) are basaltic andesites or basaltic trachyandesites, and a few of these are calc-alkaline (Jordan et al., 2004). These basalts are commonly diktytaxitic and similar in composition to those of the coeval SRP (Snake River Plain olivine tholeiite or SROT of Leeman, 1982a; Hughes et al., 2002). The basalts do not exhibit any age-progressive behavior, unlike the rhyolites, but do seem to focus in time to the axis of the HLP and to the immediate backarc region of the Cascades (Jordan et al., 2004). Basalt eruptive activity was concentrated in pulses, with distinct increases region-wide around 7.5-8 Ma, and focused activity in the western-most NWBR between 5.3 and 5.9 Ma and along the axis of the HLP from 2-3 Ma (Jordan et al., 2004). There also seems to be loci of volcanism less than ~ 50,000 years old at each end of the HLP, at Diamond and Jordan Craters to the east and around Newberry Volcano to the

west. Some vent complexes (e.g. Four Craters, Buttes of the Gods, Diamond Craters) have a NW to WNW alignment, mimicking the regional fabric of the distributed, low-relief NW-striking faults of the BFZ in the HLP and similar faults of the poorly understood and less documented Eugene – Denio Fault Zone (EDFZ) in the NWBR. There do not appear to be any vent alignments that parallel the larger offset, generally NNE striking "Basin and Range" faults in the area (Figure 3).

The < 12 Ma rhyolites of the HLP - NWBR erupted in a time transgressive manner, beginning in the eastern parts of the HLP - NWBR at around 10 to 12 Ma and younging to the west-northwest through time, with the youngest (Recent) eruptions at Newberry Volcano. Both Walker (1974) and Macleod et al. (1976) noted two generally parallel age-progressive rhyolite outcrop trends younger than 12 Ma, one within the HLP and one within the NWBR. These sets are separated by a paucity of outcrops of silicic rocks. This age progression has posed a tectonic puzzle in that it propagates in the opposite direction to the age progression among the rhyolites that define the Snake River Plain - Yellowstone trend (Pierce and Morgan, 1992), and nearly perpendicular to North American plate motion. Jordan et al. (2004), who link the two parallel trends to form a single province, term the suite the "High Lava Plains trend", which we prefer, in contrast to Humphreys et al. (2000) and Xue and Allen (2006) who refer to the trend as the "Newberry hotspot" and "Newberry trend" respectively. MacLeod et al. (1976) also noted that all rhyolites younger than 4 Ma are within 70 km of the Holocene Newberry Volcano (Higgins, 1973; MacLeod et al., 1995), but they did not link the two provinces. This work adds new age determinations on rhyolites from the HLP and NWBR and improves on earlier K-Ar ages, especially those that have large errors, showing that the HLP and NWBR form a single age-progressive volcanic province that extends to the California border.

In addition to the more than 60, generally small-volume, rhyolitic dome complexes that dot the region (Figure 4d)., three large 100 – 300 km^3 DRE (dense rock equivalent) ash-flow tuffs outcrop extensively. These include the Devine Canyon (9.63 ± 0.05 Ma – this work), Prater Creek (8.46 ± 0.18 Ma, Jordan et al., 2004) and Rattlesnake Tuff (7.09 ± 0.03 Ma, Streck and Grunder, 1995, updated by Jordan et al., 2004). In

addition, at least four smaller tuffs also have sources within the HLP while two additional tuffs might have sources within the NWBR (e.g. Silver Creek Welded Tuff and Plush Tuff). Of these units, only the Rattlesnake Tuff (RST) has been studied in detail (e.g. Streck and Grunder, 2008; 1999; 1997; 1995; Streck, 2002).

We present new data, including whole rock composition and ages for the numerous silicic domes that populate the HLP and NWBR (Table 1, Table 2, Appendix 1). The lavas and tuffs range from aphyric (e.g. Glass Buttes) to moderately porphyritic, containing up to 25% crystals, consisting of variable amounts of phenocrysts of plagioclase and (or) alkali feldspar (sanidine, sodic sanidine and anorthoclase), ± quartz. Mafic silicates are present in most porphyritic samples and consist of commonly paired augite and orthopyroxene or Fe-rich clinopyroxene and fayalite, with the latter assemblage noted only in the HLP. Amphibole and/or biotite occur as less common mafic assemblage, rarely with orthopyroxene or augite in the HLP but more commonly with other mafic phases in the NWBR. The domes are both endogenous and exogenous; while some are clearly monogenetic (e.g. the coulee-encircled Cougar Mountain, complete with glassy carapace), others are more complex and clearly polygenetic (e.g. Glass Buttes; Juniper Ridge, after MacLean, 1994). These longer-lived polygenetic dome complexes are often elongate along a northwesterly trend, parallel to the grain of the BFZ faults, and they have internal age trends that young to the west, similar to the province as a whole.

A few of the domes have vented smaller volume ash-flow tuffs that are still preserved (reference Figure 4 for many of the following locations). Frederick Butte (K-Ar age of 3.9 ± 0.4 Ma) is the likely source of the Tuff of Espeland Draw (K-Ar age of 3.6 ± 0.6 Ma) (Fiebelkorn, et al., 1983; Walker, 1974; Johnson, 1998) and based on the composition, age, and distribution, this is likely the same unit as the Hampton Tuff (^{40}Ar-^{39}Ar age of 3.80 ± 0.16 Ma) (Iademarco, 2009). The Peyerl Tuff, (K-Ar of 4.59 ± 0.89 Ma) located on the margins of and within maars of the Fort Rock Basin, maybe associated with Wart Peak and Bald Mountain (K-Ar of 5.21 ± 0.65 and 5.02 ± 0.61 Ma) (Fiebelkorn, et al., 1983; MacLeod, et al., 1976). The peralkaline tuff of Wagontire Mountain, mapped by Walker and Swanson (1968), has an approximate volume of 1 km^3

(DRE) and a postulated source just west of Wagontire Mountain but it has not been dated. The Buckaroo Lake Tuff has a ^{40}Ar-^{39}Ar age of 6.85 ± 0.04 Ma, overlapping within error of nearby Elk Mountain (6.90 ± 0.02 Ma) (Jordan et al., 2004) but no source has been identified and little additional work has been done. The Silver Creek Welded Tuff may be sourced in the Yamsay area (Hering, 1981) but MacLeod et al., (1976) disagreed based on a K-Ar age of 6.77 ± 1.10 Ma, which is older than other domes in the area. The Plush Tuff is exposed at Hart Mountain and is constrained to have erupted between 7 and 15 Ma, with a possible source of Beatys Butte (Mathis, 1993; Larson, 1965). There are likely more, yet undocumented, small volume < 12 Ma tuffs in the HLP and NWBR.

Intermediate composition (57 – 69 wt. % SiO_2) volcanic rocks are uncommon in this region and samples of these rocks make up approximately 17% of over 600 major element analyses reported (Electronic Data Supplement). Analyses of these rocks are likely over represented due to a focus and preferential sampling during earlier studies in centers known to contain a broad range of silica values, such as Burns Butte area (MacLean, 1994), Frederick Butte (Johnson, 1998) and Duck Creek Butte Eruptive Center (Johnson and Grunder, 2000) all of which are in the HLP. Outcrop exposures indicate that these compositions are a very small percentage of these centers. Gearhart Mountain and Yamsay Mountain (Figure 4d) in the NWBR are the source of many samples with intermediate compositions.

METHODS:

Sampling:

Field work consisted primarily of locating and collecting samples from silicic domes across the HLP and adjacent NWBR to provide spatial and temporal sampling of the province. We sampled centers for which no age or chemical data exists as well as augmenting existing sample collections (MacLean, 1994; Johnson, 1995; Jordan, 2001; Scarberry 2007; Iademarco, 2009) and obtaining samples for other centers identified in the literature (e.g. Wells, 1979; Hering, 1981; Walker, 1981; Berri, 1982; Brikowski, 1983; Fiebelkorn, et al., 1983; Roche, 1987; Johnson, 1998). Some areas on the Oregon

State Geologic Map (Walker and MacLeod, 1991) that were labeled as potentially rhyolite were found to be mafic (basalts or basaltic andesites) upon investigation. These minor updates to the State Geologic Map are lettered A, B, C and D in Figure 4d.

Geochemical Analyses:

New major and trace element results are reported on 118 samples with representative samples given in Table 1 (see Appendix 1 for all new data). Primarily X-ray fluorescence (XRF) and inductively coupled plasma-mass spectrometry (ICP-MS) were used with subordinate instrumental neutron activation analysis (INAA), as indicated in Tab1e 1. The majority of XRF analyses were conducted at the Washington State University (WSU) GeoAnalytical Laboratory based on the methods of Johnson et al. (1999). A small subset (10 out of 118) was analyzed by XRAL Laboratories, British Columbia. ICP-MS analyses were also performed at WSU following the methods of Knaack et al. (1994). INAA samples were activated in the Oregon State University 1 MW TRIGA reactor and analyzed at the Radiation Center, Oregon State University. For trace elements that were determined by both XRF and ICP-MS, the ICP results are preferred as this method is generally more precise. Previous workers (MacLean, 1994; Jordan, 2001; Scarberry, 2007) have shown little or no systematic differences between analyses from these different laboratories or analyses done by different techniques (e.g. INAA vs. ICP-MS) for HLP and NWBR volcanic rocks. In all cases, major element data are normalized to 100%, volatile-free with original totals given for reference. See Appendix 2 for complete information of what method was used for each sample and Appendix 3 for a list of sources of previously published data from the HLP and NWBR).

Standard errors, in either weight percent or ppm (Table 1), are given at the 95 % confidence interval for composition results and are calculated using a t-distribution from duplicate analyses (XRF, n = 4 and ICP, n = 7 except REE, n = 6). Due to the large range of values for Ba and Sr, very low concentrations for these analytes likely have smaller uncertainties than stated. This error is applicable to “silicic” (generally > ~ 60 wt. % SiO_2) samples with MTF and KCS labels and can be used in general for other samples that used the same methods (Appendix 2). The analytical uncertainties reported here are

typically similar or smaller to those quoted by the WSU laboratory, which are calculated from a very wide range of concentrations and variable substrates. Conversely, uncertainties from this work are calculated from similar igneous rocks, which typically return lower total uncertainties (R. Conrey, personal communication, 2009). Appendix 1 contains a more in depth treatment of the uncertainties including the largest uncertainties from the replicates, and uncertainties from the WSU lab, which may be more applicable to basalts or some samples that utilized different methods for whole rock geochemistry (Appendix 2). Using the two sets of errors described above yields the significant digits reported in this work for the MTF and KCS sample suites. Other samples using the same methods are treated similarly, except where data was originally received from the lab at a lower level of significance.

Geochronology by $^{40}Ar/^{39}Ar$ Incremental Heating:

Ages for nineteen rhyolitic samples, primarily from the NWBR, were determined by the $^{40}Ar/^{39}Ar$ incremental heating method at the Noble Gas Mass Spectrometry Lab (NGMSL) located in the College of Oceanic and Atmospheric Sciences at Oregon State University. Samples were prepared as either mineral separates (e.g. plagioclase, sanidine, biotite) or whole rock mini-cores. Cores were prepared from fresh, non-hydrated obsidian or from samples that were lacking in separable K-bearing minerals and appear unaltered and homogeneous. Cores were drilled from hand samples with a 5 mm diamond encrusted bit and sectioned into 2-2.5 mm thick disks weighing ~100 mg. These disks were then given an ultrasonic bath in deionized (DI) water and rinsed in acetone and DI water. Mineral separates were produced by crushing and sieving the sample to a –30+50 mesh (0.6 – 0.3 mm) and concentrating the phase of interest via Frantz Isodynamic Magnetic Separator or paper sifting. This concentrate was then washed in dilute HF and HNO_3 in ultrasonic baths, rinsed with DI water, and handpicked to obtain ~100 mg for plagioclase/sanidine, or ~50 mg for biotite.

Further sample preparation, argon extraction and analysis using either a resistance furnace (whole rock cores, n = 5) or 10W CO_2 laser (mineral separates, n = 14) follow the methods described in Duncan and Keller (2004), Duncan and Hogan (1994) and Duncan

et al. (1997) using a Fish Canyon Tuff biotite (FCT-3) monitor age of 28.02 ± 0.16 Ma (Renne et al., 1998). Irradiation was at the Oregon State University 1 MW TRIGA experimental reactor facility. The neutron flux was calculated from analyses of the FCT-3 standard. The total decay constant (λ_{tot}) incorporating the $^{40}K_{(ec,p)}{}^{40}Ar$ and $^{40}K_{(B-,n)}{}^{40}Ca$ decays was 5.543×10^{-10} a^{-1} as suggested in Steiger and Jager (1977). Data reduction was done with the ArArCALC v2.2 software package (Koppers, 2002). External errors are reported and incorporate errors on decay constants, analytical errors (regressions on peak heights vs. time) and errors in fitting measurements of monitors (J-values), as suggested by Koppers (2002) and Min et al. (2000).

Samples and standards (Fish Canyon Tuff biotite, FCT-3), were wrapped in Cu-foil and loaded in quartz tubes before irradiation. Neutron flux calibration curves were determined from analyses of the FCT-3 standard, located at several positions within the irradiation container. Subsequent to irradiation, samples were degassed at 400°C for 20 minutes. Samples were then subject to incremental heating steps (experiments) ranging from 25°C to 200°C, adjusted to optimize instrumental operating conditions and the quantity of Ar gas released, as samples were heated from 400 to 1400°C. Whole rock cores were heated with a Heine low-blank double-vacuum resistance furnace. Mineral separates (feldspars or biotite) were heated by a Merchantek integrated CO_2 continuous fire laser, operated with a diffuse beam rastered in a rectangular pattern over the sample. Gas liberated from each heating step was sequentially exposed to Zr-Al and Zr-V-Fe getters to remove active gasses and then analyzed for masses z = 35, 36, 37, 38, 39 and 40 by a 90° sector Mass Analyzer Products (MAP) 215-50 rare gas mass spectrometer with a 15 cm radius and a Nier-type source operating in peak-hopping mode following the methods of Duncan and Hogan (1994) and Duncan et al. (1997).

Concordant plateau and isochron ages indicate a trapped argon component (initial composition) that is within error of atmospheric composition. Age spectrum plots are shown in Figure 5 (Original Excel and .age files given in Electronic Data Supplement). We use the plateau age preferentially over the isochron age in all cases because age uncertainty is lower, resulting from generally low dispersion of step compositions in isochron plots. Error (external) is reported to 2σ for all analyses and in nearly all cases,

errors are less than two percent of the calculated age, and many cases, they are less than one percent.

Some samples were chosen for analysis to reduce the uncertainly or confirm the accuracy of previous K-Ar dates (generally from Fiebelkorn et al., 1983, and sources within) while other samples were from centers that had not been dated before this study. Generally, new $^{40}Ar/^{39}Ar$ dates have at least ten times better precision compared with previously reported K-Ar dates. Additionally, samples with very low Rb/Sr ratios were preferentially targeted so that with the more accurate ages, we could achieve more accurate initial radiogenic isotopic values (Ford et al., 2009).

RESULTS:

Erupted Volume:

While there have been a number of determinations of volumes of specific units in the HLP (e.g. Streck and Grunder, 1995), there has been no comprehensive reporting of the volcanic volumes for the bimodal < 12 Ma HLP – NWBR system. Our total volume estimate for volcanism < 12 Ma in the study area is 2,000 – 2,500 km^3 (Table 3) which contains sub-equal volumes of basalt and rhyolite and a minor amount of intermediate compositions. Although basalts, rhyolite domes and tuffs are widely exposed (Figure 4d), estimating the thickness and thus total volume of these 12 - 0 Ma volcanic products is difficult. Cross sections through the volcanics are exposed only in substantial fault scarps, mainly in the NWBR and in a few rare canyons in the HLP. Logs from a few energy exploration drill holes indicate that intercalated sediments and "Miocene and younger" undifferentiated volcanics extend to depths of greater than 3.5 km within the Harney Basin in the HLP and west of Lakeview in the NWBR (Popenoe, 1961; Newton et al., 1962). Recent geophysical studies (Cox, 2011) indicate that Cenozoic intercalated sediments and volcanics may be greater than 7 km thick in the eastern Harney Basin, which is likely the locus of calderas for the Devine Canyon and Prater Creek Tuffs. Field work and previous studies (see below) have indicated that the 12 - 0 Ma volcanics generally make up only a thin veneer where exposed, and while the Harney Basin may

have appreciable volumes of these younger rocks, we consider it more likely that the basin contains mostly sediments and volcaniclastic rocks. Below, we detail our estimates of rhyolites, basalts and intermediate composition for the < 12 Ma volcanics within the province.

Rhyolite Volume:

We estimate the total volume of the < 12 Ma rhyolitic volcanism in the study area is 1,000 – 1,250 km^3, the majority of which is represented by the three major ash-flow tuffs. Streck and Grunder (1995) calculated the volume of the 7.1 Ma Rattlesnake Tuff (RST) at 280 km^3 DRE. The 8.4 Ma Prater Creek and 9.6 Ma Devine Canyon Tuffs are estimated to be 100-150 km^3 and 200-300 km^3 respectively (Green, 1973). We chose the higher end of Green's estimate for the Devine Canyon Tuff as its extent and thickness are at least as great as those for the RST. The smaller tuffs, detailed above (e.g. Hampton, Peyerl, Wagontire, and others) are all likely less than 20 km^3 each and as small as 1 km^3 (Walker and Swanson, 1968). This volume estimate is based on outcrop coverage and thickness from previous reconnaissance mapping and by using the approximations of Streck and Grunder (1995) to account for erosional loss, air fall, and conversion to DRE, using the RST as an analog. The total volume of the tuffs is likely 800 – 850 km^3. Large tuffs (over 100 km^3) do not occur in the western HLP or NWBR and all appear to be greater than 7 Ma.

To the rhyolite volume from the tuffs, we add 150 – 400 km^3 from the silicic domes, many of which are less than 1 km^3, and their associated ash fall deposits. Some of the larger complexes may be as much as 50 km^3. The ~ 6.5 to 5.7 Ma Glass Buttes complex (Figure 4d) is 20 km long, 2-5 km wide and while variable in thickness, rhyolite extends to depths of at least 1 km in places, based on hydrothermal energy exploration drilling (Johnson and Ciancanelli, 1984). This yields a volume estimate of approximately 25-50 km^3 for the complex. The silicic rocks of the 9 Ma Drake Peak (Figure 4d), located in the NWBR, are likewise estimated to have a volume of 25-50 km^3 (based on cross sections of Wells, 1979). Other centers are intermediate in size, including the ~ 10.5 Ma Duck Creek Butte eruptive center, which is estimated to be 7 km^3 (Johnson and

Grunder, 2000) and Juniper Ridge, which is conservatively estimated to be 3 km^3 (MacLean, 1994). The total volume of silicic domes and flows is estimated to be 120 – 250 km^3.

The main sources of error in the volume estimate of the rhyolites are uncertainties in thickness and the unknown quantity of dispersed pyroclastic fall deposits. Two very recent, local analogs provide insight into the amount of pyroclastic fall deposits that these eruptions might have produced. The 700 C.E. eruption of the Big Obsidian Flow at Newberry Volcano (Figure 4d) has a well-documented associated plinian fall deposit of 0.1 km^3 (DRE), or about 40% of the total eruption (Jensen, 2006). Both the 950 C.E. and 1100 C.E. Little Glass Mountain and Glass Mountain of the Medicine Lake Volcano yielded about 10% by volume (DRE) of tephra (Heiken, 1978; Donnelly-Nolan, et al., 1990). Using these eruptions as proxies for HLP – NWBR volcanism would add an estimated 12 – 100 km^3 to the volume of the silicic domes in the region.

Basalt and Intermediate Composition Volume:

Most of the < 12 Ma basalts and basaltic andesites in the HLP and NWBR are low-K HAOT but subordinate calc-alkaline and alkali basalts exist (cf. Jordan, 2001, Hart et al., 1984). Areal coverage is estimated to be ~25,000 km^2, roughly 1/2 of the study area, with a greater concentration of flows along the axis of the HLP and few exposures east of 119.5º in the NWBR. HAOT flows are commonly 5 to 30 m thick (Hart et al., 1984; Mathis, 1993; Johnson, 1995; Iademarco; 2009; Scarberry, 2007) where normal faults expose cross sections of basalt. Individual flow fields commonly occur as compound stacks of several to a dozen flows with no evidence of erosion or soil development between stacks. Multiple stacks of flows, separated by tuffaceous sediments or volcanic rocks, are exposed at Hampton Buttes (2 or 3 flows, ~ 100 m, Iademarco, 2009), in drill core from Glass Buttes (3 flows, ~ 40 m, Johnson, 1984), at Abert Rim (4 to 5 flows, 50-60 m, Scarberry et al., 2010 and Burma Rim (3 to 4 flows, ~50 m, Jordan et al., 2002). Three distinct stacks of flows, ranging in age from 7.9 to 4.0 Ma (Jordan et al., 2004), each with distinctive flow thicknesses and morphologies, crop out in Dry River Canyon (HLP). These three flow stacks are separated by unconformities

and make a composite thickness of ~ 100 m, representing one of the few thick exposures of mafic lavas in the HLP. Multiple different models, some of which factor the greater aerial coverage and greater thickness along the axis of the HLP with less coverage and thickness across the NWBR, yield a total volume of basaltic and basaltic andesite volcanic rocks of 1,000 – 1,250 km^3, roughly equivalent to that of the rhyolites.

The majority of the volume of intermediate compositions (andesites and dacites) is associated with Gearhart Mountain in the NWBR (Figure 4d). Gearhart Mountain has a composite shield morphology and is primarily andesite, with subordinate volumes of basalts, dacites and rhyolites (Brikowski, 1983). Yamsay Mountain, also in the NWBR, contains a number of intermediate composition samples in the literature, but the bulk of the estimated 150 km^3 shield volcano is basaltic andesite (Hering, 1981). Hagar Mountain, again in the NWBR, has an unknown volume of intermediate rocks but a total volcanic volume likely less than 20 km^3. Intermediate compositions in the HLP are over sampled with respect to their volume and total volumes are not great, likely less than 20 km^3 in total. Thus, the total volume of intermediate rocks (andesite and dacite) from the HLP and NWBR is approximately 100 km^3, about 5% of the total volume of volcanic rocks of for the less than 12 Ma time period.

Localized Events Excluded in this Volume Estimate:

We do not include Newberry Volcano (less than 0.6 Ma) with a total volume of 800 – 1,000 km^3 (Macleod et al., 1995). While it lies within the physiographic HLP (Figure 4d), it is grouped with the Cascades and is referred to only for comparison (see Macleod et al., 1995; Donnelly-Nolan et al., 2008; Jensen et al., 2009). Likewise, we do not include the Deschutes Formation which lies primarily north of Bend and consists predominantly of pyroclastic flow deposits and volcaniclastic sediments shed from the High Cascades. The Deschutes Formation also contains isolated rhyodacite to rhyolite domes including the 6.74 ± 0.20 Ma Steelhead Falls rhyodacite and the 6.14 ± 0.06 Ma Cline Buttes (Sherrod et al., 2004), which are associated with High Cascades Arc volcanic activity (Taylor, 1981). These two exposures are of similar age to the 6.25 ± 0.02 Ma Pine Mountain, located ~40 km southwest of Bend (Figure 4c, Table 2). Given

the limited data on both Pine Mountain and Deschutes Formation rhyolites, it is difficult to assign the former to the latter but we consider it likely that the Deschutes Formation and Pine Mountain are related events. We limit the volume related to the Deschutes Formation in the HLP to ~100 km^3 (Table 3).

Age Determinations:

A majority of the new ages from this work are in broad agreement with the spatial-temporal distribution of HLP rhyolitic volcanic activity shown as isochrones in Jordan et al. (2004). Our new ages improve the density of data, reinforce and support the westward-younging age progression of rhyolite centers in the HLP and expand the age distribution to unequivocally include the NWBR.

Of the 19 samples analyzed by the incremental heating $^{40}Ar/^{39}Ar$ technique, 18 yielded plateaus with ages concordant to sample isochron ages (within 2σ) (Table 2) while one sample from Dead Indian Mountain failed to produce a reliable crystallization age. In some cases, the new dates do not differ appreciably from the previously reported K-Ar dates but in other cases, ages are significantly changed. For example, the age of the Drake Peak rhyolite has been updated from 14.7 ± 2 Ma (Fiebelkorn, et al., 1983; Wells, 1979) to 8.96 ± 0.06 Ma (Table 2).

Here we also report a new age of 9.63 ± 0.05 Ma for the Devine Canyon Tuff based on a 10-step heating plateau (Figure 5) recovering 94.9% of the radiogenic argon. This new age is from a mineral separate containing greater than two orders of magnitude more crystals than the age reported by Jordan et al (2004). Our age is subtly different from, but outside of the 2σ error, the weighted mean total fusion date of 9.74 ± 0.04 Ma returned using 9 of 10 single grain analyses (Jordan et al., 2004).

Three obsidian whole rock mini-cores were analyzed, viz: Glass Buttes "A" (5.79 ± 0.04 Ma), Glass Buttes "E" (6.49 ± 0.05 Ma) and Cougar Mountain (4.34 ± 0.05 Ma) (Table 2). These samples released the majority of their ^{39}Ar during one heating step, generally between 1075º and 1250º C, even over heating steps as small as 25º C (Figure 5), which is one quarter the temperature step of the laboratory standard for resistance furnace heating. While releasing so much of the radiogenic Ar in one heating step is

undesirable, in these cases it was unavoidable. We believe these results to be reliable estimates of the crystallization ages for these samples based on results for $^{87}Sr/^{86}Sr$ measurements on some high Rb/Sr samples (Ford et al, IP). If, for example, Glass Buttes "E" age is 0.25 m.y. older than that measured by the $^{40}Ar/^{39}Ar$ technique, the $(^{87}Sr/^{86}Sr)_i$ would be < 0.7029, a highly unlikely value given that no basalts in the region are < 0.7033.

We also report some new ages that do not fit the 12 – 0 Ma westward age sweep of the HLP - NWBR province. We identify previously unknown Middle Miocene volcanic centers at Bald Butte (17.53 ± 0.08 Ma) and Drum Hill (17.30 ± 0.09 Ma) (Figure 4b, Table 2). We report a new age of 6.25 ± 0.03 (Table 2) for rhyolite located at the top of Pine Mountain. The original K-Ar age of 22.0 ± 4 Ma (Fiebelkorn, et al., 1983) was on a sample from the flanks of the mountain indicating that there may be multiple episodes of volcanism exposed at this location, one correlative to the Deschutes Formation (7.4 – 4.0 Ma, Taylor, 1981; Sherrod et al., 2004) and the other to the John Day Formation (38.5 – 20.0 Ma, Robinson et al., 1990).

Phenocryst Assemblages in Rhyolite:

The 0-12 Ma rhyolites and dacites range from aphyric to porphyritic containing up to 25% crystals and exhibit a wide range of textural variability from pumiceous to dense glass to thoroughly devitrified, vapor-phase altered glass and lithophysae. We focus on phenocryst assemblages rather than textural variations as tracers of the magmatic history. Phenocryst assemblages among the HLP and NWBR fall into three general groups, based primarily on the mafic silicates: 1) an anhydrous Fe-rich assemblage with hedenbergite ± fayalite, 2) Augite, commonly paired with orthopyroxene ± a hydrous phase and 3) more rarely, only hydrous phases, hornblende ± biotite. The large tuffs of the HLP (DCT and RST) and the Hampton Tuff (less than 20 km^3) are of the anhydrous Fe-rich mineralogical type (Streck and Grunder, 1997; Green, 1973; Johnson, 1998; Wacaster et al., 2011). The other large tuff, Prater Creek, is very crystal poor and no mafic phenocrysts are noted (Walker, 1979). Streck and Grunder (1997) do report "several flakes" of biotite recovered from heavy mineral separation of

greater than 3 kg of crushed RST pumice but it is unclear if these are a phenocrystic or xenocrystic in nature.

With respect to the felsic assemblage, the large tuffs have alkali feldspar (sodic sanidine to anorthoclase) and lack plagioclase (Wacaster et al., 2011) with only a few crystals of oligoclase reported from the most evolved compositions of the RST (Streck, 1994). All three contain quartz, with prominent pink to clear quartz in the DCT but sparse amounts in the PCT and RST. In contrast, the Hampton Tuff, which is less silicic than the large tuffs, has plagioclase but lacks alkali feldspar and quartz (Johnson, 1998). Similarly, all dacite samples from Frederick Butte, the likely source of the Hampton Tuff, lack quartz and sanidine but contain plagioclase. The remaining rhyolites (domes) contain variable combinations of sanidine, plagioclase and quartz. While many of the peralkaline samples are aphyric, some do contain quartz and sanidine, and in a few cases, plagioclase.

In our phenocryst analyses, just over 25 % of the porphyritic samples of dacite to rhyolite domes or flows within the HLP contain hydrous phases; about one third of all samples (71 from this work; Table 4, 134 in total; Appendix 4) are aphyric, either obsidian, felsite or devitrified glass (based on compilations from Berri, 1982; Roche, 1987; MacLean, 1994; Johnson, 1998; Johnson and Grunder, 2000). Within the NWBR, 80% of the silicic porphyritic samples contain a hydrous phase while only 12% of all samples (32 from this work; Table 4, 76 in total; Appendix 4) were aphyric (based on compilations from Wells, 1979; Hering, 1981; Brikowski, 1983; Scarberry, 2007). This analysis indicates that the vast majority of the HLP silicic magma (dacite to rhyolite) does not contain any hydrous phases while the vast majority of the NWBR lavas do contain hydrous phases.

Whole Rock Major and Trace Element Compositions:

The compositional data used for this study include 118 major and trace element analyses (Table 1, Appendix 1), 75% of which are rhyolites, plus a compilation from theses, open file reports and literature sources. The resultant database contains over 600 samples that are less than ~12 Ma (Electronic Data Supplement). Samples that were not

in our repository and that were described in the literature as “altered” or “contaminated” or other such descriptors and most samples that had documented analytical totals below 96% were eliminated from the database and are not included in subsequent figures. As described above, Deschutes Formation volcanism is excluded from the following presentation and samples from Newberry Volcano are plotted with a separate symbol and not included in the database.

The suite of volcanic rocks < 12 Ma old from the HLP and NWBR is strongly basalt - rhyolite bimodal (Figure 6a, b) and contains roughly equal volumes of each. Greater than 60% of mafic compositions are basalts and 70% of these are 48.5 ± 1 wt. % SiO_2. Nearly 40% are basaltic andesites (normalized, volatile free 52 - 57 wt. % SiO_2) and samples are distributed throughout this SiO_2 compositional range without any apparent groupings. Intermediate compositions, classified as andesite or dacite, and their high alkali equivalents, make up only 5% of the volume of erupted rocks but ~15% of the samples analyzed. In the histogram (Figure 6b), 49 of the intermediate samples come from Gearhart Mountain (Brikowski, 1983) and Yamsay Mountain (Hering, 1981), showing the disproportionate sampling of some volcanic centers. A few other localities contain relatively dense sampling for intermediate composition such as eastern Juniper Ridge (MacLean, 1994) and the Duck Creek Butte eruptive center (Johnson, 1995). The spectrum of compositions at some centers with only a few analyses is likely underrepresented (e.g. Hagar Mountain) while others are likely fully represented with only one or a few samples (e.g. the monogenetic Cougar Mountain). Given the size of the database and bearing sampling caveats in mind, data plots presented below are a reasonable representation of the composition of the < 12 Ma volcanic rocks as a whole.

In the next sections, we first focus on rhyolite classification and composition with a focus on specific centers and geographic areas that have slight compositional variations from the general trends. We then detail spatial differences between HLP and NWBR rhyolites and examine east to west variations. Finally, we briefly characterize intermediate and basaltic compositions within the cast of the HLP and NWBR provinces.

Rhyolitic Classification and Compositions:

In the 0 – 12 Ma database, 275 samples are rhyolites. Approximately 60% of these compositions are classified as high silica rhyolites (SiO_2 > 75 wt. %) with the remainder split between low silica (69 – 72 wt. % SiO_2) and moderate silica (72 – 75 wt. % SiO_2) rhyolites. In terms of eruptive volume, a significant majority, a minimum of 80%, of the silicic rocks are high silica rhyolites, largely because the three major tuffs are high in silica. No attempt is made to calculate the relative volumes of low, moderate and high silica domes.

Using the alumina saturation index (ASI) classification (Figure 7, after Shand, 1927), a majority of rhyolite compositions are metaluminous but range to mildly peraluminous and peralkaline. Peraluminosity, present in about a third of the rhyolite samples, is only modest, with normative corundum always less than one percent. The composition and mineralogy classifies these samples as weakly peraluminous (Miller, 1985) as Al-bearing phases such as hornblende and biotite take up this "excess Al_2O_3" and indeed, these phases are commonly found in these samples. This low level of normative corundum does not fit the classification of "S-type", as first described by Chappell and White (1974). The mix of mildly peralkaline, weakly peraluminous and metaluminous compositions generally preclude the melting of sediment as the sole source for these rhyolites. This ASI classification, coupled with anhydrous phenocryst assemblages, high temperatures for some tuffs (RST, Streck and Grunder, 1997; 2008) and trace element composition (below) are all characteristics of "A-type" granites and rhyolites (Loiselle and Wones, 1979). These attributes are similar in many regards to the A-type rhyolites of the coeval Snake River Plain (Christiansen and McCurry, 2008, McCurry et al., 2008).

Nearly all peraluminous samples with molar Al/(Na+K+Ca) > 1.12 are from Glass Buttes, in the HLP, and all of these samples are from previous workers (Berri, 1982; Roche, 1987). These correspond to all samples that are > 74 wt. % SiO_2 and < ~7.7 wt. % total alkalis (Figure 6a), resulting in peraluminous samples (Figure 7). These samples may have been subject to glass hydration and attendant leaching of Na_2O (cf. Lipman, 1965), as Glass Buttes is one of a few dome sets that contain pervasive

hydrothermal alteration. Alternatively, low Na_2O concentrations may be due to systematic analytical shifts, as Na_2O is low in all samples from these studies but analyses of Glass Buttes samples from this study do not have low total alkalis relative to other rhyolite samples. Samples analyzed for this work do not appear to have been altered and often plot within the larger rhyolite group. Trace elements do not seem to be affected much by the alteration suggested by low Na_2O and noted above. Trace element data for Glass Buttes from both this study and previous work tend to plot within the range of high silica rhyolites except that a few samples are elevated in U and Th. This area is one of the few places in the HLP and NWBR where minable concentrations of metals occur, in this case, Hg.

A subordinate numbers of samples are peralkaline and, excepting one sample from Yamsay Mountain, all of these are from the physiographic HLP (Figure 7). These comendites have molar (Na+K)/Al up to 1.3 but do not have enough FeO* at a given Al_2O_3 to be pantellerites (after Macdonald, 1974). In addition to the geographic separation, many of the large ignimbrites, including RST and DCT, are mildly peralkaline. While there are nearly no < 12 Ma peralkaline samples from the NWBR, some Oligocene to middle Miocene rhyolites from the NWBR are peralkaline including Bald Butte and the pantellerites and comendites of Hart Mountain (Mathis, 1993; Noble and Parker, 1974).

Using the Fe-number (FeO/(FeO+MgO)) classification method (Frost, et al., 2001), a majority of the rhyolite samples are ferroan and nearly all of the tuffs are. There is only a loose connection between ASI and Fe-number whereas nearly all peralkaline samples are ferroan, many metaluminous and peraluminous samples are as well. Another classification, the modified alkali-lime index (MALI; Frost et al., 2001) classifies most rhyolites as either alkali-calcic or calc-alkalic with only a few samples classified as alkali. Most of the tuff samples are alkali-calcic.

Harker Diagrams (Figure 8) are not particularly illustrative when examining only the rhyolitic samples and samples are not separated geographically, into the HLP and NWBR. This is due to the closed geochemical array, the forced correlations of variables that sum to 100%, which is also called the constant sum problem (Rollinson, 1993). Due

to the high concentrations of SiO_2 and Al_2O_3, totaling up to 90 wt. %, there can be only limited variation among the remaining major elements. The peralkaline samples do stand out in being lower in Al_2O_3, higher in FeO* and marginally higher in Na_2O and K_2O at a given SiO_2 (Figure 8). The potential hydrothermal alteration in many Glass Buttes samples is especially evident with the major elements with typically higher SiO_2, Al_2O_3, and CaO and lower Na_2O and K_2O (Figure 8).

Selected trace element variation diagrams (Figure 9) show the generally expected incompatible behavior and enrichment for some elements (Rb, U, Th), although some analytes values are highly elevated (e.g. eastern HLP sample for Rb in Figure 9). Generally compatible elements (Sr, Eu) are depleted and these depletions are related to crystalizing feldspars (cf. Ren et al., 2003; Ren, 2004). Many trace elements span a large range, for example Ba at ~76% SiO_2 can range from 50 - 2000 ppm. Sanidine can appear as part of the crystallizing assemblage in high silica rhyolites and it has mineral-melt partition coefficients as high as 20 for Ba (in the RST: Streck and Grunder, 1997). The timing of the appearance of sanidine on the liquid line of decent can cause such a wide variation for alkali-feldspar compatible elements. The onset of crystallization of certain phases (e.g. sanidine, zircon) results in geochemical behavior that appears to be compatible for some samples and incompatible for others (Ba, Hf, Zr, Nb).

The peralkaline samples have very low Ba and Sr concentrations, nearly all of which are < 300 ppm and < 30 ppm respectively. While many samples from both the HLP and NWBR have similarly low concentrations of Ba and Sr, they also extend to significantly higher values and have a greater range than the peralkaline rhyolite subset. The peralkaline rhyolites also have the highest high field strength elements (HFSE: Ta, Hf, Zr, Nb) concentrations and range to higher values for Y, Zn, and Ga and to the lowest values for Sc (Figure 9).

Seven samples collected near 42.35^o N, 120.6^o W, locally termed Cox Flat and Thomas Creek (NWBR), have double the U content as compared to average rhyolites. These samples also have elevated SiO_2, Rb, Th, Pb and Cs values and some of the lowest Sr values recorded (Figure 9). There are several more rhyolites from this area that have higher than average Pb concentrations but are not displaced in other element space.

Some of these samples might be altered, similarly to the Glass Buttes samples, as evidenced by the relatively strong peraluminousity (Figure 7). This general location is known as the Lakeview Uranium Area and at least two uranium mines were active in the area during the 1950's and 60's (Peterson, 1959).

N-MORB normalized rare earth element (REE) show a wide range of enrichment in the rhyolites ranging from 3 to 50 times N-MORB concentrations (Figure 10). $(La/Yb)_n$ values range from 2 to 12 and Eu anomalies $(Eu/Eu^*)_n$ range from 0.85 to < 0.1. Peralkaline compositions are particularly enriched in REE and have some of the greatest Eu anomalies (smallest $(Eu/Eu^*)_n$) values.

Rhyolites - Comparing the HLP and NWBR:

When separating samples based on physiographic location, either HLP or NWBR, there are some compositional differences. While rhyolites dominate the silicic samples (> 63 wt. % SiO_2) with dacites and trachydacites uncommon, compositional separation between the HLP and NWBR is apparent for dacite compositions for the total alkalis and most of the major elements, and this separation continues up to low silica rhyolites (< 72 wt. % SiO_2) for some elements (Figure 6a, Figure 8). At the higher silica values, there is little separation between the HLP and NWBR due to the closed geochemical array. Many of the classification schemes discussed above do not show much of a difference between the HLP and NWBR. The ASI classification (Shand, 1927) does not clearly divide the two physiographic provinces and roughly equal numbers of rhyolite and dacite analyses from the HLP and NWBR are metaluminous and mildly peraluminous (Figure 7). Almost all of the peralkaline compositions are in the HLP however. Silicic samples from the HLP and NWBR also are not clearly distinguished by the Fe-number (FeO/(FeO+MgO)) and MALI of Frost, et al. (2001).

While the rhyolites do not show any discernable difference in total alkali content between the HLP and NWBR (Figure 6a), one clear difference between the two provinces is that there is a higher proportion of high silica rhyolites (> 75 wt. %) in the HLP, including not only the voluminous tuffs like the RST but also among the domes, and a greater percentage of low silica rhyolites (< 72 wt. %) in the NWBR (Figure 6a). While

there is considerable overlap on major element diagrams, at a given SiO_2, HLP rhyolites are generally higher in TiO_2 and FeO* (Figure 8) and among and high silica samples (> 75 wt. % SiO_2) rhyolites from the HLP have elevated K_2O relative to NWBR samples. Higher silica samples from the NWBR are typically higher in Al_2O_3 than HLP samples. Trace element differences at a given silica concentration include elevated HFSE concentrations for HLP samples, but lower Pb and Sr values compared to the NWBR (Figure 9, cf. Figure 11). The HLP rhyolites are commonly enriched in REE and on average, have higher REE concentrations and a greater Eu anomaly than those of the NWBR (Figure 10). This enrichment in the HLP is slightly greater for the mid to heavy REE concentrations than the enrichment in the LREE concentrations (Figure 10).

The separation between the HLP and NWBR shown in the FeO* Harker diagram (Figure 8) is also displayed in plots comparing calc-alkaline to tholeiitic provinces, (Figure 12). Separation is generally best for compositions ranging from andesite to low silica rhyolite. A line can be drawn that separates samples from the HLP - NWBR province and has the equation $y = -0.3523x + 27.83$ with (SiO_2, FeO*) end points at (57, 7.75) and (79, 0) and we term this the "Fe-line". Of the greater than 57 wt. % SiO_2 samples, nearly 73% of the HLP points plot above the Fe-line while nearly 90% of the NWBR points plot below this line, separating the two provinces close to 80% of the time into high-FeO* (at given SiO_2) HLP and low-FeO* NWBR. When the Fe-line is superimposed on the Iceland-Cascade dataset (Figure 12, inset), it correctly separates the two provinces into high- and low-FeO suites over 90% of the time. Thus, there does seem to be some compositional differences between rhyolites from this temporally linked volcanic province.

A subset of samples from Yamsay Mountain, rhyolites above 73 wt. % SiO_2 are nearly identical to Newberry samples (discussed next) of the same SiO_2 content, and, if included in the NWBR set, usually make up the upper or lower boundary for that group for any given element. Samples from Newberry Volcano (MacLeod et al., 1995; Higgins, 1973) are more similar to those from the NWBR plotting within the NWBR field or plotting between the HLP and NWBR sets where there is separation (Figure 6a, Figure 8). Newberry has some of the lowest CaO and highest Al_2O_3 at any given silica

values and has high Na_2O, like the NWBR and, excepting the hydrated Glass Buttes samples, a larger percentage of the Newberry samples are slightly peraluminous (Figure 7). In trace element composition, Newberry samples again plot either similarly to NWBR samples or between the two provinces except for Rb and Cs, where it plots towards the upper limits of the measured concentrations (Figure 9).

Rhyolites - Additional Spatial Considerations:

There are a number of trends in composition with respect to longitude. From east to west, the rhyolites increase in Na_2O and decrease in K_2O for both provinces and the magnitude of these changes is greater for the NWBR rhyolites than for HLP rhyolites (Figure 13). Another notable E-W trend is that the peralkaline rhyolites are present only east of ~ 120.3º. In the HLP, there is a slight increase in the Zr/Nb ratio to the west (Figure 14) while the NWBR rhyolites increase in Zr, Nb, Y, and Hf west of 121º. We did not see any other trends in HLP trace element composition except that there is less scatter in the data west of ~120.6º and some of the easternmost lavas show a slight displacement, discussed next.

Located on the extreme eastern margin of the HLP, the Duck Butte Eruptive Center (DBEC) is one of the few centers that have received in-depth study (Johnson, 1995; Johnson and Grunder, 2000). Compared to other low silica rhyolites in the HLP, the low silica rhyolites of the DBEC are enriched in Rb, Ba, Sr, Cr, U and Th whereas the DBEC high silica rhyolites are only enriched in Rb, Th, U and possibly Pb, but have low Zr, Hf and Y concentrations as compared to most other high silica HLP samples. This is not a trend that stretches across the HLP, as these compositional differences are only present in this extreme eastern section. Other rhyolite samples from the eastern sections of the HLP, such as Stockade Butte and Crane Creek Dome, are similar in trace element composition to the DBEC high silica rhyolites. They are higher in Rb, U, Th and Pb but they are also enriched in Sr, Cs, and for Stockade Butte, Cr and show slight depletions in Zr, Hf and Y, as compared to most HLP rhyolites (Figure 9).

Intermediates - Comparing the HLP and NWBR:

On nearly all of the Harker variation diagrams (Figure 8), the intermediate compositions (57 – 69 wt % SiO_2) from the HLP plot separately from the NWBR samples. Intermediates from the HLP have higher FeO*, K_2O, and TiO_2 and lower Na_2O, Al_2O_3 and total alkali than those of the NWBR. For some plots (e.g. Na_2O, Al_2O_3), there is essentially no overlap between 55 and 69 wt. % SiO_2 between the two provinces. With respect to trace elements, the HLP intermediate samples have higher concentrations of Rb and may be higher in HFSE (Zr, Nb, Hf, Ta), Y, Zn, Sc, Ni and Cr (Figure 9). Most intermediate HLP analyses are lower in Sr compared to the NWBR and at least some samples from the HLP seem to lie along linear trends (potentially mixing lines) that would connect mafic and silicic compositions. REE data plot in a narrow range for intermediate compositions from both provinces (Figure 10). Samples from Hagar Mountain located at N 43.0º, W 121.0º, near the northern border of the physiographic NWBR, are more similar to those from the HLP in both major and trace elements, and they plot towards the upper limit for Rb, U and Th of all intermediate compositions. Roughly equal numbers of dacites from both provinces are metaluminous or peraluminous but none are peraluminous (Figure 7). The intermediate compositions of the eastern DBEC samples are elevated in TiO_2, FeO*, K_2O, and P_2O_5 and many trace elements including Rb, Ba, Zr, Nb, Ga, U, Th, Hf, Ta and REE but have some of the lowest Al_2O_3 concentrations in the study. At least some of the intermediate compositions from the DBEC are interpreted to be mixed silicic and mafic magma (Johnson and Grunder, 2000). Other east to west changes in intermediate compositions trends are difficult to discern due to the paucity of data, but they generally seem to mimic the basalts (discussed below) and grade into the rhyolite trends without any obvious inflections.

One other noteworthy observation is that west of Frederick Butte, or about 120.6º, there is only one HLP lava reported that has between 57 and 72 wt. % SiO_2. East of this same line, there are only 3 compositions from the NWBR that fall between 55 and 70 wt. % SiO_2. Surface exposures of intermediate lavas are nearly nonexistent in the western

HLP, but are prevalent in the NWBR. Conversely, intermediate lavas are nearly nonexistent in the eastern NWBR but become more common in the HLP.

Basalts and Basaltic Andesites - Comparing the HLP and NWBR:

Many authors have noted the uniformity in major and trace element composition for HAOT magmas across a broad swath of the western United States (Hart et al., 1984; Hart, 1985; Hart et al., 1997), including grouping all the HAOT lavas of Oregon, whether in the HLP or NWBR, as one geochemical province. Previous workers did not investigate compositional differences when samples were split into physiographic sub-sets. Overall, the compositional variability among the mafic rocks is less than among the rhyolites, but there are subtle differences between the HLP and NWBR, as well as spatial (east-west) differences.

Basalts and basaltic andesites of the HLP commonly have higher TiO_2 and P_2O_5 than those from the NWBR at comparable SiO_2 (Figure 8). The HLP basaltic andesites also tend to have lower Al_2O_3 and Na_2O, grading into the separation seen in the intermediate compositions (Figure 8). HLP basalts extend to higher concentrations in Rb, Ba, Zr, Nb, U, Th, Hf, and Ta Figure 11). Most HLP basalts are lower in Sr (Figure 11) and many samples extend to lower concentrations (at given SiO_2) for V, and Cu. Although the basalts from the two provinces are very similar in REE concentrations, the basaltic andesites from the HLP are slightly more enriched (Figure 10).

The basaltic andesite of Paiute Butte (formerly Squaw Butte) in the HLP is a special case, and it is often distinct from other basaltic andesites, with high FeO* and MnO (double other concentrations) and low MgO and CaO. It is also very high in Zr, Nb, Y, Zn, Ga, Ta and Hf, slightly higher in Rb, Ba, Pb, Sc, Th, slightly lower in Sr, Cu, Cr and very low in V as compared to other basalts in this study (Figure 9, Figure 11). MacLean (1994) attributes this unusual composition to a series of magma recharge and crystallization events which can strongly enrich incompatible elements while only moderately depleting compatible elements. Like the intermediates, the basalts and basaltic andesites of the DBEC are enriched in many constituents but are depleted in Al_2O_3 as compared to most other HLP samples.

When the HLP and NWBR mafic rocks are viewed separately, we discern some changes in composition from east to west in the HLP. For example, the Zr/Nb ratio (Figure 14) generally increases from 3-15 in the east to 10-25 in the west for HLP samples while in the NWBR, values are widely scattered and especially high in the Coleman Hills region (Scarberry, 2007). Likewise, Ba/Nb ratios rarely exceed 50 in the eastern HLP samples while samples to the west range from 10 to 100, with many samples above 50 (Figure 14). In many cases, the compositional range of NWBR basalts is more widely scattered than that of HLP basalts.

There is a westward decrease in $^{87}Sr/^{86}Sr$ among HAOT, dropping below 0.704 for primitive basalts around 119.5º in the HLP (Oregon Plateau of Hart, 1985, Leeman, 1982b), coinciding with the increasing Zr/Nb ratio. Jordan (2001) remarks on the isotopic shift and also points out that nepheline normative basalts are restricted to the eastern HLP and that there is a slight silica enrichment from east to west resulting in a greater percentage of basaltic andesites in the western half of the HLP and NWBR (Jordan, 2001). This latter observation is in contrast to Draper (1991) who argues for a slight increase in MgO among HAOT basalts from the central to western HLP. While we have not found an increase in MgO to the west, neither can the decrease in basaltic andesite be substantiated, as the eastern HLP centers Stockade Butte and the DBEC, contain substantial numbers of basalts and basaltic andesites.

Compositional Review:

The vast majority of the over 600 compositions discussed in this work form identifiable chemical trends for the HLP and NWBR. The variability among rhyolites is not reflected in a comparable variability among basalts. While there are subtle shifts in the basalt compositions, these do not correspond in a direct fashion to the geochemical trends seen in the rhyolites. A few silicic centers have compositional attributes that fall outside the regional trends including Hagar Mountain (NWBR, 3 samples), which is more similar to HLP compositions. The Lakeview Uranium Area (NWBR, 8 samples) and to a lesser degree Glass Buttes (HLP) (Figure 4d) have U and Th concentrations higher than elsewhere and both likely have hydrothermal alteration histories. Pervasive alteration of

Glass Buttes has also slightly altered the major element composition but most trace elements do not appear to be affected. Finally, a few samples from Juniper Ridge (HLP, 4 samples) have previously been described as mixtures of two "common" end-member compositions and approximately 4 other samples from the HLP show similar compositional trends.

Rhyolites of the HLP are typically higher in SiO_2 and TiO_2 and, at any given silica, are higher in FeO*, when compared to NWBR rhyolites. They are also elevated in HFSE and REE and K_2O (at high silica) but lower in Pb and Sr with greater Eu anomalies and lower Al_2O_3 (at high silica). Peralkaline rhyolites are generally restricted to the HLP and accentuate the above features, showing an especially strong Fe enrichment. Basalt through rhyolite samples from the extreme eastern HLP, including DBEC indicate that there might be slight, but fundamental differences with respect to longitude.

DISCUSSION:

In the following section we examine the spatial-temporal patterns of the age progressive volcanism, compare the timing of basalt and rhyolitic emplacement and investigate some of the tectonic implications for these patterns and relationships. Next, we compare geochemistry between the HLP, NWBR and other volcanic suites and imply generic petrologic models based on these comparisons. We then investigate, in more detail, individual centers and how they change over time and relate the tectonic history to the geochemical data.

Age Progressive Volcanism:

Our data allow us to refine the isochrons representing westward migration of rhyolites across the HLP established by MacLeod et al. (1976) and modified by Jordan et al. (2004) and include the NWBR. We have applied an inverse distance (squared) weighted stretched color ramp (IDW interpolation: Shepard, 1968; Naoum and Tsanis, 2004) to the age data, rather than fitting specific isochrons through the data. The resultant color-coded map (Figure 15) with interpolated ages largely conforms the earlier work within the HLP (MacLeod et al., 1976; Jordan et al., 2004) and shows that the west-

northwest younging pattern applies to silicic rocks as far south as the California border. From this, we draw the important conclusion that the HLP and NWBR constitute a single, basalt - rhyolite bimodal, age-progressive volcanic province that has been active over the past 12 m.y.

In addition, although the isochrons of Jordan et al. (2004) display the westward sweep of silicic volcanism, each isochron also represents only the *onset* of silicic volcanism (no older ages on the younger side of the isochron) and includes a hypothetical 2 million year lifespan for each volcanic system. This leads to some young ages, such as the 5.77 Ma Spodue Mountain (Table 2; previously determined K-Ar age, 5.5 Ma) lying on an older isochron, 7 Ma in this case (cf. Figure 3 and Figure 8 of Jordan et al., 2004). Our graduated interpolation has the advantage of not forcing a particular isochron through the data, therefore reducing the number of apparent misfits, and shows the age progression as a more systematic sweep than as depicted by the isochrons. It should be noted that one limitation of the IDW interpolation is the radial symmetry (Watson and Philip, 1985) or "halo" effect created by some isolated data points (e.g. the 9.5 Ma K-Ar age in the eastern HLP). However, despite the proclivity for the IDW interpolation to form radial patterns, highlighting anomalous ages, there are enough consistent data within the HLP – NWBR system to discern a broadly linear WNW volcanic transgression.

Excluded from this analysis are two older episodes of silicic volcanism that crop out in the area, 1) the 38.5-20 Ma, region-wide events of subduction-related calc-alkaline John Day volcanism (Robinson et al., 1990) and 2) volcanism coeval with the Steens Basalts emplacement, generally 17-14 Ma. Exposures of John Day-aged volcanism crop out at the margins of the HLP volcanism or in scarps created by Basin and Range faults within the NWBR (cf. Iademarco, 2009; Scarberry et al., 2010). A few paleotopographic highs of Steens-age felsic volcanic rocks manifest as kipukas in both the HLP (e.g. Horsehead and Little Juniper Mountain, both at 15.64 ± 0.08; Jordan et al., 2004) and in the NWBR (e.g. Bald Butte at 17.53 ± 0.08 Ma and Drum Hill at 17.30 ± 0.09 Ma).

Only two of the < 12 Ma rhyolites do not conform to the westward age sweep. One is Iron Mountain, which has an age of 2.89 ± 0.16 Ma, but lies in an area of rhyolitic

volcanism that is about 7 Ma (Jordan et al., 2004) (Figure 15). We interpret this center to be part of the HLP, but it is clearly a post-age-progressive rhyolite and may be associated with young basaltic activity that extends along the length of the HLP. Iron Mountain is analogous to post rhyolite-sweep centers in the eastern SRP that are associated with younger basaltic volcanism (e.g. Big Southern Butte, Cedar Butte, East Butte; McCurry et al., 2008). In contrast, there are no centers in the NWBR younger than the age progression.

The second center that does not conform to the westward age sweep is the 6.25 ± 0.03 Ma rhyolite at Pine Mountain, which crops out in an area where the age trend would indicate rhyolitic volcanism that is less than 1 Ma (Figure 4c). This is similar in age to Cline and Steelhead Falls Buttes of the Deschutes Formation, which are related to Cascade volcanism (Sherrod, et al., 2004) and we believe this to be the southeastern-most exposure of this formation, although further study is needed. Neither of these two centers is included in the determination of the color ramp for Figure 15.

While the combined HLP and NWBR show a 12 - 0 Ma sweep of volcanism across Oregon, eruption rates vary across the province. Voluminous tuffs (RST, PCT and DCT) erupted only from the HLP and only between 10 – 7 Ma, accounting for well over half of the total volume of silicic volcanics. A further difference between the two sub-provinces is that the HLP yields samples from over the entire 12 - 0 Ma time span whereas the NWBR does not contain rhyolites younger than about 5 Ma. Finally, the age color ramp map (Figure 15) reveals gaps in the rhyolite ages, or at least gaps in rhyolite exposures, within the HLP including the intervals from 9.6 – 8.4 Ma, 8.2 – 7.3 Ma and 5.8 - 4.34 Ma while the NWBR shows no gaps in activity greater than 0.75 m.y., despite having substantially fewer dated samples than the HLP. These gaps may be due to lulls in rhyolitic activity or may indicate subsidence of existing domes into the subsurface and/or younger cover, including basaltic flows, but are not due to under-sampling. Each of these possibilities is discussed below.

Basalt - Rhyolite Connection and Timing of Volcanism:

Regardless of the particular tectono-magmatic mechanism responsible for the formation of the HLP and NWBR rhyolites, a flux of basalt is required as either a thermal or material source for rhyolitic magma production (e.g. Hildreth, 1981; Huppert and Sparks, 1988; Nekvasil et al., 2000). Unlike the rhyolites, however, the coeval basalts of the HLP-NWBR do not show a comparable age sweep and instead occur in episodes. Here we examine the link between the timing of basaltic pulses and rhyolite production, primarily in the HLP. In some cases, basaltic magmas may be stalled in the crust (intraplated) if regional tectonics or crustal lithology (density) are not conducive to eruption, similar to the conditions inferred for some basalts of the SRP (McCurry and Rodgers, 2009). In other cases, the related basalts may simply be covered by younger volcanic rocks or, in the case of the Harney Basin, located only in the subsurface due to basin subsidence.

Basaltic magmas erupted widely across much of the HLP from 7.8 – 7.5 Ma (Jordan et al., 2004). This pulse is shortly followed by voluminous rhyolite volcanism within the HLP from 7.3 – 6.9 Ma, including many domes and the 280 km^3 RST at 7.1 Ma (Streck and Grunder, 1995; Jordan et al., 2004), representing approximately a quarter of the total volume of silicic magmatism (Figure 4d, Figure 15). There are a few centers within the NWBR, west of Lakeview, that also fall within this age range (Figure 15). This episode of rhyolitic volcanism slightly postdates the time of significantly elevated basaltic volcanism by 0.3 to 0.8 m.y. In part, the basaltic flows and voluminous RST may well have covered coeval rhyolites or there may be a thermal lag between basalt and rhyolite activity (Jackson et al., 2003). The spatial relationships of basalts to rhyolite eruption and the delay between the two, however, demonstrates that basalt eruption is not directly coupled to rhyolitic volcanism as the geographic extent of the 7.8 – 7.5 Ma basalts are not accompanied by a similar distribution of rhyolites or, alternatively, the 7.3 – 6.9 Ma flare-up of rhyolitic volcanism is not accompanied by widespread basaltic volcanism. Furthermore, there are limited basalts in the NWBR at this time and less basalt overall, compared to the HLP, outcropping only at Abert Rim (Scarberry et al., 2010) and Burma Rim (Jordan et al., 2002). This indicates a decoupling between the

injection of basalt to drive silicic magmatism and the eruption of the basalt. Additionally, regional tectonic events (e.g. initiation of the High Cascades, a change in Pacific Plate motion) likely triggered deformation and the widespread eruption of basalts that is strongly concentrated in the HLP, as discussed in Jordan et al. (2004). It is unclear if localization of crustal stresses induced pathways for basaltic magmas to reach the surface or if increased melt volumes in the crust reduced rock strength to facilitate faulting (Rosenberg et al., 2007; Trench, 2008). Trench (2008) shows that NWBR extension still has a kinematic link to the BFZ in the HLP.

Another, less pronounced pulse of basaltic volcanism occurred province-wide from 3 – 2 Ma (Jordan et al., 2004). While widespread, extending the length of the HLP, it is unclear if this pulse is represented in the NWBR due to more limited exposure, but if it exists, it is relatively minor. This more recent pulse in basaltic eruptions is also smaller than that at ~ 7.5 Ma, suggesting a general waning of the basaltic flux, but still sufficient to produce rhyolite as indicated by the emplacement of the 2.8 Ma Iron Mountain example. We are not aware of any region tectonic shifts at this time, unlike at ~ 7.5 Ma, but work by Trench (2008) indicates a decoupling of the kinematic link between the HLP and NWBR at ~5.7 Ma, resulting in an independent slip history for the HLP and a reduction in deformation rates. This could be the reason that the 3 – 2 Ma basaltic pulse is relegated to the HLP whereas the ~7.5 Ma pulse covered a greater area. Relative volumes of the 7.8 – 7.5 and 3 – 2 Ma basaltic pulses could not be determined.

Jordan et al. (2004) also postulated a small pulse of basaltic volcanism between 5.9 – 5.3 Ma which is restricted to the western part of the HLP – NWBR border. This increased activity is coeval with or slightly older than nearby rhyolitic volcanism (e.g. Hagar Mountain, North Connelly Hills, Yamsay Mountain; Figure 4d, Table 2). Due to the paucity of basalt ages within the NWBR, it is not clear if mafic volcanism of this age extends throughout the province and relates to the 6 – 5 Ma rhyolitic volcanism in the NWBR but a weak correlation is suggested. It is at this time that Trench (2008) suggests the influence of NWBR extension on the BFZ was greatly reduced or eliminated.

A correlation between basaltic volcanism and the older set of voluminous tuffs (PCT at 8.4 Ma and DCT at 9.63 Ma), which account for approximately a quarter of the

rhyolitic volcanism, is more difficult to establish. Basalts of a broadly similar age are associated with the ~10.5 Ma emplacement of the DBEC (Johnson and Grunder, 2000), while a 10.42 Ma basalt is in the Malheur caves area (Jordan et al., 2004) and the 12 – 9 Ma "Southern Harney Basin Group" (Brown et al., 1980) crops out less than 20 km east or south of the proposed source location of the DCT (Figure 4d). In addition to these basalts, the more widely distributed ~12.5 – 10 Ma Keeney sequence flows crop out less than 45 km east of the source of the DCT (Hooper, et al., 2002; Camp et al., 2003). The only known basalts in the NWBR from this period are also exposed at Abert Rim (8.7 Ma; Scarberry et al., 2010). Other basalts that might have been erupted near the time of the PCT and DCT eruptions are relegated to the subsurface in the Harney Basin, as basalt – sediment interbeds extend to greater than 1000 m depths in many places (Newton et al., 1962; Milliard, 2010). Much of this sediment was deposited after the rapid onset of subsidence in the basin starting at approximately 10 Ma and ending or slowing significantly by the time of the emplacement of the 7.25 Ma Drinkwater basalt (Milliard, 2010). Additionally, the voluminous PCT and DCT and younger flows and sediment may cover many basalt flows that are related to this period. An alternative which can not be disproved with current information is that due to different tectonic stresses at this time, basalts associated with these rhyolites did not erupt to the same degree as younger basalts. It is unclear if basalt "bedrock" encountered in the well logs at depth is the middle Miocene Steens Basalt or a younger, "HLP-aged" flow. Either there are no basaltic flows associated with voluminous rhyolitic eruptions of this time, or they are only sparsely exposed at the surface.

The most recent pulse of HLP-wide basaltic volcanism spans the past 50 ka. While much of this young basaltic volcanism is centered around Newberry Volcano and to the east of Newberry (Potholes, Devils Garden, Four Craters and East Lava Flows) (Jenson, 2006; Jordan et al., 2004), some of this young volcanism extends to the western HLP, including Diamond Craters (Russell and Nicholls, 1986; D. Sherrod, pers. comm., 2009) and Jordan Craters (Otto and Hutchison, 1977; Hart and Mertzman, 1983). Except for Holocene rhyolites at Newberry Volcano (e.g. Big Obsidian Flow), there are no rhyolites associated with this youngest pulse of basaltic activity, either because rhyolites

have not had a sufficient incubation period, the basalt flux is insufficient, or the crust is too refractory to produce rhyolite via partial melting. No such young basalts are present in the NWBR based on flow morphologies and available (sparse) age determinations.

Tectonic Factors in Rhyolite Outcrop Distribution:

There is a paucity of rhyolite domes exposed in some regions (e.g. eastern Harney Basin; western Harney Basin, south of the RST source; south of the proposed Hampton Tuff source at Frederick Butte), and this lack of silicic outcrops can be related to apparent age gaps in volcanic activity (9.6 – 8.4 Ma, 8.2 – 7.3 Ma and 5.8 – 4.34 Ma) in the HLP (Figure 4d, Figure 15). The paucity of rhyolites of 9.6 – 8.4 Ma and 8.2 – 7.3 Ma age we attribute to subsidence of the HLP and cover by younger volcanics and sediments so that rhyolitic activity during this time is now hidden in the subsurface. We suggest that basin subsidence is the primary cause for these "missing" rhyolites. The paucity of rhyolites of 5.8-4.34 Ma age is partly a result of cover by younger volcanics (± limited sediment), especially on the flanks of Newberry Volcano, but may also reflect basin subsidence and/or a tectonic change. Each of these processes is explored in greater detail below.

The Harney Basin is the likely vent area for all three of the large ash flow tuffs (Figure 4d), and thus other smaller rhyolitic centers are also likely preserved at depth but covered by younger basaltic flows and sedimentary cover (e.g. the 2.54 Ma Wrights Point basalt of the western Harney Basin; Jordan, 2001). Volcanic units exposed along the northern margin of the HLP dip to the south, as evidenced by the originally horizontal ash flow beds that now dip into the plain. The dips on these beds increase with increasing age, so that the 9.6 Ma Devine Canyon Tuff has a dip of 6º, the 8.4 Ma Prater Creek Tuff dips at 3º and the 7.1 Ma RST dips less than ~ 1º (Milliard, 2010). These dips were not caused by any uplift in the adjacent Blue Mountain province within the past 10 Ma as that region had transitioned from a compressional to an extensional tectonic environment starting in the middle Miocene (Walker and Robinson, 1990). Broad, gentle folds located along the southern margin of the Harney Basin in RST-age volcanics and in-filled with 6.1 Ma (K-Ar) basaltic flows plunge toward the center of the basin (Brown et al., 1980). Additionally, to the southwest of the Harney Basin, there is a 5º angular discordance

between a ~7.7 Ma basalt and the 7.1 Ma RST, which has a 5º dip to the northeast (towards the basin) which Scarberry et al. (2010) attribute this to active faulting in the area.

These observations might indicate that the region has experienced downward crustal flexure or sag in a manner similar to that of the SRP (McQuarrie and Rodgers, 1998), with crustal loading due to mass transfer from the mantle to the crust via intraplated basaltic magmas, diking and volcanism, with additional mass added by basin sedimentation. Even such shallow dips could easily be an indication of multiple kilometers of crustal downwarping on the scale of the study area. Well logs from the eastern part of the Harney Basin indicate 0.75 to more than 1.5 km of sediment (Milliard, 2010) while recent geophysical studies (Cox, 2011) indicate volcanics and sediments may extend to as deep as 7 km in the Harney Basin. The timing of this subsidence coincides with rhyolitic eruptions, with subsidence waning after the focus of silicic volcanism moved westward. This would explain the general lack of domes in the Harney Basin and along the border of the HLP and NWBR between 119º and 120º longitude (Figure 4d), as any domes and older basalt flows would have subsided to maintain isostatic equilibrium and currently exist in the subsurface, covered by subsequent basalt flows and sediment. The only exposed rhyolite dome complex constructed during between 8.2 – 7.3 Ma contains the 7.68 Ma Burns Butte, located on the northern margin of the HLP, outside of the Harney Basin, where little effect from the subsidence would be manifested. While the regionally extensive RST might obscure older, localized basalt flows, it likely hides few if any coeval rhyolite domes as it generally less than 30 m thick (Streck and Grunder, 1995).

The lack of exposed silicic volcanism from 5.8 - 4.34 Ma in the HLP might also be a result of basin subsidence, although there is less evidence for this than in the case of the Harney Basin. A 7.8 Ma basalt from Hampton Butte (Figure 4a), just north of this rhyolite gap, dips south into the HLP by 5º (Iademarco, 2009). Also, the Frederick Butte-sourced ~ 3.8 Ma Hampton Tuff outcrops from this same area dip from 4º – 6º into the plain (Iademarco, 2009), indicating that there could have been subsidence in this area since ~4 Ma. The area also has widespread 2 - 1 Ma age basalts. But, unlike the Harney

Basin, there are no structural indications from other areas indicating a down flexure, no deep well logs or geophysical data to indicate sediment fill on the scale of the Harney Basin, and the area lacks the voluminous rhyolites, which would require substantial additions of basalt, a catalyst of such basin formation. Given the amount of mass addition to the mid-crust required to produce flexure of the SRP (McQuarrie and Rodgers, 1998), we consider it unlikely that the relatively small amounts of mass added to the crust in this area could cause downwarping. Alternatively, recent geophysical studies (Cox, 2011) indicate a 2 – 3 km thick higher density region (SD2) in the uppermost crust in this region, and this shallow dense layer might have a greater effect on surface downwarping than deeper dense layers.

The lack of exposed silicic volcanism in the area south of Frederick Butte, ranging between ~120.3º and 121º longitude may have a cause other than crustal flexure. The volume of rhyolite greatly diminishes after the eruption of the 5.79 Ma Glass Butte in the HLP, and is further constrained to a narrow band of small volume domes on the eastern flank of the Newberry shield less than 3.7 Ma. Rhyolitic volcanism in the NWBR completely ceases by ~5 Ma. Extension via Basin and Range faults has propagated in episodic steps westward (and northward) across the NWBR over at least the past 10 Ma, most recently transferring strain to the High Cascades graben by ~ 5 Ma (Scarberry, et al., 2010). While the Cascades graben may have started to form in southern Oregon between 8 – 7 Ma, the onset of extensional activity is well constrained in central Oregon at 5.4 Ma, leading some workers to conclude that the intra-arc extension (rift) is propagating northward (Smith et al., 1987; Conrey et al., 1997). This westward propagation into the Cascades corresponds with an increase in volcanic activity within the arc in central Oregon at about the same time, just prior to 4.5 Ma (Hughes and Taylor, 1986). This model is consistent with the margin-ward migration of basalt or bimodal basalt - rhyolite volcanism throughout the entire Basin and Range province (e.g. Coso Volcanic Field; Snake River Plain) and the general westward sweep of rhyolitic volcanism in the northern Basin and Range from 12 – 5 Ma (Finton et al. 1991; Luedke and Smith, 1984). This transfer and reorganization of crustal stresses to the axis of the active arc may have greatly reduced either the formation of rhyolitic magmas or their

ability to reach the surface in the HLP and NWBR. Also, Pliocene and younger basalt coverage is more extensive in this area than in other parts of the HLP, especially as one approaches the Newberry shield, and this may have covered some small volume domes. Basin subsidence does not appear to be a primary factor obscuring rhyolite exposures in the western HLP, which would be consistent with a decrease in crustal loading and intraplated basaltic magmas.

Geochemical Comparisons:

HLP and NWBR Compared to Other Provinces; Intermediates and Rhyolites:

The following section compares and contrasts compositions from the HLP and NWBR to the Cascades, a nearby calk-alkaline province, the adjacent bimodal tholeiitic Snake River Plain (SRP) province (Figure 2) and Iceland, an archetypal bimodal tholeiitic province. As one might suspect, there is often separation between the tholeiitic suites and the calc-alkaline suite in major element space, and this separation is especially pronounced in the intermediate compositions. At the higher silica compositions (rhyolites), the separation of the tholeiitic and calc-alkaline suites gets more difficult to discern due to the closed geochemical array, resulting in overlapping data sets.

One example, given earlier, where there is separation between the HLP and NWBR datasets is FeO* vs. SiO_2 (Figure 8) and this is clearly demonstrated in plots comparing tholeiitic to calc-alkaline provinces (Figure 12, inset). We term the line that separates these two data sets the Fe-line, (equation $y = -0.3523x + 27.83$ and end points at (57, 7.75) and (79, 0)) (Figure 12). A similar strong separation is noted for Al_2O_3 vs. SiO_2 with the calc-alkaline suite typically yielding higher values (at given silica) than the tholeiitic (not shown), and the NWBR likewise generally plots at higher Al_2O_3 than the HLP (Figure 8).

The separation into more tholeiitic character of the HLP and the more calk-alkaline character of the NWBR does not derive from high CaO in the latter (Figure 8, Figure 16). While there is appreciable overlap, especially at high silica, at intermediate compositions the HLP generally has higher CaO (at given SiO_2) than the NWBR. Some

of the other tholeiitic suites also have higher CaO than the calc-alkaline Cascades (Figure 16, inset). The SRP intermediate to silicic volcanic rocks have a range in CaO that is similar to the overall HLP – NWBR dataset. A subset of the SRP samples that have some of the highest CaO at a given SiO_2 comes from Unnamed Butte, a Quaternary dome that yields intermediate compositions that are clearly mixes of mafic and silicic end-members and often show very different variation diagram trends than the liquid line of decent, fractionated Quaternary lavas of the Craters of the Moon (COM) - Cedar Butte trend of the SPR (McCurry et al., 2008). The Iceland dataset is bifurcated and a set of dacitic to rhyolitic compositions from Iceland contain higher CaO than samples of similar SiO_2 from the Cascades (Figure 16). This set includes samples from Krafla (Jonasson, 1994), Askja (Sigurdsson and Sparks, 1981), Hekla (Sverrisdottir, 2007), and a few others. Nearly all of these workers report magma mixing or hybridization and/or disequilibrium phenocryst assemblages. This set of high-CaO dacites and rhyolites from the Iceland data set closely matches the concentrations observed from the HLP whereas the NWBR compositions are more similar to the Cascades dataset. A similar phenomenon occurs with MgO vs. SiO_2 and TiO_2 vs. SiO_2 (not shown) with higher values for intermediate composition from the HLP, mixed Quaternary SRP and the subset of Icelandic samples mentioned above, although there is significantly less distinction at the high silica end. The other major elements don't clearly break into two discernable groups for either the tholeiitic – calc-alkaline plots or the HLP – NWBR plots (see Figure 8 and discussion above).

Volcanic rocks from the HLP – NWBR also show evidence of a subduction component, something not seen in the Iceland or the SRP suite. Depletion of HFSE and enrichment in large ion lithophile elements (LILE) are the quintessential tracers for the presence of subducted slab fluids, and thus a signature that occurs in many calc-alkaline suites (Pearce, 1982). Accordingly, in the comparison suites used here, the Cascades suite exhibits elevated and variable Ba/Nb ratios over a range of silica content whereas Iceland remains low and constant (Figure 17). A subduction component is also present in both the HLP and NWBR mafic compositions, as evidenced by the enrichment of fluid mobile elements like Rb, Ba, K, Pb and Sr and relative depletion of the HFSE, especially

Nb and Ta, with resultant high (> 20) Ba/Nb or Ba/(17.6*Ta) ratios (Figure 11, Figure 17, and Carlson et al., 2009). The NWBR has similar normalized LILE and lower HFSE than the HLP basalts and they form the upper margin of the data over a range of silica in Ba/Nb (Figure 11, Figure 17), at least until a strong Ba-fractionating phase begins to dominate the ratio, generally above ~ 74 wt. % SiO_2. This Ba-removing phase is likely alkali feldspar, which has K_d values approaching 20 in the RST high silica rhyolite tuff of the HLP (Streck and Grunder, 1997). Such a fractionation, where Ba/Nb values drop by a factor of 5 to 50, as compared to mafic and intermediate rocks, is not seen in either the Cascades or Iceland, whereas such precipitous drops are common in the SRP silicic ash flow tuffs (not shown) and are ubiquitous in the evolved Quaternary fractionates (COM – Cedar Butte trend).

Comparison of Basalts, the Drivers of Volcanism:

Basalts of the HLP – NWBR have been classified as high-alumina olivine tholeiites (HAOT: Hart et. al., 1984) and are similar to mid-ocean ridge olivine tholeiites and back-arc basin basalts in major element composition; that is they are characterized by high Mg/Fe, high Al_2O_3 and low K_2O. They differ in trace elements, being lower in Nb, Ta and other high-field-strength elements and enriched in Ba, Sr and Pb. As HLP - NWBR basalts become more silica rich, there is wider geochemical variation and an increasing number of samples are classified as calc-alkaline (Figure 18; cf. Jordan, 2001). Slight perturbations in the primary tholeiitic parental magmas are most likely due primarily to small differences in mantle source peridotite composition and conditions of melting, while the overlap between the two provinces and production of evolved basalts (Figure 18) is explained by magma evolution, including fractional crystallization for samples > 7 wt. % MgO and assimilation – fractional crystallization (AFC) processes for those < 7 wt. % MgO (Jordan, 2001, Draper, 1991). The assimilant used in modeling by Jordan (2001) is an average low silica rhyolite from the age-progressive set.

HAOT basalts or low-potassium (K) tholeiites (LKTs) are widespread across the northwestern United States, and are found in broadly coeval neighboring volcanic provinces including the Owyhee area and the northwestern Basin and Range of California

and Nevada (Hart et al., 1984), in the Cascades Arc (Conrey et al., 1997; Bacon et al., 1997; Schmidt et al., 2008), and as dikes within the Picture Gorge member of the Columbia River Basalt in central Oregon (Bailey and Conrey, 1992). Thus, much of the volcanism in Oregon and adjacent areas has been driven by a common, generally uniform mafic input (HAOT) over the past 16 Ma. The widespread olivine tholeiites of the SRP (SROT) are similar to the HAOT in bulk chemistry (Leeman, 1982a; Hughes et al., 2002). SROT likely have a different mantle parent as inferred from isotope geochemistry (Graham et al., 2009) and some trace elements (LREE, HFSE, U, Th) for the most primitive basalts are enriched over those of HLP primitive basalts. Thus, mantle conditions under the accreted terranes of Oregon and Washington are likely similar, producing HAOT basaltic magmas and these conditions control melting from different mantle sources under the craton of Idaho (Carlson and Hart, 1987).

Mafic samples from the two comparison suites show considerable overlap in Harker diagrams due to magma evolution. In the tholeiitic suite (SRP, Iceland), this is caused largely by fractional crystallization which creates a broad range of many major elements over a relatively small change in silica and in the Cascades, due to the multitude of primitive magmas (CAB, OIB, LKT, etc.) coupled with AFC processes (Conrey et al., 1997). Additionally, over the time and length scales considered here, along the Cascades Arc or across Iceland, mantle source heterogeneity also results in a range of parental mafic compositions (cf. Schmidt et al., 2008; review by Sigmarsson and Steinthorsson, 2007 and source therein).

From the spider diagrams for mafic through intermediate samples (Figure 11) and from the Harker diagrams and Ba/Nb plots (Figure 9, Figure 17), it is clear that subduction fluids have enriched the LILE, including the Ba and Sr, concentrations in basaltic samples. In the NWBR, Sr continues to increase through basaltic andesite before decreasing in andesites and more silica rich compositions whereas HLP samples peak at the basalt – basaltic-andesite boundary before declining. As with the dacites and low silica rhyolites, the HLP basalts to basaltic andesites more closely mimic Iceland compositions whereas the NWBR rocks are more similar to the Cascades. However, the Cascades data are more variable, perhaps due to the larger number of analyses, the large

number of parental basaltic compositions (Conrey et al., 1997) or the suppression of plagioclase fractionation in wet systems (e.g. Sisson and Grove, 1993). While parental basaltic compositions are similar and cover a wide range in these systems, most of the high silica rhyolites are indistinguishable from each other, with only the intermediate to low silica rhyolites breaking out into separate compositional groups. Thus, extensive fractionation and/or crustal processing can completely obscure the true parentage of the high silica rhyolites.

Petrologic Implications for the HLP – NWBR Province:

The analogs discussed (see Appendix 5 on petrogenetic summaries of Iceland, SRP and Cascades) and used in this geochemical comparison yield four different petrogenetic models to explain rhyolite formation and differences among sub-provinces. These models propose that the rhyolites of the HLP and NWBR are: 1) principally partial melts of recent, mantle-derived basaltic magmas – as per the SRP ignimbrites (e.g. Christiansen and McCurry, 2008; Leeman et al., 2008) and genetically related to the basaltic pulse of volcanism, 2) partial melts of primarily mafic crust by younger, intraplating basaltic magmas – as per much of Iceland (e.g. Jonasson, 1994; Jonasson, 2007; Lacasse et al., 2007; Martin and Sigmarsson, 2007) except that in this case, this mafic crust is composed of accreted terranes re-melted by more recent basalt injection, 3) extreme fractionates of mantle-derived basaltic magmas – as per COM-Cedar Butte trend and other isolated anorogenic high silica rhyolites (McCurry et al., 2008), and 4) the results of complex multi-stage recharge, crustal assimilation and fractional crystallization (RAFC) processes to derive intermediate magmas which then evolve to silicic melts – as per the Cascades Arc (e.g. Hildreth and Moorbath, 1988; Bohrson and Spera, 2001; Spera and Bohrson, 2001). We apply additional geochemical constraints to generate a generic petrologic model for the HLP and NWBR.

Intermediate Composition: HLP Are Mixed Magmas; NWBR Are Not:

Some of the intermediate composition magmas from the HLP have previously been described as mixtures of mafic and silicic end-members, including some

intermediate samples from the DBEC (Johnson and Grunder, 2000) and mixed dacite pumices from the RST (Streck, 2002). We note that eight additional samples from the HLP fall along straight lines on trace element diagrams where there is a great change in elemental compatibility through the intermediate rocks such as for Ba, Sr, Zr, Y, Ni and possibly Pb and Cr (Figure 9). These include some Juniper Ridge lavas including three intermediate compositions which show disequilibrium textures and xenocrysts as well as one rhyolite that contains 10 to 15% basaltic xenoliths. These four samples have been modeled by MacLean (1994) to be mixed magmas (intermediate compositions) or mingled magmas. Four other samples, three from the Malheur Caves area, fall along the same composition trajectory, and we consider them to be compositionally mixed or mingled magmas.

We believe these HLP intermediate magmas to be petrologically similar to the high CaO intermediate magmas from the SRP and Iceland. For the high CaO subset of Iceland samples (Figure 16), many of the intermediate composition rocks (andesites to dacites) contain disequilibrium phenocrysts textures, with some workers calling on magma mingling or mixing of more silicic and mafic end-members for their formation (e.g. Askja: Sigurdsson and Sparks, 1981, Krafla volcano: Jonasson, 1994; Katla: Lacasse et al., 2007) while others invoke magma hybridization of two parental end-member compositions (e.g. Hekla: Sigmarsson et al., 1992; Schuessler, et al., 2009). Partial melting of crustal rocks or extensive fractional crystallization of basalt (RAFC models) are generally discounted as a mechanism to form the intermediate rocks in these systems.

The high CaO at a given SiO_2 intermediate composition samples of Unnamed Butte from the SRP show markedly different variation diagram trends than well characterized liquid line of decent, fractionated Quaternary lavas from elsewhere on the SRP. McCurry et al. (2008) believe these to be mixes of mafic and silicic end-members. Thus, we infer that similar to Iceland and Unnamed Butte of the SRP, most, if not all of the intermediate HLP lavas are a result of mixing of a bimodal assemblage of basalt or basaltic andesite and low to high silica rhyolite.

In the NWBR, many of the intermediate samples have the highest values for some analytes, precluding magma mixing to obtain most of these compositions. The highest Sr values occur for samples ranging from ~53 to ~63 wt. % SiO_2 and the highest Na_2O values are in samples from 60 to ~70 wt. % SiO_2 (Figure 8, Figure 9). This mimics the results from the Cascade dataset, except that Na_2O decreases in NWBR samples but remains nearly constant in Cascade samples above 70 wt. % SiO_2. FeO and CaO (Figure 12, Figure 16) for the NWBR also are more similar to the Cascades than they are for the tholeiitic suites. Additionally, phenocrysts of plagioclase from the NWBR intermediate to low SiO_2 rhyolite samples are commonly resorbed, sieve-textured and inclusion rich (this work; Wells, 1979; Hering, 1981), as is typical of feldspars from the Cascades (e.g. Bacon and Druitt, 1988, many others). We infer that intermediate through rhyolitic compositions of most samples from the NWBR are likely the result of crustal assimilation, likely of amphibolitic crust, and fractional crystallization (AFC) processes, in a manner that is similar to the Cascades.

Low SiO_2 Rhyolitic Composition - HLP Are Partial Melts; NWBR Are AFC:

In a similar manner to intermediate compositions above, we compare the HLP – NWBR system to others. The Sr/Y ratio is used to show the relative importance of plagioclase versus amphibole, either as a fractionating phase or as a component of the partially melting crustal rock. The major control on Sr concentration at all silica levels is plagioclase, except at high silica (> ~74 wt. %) where potassium feldspar also has a strong effect (Ren, 2004). Similarly, Y tracks the involvement of amphibole, although pyroxene also has K_d values greater than 1 as compositions become dacitic (Ewart and Griffin, 1994). For most samples from 50 - ~72 wt. % SiO_2, Sr/Y is greater for the NWBR than for the HLP (Figure 19).

Examining Y and Sr/Y systematics from Iceland and the Cascades is illustrative (Figure 19). Yttrium in Icelandic samples, taken in a broad sense, show a 3 to 6 fold increase as SiO_2 increases from basalts to rhyolites. This indicates that while fractional crystallization of non-Y compatible minerals cannot be ruled out, partial melting of amphibolite is strong possibility. This is especially true when one considers that high

silica compositions that are similar to Icelandic samples have been generated experimentally by small degrees of partial melts of amphibolites, and that generally, even these small degree partial melts completely, and incongruently, melt the amphibole phase (Beard and Lofgren, 1991; Sisson, et al., 2005), thus releasing Y into the melt. Cascades samples, on the other hand, show steady or declining Y with increases in SiO_2, thus indicating that amphibolitic crust is only a minor component in the generation of evolved melts (e.g. Conrey et al., 2001; Schmidt and Grunder, 2011; many others) and that Y is removed as suites evolve via fractional crystallization. Thus, in Icelandic suites (again, a broad generalization), Sr/Y values decrease as Sr decreases, if plagioclase is fractionating, or remains generally constant as Y increases, due to complete dissolution of amphibole in a partial melt of an amphibolite, or at least no fractional crystallization of amphiboles in this dry system. In Cascades suites, Sr increases due to the suppression of plagioclase fractionation (Sisson and Grove, 1993) while Y decreases due to amphibole crystallization or remains relatively constant due to the interplay of amphibolite partial melt followed by amphibole fractionation in some systems (Figure 19).

To a large degree, the HLP more closely mimics the Icelandic suites, except that Y increases are not as pronounced, whereas the NWBR more closely mimics the Cascades suite (Figure 19). Strong Y enrichments above about 73 wt. % SiO_2 in the HLP are likely due to fractional crystallization, and at least part of the enrichment trend in higher silica Iceland samples is as well. Few samples from the SRP contain Y data and the paucity of intermediate samples associated with the voluminous ignimbrite erupts precludes information on system evolution using solely Sr compositions. The Sr pattern of the A-type rhyolites of the SRP (COM – Cedar Butte trend) strongly suggests feldspar fractionation (McCurry et al., 2008).

Fractional crystallization of basalts to form rhyolites is precluded for the HLP. If Rb is modeled as completely incompatible, parental basalt at 5 ppm Rb require 95% fractional crystallization to produce a low silica rhyolite (70 wt. %) with 100 ppm Rb. This percentage is similar to what is calculated for both the Cedar Butte trend (McCurry et al., 2008) and in crystal fractionation experiments (Whitaker, et al., 2008) on similar basalts from the SRP. Plagioclase remains on the liquidus over this extreme

fractionation, resulting in large bulk distribution coefficients, strongly depleting Sr. This is observed in the above systems and in the Blackfoot Volcanic Field (Ford, 2005), and results in Rb/Sr ratios of 5 – 10 for low silica rhyolites and 100 or more in high silica rhyolites. In the HLP, there is only a modest difference in the Sr concentration from basalt to rhyolite (up to a three-fold reduction) and the resultant Rb/Sr ratios range from ~0.3 to 2 in low silica rhyolites.

Many low silica rhyolites do evolve to high silica rhyolites through fractional crystallization (e.g. Streck and Grunder, 2008). Rb contents in high silica rhyolites do not increase much over those for low silica rhyolites, indicating that trace phases or perhaps alkali feldspar crystallization help buff the melt (Ewart and Griffin, 1994; Ren, 2004). With the continued crystallization of plagioclase, and onset of alkali feldspar crystallization in some systems, Sr content drops markedly as silica increases from 70 – 77 wt. % (Figure 9), resulting in Rb/Sr ratios approaching 10. Some peralkaline compositions show extreme depletions in Sr due to very high distribution coefficients for the feldspars (cf. Streck and Grunder, 1997).

Glass Buttes and Juniper Ridge Systems – a Microcosm of Crustal Change:

Two areas where we have protracted volcanism within the HLP are Glass Buttes and Juniper Ridge (Figure 4d). New and previous ^{40}Ar-^{39}Ar ages (Table 2; Jordan et al., 2004) and field relationships indicate that rhyolite volcanism occurred over approximately 0.7 m.y. at Glass Buttes and 1.2 m.y. at Juniper Ridge, younging to the WNW in a trend similar to that of the BFZ (Figure 3). In each case, and at nearly the same rate, rhyolites evolve to higher FeO* at a given silica content over time (Figure 20). Intraplated basaltic magmas drive this silicic system and over time, an increased heat flux caused by these intraplated basalts creates a feedback in the crust that yields both a more mafic crust and higher FeO* crustal melts from a “drier” source (cf. Beard and Lofgren, 1991; Sisson, et al., 2005). We use the term “basaltification” of the crust for this change where both basaltic magmas are added to the crust and less refractory components are preferentially removed early in the cycle, resulting in a more dense, more refractory crustal block.

We argue that more basaltification occurred in the crust in the vicinity of Juniper Ridge as compared to Glass Buttes. The suite at Juniper Ridge starts at a higher FeO* content as compared to the Glass Buttes suite, likely because it is closer in time and space to the voluminous RST source. This ignimbrite required a substantial volume of mafic magma, added over time in multiple cycles to both provide the heat to drive the partial melt system and to create the geochemical signature of basaltic andesite inclusions in the RST (Streck and Grunder, 1999).

This basaltification can be applied to the HLP as a whole. When compared to the NWBR, the HLP has a much greater number of high FeO* at a given silica concentration (Figure 12, Figure 21). Similarly to that described above for Juniper Ridge and Glass Buttes, the HLP overall evolves to higher FeO* at given silica from east to west (Figure 21). This is a direct result of mafic volcanism having more time to alter the crust to the west prior to the onset of silicic volcanism. To form low silica rhyolites in the HLP, we see a greater basalt flux, resulting in both a hotter crust and a more mafic crust. This influx of heat results in more partial melt, despite the crust becoming more mafic, and the partial melts are at progressively higher in FeO* at a given SiO_2 composition. The high FeO* rhyolites are also higher in Y (and lower in Sr/Y). This low silica (parental) rhyolite then evolves to high silica rhyolite by fractional crystallization, a process documented in the RST (Streck and Grunder, 2008). Only binary mixes of rhyolite with basaltic andesite (or more rarely basalt) produce intermediate compositions and the province is bimodal. By contrast, most NWBR low silica rhyolites are generally produced by AFC processes, where assimilation of an amphibolitic crust is coupled with fractional crystallization to form a continuum of compositions from basalt to low silica rhyolite.

The one post-progression rhyolite dome (Iron Mountain at 2.89 Ma) also fits the above model. Its presence, coupled with existence of 2-3 Ma basalts in the region (Jordan et al., 2004) suggests that despite strongly waning in the area, rhyolitic volcanism is still possible. In contrast to most other HLP rhyolites, it has low FeO* at a given SiO_2 and also has a low Y content and correspondingly high Sr/Y. This is what would be expected from a partial melt in an area where the basaltic influx has slowed and the mafic

crust has cooled. A smaller degree of partial melt of the mafic crust in this system results in a lower FeO* at a given SiO_2 (cf. Sisson et al., 2005) and the low Y indicates that much of the amphibole had been previously partially melted in the area.

The HLP – NWBR Age Progressive Trend and Asthenopheric Flow:

An unresolved question is what has caused the age progressive volcanism in the HLP and NWBR? Previous authors have suggested a number of models which are briefly described here. Carlson and Hart (1987) suggest the trend results from the clockwise rotation of the Klamath and Cascades terranes (Figure 1) resulting in a wedge-shaped time transgressive pattern to rhyolitic eruptions where the propagation rate would be faster in southern Oregon and slower in central Oregon, along the BFZ. Draper (1991) suggests that a plume head, entrained in the asthenospheric counterflow of the subducting Juan de Fuca plate, spreads out over time, thus younger (5-7 Ma) silicic volcanics have a wider age distribution than the older (7-12 Ma) volcanics. Jordan et al (2004) liken the trend in ages to plume material flow along the slope of a westward thinning lithosphere, creating age-progressive volcanism that wanes to the west as flow "up the lithospheric slope" decreases. Decompression and partial melting due to lithospheric extension (cf. Langmuir et. al., 1992) along the diffuse BFZ is unlikely due to the small rates of extension over the past ~8 Ma, ranging from 0.05% to a maximum of 1% (Trench, 2008).

We propose that the volcanism in the HLP and NWBR can be driven solely by Cascadia slab plate-driven asthenopheric flow. Surface expression of HLP rhyolitic volcanism moves approximately N20ºW at ~33 km/Ma, from 12 Ma until 4 Ma (this work; Jordan et al., 2004) and the North American Plate moves S40ºW at ~26 km/Ma (Gripp and Gordon, 2002). Simple vector addition of North American plate motion and the HLP age-progressive rhyolitic volcanism trend very closely matches the direction of asthenopheric flow, as recently determined by shear wave splitting (SKS phases) delay times (Long, et al., 2009) (Figure 22). These seismic anisotropies can be generated by rollback, steepening and down-dip motion of the Cascadia slab portion of the Juan de Fuca plate (Druken et al., 2011). The calculated asthenopheric flow is ~53 km/Ma, which is fairly rapid when compared to current plate velocities but such a fast rate is

predicted by the magnitude of the s-wave delay times which are some of the largest recorded, indicating very strong anisotropy and alignment in the asthenosphere (Long et al., 2009).

The progressive steepening of the slab from south to north focuses the increased counterflow or upwelling to a more narrow band, which results in the HLP track, although there is still upwelling to a lesser degree in the NWBR. This focused flow results in a greater flux of basaltic magmas, resulting in intraplated basalts and mafic residuum from partial melts (basaltification) of the crust in the HLP and the iron-rich rhyolites resulting from crustal partial melt. If the HLP volcanic trend continued to move at 33 km/Ma, instead of appearing to slow at about 4 Ma, the current location of volcanic activity would be on the apex of the Cascade range, approximately 25 km south of South Sister volcano (Figure 22).

CONCLUSIONS:

In this work, we extend the westward age progression of rhyolites in the HLP to include the NWBR into a single, age-progressive series that extends to nearly the California border. The basalts are not time transgressive and we establish that the timing of basaltic pulses are decoupled from the age-progressive rhyolites. Basin subsidence, in a process similar to that invoked for the SRP (McQuarrie and Rodgers, 1998), and caused by dense intraplated basaltic magmas and residuum from partial melting, has likely buried some silicic centers in the subsurface (such as in the Harney Basin).

We describe three types of rhyolites from the HLP – NWBR. The first is a high FeO*, high silica rhyolite with anhydrous phase assemblage containing hedenbergite ± fayalite which is found only in the HLP and can be peralkaline. A moderately high FeO* rhyolite with augite, commonly paired with orthopyroxene ± a hydrous phase is common in both the HLP and NWBR. More rarely, a lower FeO* rhyolite containing only hydrous phases, hornblende ± biotite is also found in the HLP and NWBR. Rhyolites from the HLP are typically higher in FeO* at any given silica value than those from the NWBR, among other, more subtle geochemical differences. These differences in rhyolite composition are not reflected by similar changes in basalt composition. Comparisons to

SRP, Iceland, and the Cascades indicate that low silica (parental) rhyolites of the HLP are more like crustal partial melts of Iceland and the SRP, with most intermediate composition likely mixtures of basalt to basaltic andesite and low silica rhyolite end member mixtures. The continuum of compositions in the NWBR is more similar to what is observed in the Cascades and is driven by AFC processes.

Greater amounts of basaltic volcanism in the HLP results in both crustal mass addition via intraplated basaltic magmas and an increased heat flow to the crust. This results in progressively greater amounts of partial melt of an ever increasingly mafic crust, a process we term basaltification. These low silica rhyolite partial melts evolve to higher FeO* at any given silica over time, both province wide, and within any polygenetic suite, produce the phenocryst assemblages and add density to the crust to create subsidence. The westward asthenopheric flow required to produce the HLP volcanic trend, given the southwestward North American Plate motion, is nearly identical to seismically imaged flow (via anisotropy) and has been reproduced in laboratory tank models (Long et al., 2009; Druken et al., 2011).

REFERENCES:

Bachmann, O., Miller, C. F. and de Silva, S. L., 2007, The volcanic–plutonic connection as a stage for understanding crustal magmatism: J. of Volcanology and Geothermal Research, v. 167, p. 1-23.

Bachmann, O. and Bergantz, G.W., 2004, On the origin of crystal-poor rhyolites: extracted from batholithic crystal mushes: J of Petrology v. 45, p. 1565–1582.

Bacon, C. R., Bruggman, P. E., Christiansen, R. L., Clynne, M. A., Donnelly-Nolan, J. M., and Hildreth, W., 1997, Primitive magmas at five Cascade volcanic fields; melts from hot, heterogeneous sub-arc mantle: Canadian Mineralogist, v. 35, no. 2, p. 397-423.

Bacon, C. R. and Druitt, T. H., 1988, Compositional evolution of the zoned calcalkaline magma chamber of Mount Mazama, Crater Lake, Oregon: Contributions to Mineralogy and Petrology, v. 98, p. 224-256.

Barnes, C. G., Petersen, S. W., Kistler, R. W., Murray, R., Kays, M. A., 1996, Source and tectonic implications of tonalite-trondhjemite magmatism in the Klamath Mountains: Contributions to Mineralogy and Petrology, v. 123, p. 40-60.

Bailey, D. G. and Conrey, R. M., 1992, Common parent magma for Miocene to Holocene mafic volcanism in the northwestern United States: Geology, v. 20, p. 1131-1134.

Beard, J. S. and Lofgren, G. E., 1991, Dehydration melting and water-saturated melting of basaltic and andesitic greenstones and amphibolites at 1, 3, and 6.9 kb: J. of Petrology, v. 32, p. 365-401.

Beard, J. S., Abitz, R. J. and Lofgren, G. E., 1993, Experimental melting of crustal xenoliths from Kilbourne Hole, New Mexico and implications for the contamination and genesis of magmas: Contributions to Mineralogy and Petrology, v. 115, p. 88-102.

Beard, J. S., Lofgren, G. E., Sinha, A. K. and Tollo, R. P., 1994, Partial melting of apatite-bearing charnockite, granulite, and diorite: melt compositions, restite mineralogy, and petrologic implications: J. of Geophysical Research, v. 99, p. 21591-21603.

Berri, D. A., 1982, Geology and hydrothermal alteration of Glass Buttes, Southeast, Oregon: Portland State University MS Thesis, 125p.

Bohrson,W. A. and Spera, F. J., 2001, Energy-constrained open-system magmatic processes II: Application of energy-constrained assimilation-fractional crystallization (EC-AFC) model to magmatic systems: J. of Petrology, v.42, p. 1019-1041.

Bonnichsen, B., Leeman, W. P., Honjo, N., W. C., McIntosh, and Godchaux, M. M., 2008, Miocene silicic volcanism in southwestern Idaho: geochronology, geochemistry, and evolution of the central Snake River Plain: Bulletin of Volcanology, v. 70, no. 3, p. 315-342.

Bowen, N.L., 1928, The evolution of igneous rocks: Dover, NewYork, 332 p.

Brikowski, T. H., 1983, Geology and petrology of Gearhart Mountain: A study of calc-alkaline volcanism east of the Cascades in Oregon: University of Oregon PhD thesis, 157 p.

Brown, D. E., McLean, G. D. and Black, G. L., 1980, Preliminary geology and geothermal resource potential of the southern Harney Basin, Oregon: Oregon Department of Geology and Mineral Industries Open File Report O-80-07, 90 p.

Camp, V. E., Ross, M. E. and Hanson, W. E., 2003, Genesis of flood basalts and Basin and Range volcanic rocks from Steens Mountain to the Malheur River Gorge, Oregon: Geological Society of America Bulletin, v. 115, p. 105-128.

Carlson, R. W., Hart, W. K. and Grove, T. L., 2009, Cenozoic basaltic volcanism in the Pacific Northwest: Geological Society of America Abstracts with Programs, v. 41, p. 571

Carlson, R. W. and Hart, W. K., 1987, Crustal Genesis on the Oregon Plateau: J. of Geophysical Research, v. 92, p. 6191-6206.

Chappell, B. W. and White, A. J. R., 1974, Two contrasting granite types: Pacific Geology, v. 8, p. 173-174.

Christiansen, E. H. and McCurry, M., 2008, Contrasting origins of Cenozoic silicic volcanic rocks from the western Cordillera of the United States: Bulletin of Volcanology, v. 70, no. 3, p. 251-267.

Conrey,R. M., Hooper, P. R., Larson, P. B., Chesley, J. and Ruiz, J., 2001, Trace element and isotopic evidence for two types of crustal melting beneath a High Cascade volcanic center, Mt. Jefferson, Oregon: Contributions to Mineralogy and Petrology, v. 141, p. 710-732.

Conrey, R. M., Sherrod, D. R., Hooper, P. R. and Swanson, D. A., 1997, Diverse primitive magmas in the Cascade Arc, northern Oregon and southern Washington: Canadian Mineralogist, v. 35, no. 2, p. 367-496.

Cox, C., 2011, A Controlled- Source Seismic and Gravity Study of the High Lava Plains (HLP): University of Oklahoma MS Thesis, 110 p.

DeMets, C., Gordon, R. G., Argus, D. F. and Stein, S., 1994, Effect of recent revisions to the geomagnetic reversal time scale on estimate of current plate motions: Geophysical Research Letters, v. 21, no. 20, p. 2191-2194.

Dicken, S. N., 1950, Oregon Geography: First Preliminary Edition: Ann Arbor, MI, Edwards Brothers, 104 p.

Donnelly-Nolan, J. M., Grove, T. L., Lanphere, M. A., Champion, D. E. and Ramsey, D. W., 2008, Eruptive history and tectonic setting of Medicine Lake Volcano, a large rear-arc volcano in the southern Cascades: J. of Volcanology and Geothermal Research, v. 177, p. 313-328.

Donnelly-Nolan, J. M., Champion, D. E., Miller, C. D., Grove, T. L. and Trimble, D. A, 1990, Post-11,000-year volcanism at Medicine Lake Volcano, Cascade Range, northern California: J. of Geothermal Research, v. 95, no. B12, p. 19693-19704.

Draper, D. S., 1991, Late Cenozoic bimodal magmatism in the northern Basin and Range Province of southeastern Oregon: J. of Volcanology and Geothermal Research, v. 47, p. 299-328.

Druken, K. A., Long, M. D. and Kincaid, C., 2011, Patterns in seismic anisotropy driven by rollback subduction beneath the High Lava Plains: Geophysical Research Letters, v. 38, L13310, p. 1-6.

Duncan, R. A. and Hogan, L. G., 1994, Radiometric dating of young MORB using the ^{40}Ar-^{39}Ar incremental heating method: Geophysical Reasearch Letters, v. 21, p. 1927-1930.

Duncan, R. A. and Keller, R. A., 2004, Radiometric ages for basement rocks from the Emperor Seamounts, ODP Leg 197: Geochemistry, Geophysics, Geosystems, v. 5, Q08L03.

Duncan, R. A., Hooper, P. R., Rehacek, J., Marsh, J. S. and Duncan, A. R., 1997, The timing and duration of the Karoo igneous event, southern Gondwana: J. of Geophysical Research, v. 102, p. 18127-18138.

Ewart, A. and Griffin, W. L., 1994, Application of proton-microprobe data to trace-element portioning in volcanic rocks: Chemical Geology, v. 117, p. 251-284.

Fenneman, N. M., 1916, Physiographic divisions of the United States: Annals of the Association of American Geographers, v. 6, p. 19-98.

Fiebelkorn, R. B., Walker, G. W., MacLeod, N. S., McKee, E. H., and Smith, J. G., 1983, Index to K-Ar determinations for the state of Oregon: Isochron Weast, no. 37, p. 3-60.

Fitton, J. G., James, D. and Leeman, W. P., 1991, Basaltic Magmatism associated with late Cenozoic extension in the western United States: Compositional variations in space and time: J. of Geophysical Research, v. 96, p. 13693-13711.

Ford, M. T., 2005, The petrogenesis of Quaternay rhyolite domes in the bimodal Blackfoot Volcanic Field, southeastern Idaho: Idaho State University MS thesis, 133p.

Ford, M. T., Carlson, R. W. and Grunder, A. L., 2009, Isotopic Compositional Changes Across Space, Time, and Bulk Rock Composition in the High Lava Plains and Northwestern Basin and Range, Oregon: Geological Society of America Abstracts with Programs, v. 41, p. 571.

Frost, B. R., Barnes, C. G., Collins, W. J., Arculus, R. J., Ellis, D. J. and Frost C. D., 2001, A geochemical classification for granitic rocks: J. of Petrology, v. 42, p. 2033-2048.

Furman, T., Frey, F. A., Meyer, P. S., 1992, Petrogenesis of evolved basalts and rhyolites at Austurhorn, southeastern Iceland: the role of Fractional Crystallization: J. of Petrology, v. 33, p. 1405-1445.

Graham, D. W., Reid, M. R., Jordan, B. T., Grunder, A. L., Leeman, W. P., and Lupton, J. E., 2009, Mantle source provinces beneath the Northwestern USA delimited by helium isotopes in young basalts: J. of Volcanology and Geothermal Research, v. 188, p. 128-140.

Green, R. C., 1973, Petrology of the welded tuff of Devine Canyon, southeastern Oregon: US Geological Survey Professional Paper 797, p. 1-26.

Gripp, A. E. and Gordon, R. G., 2002, Young tracks of hotspots and current plate velocities: Geophysics Journal International, v. 150, p. 321-361.

Hampton, E.R., 1964, Geologic factors that control the occurrence and availability of groundwater in the Fort Rock Basin, Lake County, Oregon: U.S. Geological Survey Professional Paper 383-B, p. B1-B29.

Hart, W. K. and Mertzman, S. A., 1983, Late Cenozoic volcanic stratigraphy of the Jordan Valley area, southeastern Oregon: Oregon Geology (Ore Bin), v. 45, p. 15-19.

Hart, W. K., Aronson, J. L., and Mertzman, S. A., 1984, Areal distribution and age of low-K, high-alumina olivine tholeiite magma in the northwestern Great Basin: Geological Society of America Bulletin, v. 95, p. 186-195.

Hart, W. K., Carlson, R. W., and Shirey, S. B., 1997, Radiogenic Os in primitive basalts from the northwestern U. S. A.: Implications for petrogenesis: Earth and Planetary Science Letters, v. 150, p. 103-116.

Hart, W. K., 1985, Chemical and isotopic evidence for mixing between depleted and enriched mantle, northwestern USA: Geochimica et Cosmochimica Acta, v. 49, p. 131-144.

Heiken, G., 1978, Plinian-type eruptions in the Medicine Lake highland, California, and the nature of the underlying magma: J. of Volcanology and Geothermal Research, v. 4, p. 375-402.

Hering, C. W., 1981, Geology and petrology of the Yamsay Mountain Complex, south-central Oregon: A study of bimodal volcanism: University of Oregon PhD thesis, 189 p.

Higgins, M. W., 1973, Petrology of Newberry Volcano, central Oregon: Geological Society of America Bulletin, v. 84, no. 2, p. 455-488.

Hildreth, W., 1981, Gradients in silicic magma chambers: Implications for lithospheric magmatism: J. of Geophysical Research, v. 86, is. B11, p. 153-192.

Hildreth, W., and Moorbath, S., 1988, Crustal contributions to arc magmatism in the Andes of central Chile: Contributions to Mineralogy and Petrology, v. 98, p. 455-489.

Hooper, P. R., Binger, G. B. and Lees, K. R., 2002, Ages of the Steens and Columbia River flood basalts and their relationship to extension-related calc-alkalic volcanism in eastern Oregon: Geological Society of America Bulletin, v. 114, p. 43-50.

Hughes, S. S. and Taylor, E. M., 1986, Geochemistry, petrogenesis, and tectonic implications of central High Cascade mafic platform lavas, Geological Society of America Bulletin, v. 97, p. 1024-1036

Hughes, S. S., McCurry, M. and Geist, D. J., 2002, Geochemical correlations and implications for the magmatic evolution of basalt flow groups at the Idaho National Engineering and Environmental Laboratory, in Link, P. K. and Mink, L. L., eds., Geology, Hydrogeology, and Environmental Remediation: Idaho National Engineering and Environmental Laboratory, Eastern Snake River Plain, Idaho: Geological Society of America Special Paper 353, p. 151-173.

Humphreys, E. D., Dueker, K. G., Schutt, D. L. and Smith, R. B., 2000, Beneath Yellowstone: Evaluating plume and nonplume models using teleseismic data: GSA Today, v. 10, p. 1-7.

Huppert, H. E. and Sparks, R. S. J., 1988, The generation of granitic magmas by intrusion of basalt into continental crust: J. of Petrology, v. 29, p. 599 – 634.

Iademarco, M. J., 2009, Volcanism and faulting along the northern margin of Oregon's High Lava Plains: Hampton Butte to Dry Mountain: Oregon State University MS thesis, 141 p.

Jackson, M. D., Cheadle, M. J. and Atherton, M. P., 2003, Quantitative modeling of granitic melt generation and segregation in the continental crust: J. of Geophysical Research, v. 108, no. 2332. DOI: 10.1029/2001JB001050

Jensen, R. A., 2006, Roadside guide to the geology and history of Newberry Volcano, 4th ed., CenOreGeoPub, Bend, OR, 182 p.

Jensen, R. A., Donnelly-Nolan, J. M. and Mckay, D., 2009, A field guide to Newberry Volcano, Oregon. In O'Connor, J. E., Dorsey, R. J. and Madin, I. P., eds., Volcanoes to Vineyards: Geologic Field Trips Through the Dynamic Landscape of the Pacific Northwest: Geological Society of America Field Guide 15, p. 53-79.

Johnson, D. M., Hooper, P. R. and Conrey, R. M., 1999, XRF analysis of rocks and minerals for major and trace elements on a single low dilution Li-tetraborate fused bead: Advances in X-ray analysis, v. 41, p. 843-867.

Johnson, J. A., 1995, Geologic evolution of the Duck Creek Butte eruptive center, High Lava Plains, southeastern Oregon: Oregon State University MS thesis, 151 p.

Johnson, J. A., 1998, Geologic map of the Frederick Butte volcanic center, Deschutes and Lake counties, south-central Oregon: USGS Open File Report 98-208, scale 1:40,000.

Johnson, J. A., and Grunder, A. L., 2000, The making of intermediate composition magma in a bimodal suite: Duck Butte Eruptive Center, Oregon, USA: J. of Volcanology and Geothermal Research, v. 95, p. 175-195.

Johnson, K. E., and Ciancanelli, E. V., 1984, Geothermal exploration at Glass Buttes, Oregon: Oregon Geology, v. 46, p. 15-20.

Johnson, M. J., 1984, Geology, alteration, and mineralization of a silicic volcanic center, Glass Buttes, Oregon: Portland State University MS thesis, 129 p.

Jonasson, K., 2007, Silicic volcanism in Iceland: Composition and distribution within the active volcanic zones: J. of Geodynamics, v. 43, p. 101-117.

Jonasson, K., 1994, Rhyolite volcanism in the Krafla central volcano, north-east Iceland: Bulletin of Volcanology, v. 56, p. 516-528.

Jordan, B. T., 2001, Basaltic volcanism and tectonics of the High Lava Plains, southeastern Oregon: Oregon State University PhD thesis, 218p.

Jordan, B. T., Streck, M. J. and Grunder, A. L., 2002, Bimodal volcanism and tectonism of the High Lava Plains, Oregon in Moore, G. W., ed., Field Guide to Geologic Processes in Cascadia: Oregon Department of Geology and Mineral Industries Special Paper 36, p. 23-46.

Jordan, B. T., Grunder, A. L., Duncan, R. A., and Deino, A. L., 2004, Geochronology of age-progressive volcanism of the Oregon High Lava Plains: Implications for the plume interpretation of Yellowstone: J of Geophysical Research, v. 109, issue B10, p. 1-19.

Kistler, R. W. and Peterson, Z. E., 1978, Reconstruction of crustal blocks of California on the basis of initial strontium isotopic compositions of Mesozoic granitic rocks: USGS Professional Paper 1071, 17 p.

Knaack, C., Cornelius, S. B., and Hooper, P. R., 1994, Trace element analyses of rocks and minerals by ICP-MS: Washington State University, open file report, http://www.sees.wsu.edu/Geolab/note/icpms.html, checked 11/22/11.

Koppers, A. A. P., 2002, ArArCalc – software for $^{40}Ar/^{39}Ar$ age calculations: Computers and Geosciences, v.28, p. 605-619.

Lacasse, C., Sigurdsson, H., Carey, S. N., Jóhannesson, H., Thomas, L. E., Rogers, N. W., 2007, Bimodal volcanism at the Katla subglacial caldera, Iceland: insight into the geochemistry and petrogenesis of rhyolitic magmas: Bulletin of Volcanology, v. 69, p. 373-399.

Langmuir, C. H., Klein, E. M. and Plank, T., 1992, Petrological Systematics of Mid-Ocean Ridge Basalts: Constraints on Melt Generation Beneath Ocean Ridges: AGU Monograph, v. 71, p. 183-280.

Larson, E. E., 1965, The structure, stratigraphy, and paleomagnetics of the Plush area, southeastern Lake County, Oregon: University of Colorado PhD thesis, 166 p.

Lawrence, R. O., 1976, Strike-slip faulting terminates the Basin and Range province in Oregon: Geological Society of America Bulletin, v. 87, p. 846-850.

Le Bas, M. J., Le Maitre, R. W. and Woolley, A. R., 1992, The construction of the Total Alkali-Silica chemical classification of volcanic rocks: J. of Mineralogy and Petrology, v. 46, No. 1, p. 1-22..

Leeman, W. P., 1982a, Olivine Tholeiites of the Snake River Plain, Idaho, in Bonnichsen, W and Brekenridge, R. M., eds., Cenozoic Geology of Idaho: Bureau of Mines and Geology Bulletin 26, p. 181-191.

Leeman, W. P., 1982b, Tectonic and magmatic significance of strontium isotope variations in Cenozoic volcanic rocks from the western United States: Geological Society of America Bulletin, v. 93, p. 487-503.

Leeman, W. P., Annen,C., Dufek, J., 2008, Snake River Plain-Yellowstone silicic volcanism: implications for magma genesis and magma fluxes: Geological Society of London Special Publication, v. 304, p. 235-259.

Lipman, P. W., 1965, Chemical comparison of glassy and crystalline volcanic rocks: U.S. Geological Survey Bulletin 1201-D, p. D1-D24.

Loiselle, M. C. and Wones, D. R., 1979, Characteristics and origin of anorogenic granites: Geological Society of America Abstracts with Programs, v. 11, p. 468.

Long, M. D., Gao, H., Klaus, A., Wagner, L. S., Fouch, M. J., James, D. E., and Humphreys, E., 2009, Shear wave splitting and the pattern of mantle flow beneath eastern Oregon: Earth and Planetary Science Letters, v. 288, p. 359-369.

Luedke, R. G. and Smith, R. L., 1984, Map showing distribution, composition, and age of late Cenozoic volcanic centers in the western conterminous United States: US Geological Survey Miscellaneous Investigations Map I-1523, scale 1:2,500,000.

MacDonald, R., 1974, Nomenclature and petrochemistry of the peralkaline oversaturated extrusive rocks: Bulletin of Volcanology, v. 38, p. 498-516.

MacLean, J. W., 1994, Geology and geochemistry of Juniper Ridge, Horsehead Mountain and Burns Butte: implications for the petrogenesis of silicic magma on the High Lava Plains, southeastern Oregon: Oregon State University MS Thesis, 141 p.

MacLeod, N. S., Walker, G. W. and McKee, E. H., 1976, Geothermal significance of eastward increase in age of upper Cenozoic rhyolitic domes in southeastern Oregon, Second United Symposium on the development and use of geothermal resources, Proceedings v. 1, p. 465-474.

MacLeod, N. S., Sherrod, D. R., Chitwood, L. A. and Jensen, R. A., 1995, Geologic Map of Newberry Volcano, Deschutes, Klamath, and Lake Counties: Oregon, USGS Miscellaneous Investigations Series Map I-2455, scale 1:62,500 and 1:24,00.

Martin, E. and Sigmarsson O., 2007, Crustal thermal state and origin of silicic magma in Iceland: the case of Torfajokull, Ljosufjoll and Snaefellsjokull volcanoes: Contributions to Mineralogy and Petrology, v. 153, p. 593-605.

Mathis, A. C., 1993, Geology and petrology of a 26-Ma trachybasalt to peralkaline rhyolite suite exposed at Hart Mountain, Oregon: Oregon State University MS thesis, 141 p.

McCurry, M. and Rodgers, D. W., 2009, Mass transfer along the Yellowstone hotspot track 1: Petrologic constraints on the volume of mantle-derived magma: J. of Volcanology and Geothermal Research, v. 188, p. 86-98.

McCurry, M., Hayden, K. P., Morse, L. H. and Mertzman, S., 2008, Genesis of post-hotspot, A-type rhyolite of the Eastern Snake River Plain volcanic filed by extreme fractional crystallization of olivine tholeiite: Bulletin of Volcanology, v. 70, p. 361-383.

McKee, E. H. and Walker, G. W., 1976, Potassium-argon ages of late Cenozoic silicic volcanic rocks, southeastern Oregon: Isochron West, v. 15, p. 37-41.

McQuarrie, N. and Rodgers, D. W., 1998, Subsidence of a volcanic basin by flexure and lower crustal flow: The eastern Snake River Plain, Idaho: Tectonics, v. 17, no. 2, p. 203-220.

Meigs, A., Scarberry, K., Grunder, A., Carlson, R., Ford, M. T., Fouch, M., Grove, T., Hart, W. K., Iademarco, M., Jordan, B., Milliard, J., Streck, M., Trench, D. and Weldon, R., 2009, Geological and geophysical perspectives on the magmatic and tectonic development, High Lava Plains and northwest Basin and Range, in O'Connor, J.E., Dorsey, R.J. and Madin, I.P., eds., Volcanoes to Vineyards: Geologic Field Trips through the Dynamic Landscape of the Pacific Northwest: Geological Society of America Field Guide 15, p. 435-470.

Miller, C. F., 1985, Are strongly peraluminous magmas derived from pelitic sedimentary sources?: J. of Geology, v. 93, p. 673-689.

Milliard, J., 2010, Two-stage opening of the northwestern Basin and Range in eastern Oregon: Oregon State University MS thesis, **81** p.

Min, K., Mundil, R., Renne, P. R and Ludwig, K. R., 2000, A test for systematic errors in $^{40}Ar/^{39}Ar$ geochronology through comparison with U/Pb analysis of a 1.1-Ga rhyolite: Geochimica et Cosmochimica Acta, v. 64, p. 73-98.

Miyashiro, A., 1974, Volcanic rock series in island arcs and active continental margins: American J. of Science, v. 274, p. 321-355.

Nekvasil, H., Simon, A., and Lindsley, D. H., 2000, Crystal fractionation and the evolution of intra-plate hy-normative igneous suites: Insights from their feldspars: J. of Petrology, v. 41, p. 1743-1757.

Naoum, S. and Tsanis, I. K., 2004, Ranking spatial interpolation techniques using a GIS-based DSS: Global Nest: The International Journal, v. 6, p. 1-20.

Newton, V. C., Corcoran, R. E. and Deacon, R. J., 1962, Oregon, still without oil, offers favorable pay areas, in Petroleum Exploration in Oregon: Oregon Department of Geology and Mineral Industries Miscellaneous Paper No. 9, p. 1-5.

Noble, D. C. and Parker, D. F., 1974, Peralkaline silicic volcanic rocks of the western United States: Bulletin of Volcanology, v. 38, p. 803-827.

Otto, B. R. and Hutchison, D. A., 1977, The geology of Jordan Craters, Malheur County, Oregon: The Ore Bin, v. 39, p. 125-140.

Parman, S. W and Grove, T. L., 2004, Harzburgite melting with and without H2O: Experimental data and predictive modeling: J. of Geophysical Research, v. 109, is. B2, article number B02201.

Pearce, J. A., 1982, Trace element characteristics of lavas from destructive plate boundaries, in Thorpe, R.S., ed., Andesites: Orogenic andesites and related rocks: Chichester, England, John Wiley and Sons, p. 525-548.

Pearce, J. A. and Parkinson, I. J., 1993, Trace element models for mantle melting: application to volcanic arc petrogenesis, in Prichard, H. M., Alabaster, T., Harris, N. B. W. and Neary, C. R., eds, Magmatic Processes and Plate Tectonics: Special Publication of the Geological Society of London, v. 76, p. 373-403.

Peccerillo, A., Barberio, M. R., Yirgu, G., Ayalew, D., Barberi, M. and Wu, T. W., 2003, Relationships between mafic and acid peralkaline magmatism in continental rift settings: a petrological, geochemical and isotopic study of the Gedemsa volcano, central Ethiopian Rift: J. of Petrology v. 44, p. 2003–2032

Peterson, N. V., 1959, Preliminary geology of the Lakeview Uranium Area, Oregon: The Ore Bin, v 21, p 11-16.

Pezzopane, S. K. and Weldon, R. J., 1993, Tectonic role of active faulting in central Oregon: Tectonics, v. 12, p. 1140 – 1169.

Pierce, K. L. and Morgan, L. A., 1992, The track of the Yellowstone hotspot: Volcanism, faulting and uplift, in Link, P. K, Kuntz, M. A. and Platt, L. B., eds., Regional Geology of Eastern Idaho and Western Wyoming: Geological Society of America Memoir 179, p. 1-53.

Popenoe, H. L., 1961, Developments in west coast area in 1960; Bulletin of the American Association of Petroleum Geologists, v. 45, p. 959-973.

Ren, M., 2004, Partitioning of Sr, Ba, Rb, Y, and LREE between alkali feldspar and peraluminous silicic magmas: American Mineralogist, v. 89, p. 1290-1303.

Ren, M., Parker, D. F. and White, J. C., 2003, Partitioning of Sr, Ba, Rb, Y, and LREE between plagioclase and peraluminous silicic magmas: American Mineralogist, v. 88, p. 1091-1103.

Renne, P. R., Swisher, C. C., Deino, A. L., Karner, D. B., Owens, T. L. and DePaolo, D. J., 1998, Intercalibration of standards, absolute ages and uncertainties in $^{40}Ar/^{39}Ar$ dating: Chemical Geology, v. 145, p. 117-152.

Robinson, P. T., Walker, G. W. and McKee, E. H., 1990, Eocene (?), Oligocene, and lower Miocene rocks of the Blue Mountains Region: US Geological Survey Professional Paper, 1437, p. 29 – 62.

Roche, R. L., 1987, Stratigraphic and geochemical evolution of the Glass Buttes Complex, Oregon: Portland State University MS Thesis, 99p.

Rollinson, H., 1993, Using geochemical data: Evaluation, presentation, interpretation: Longman Group,Essex, England, 352 p.

Rooney, T., Furman, T., Bastow, I., Ayalew, D. and Yirgu, G., 2007, Lithospheric modification during crustal extension in the Main Ethiopian Rift, J. of Geophysical Research v. 112, p. B10201.

Rosenberg, C. L., Medvedev, S. and Handy, M. R., 2007, Effects of melting on faulting and continental deformation, in Handy, M. R., Hirth, G. and Hovius, N, eds., Tectonic faults: Agents of change on a dynamic earth: The MIT Press, Cambridge, MA.

Rubin, K. H., Smith, M. C., Bergmanis, E. C., Perfit, M. R., Sinton, J. M. and Batiza, R., 2001, Geochemical heterogeneity within mid-ocean ridge lava flows: insights into eruption, emplacement and global variations in magma generation: Earth and Planetary Science Letters, v. 188, is. 3-4, p. 349-367.

Russell, I. C., 1884, A Geological Reconnaissance in Southern Oregon: US Geological Survey, Annual Report 4, p. 431-464.

Russell, J. K. and Nicholls, J., 1987, Early crystallization history of alkali olivine basalts, Diamond Craters, Oregon: Geochimica et Cosmochimica Acta, v. 51, p. 143-154.

Scarberry, K. C., 2007, Extension and volcanism: Tectonic development of the northwestern margin of the Basin and Range Province in southern Oregon: Oregon State University PhD thesis, 168p.

Scarberry, K. C., Meigs, A., and Grunder, A., 2010, Faulting in a propagating continental rift: Insights from the late Miocene structural development of the Abert Rim fault, southern Oregon, USA: Tectonophysics v. 488, p. 71-86.

Schmidt, M. E. and Grunder, A. L., 2011, Deep mafic roots to arc volcanoes: Mafic recharge and differentiation of basaltic andesite at North Sister Volcano, Oregon Cascades: J. of Petrology, v. 52, p. 603-641.

Schmidt, M. E., Grunder, A. L. and Rowe, M. C., 2008, Segmentation of the Cascade Arc as indicated by Sr and Nd isotopic variations among diverse primitive basalts: Earth and Planetary Science Letters, v. 266, p. 166-181.

Schuessler, J. A.; Schoenberg, R. and Sigmarsson, O, 2009, Iron and lithium isotope systematics of the Hekla volcano, Iceland — Evidence for Fe isotope fractionation during magma differentiation: Chemical Geology, v. 258, p. 78-91.

Shand, S. J., 1927, Eruptive Rocks: Their Genesis, Composition, Classification and Their Relation to Ore-deposits: Murby, London, 360 p.

Shepard, D., 1968, A two-dimensional interpolation function for irregularly-spaced data: Proceedings of the Association of Computing Machinery (ACM) National Conference, p. 517-524.

Sherrod, D. R., Taylor, E. M., Ferns, M. L., Scott, W. E., Conrey, R. M., and Smith, G. A., 2004, Geologic map of the Bend 30- X 60- minute quadrangle, central Oregon: US Geological Survey Geologic Investigations Series I-2683, 48 p.

Sigmarsson, O. and Steinthorsson, S., 2007, Origin of Iceland basalts: A review of their petrology and geochemistry: J. of Geodynamics, v. 43, p. 87-100.

Sigmarsson, O., Condomines, M., and Fourcade, S., 1992, A detailed Th, Sr and O isotope study of Hekla: differentiation processes in an Icelandic Volcano: Contributions to Mineralogy and Petrology, v. 112, p. 20-34.

Sigurdsson, H and Sparks, R S J, 1981, Petrology of rhyolitic and mixed magma ejecta from the 1875 eruption of Askja, Iceland: J. of Petrology, v. 22, p. 41-84.

Sisson, T.W. and Grove, T. L., 1993. Experimental investigations of the role of H2O in calc-alkaline differentiation and subduction zone magmatism: Contributions to Mineralogy and Petrology, v. 113, p. 143-166.

Sisson, T. W., Ratajeski, K., Hankins, W. B., Glazner, A. F., 2005, Voluminous granitic magmas from common basaltic sources: Contributions to Mineralogy and Petrology, v. 148, p. 635-661.

Smith, G. A., Snee, L. W., and Taylor, E. M., 1987, Stratigraphic, sedimentologic, and petrologic record of the late Miocene subsidence of the Oregon High Cascades: Geology, v. 15, p. 389-392.

Smith, R.L. and Luedke, R.G., 1984, Potentially active volcanic lineaments and loci in western conterminous United States, in, Explosive Volcanism: Inception, Evolution and Hazards, National Research Council, p. 47-66.

Spera, F. J. and Bohrson,W. A., 2001, Energy-constrained open-system magmatic processes I: General model and energy-constrained assimilation and fractional crystallization (EC-AFC) Formulation: J. of Petrology, v. 42, p. 999-1018.

Spulber, S. D. and Rutherford, M. J., 1983, The origin of rhyolite and plagiogranite in oceanic crust: An experimental study: J. of Petrology, v. 24, p. 1-25.

Steiger, R. H. and Jager, E., 1977, Subcommission on Geochronology – convention on the use of decay constants in geochronology and cosmochronology: Earth and Planetary Science Letters, v. 36, p. 359-363.

Streck, M, J., 2002, Partial melting to produce high-silica rhyolites of a young bimodal suite: compositional constraints among rhyolites, basalts, and metamorphic xenoliths from the Harney Basin, Oregon: International J. of Earth Sciences, v. 91, p. 583-593.

Streck, M. J. and Grunder, A. L., 1995, Crystallization and welding variations in a widespread ignimbrite sheet; the Rattlesnake Tuff, eastern Oregon, USA: Bulletin of Volcanology, v. 57, p. 151-169.

Streck, M. J. and Grunder, A. L., 1997, Compositional gradients and gaps in high-silica rhyolites of the Rattlesnake Tuff, Oregon: J. of Petrology, v. 38, p. 133-163.

Streck, M. J. and Grunder, A. L., 1999, Enrichment of basalt and mixing of dacite in the rootzone of a large rhyolitic chamber: inclusions and pumices from the Rattle Snake Tuff, Oregon: Contributions to Mineralogy and Petrology, v. 136, p. 193-212.

Streck, M. J. and Grunder, A. L., 2008, Phenocryst-poor rhyolites of bimodal, tholeiitic provinces: the Rattlesnake Tuff and implications for mush extraction models: Bulletin of Volcanology, v. 70, p. 385-401.

Sun, S. S. and McDonough, W. F. (1989) Chemical and Isotopic Systematics of oceanic basalts: implications for Mantle Composition and Processes, in Saunders, A. D. and Norry, M. J., eds., Magmatism in the Ocean Basins: Special Publication Geological Society of London, no. 42, p. 313-345.

Sverrisdottir, G., 2007, Hybrid magma generation preceding Plinian silicic eruptions at Hekla, Iceland: Evidence from mineralogy and chemistry of two zoned deposits: Geological Magazine, v. 144, p. 643-659.

Taylor, E. M., 1981, Central High Cascade roadside geology, in Johnston, D. A. and Donnelly-Nolan, J. M., eds., Guides to some volcanic terranes in Washington, Idaho, Oregon, and northern California: US Geological Survey Circular 838, p. 55-83.

Trench, D., 2008, The Termination of the Basin and Range Province into a Clockwise Rotating Region of Transtension and Volcanism, Central Oregon: Oregon State University MS thesis, 71 p.

Vigil, J. F., Pike, R. J. and Howell, D. G., 2000, A tapestry of time and terrain: U.S. Geological Survey Geologic Investigations Series 2720, scale 1:3,500,000.

Wacaster, S., Streck, M. J., Belkin, H. E., and Bodnar, R. J., 2011, Compositional zoning of the Devine Canyon Tuff, Oregon: American Geophysical Union Fall 2011 Meeting abstract V21C-2517.

Walker, G. W., 1974, Some implications of Late Cenozoic volcanism to geothermal potential in the High Lava Plains of south-central Oregon: Ore Bin, v. 36, p. 109-119.

Walker, G. W., 1979, Revisions to the Cenozoic stratigraphy of Harney Basin, southeastern Oregon: U.S. Geological Survey Bulletin 1475, 35 p.

Walker, G. W., 1981, Uranium, thorium, and other metal associations in silicic volcanic complexes of the northern Basin and Range, a preliminary report: U.S. Geological Survey Open File Report no 81-1290, 45 p.

Walker, G. W. and Swanson, D.A., 1968, Laminar flowage in a Pliocene soda rhyolite ash-flow tuff, Lake and Harney Counties, Oregon: U.S. Geological Survey Professional Paper 600-B, p. B37-B47.

Walker, G.W., and MacLeod, N.S., 1991, Geologic map of Oregon: U. S. Geological Survey, scale 1:500,000.

Walker, G. W. and Robinson, P. T., 1990, Cenozoic tectonism and volcanism of the Blue Mountains region, in Walker, G. W., ed., Geology of the Blue Mountains Region of Oregon, Idaho, and Washington: US Geological Survey Professional Paper 1437, p. 119-135.

Watson, D. F. and Philip, G. M., 1985, A refinement of inverse distance weighted interpolation: Geo-Processing, v. 2, p. 315-327.

Wells, R. E., 1979, Drake Peak – A structurally complex rhyolite center in southeastern Oregon: US Geological Survey Professional Paper 1124, p. E1-E16.

Wells, R. E., Weaver, C. S. and Blakely, R. J., 1998, Fore arc migration in Cascadia and its neotectonic significance: Geology, v. 26, p. 759-762.

Whitaker, M. L., Nekvasil, H., Lindsley, D. H., McCurry, M., 2008, Can crystallization of olivine tholeiite give rise to potassic rhyolites? – an experimental investigation: Bulletin of Volcanology, v. 70, p. 417-434.

Xue, M. and Allen, R. M., 2006, Origin of the Newberry Hotspot Track: Evidence from shear-wave splitting: Earth and Planetary Science Letters, v. 244, p. 315-322.

FIGURES:

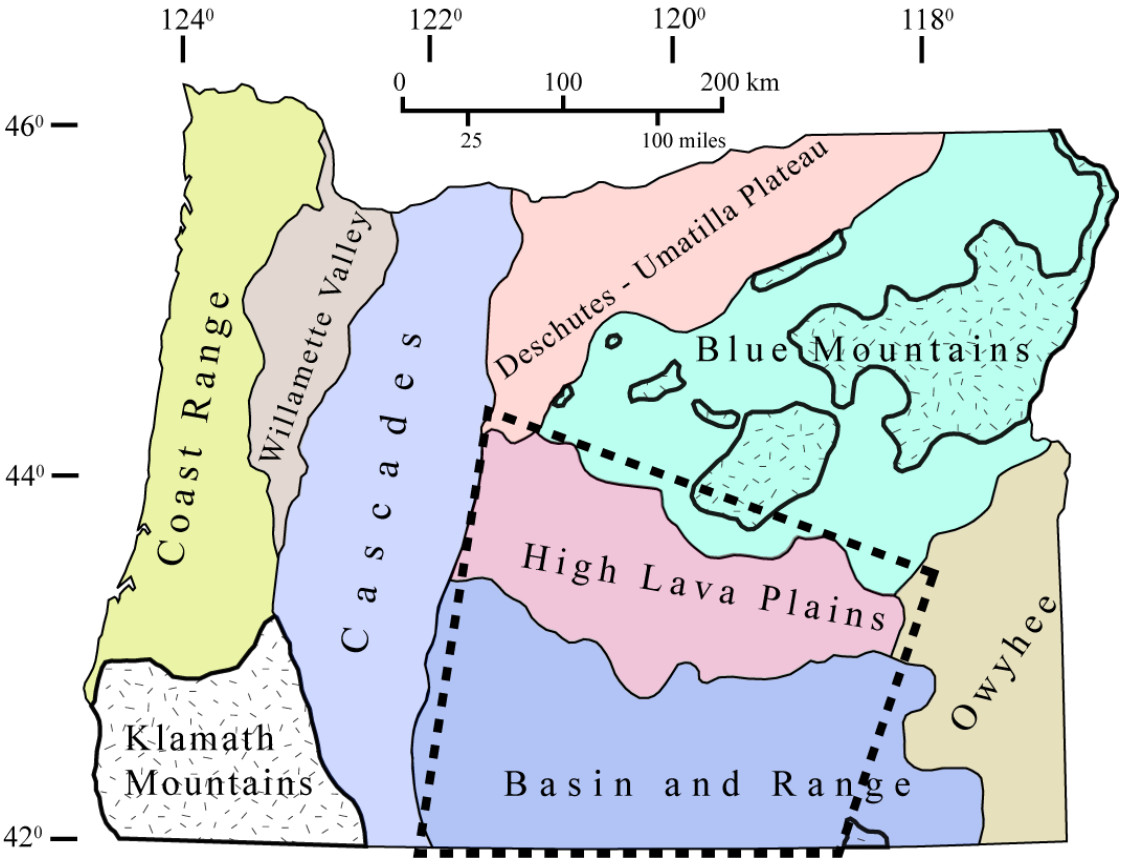

Figure 1: Physiographic provinces of Oregon and study area outlined by dashed line. The approximate extent of pre-Tertiary outcrops are given in a stipple pattern (adapted after Dicken, 1950 and MacLeod, et al., 1995; Walker and MacLeod, 1991).

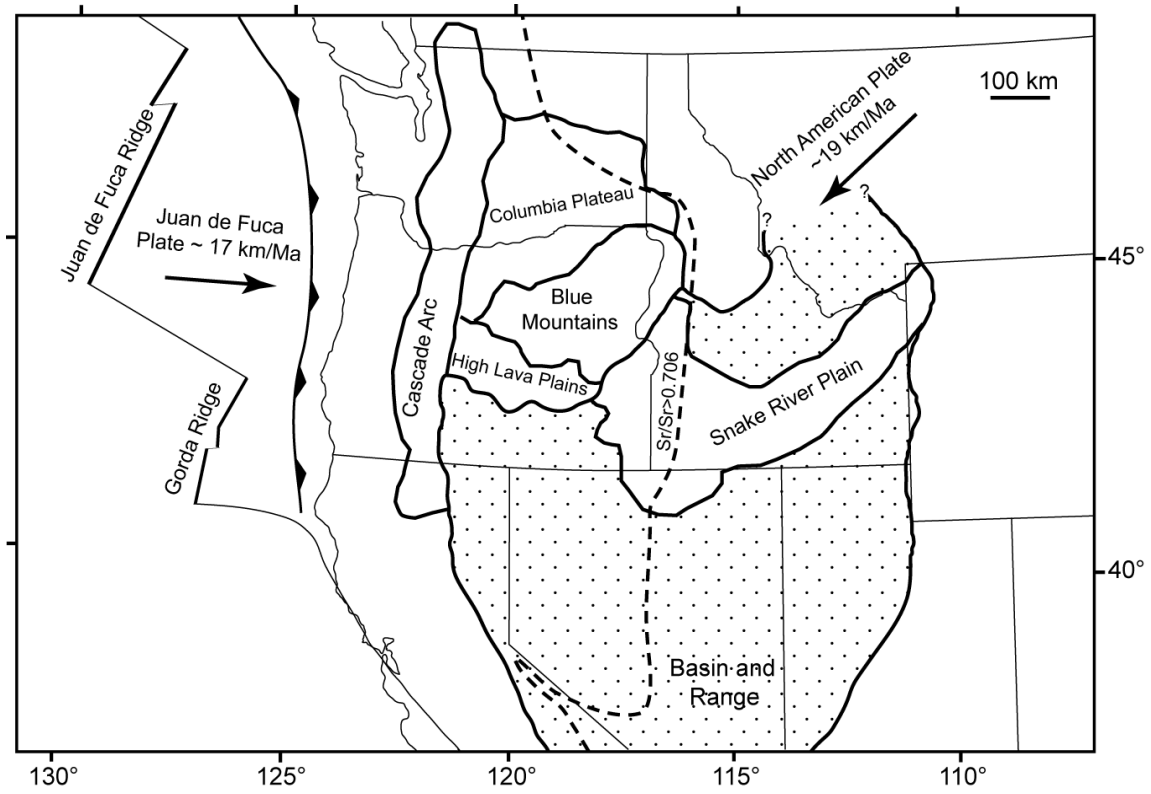

Figure 2: Regional tectonic setting of the High Lava Plains and surrounding provinces. Dashed line indicates approximate position of the $^{87}Sr/^{86}Sr$ 0.706 line (after Kistler and Peterson, 1978), representing the western edge of the Proterozoic or older craton of North America with generally Mesozoic and younger accreted terranes to the west. Stippled region indicates middle Miocene and younger extensional normal faulting (Basin and Range style, after Pezzopane and Weldon, 1993). Arrows give the absolute plate motions and velocities based on models of DeMets, et al., 1994 (no net rotation NUVEL-1A model) relative to 43° N latitude, 120° W longitude, near the center of the studied area (Figure 1). Modified after Jordan, et al., 2004.

Figure 3: Simplified geologic map. Fault and generalized geologic map of south-central and south-eastern Oregon with fault zones and major NWBR faults. Stipple pattern are basalts and basaltic andesites, gray areas are rhyolites and rhyodacites including major tuffs, white areas are sedimentary cover, except not all units are expressed in the Cascades Range. HB is the Harney Basin, BFZ is the Brothers Fault Zone and EDFZ is the Eugene – Denio Fault Zone. Major, generally NNE trending Basin and Range type faults are shown with thick lines. Figure is adapted from the Oregon State Geologic Map (Walker and MacLeod, 1991).

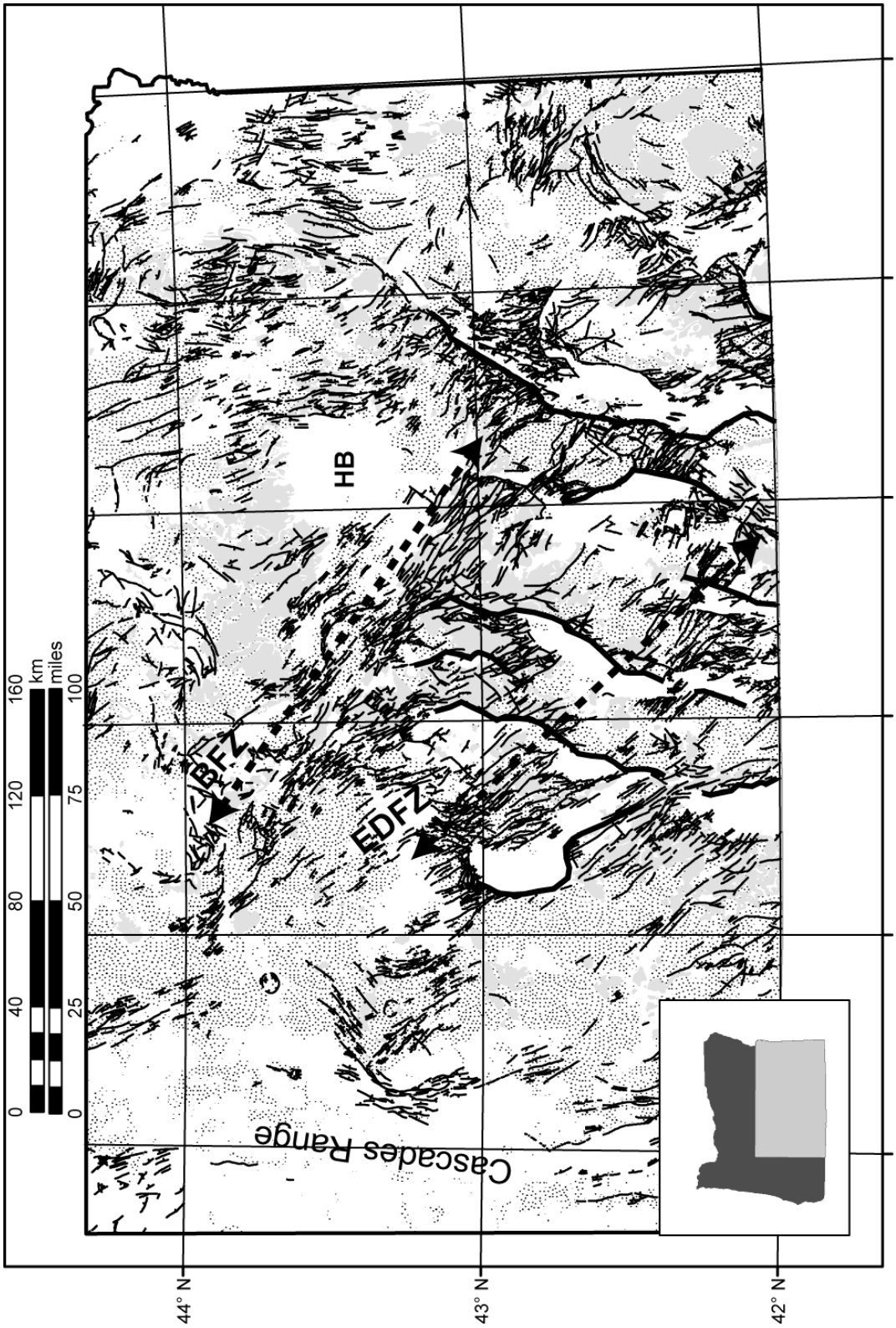
HB
BFZ
EDFZ
Cascades Range
0
40
80
120
160
km
0
25
50
75
100
miles
44° N
43° N
42° N
122° W
121° W
120° W
119° W
118° W
117° W

Figure 3:

Figure 4: Distribution of eastern Oregon rhyolites and basalts through time. Map of eastern Oregon shows the spatial distribution of basalts and rhyolite lavas and tuffs though time. (A) John Day age (37-20 Ma), (B) Steens age (~18-15 Ma), (C) Deschutes age (7-6 Ma) and (D) Age-progressive HLP and NWBR less than 12 Ma province. Lettered, outlined, areas on 4D indicate units that differ from the Walker and MacLeod (1991) Oregon State geologic map as follows: A) basalt of Dry Mountain (originally mapped as an andesite, Iademarco, 2009) B) basalt or basaltic andesite with local hydrothermal silica sinter, C) basalt or basaltic andesite, D) basalt or basaltic andesite. Units B, C, and D were originally mapped as rhyolite. Proposed location for the Rattlesnake Tuff (Streck and Grunder, 1997) given. Black lines are major roads; heavy black dashed line outlines the HLP physiographic province as described in the text and Figure 1. The locations of many localities mentioned in the text are given. All four maps cover the same region.

Figure 4:

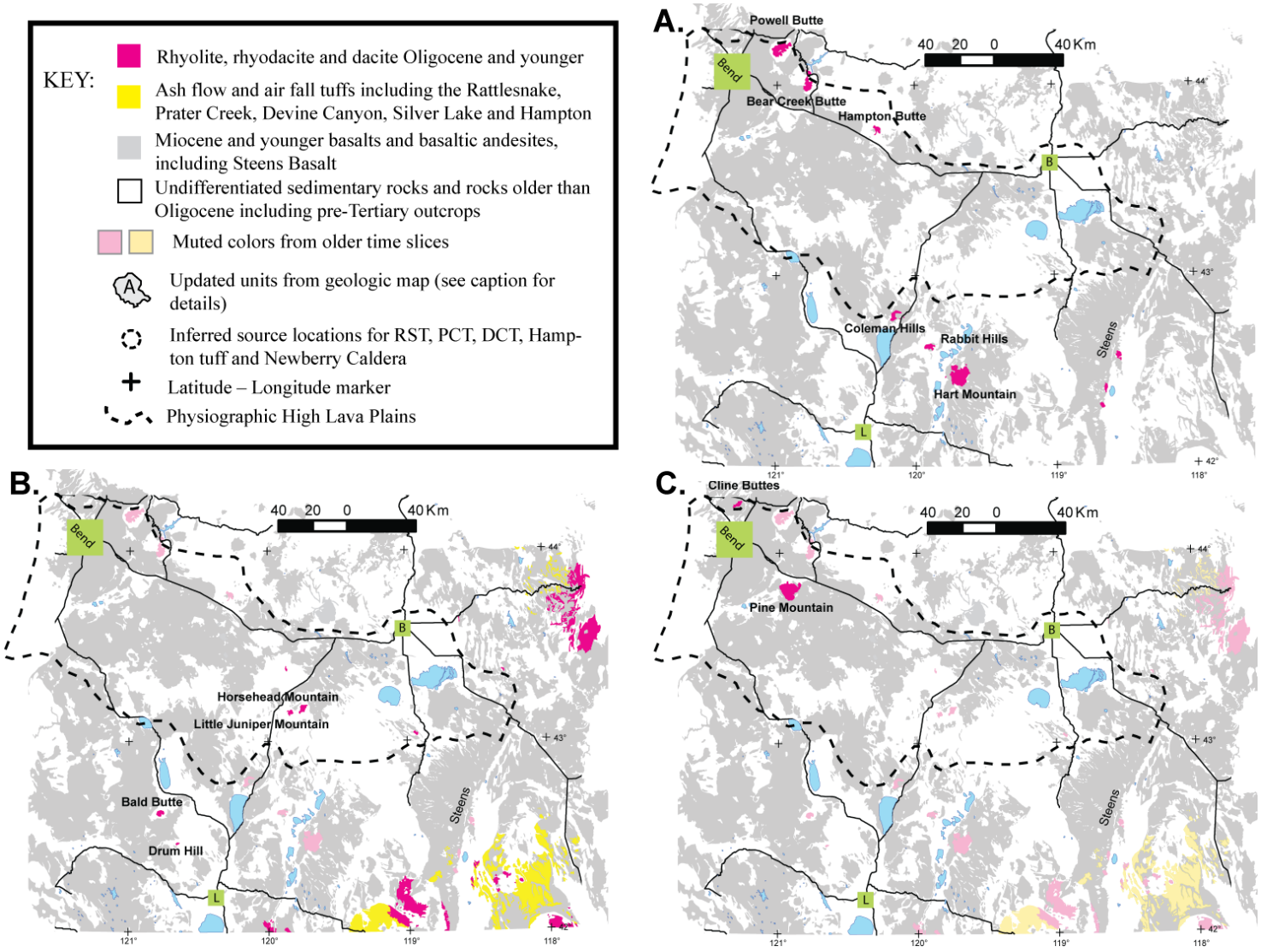
KEY:
Rhyolite, rhyodacite and dacite Oligocene and younger
Ash flow and air fall tuffs including the Rattlesnake, Prater Creek, Devine Canyon, Silver Lake and Hampton
Miocene and younger basalts and basaltic andesites, including Steens Basalt
Undifferentiated sedimentary rocks and rocks older than Oligocene including pre-Tertiary outcrops
Muted colors from older time slices
A
Updated units from geologic map (see caption for details)
Inferred source locations for RST, PCT, DCT, Hampton tuff and Newberry Caldera
Latitude – Longitude marker
Physiographic High Lava Plains
A.
Powell Butte
Bend
40 20 0 40 Km
Bear Creek Butte
Hampton Butte
B
Coleman Hills
Rabbit Hills
Steens
Hart Mountain
L
121°
120°
119°
118°
44°
43°
42°
B.
Horsehead Mountain
Little Juniper Mountain
Bald Butte
Drum Hill
C.
Cline Buttes
Pine Mountain

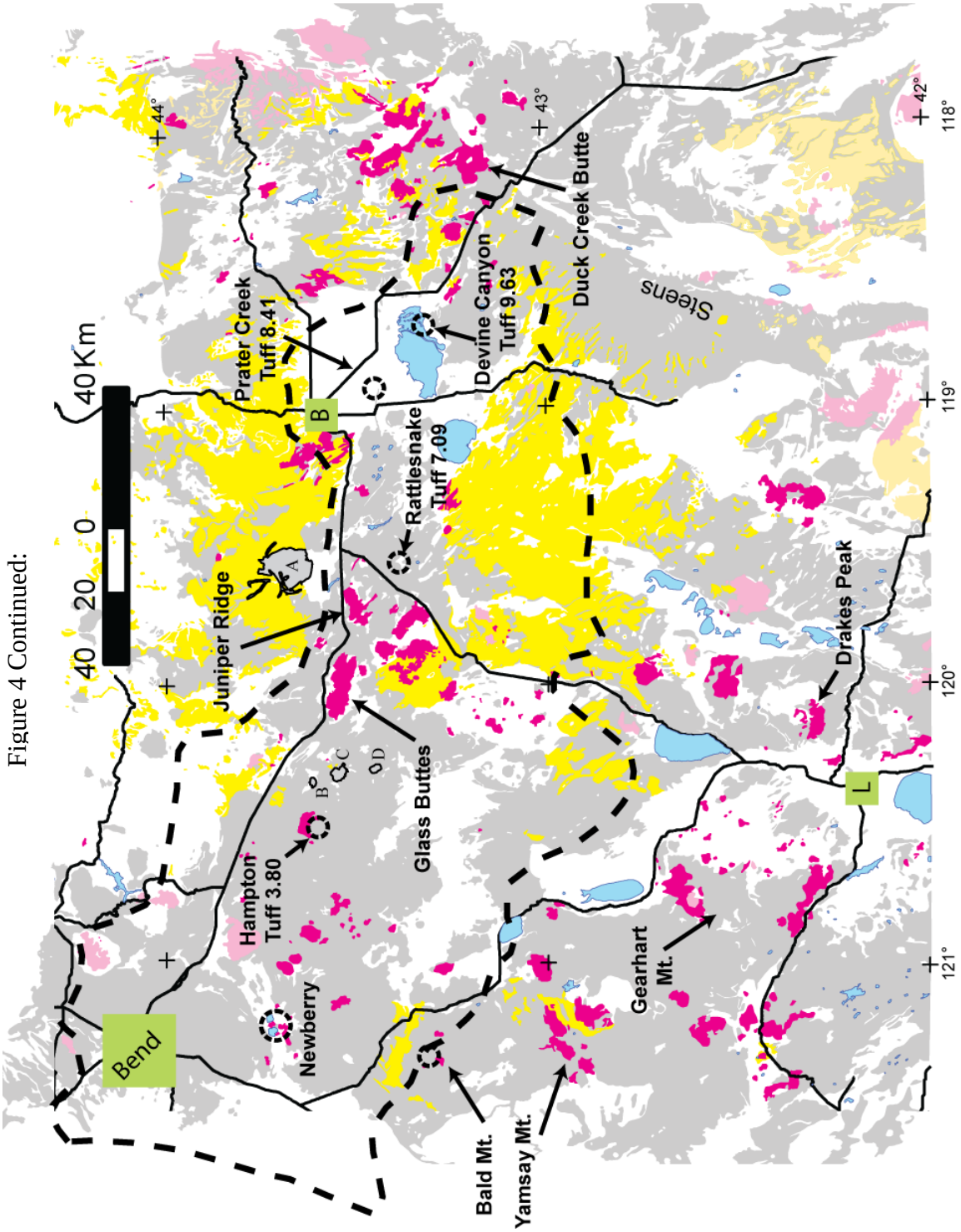

Figure 4 Continued:

Figure 5: New ages for the HLP and NWBR. Eighteen $^{40}Ar/^{39}Ar$ age plateaus from the current study, 15 of which are from less than 12 Ma samples from the NWBR or HLP of which, one (Pine Mountain, 6.25 Ma) has been ascribed to the Deschutes Formation (see text). The remaining three samples fall within the "Steens-age" time slice from 18 to 15 Ma (Figure 4b). Dashed lines on the diagrams indicate the heating steps that were integrated into the age calculation, the width of each box is the percent of total ^{39}Ar released for that temperature step, and the height of each box is the 2σ uncertainty for that heating step. See Table 2 and Electronic Data Supplement for additional sample information including Excel files and original .age (ArArCalc) files.

Figure 5:

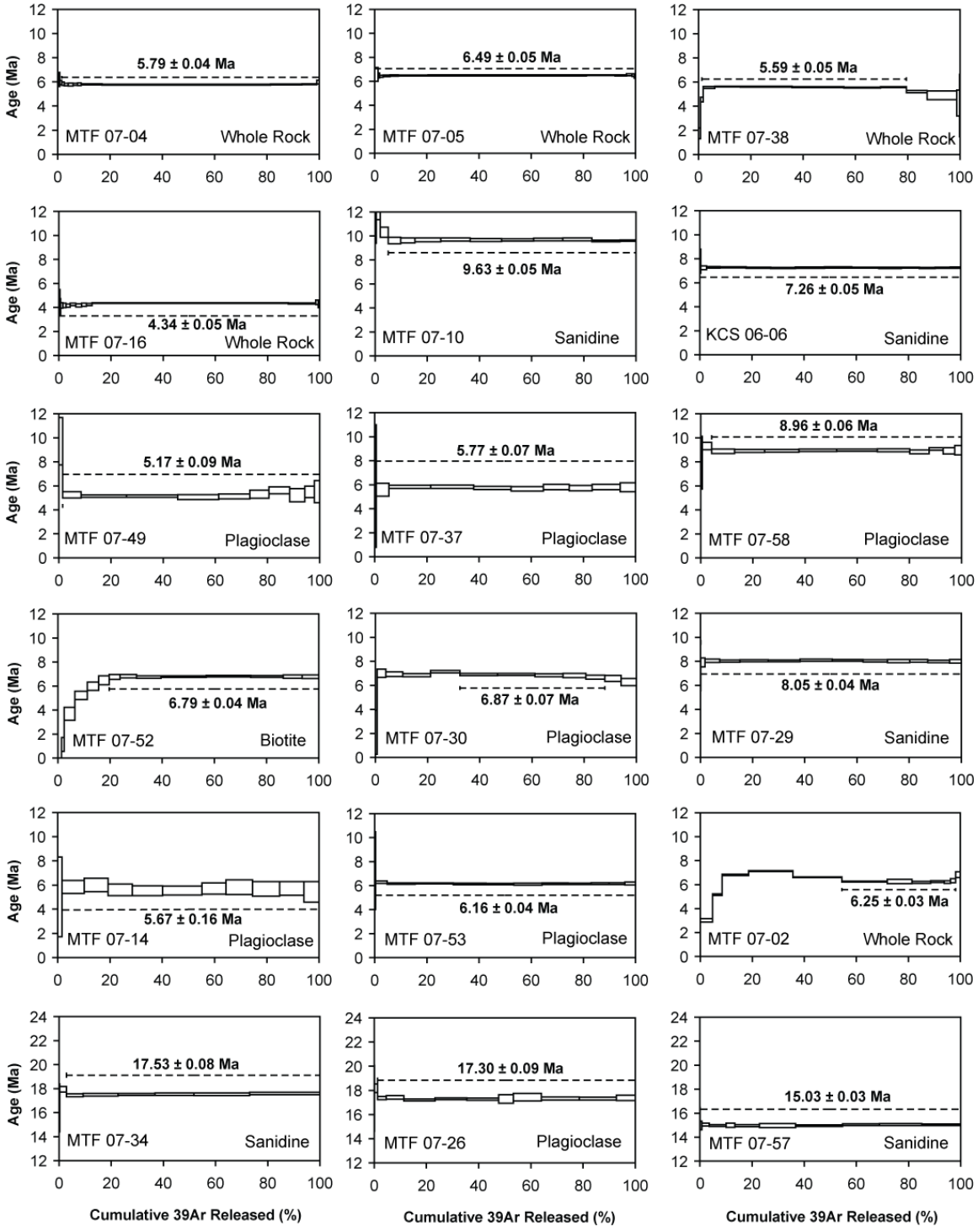
5.79 ± 0.04 Ma
MTF 07-04
Whole Rock
6.49 ± 0.05 Ma
MTF 07-05
Whole Rock
5.59 ± 0.05 Ma
MTF 07-38
Whole Rock
4.34 ± 0.05 Ma
MTF 07-16
Whole Rock
9.63 ± 0.05 Ma
MTF 07-10
Sanidine
7.26 ± 0.05 Ma
KCS 06-06
Sanidine
5.17 ± 0.09 Ma
MTF 07-49
Plagioclase
5.77 ± 0.07 Ma
MTF 07-37
Plagioclase
8.96 ± 0.06 Ma
MTF 07-58
Plagioclase
6.79 ± 0.04 Ma
MTF 07-52
Biotite
6.87 ± 0.07 Ma
MTF 07-30
Plagioclase
8.05 ± 0.04 Ma
MTF 07-29
Sanidine
5.67 ± 0.16 Ma
MTF 07-14
Plagioclase
6.16 ± 0.04 Ma
MTF 07-53
Plagioclase
6.25 ± 0.03 Ma
MTF 07-02
Whole Rock
17.53 ± 0.08 Ma
MTF 07-34
Sanidine
17.30 ± 0.09 Ma
MTF 07-26
Plagioclase
15.03 ± 0.03 Ma
MTF 07-57
Sanidine
Age (Ma)
Cumulative 39Ar Released (%)

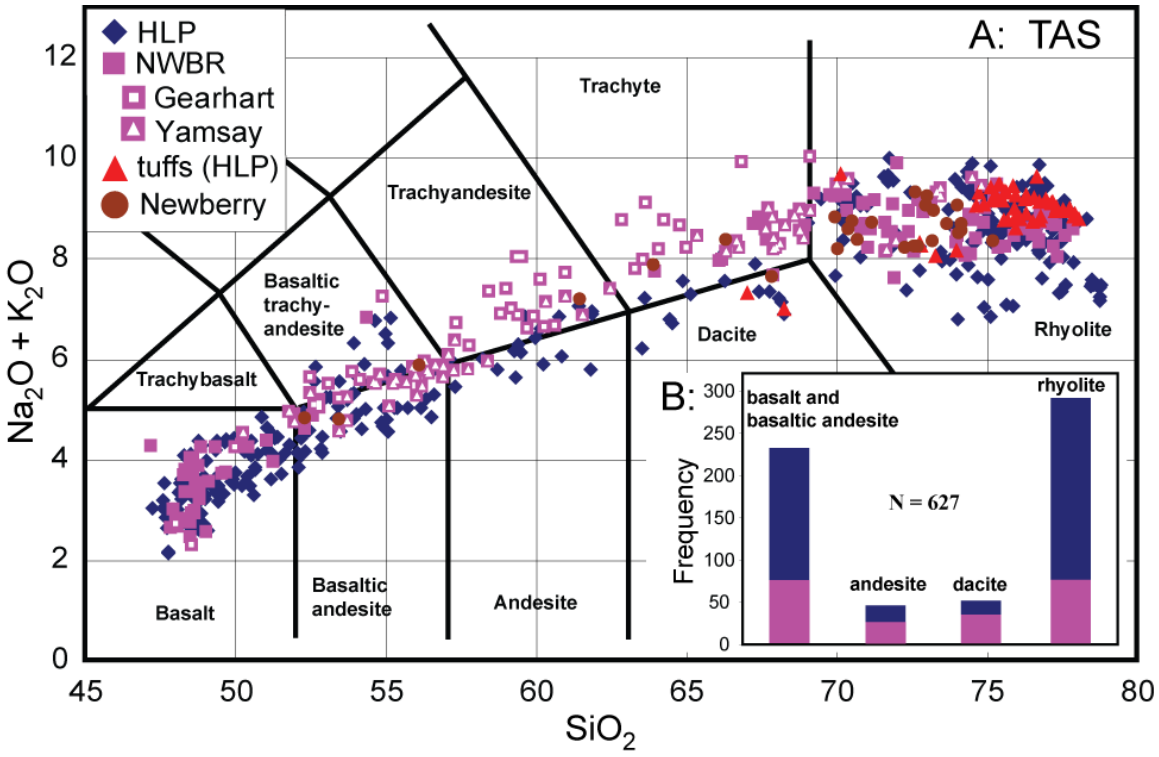

Figure 6: TAS diagram and histogram of < 12 ma HLP and NWBR volcanics. 6A is a total alkali-silica (TAS) (after Le Bas, et al., 1992) of all HLP and NWBR samples less than 12 Ma with major element analyses. Note that the Gearhart Mountain and Yamsay Mountain sample subsets from the NWBR make up many of the intermediate compositions. Some of the samples from Glass Buttes (HLP) have lower total alkalis than most other rocks of the study area. This appears to be either an artifact of glass hydration and attendant leaching of Na_2O or the analytical technique used for some samples yielding lower values for Na_2O (see text for discussion). Samples from Newberry Volcano (MacLeod et al., 1995; Higgins, 1973) are plotted as a separate symbol. 6B is a histogram showing the strongly bimodal nature of compositions from the HLP and NWBR with intermediate compositions likely over represented (see text).

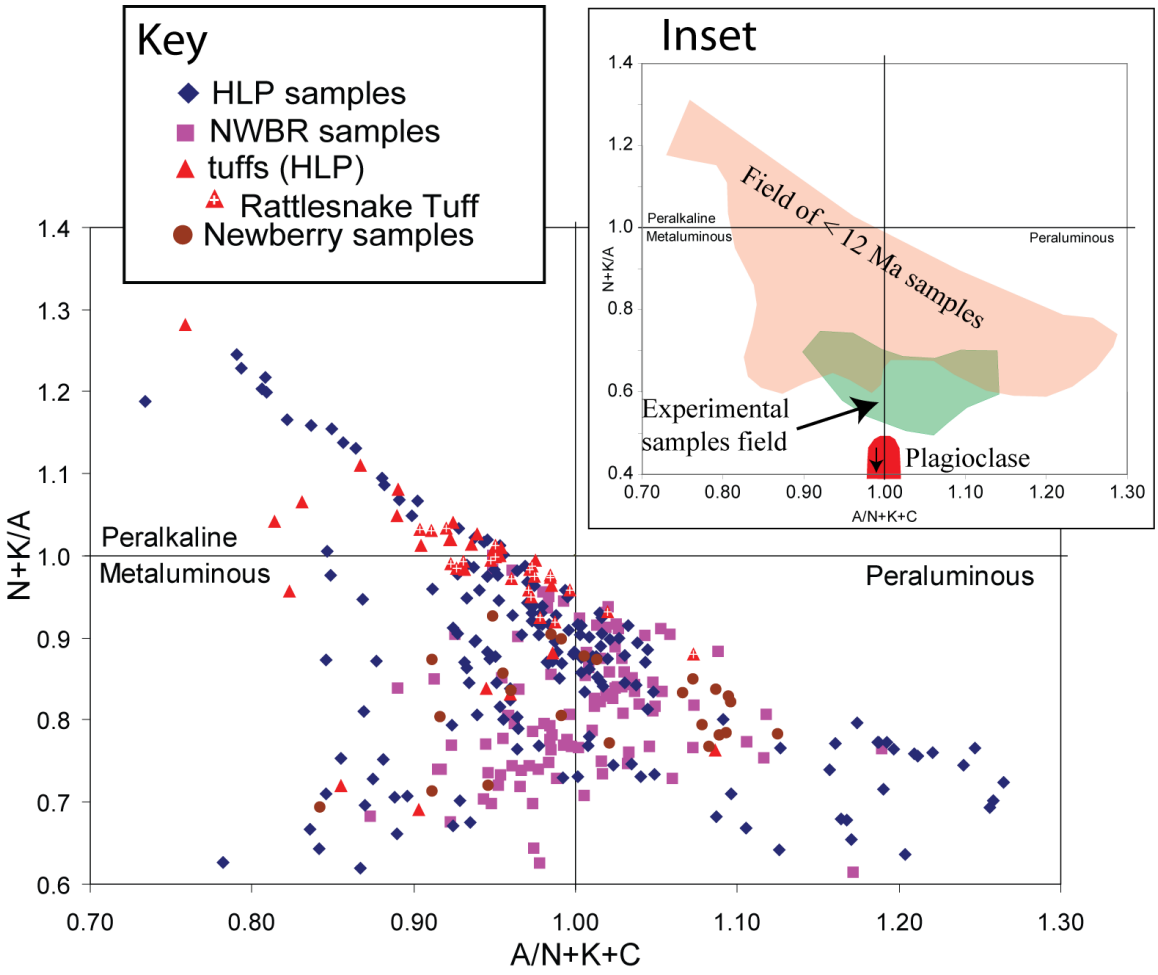

Figure 7: Alumina saturation index. ASI (after Shand, 1927) of less than 12 Ma samples (dacites and rhyolites) from the HLP and NWBR. There are no peralkaline samples from the NWBR and tuffs are generally more peralkaline than the lavas. The overall distribution for the NWBR samples is similar to Newberry Volcano samples (MacLeod et al., 1995; Higgins, 1973) and there is no clear delineation between NWBR and HLP samples. Some of the strongly peraluminous samples may be an artifact caused by glass hydration (see text for discussion). Inset shows the field of < 12 Ma samples with fields for low degree partial melting experimental results (Sisson et al., 2005; Beard and Lofgren, 1991; Spulber and Rutherford, 1983) and plagioclase (An_{50-99}), which would extend to near 0 in N+K/A (y-axis). Plagioclase is present and contributes to the melt in all of the experimental studies. Most of the experimental melts contain more normative plagioclase (cf. Figure 2 of Sisson, et al., 2005) than silicic rocks from this study. Partial melts with less plagioclase or fractional crystallization of some plagioclase would move compositions up on this diagram.

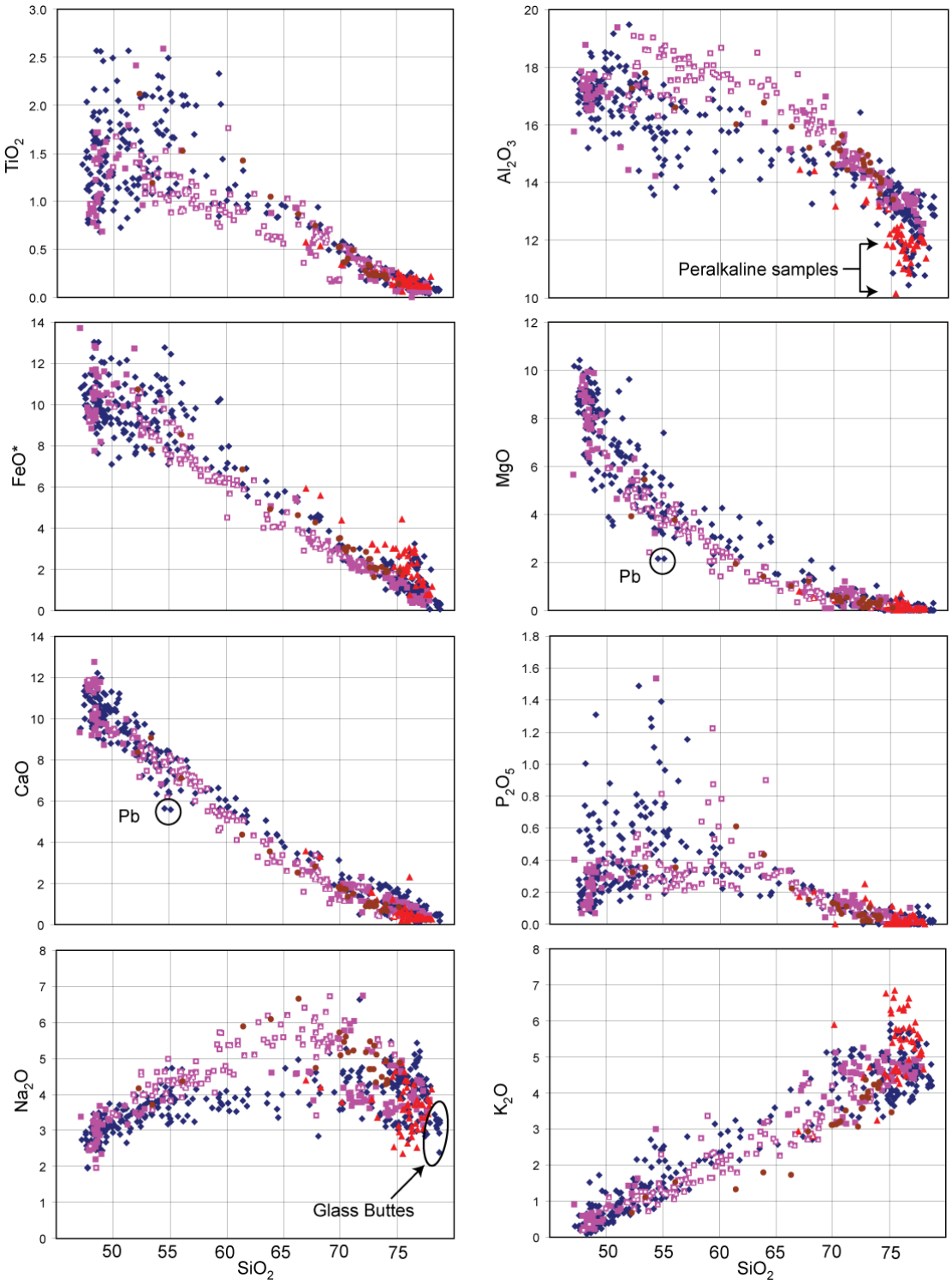

Figure 8: Harker diagrams for HLP and NWBR for selected major elements. Some general fields delineated such the potential hydrothermal alteration in many Glass Buttes samples, the peralkaline samples and Paiute Butte (PB) (see text for discussion). Symbols as is Figure 6.

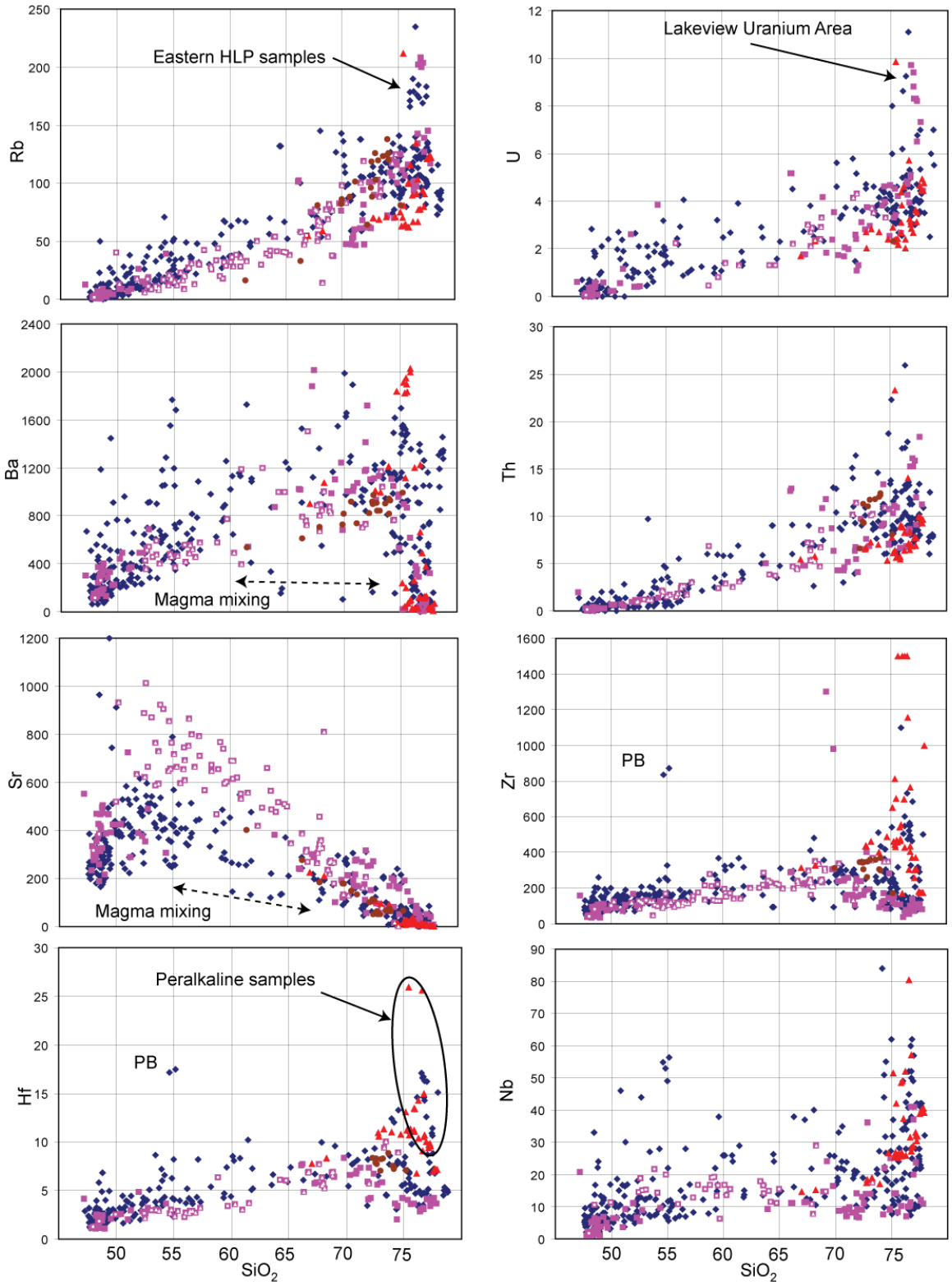

Figure 9: Selected trace elements variation diagrams for the HLP and NWBR. See text for discussion of labeled areas, PB = Paiute Butte, symbols as in Figure 6.

Figure 10: Normalized rare-earth element diagrams. N-MORB normalized (Sun and McDonough, 1989) rare-earth element diagram for HLP and NWBR separated into A: basalts (<52 wt % SiO_2) and basaltic andesites (52 – 57 wt. % SiO_2) with PB = Paiute Butte (see text) and B: rhyolites (69 - ~78% SiO_2) and intermediate compositions (57 – 69 wt. % SiO_2). All intermediate compositions (andesites and dacites) are plotted together due to the general lack of data points and the narrow range in which they fall. Average composition for each group is also given.

Figure 10A:

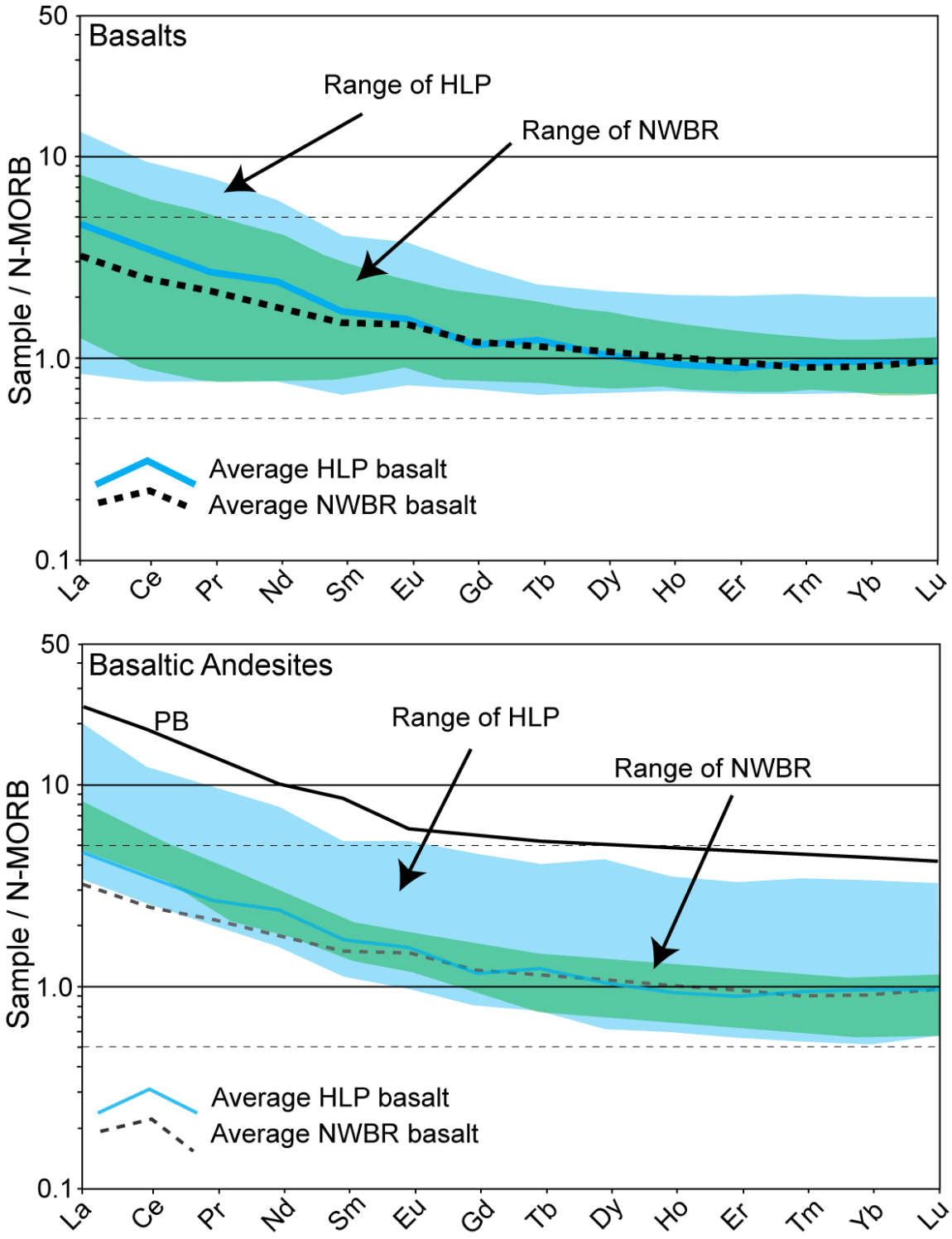
Basalts
Range of HLP
Range of NWBR
Sample / N-MORB
50
10
1.0
0.1
Average HLP basalt
Average NWBR basalt
La
Ce
Pr
Nd
Sm
Eu
Gd
Tb
Dy
Ho
Er
Tm
Yb
Lu
Basaltic Andesites
PB
Range of HLP
Range of NWBR
Sample / N-MORB
50
10
1.0
0.1
Average HLP basalt
Average NWBR basalt
La
Ce
Pr
Nd
Sm
Eu
Gd
Tb
Dy
Ho
Er
Tm
Yb
Lu

Figure 10B:

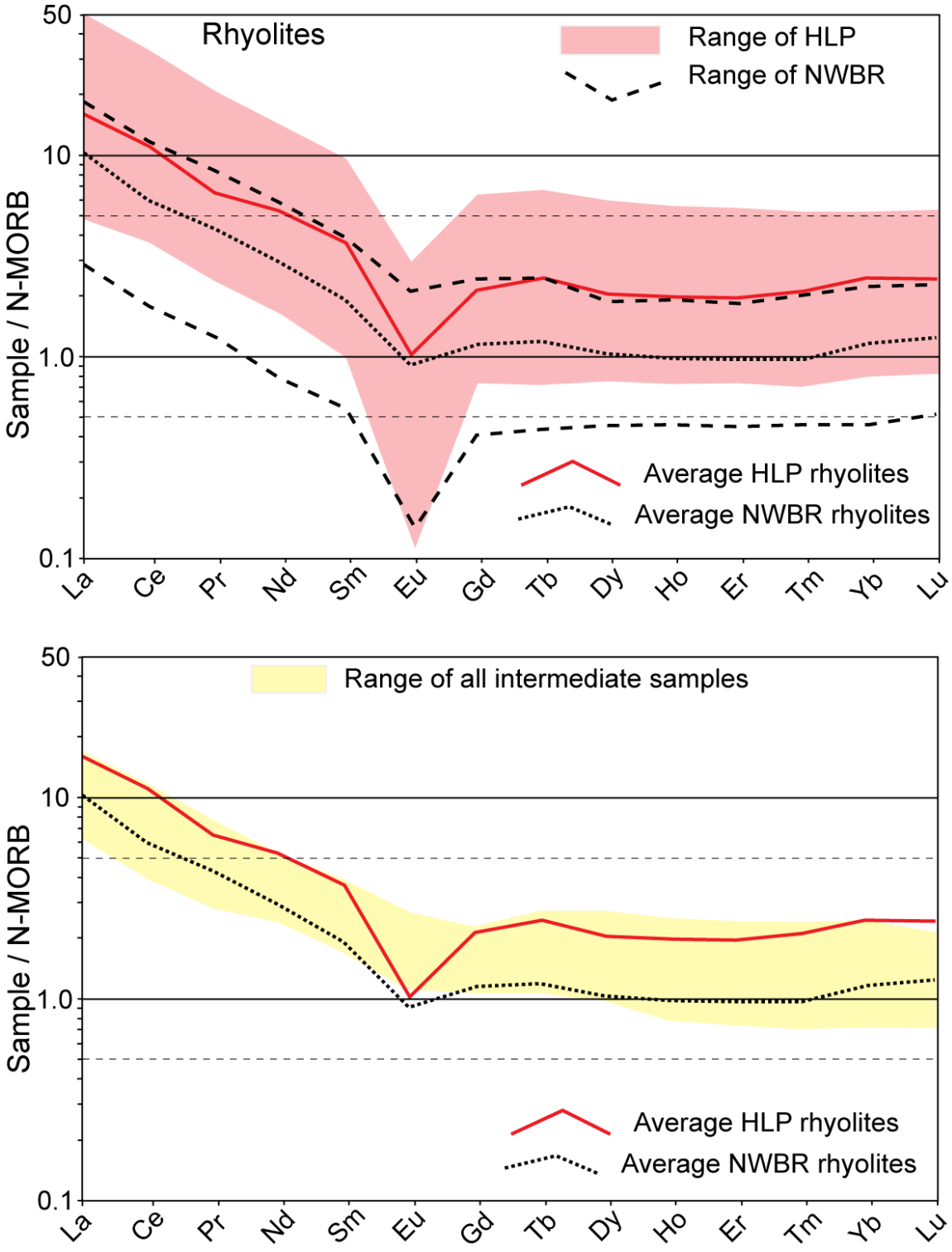
Rhyolites
Range of HLP
Range of NWBR
Average HLP rhyolites
Average NWBR rhyolites
Sample / N-MORB
50
10
1.0
0.1
La
Ce
Pr
Nd
Sm
Eu
Gd
Tb
Dy
Ho
Er
Tm
Yb
Lu
Range of all intermediate samples
Average HLP rhyolites
Average NWBR rhyolites
Sample / N-MORB
50
10
1.0
0.1
La
Ce
Pr
Nd
Sm
Eu
Gd
Tb
Dy
Ho
Er
Tm
Yb
Lu

Figure 11: Normalized spider diagrams. N-MORB normalized (Sun and McDonough, 1989) spider diagrams using the element order of Pearce and Parkinson (1993) with color-coding similar to that of Figure 10. A: basalts and basaltic andesites. Paiute Butte is shown dashed where inferred, based on similar patterns for other basaltic andesites. Ranges for NWBR basaltic andesites for REE, Cs, U, and Pb are likely underestimated due to limited data. B: Rhyolites and intermediate compositions. Data for some REE (Pr, Gd, Dy, Ho, Er, Tm) inferred for some samples, based on similar samples with complete data, for the HLP only.

Figure 11A:

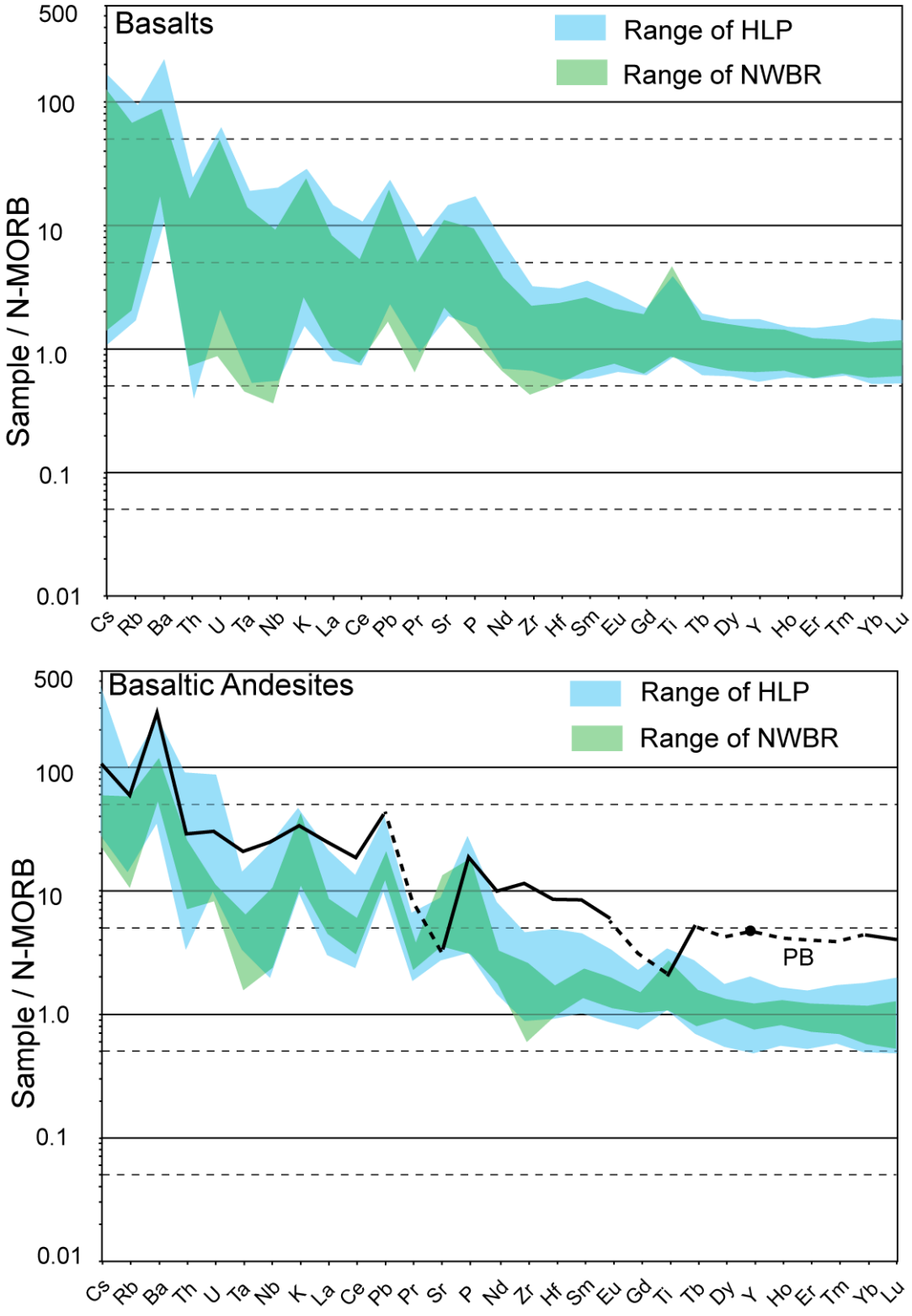
Basalts
Range of HLP
Range of NWBR
Sample / N-MORB
500
100
10
1.0
0.1
0.01
Cs Rb Ba Th U Ta Nb K La Ce Pb Pr Sr P Nd Zr Hf Sm Eu Gd Ti Tb Dy Y Ho Er Tm Yb Lu
Basaltic Andesites
Range of HLP
Range of NWBR
PB
Sample / N-MORB
500
100
10
1.0
0.1
0.01
Cs Rb Ba Th U Ta Nb K La Ce Pb Pr Sr P Nd Zr Hf Sm Eu Gd Ti Tb Dy Y Ho Er Tm Yb Lu

Figure 11B:

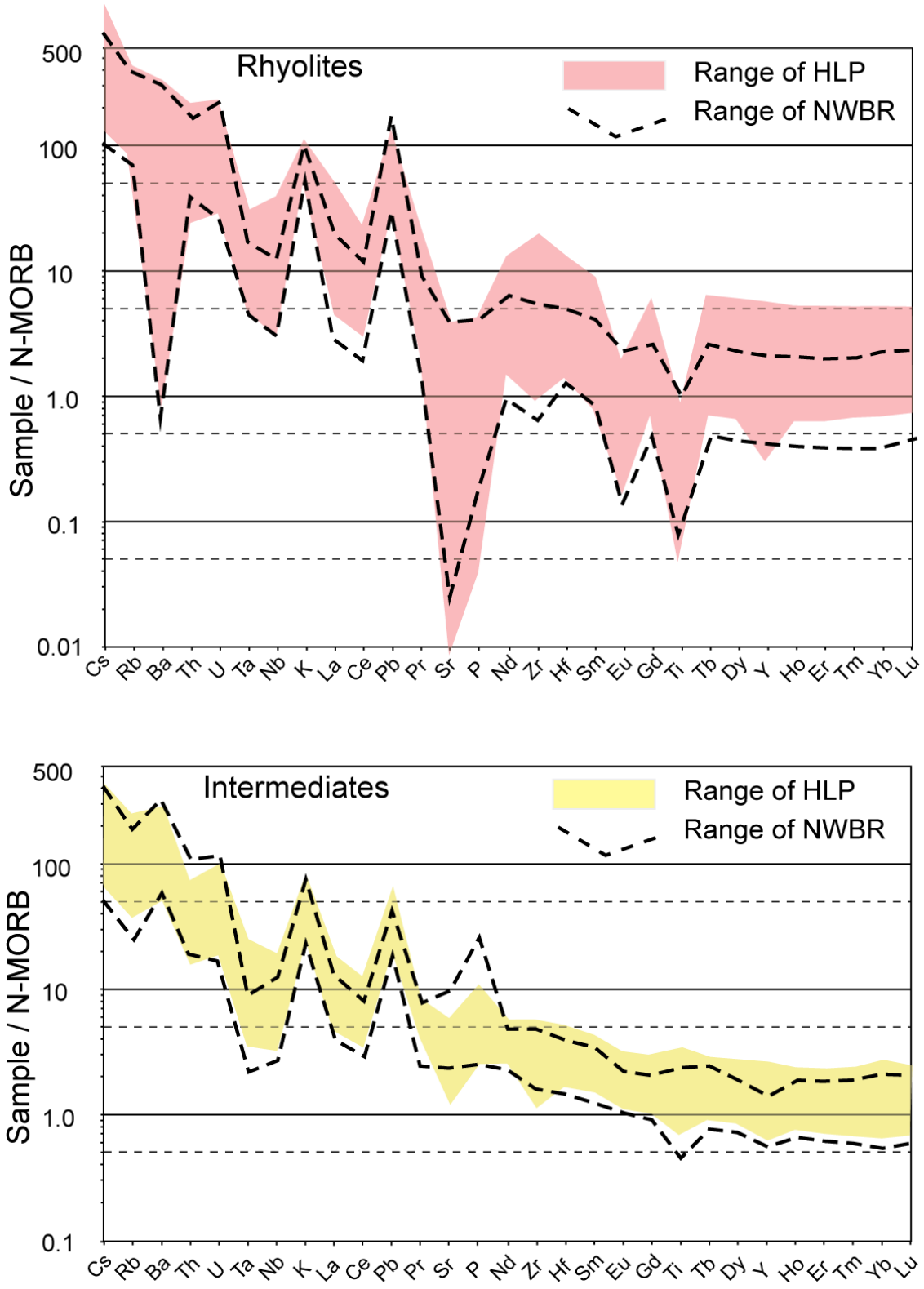
Rhyolites
Range of HLP
Range of NWBR
Sample / N-MORB
500
100
10
1.0
0.1
0.01
Cs Rb Ba Th U Ta Nb K La Ce Pb Pr Sr P Nd Zr Hf Sm Eu Gd Ti Tb Dy Y Ho Er Tm Yb Lu
Intermediates
Range of HLP
Range of NWBR
Sample / N-MORB
500
100
10
1.0
0.1
Cs Rb Ba Th U Ta Nb K La Ce Pb Pr Sr P Nd Zr Hf Sm Eu Gd Ti Tb Dy Y Ho Er Tm Yb Lu

Figure 12: FeO* vs. SiO_2 for the HLP, NWBR and other provinces. FeO* vs. SiO_2 plot for samples > 57% SiO_2 of the HLP and NWBR with symbols the same as in Figure 6 and Figure 7. A heavy black line separates the more tholeiitic samples from the physiographic HLP, including voluminous tuffs, and the more calc-alkaline samples of the northern Basin and Range (cf. Christiansen and McCurry, 2008). Newberry Volcano samples generally fall along the line. Fields represent more than 600 samples from Iceland and more than 900 samples from the Cascades along with an inset showing these data points. A field for the nearby SRP is also represented. The line generally separates HLP and Basin and Range (south of the HLP samples) andesite to low silica rhyolite (57 - 72 wt. % SiO_2) compositions but does not distinguish between high silica rhyolites well. High silica rocks of the study area are also not readily separated in other element variation diagrams, a characteristic that has been noted in other provinces (e.g. SRP by Christiansen and McCurry, 2008). Within the ellipse are mildly peralkaline compositions. The Cedar Butte trend (double headed arrow) is generally believed to be part of a fractionation trend from tholeiitic basalt to rhyolite in the SRP (McCurry et al., 2008). Stared points are from Whitaker et al. (2008) and are fractional crystallization experiments that started with tholeiitic basalt. The highest silica star (~69 wt. %) represents over 85% crystallization. Experimental partial melts inset shows results from the literature for partial melts of various basalts and amphibolite samples including red triangles – basaltic to basaltic andesite greenschists, Beard and Lofgren (1991); black triangles – a charnokitic xenolith from Kilbourne Hole, Beard et al. (1993); Open boxes – an amphibole-containing andesitic gneiss, Beard et al. (1994); diamonds, circles and purple squares – three different hornblende gabbors, Sisson et al. (2005) and brown box – Spulber and Rutherford (1983). Most of these partial melts are somewhat higher in Al_2O_3 and CaO and lower in K_2O than most HLP and NWBR compositions. This indicates a higher percentage of plagioclase is partially melted in most of these compositions than is required to produce the parental (low silica) rhyolites of the HLP and NWBR (cf. Figure 7).

Figure 12:

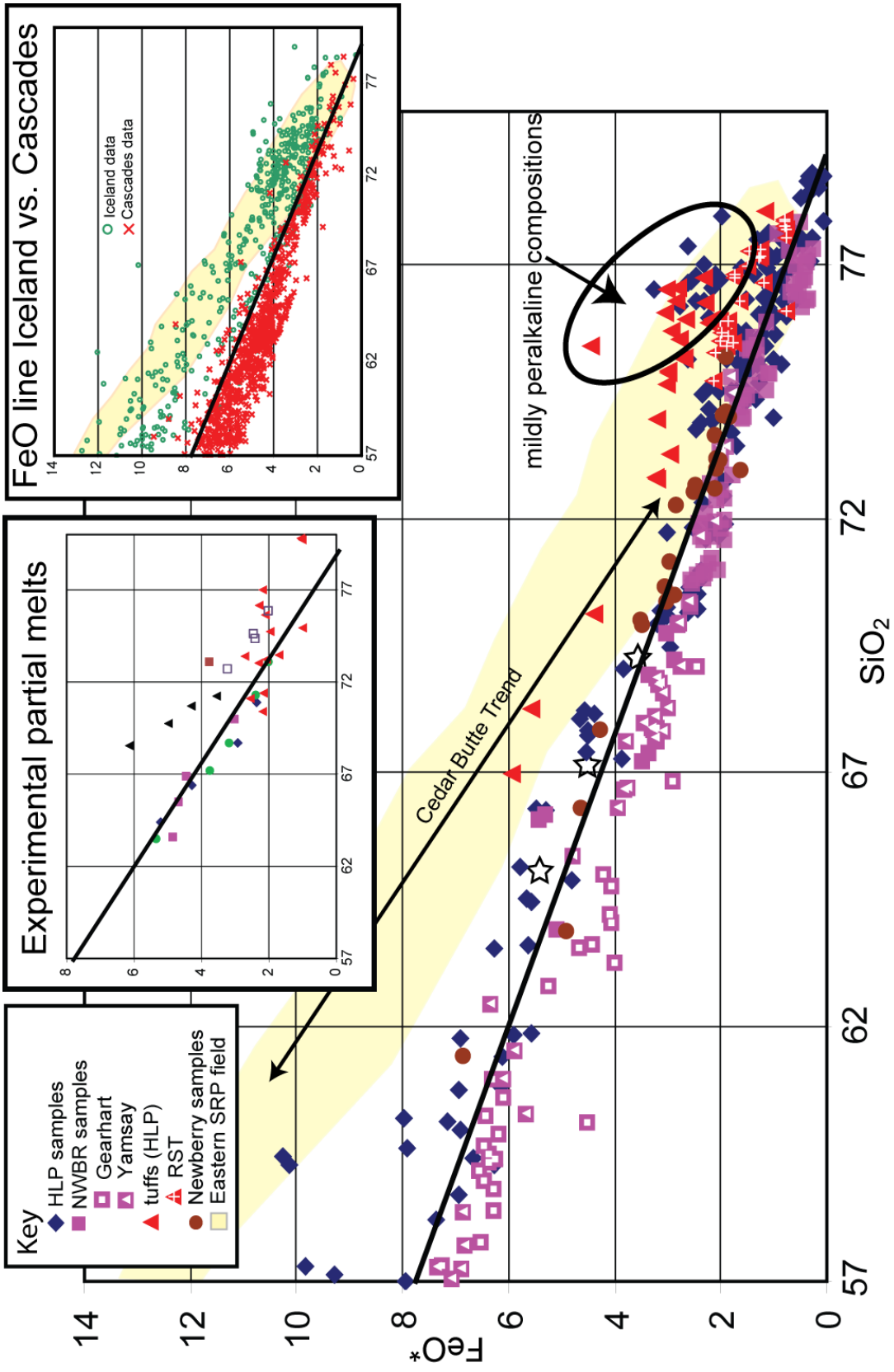
Key
HLP samples
NWBR samples
Gearhart
Yamsay
tuffs (HLP)
RST
Newberry samples
Eastern SRP field
Experimental partial melts
FeO line Iceland vs. Cascades
Iceland data
Cascades data
Cedar Butte Trend
mildly peralkaline compositions
FeO*
SiO2
0
2
4
6
8
10
12
14
57
62
67
72
77

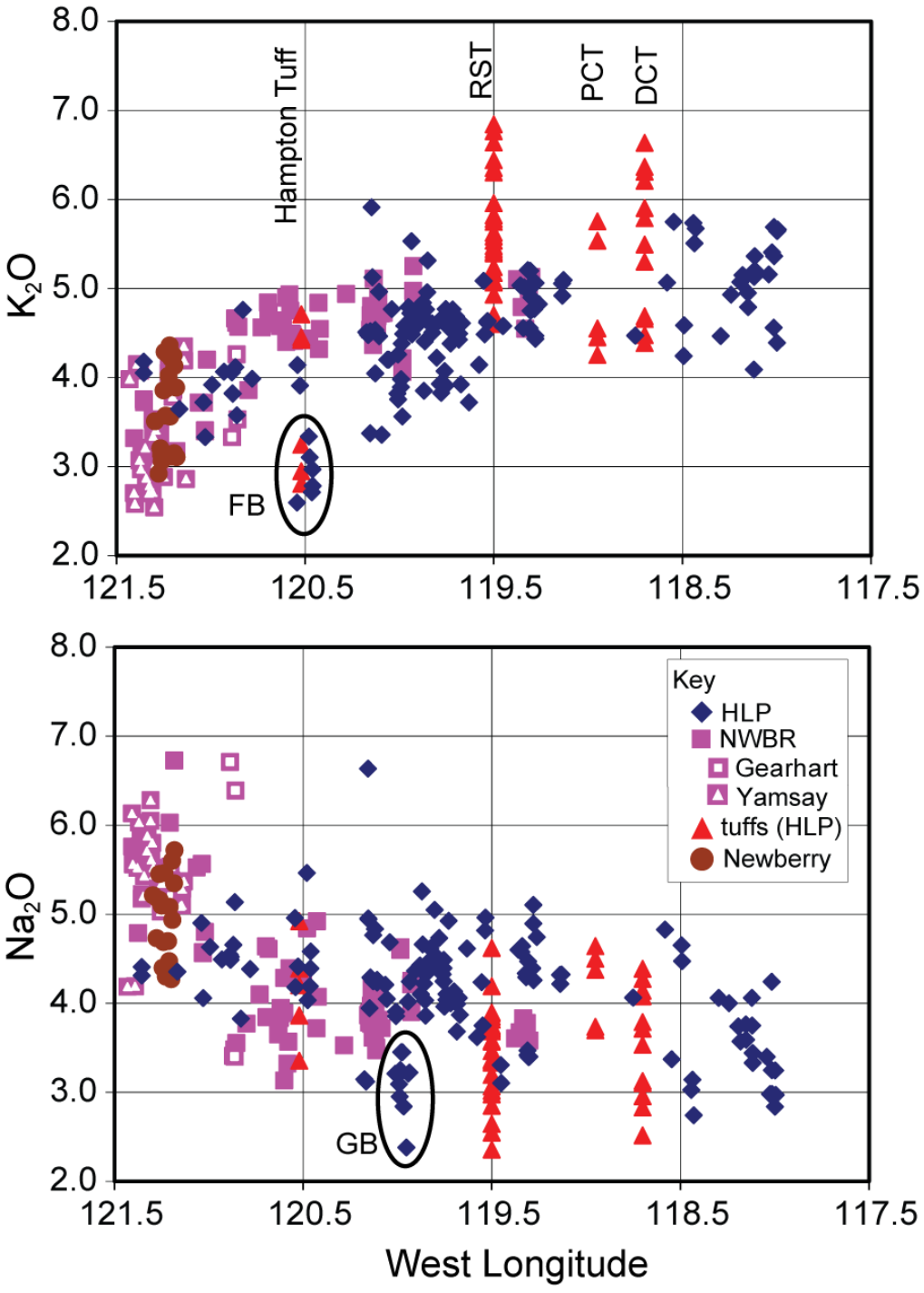

Figure 13: K_2O and Na_2O vs. longitude for HLP and NWBR silicic rocks > 66 wt. % SiO_2. Circled analyses in K_2O are from Frederick Butte (FB) rhyodacites while rhyolites from the same area plot with the larger HLP group. Some analyses from Glass Buttes (GB) have low Na_2O, perhaps due to glass hydration (see text). Major tuffs of the HLP are listed and symbols as in Figure 6.

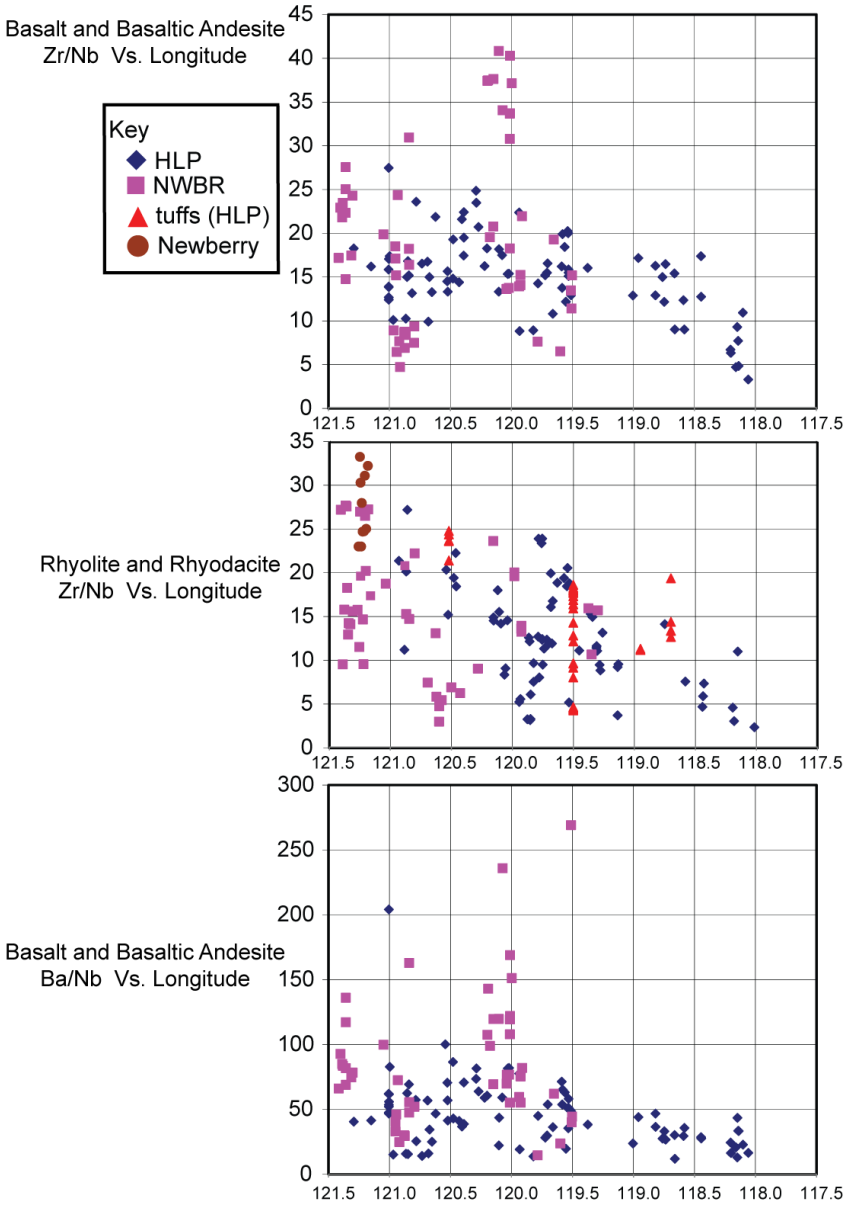

Figure 14: Zr/Nb and Ba/Nb ratios. Zr/Nb for basalts and basaltic andesites (up to 57 wt. % SiO_2) and rhyodacites and rhyolites (above 67 wt. % SiO_2) and Ba/Nb ratios for basalts and basaltic andesites versus longitude. Note that for basalts, NWBR samples have wider scatter and HLP ratios increase to the west. Rhyolite Ba/Nb not shown due to the effects of sanidine crystallization on Ba above about 74 wt. % SiO_2 (e.g. RST Ba/Nb ranges from 0.3 to 80 for units A to E) but intermediate to low silica rhyolites show a similar distribution as the basalts, with more scatter in the NWBR samples. Symbols are as in Figure 6 except that Gearhart Mountain and Yamsay Mountain are not differentiated from other NWBR samples.

Figure 15: Stretched color ramp of interpolated ages. Map with interpolated ages over much of the study area, with HLP and NWBR silicic centers in purple. Known ages less than 12 Ma represented (see key). Coloring indicates age and was created by an inverse distance (squared) weighted stretched color ramp. White space indicates that there was not sufficient data for interpolation. Green boxes are towns (B = Burns, L = Lakeview), heavy dashed line outlines physiographic HLP (Figure 1) and black lines are major roads. Proposed location for the RST from Streck and Grunder, 1997 and proposed locations, based in part from this map and field evidence (Grunder, unpublished) for other tuffs (Hampton, Prater Creek and Devine Canyon) shown with dashed circles. ^{40}Ar-^{39}Ar age for the Hampton Tuff from Iademarco, 2009. The following points were removed for this interpolation: The Deschutes Formation-aged 6.25 Ma Pine Mountain and 6.8 Ma China Hat and the 2.89 Ma Iron Mountain (shown in yellow text).

Figure 15:

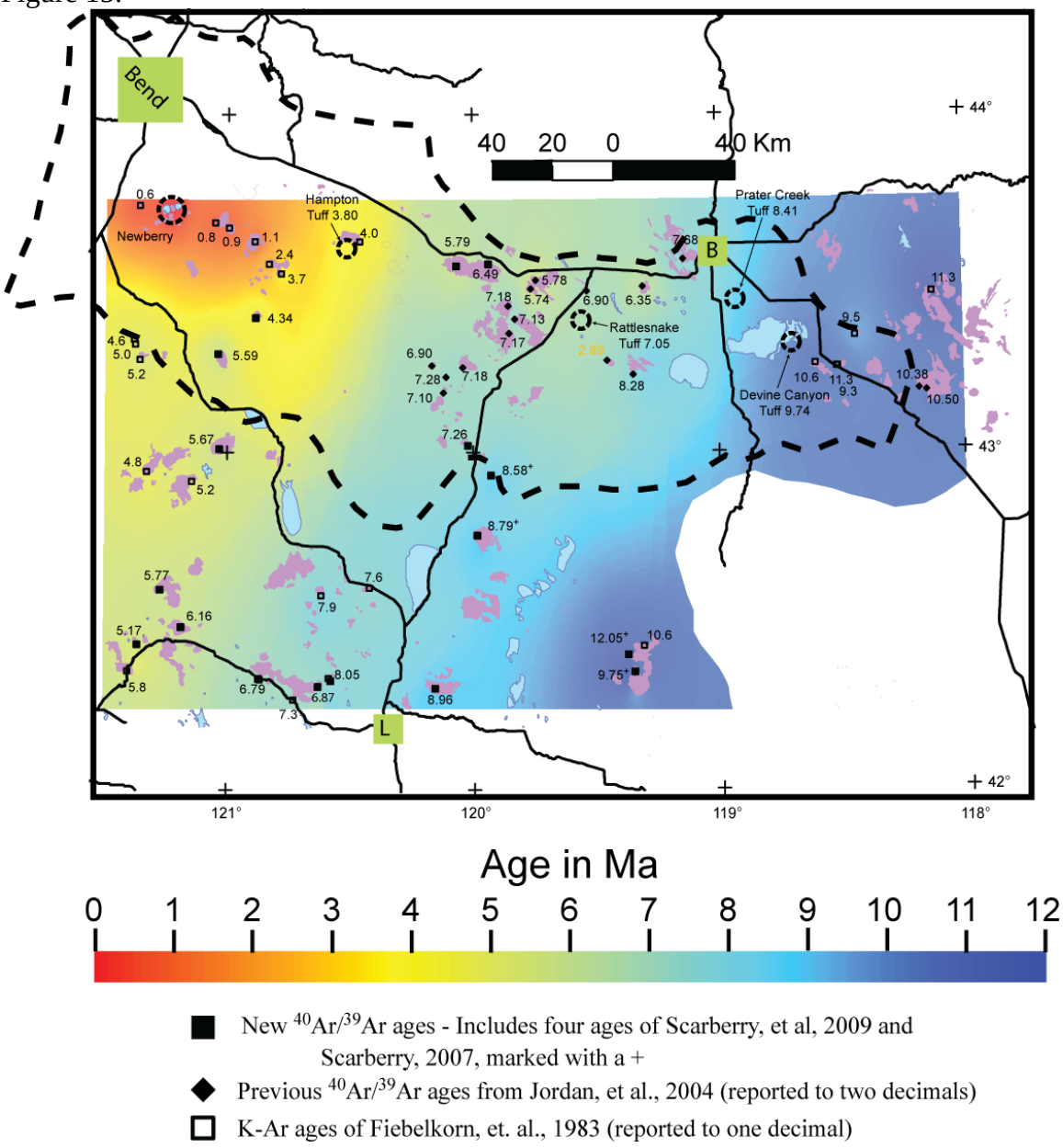
Bend
40 20 0 40 Km
Hampton Tuff 3.80
Prater Creek Tuff 8.41
Rattlesnake Tuff 7.05
Devine Canyon Tuff 9.74
Newberry
B
L
44°
43°
42°
121°
120°
119°
118°
Age in Ma
0 1 2 3 4 5 6 7 8 9 10 11 12
New 40Ar/39Ar ages - Includes four ages of Scarberry, et al, 2009 and Scarberry, 2007, marked with a +
Previous 40Ar/39Ar ages from Jordan, et al., 2004 (reported to two decimals)
K-Ar ages of Fiebelkorn, et. al., 1983 (reported to one decimal)

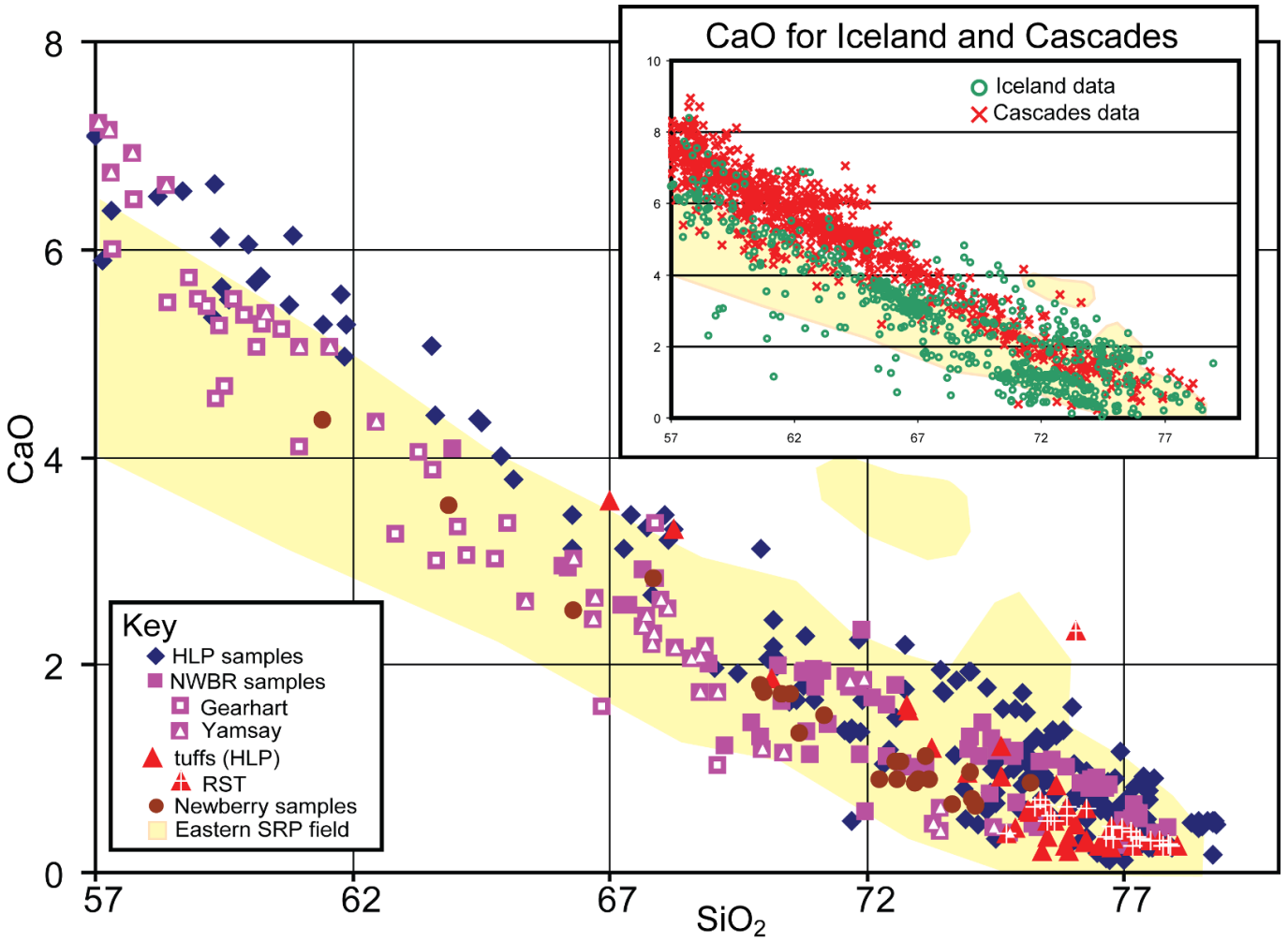

Figure 16: CaO vs. SiO_2 for the HLP, NWBR and other provinces. CaO vs. SiO_2 for samples > 57% SiO_2 of the HLP and NWBR with same key as in Figure 12 with similar inset from the Cascades, Iceland and SRP. While many HLP samples have higher CaO than NWBR samples, a subset of Icelandic samples also have higher CaO than Cascade samples. Peralkaline samples are uniformly low in CaO.

Figure 17: Log of Ba/Nb vs. SiO_2. Figure shows the log of Ba/Nb vs. SiO_2 for all samples of the HLP and NWBR with a similar key as Figure 12. Where no Nb values exist, 17.6 * Ta values were used. These ratios, either Ba/Nb or Ba/17.6*Ta, approximate closely N-MORB normalized values. Inset represents Cascade and Iceland data (Ba/Nb only), with linear scale. Heavy dashed line is at Ba/Nb = 20 in both plots. Double arrow line shows likely mixing of mafic and silicic samples, as discussed earlier.

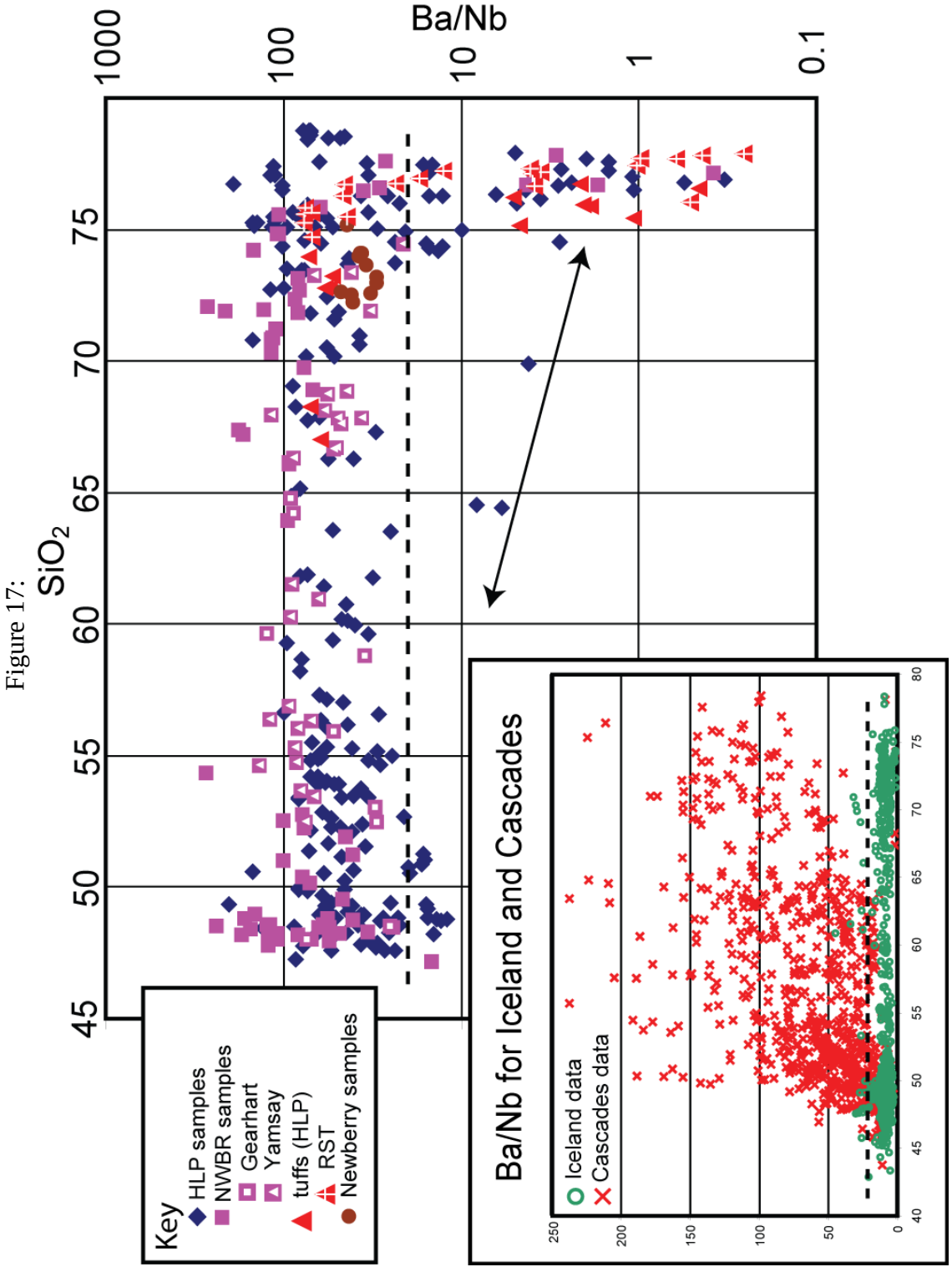
Ba/Nb
1000
100
10
1
0.1
SiO2
45
50
55
60
65
70
75
Key
HLP samples
NWBR samples
Gearhart
Yamsay
tuffs (HLP)
RST
Newberry samples
Ba/Nb for Iceland and Cascades
Iceland data
Cascades data
250
200
150
100
50
0
40
45
50
55
60
65
70
75
80

Figure 17:

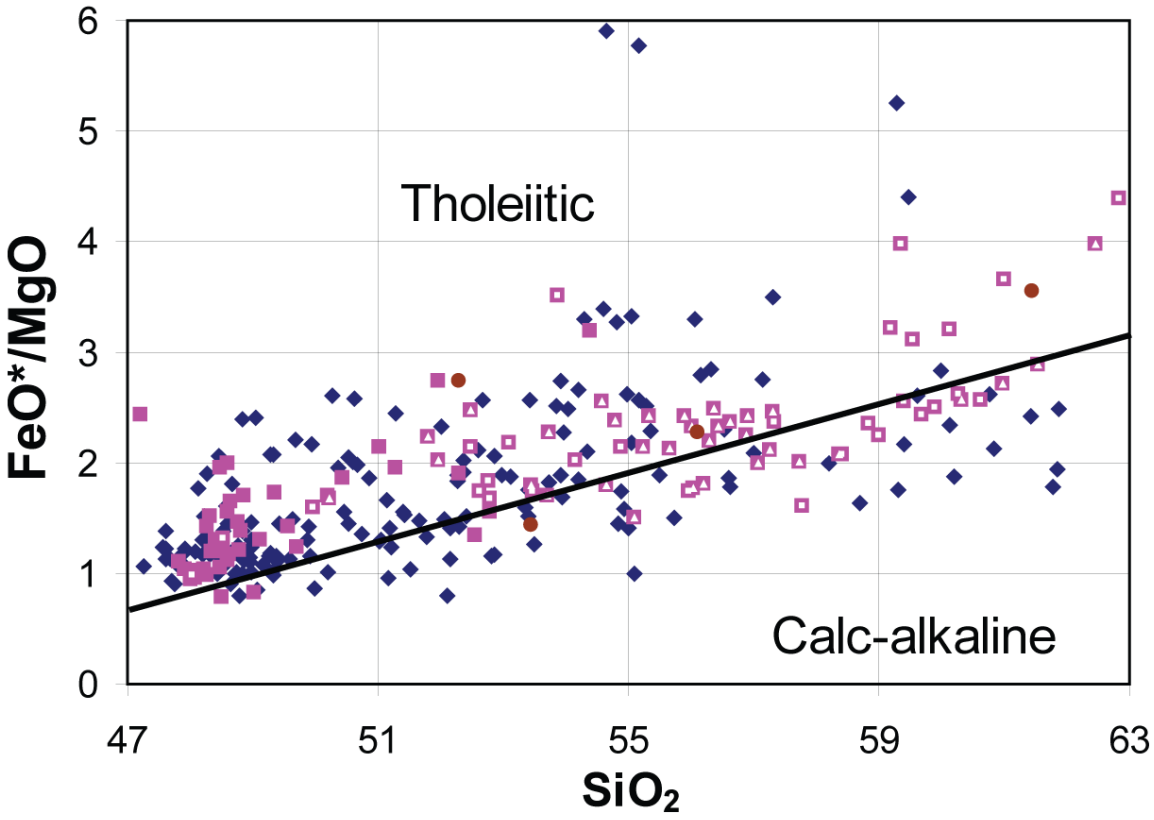

Figure 18: Miyashiro (1974) classification of mafic rocks from the HLP and NWBR. A majority of basalts or basaltic andesites are tholeiitic. There is no east-west spatial separation of the samples (Jordan, 2001) and no HLP vs. NWBR separation based on this classification. As basalts become more silica rich or "evolved", there is wider scatter and an increasing number samples classified as calc-alkaline (cf. Jordan, 2001). Symbols as in previous figures.

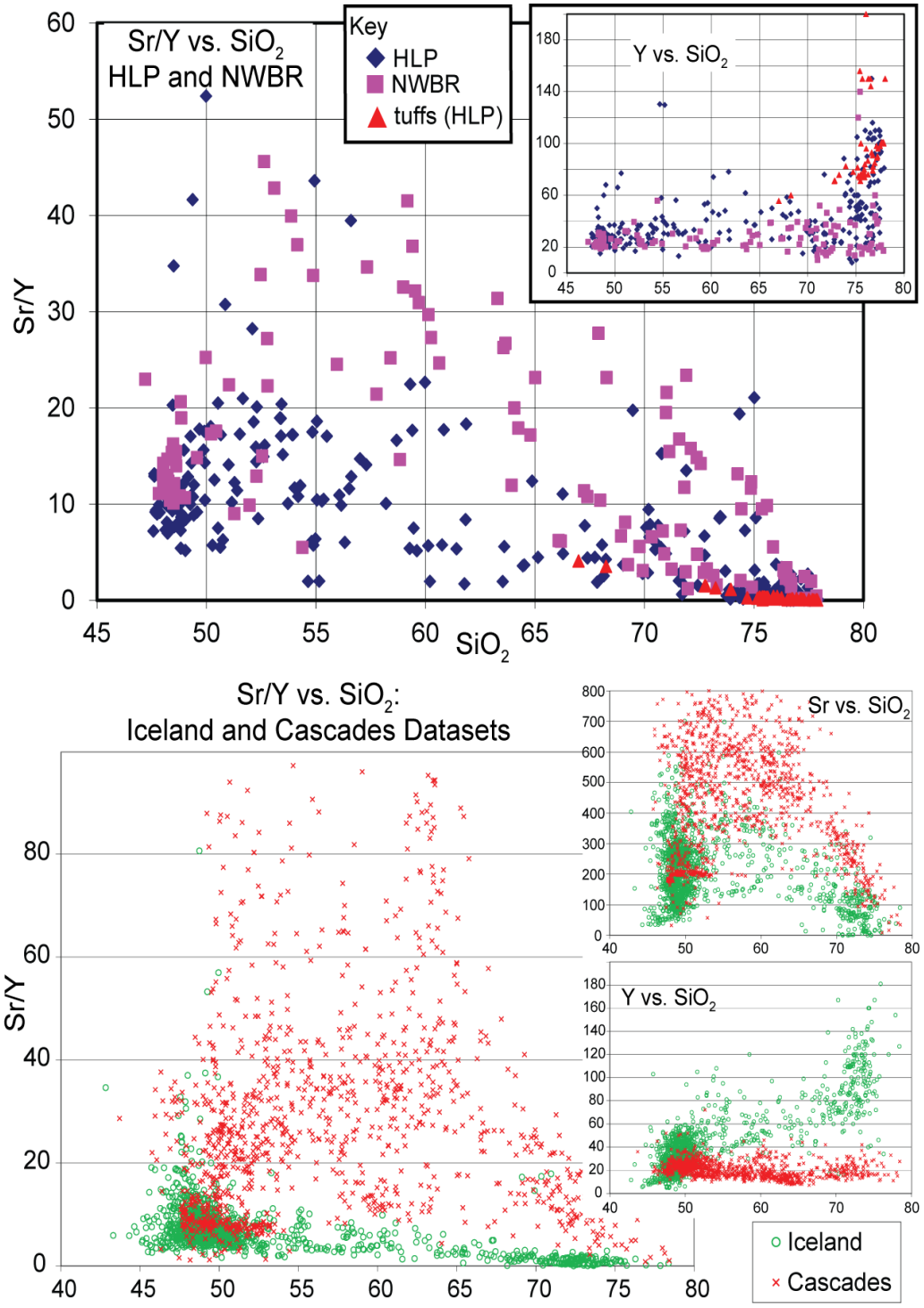

Figure 19: Sr/Y vs. SiO_2 for the HLP and NWBR (top) and for Iceland and Cascades (bottom). Inset for HLP- NWBR diagram shows data for Y vs. SiO_2 (see Figure 9 for Sr vs. SiO_2). Inset for Iceland – Cascades suite shows data for both Y and Sr vs. SiO_2. Symbols are similar to Figure 12. There are no Y data from Newberry Volcano.

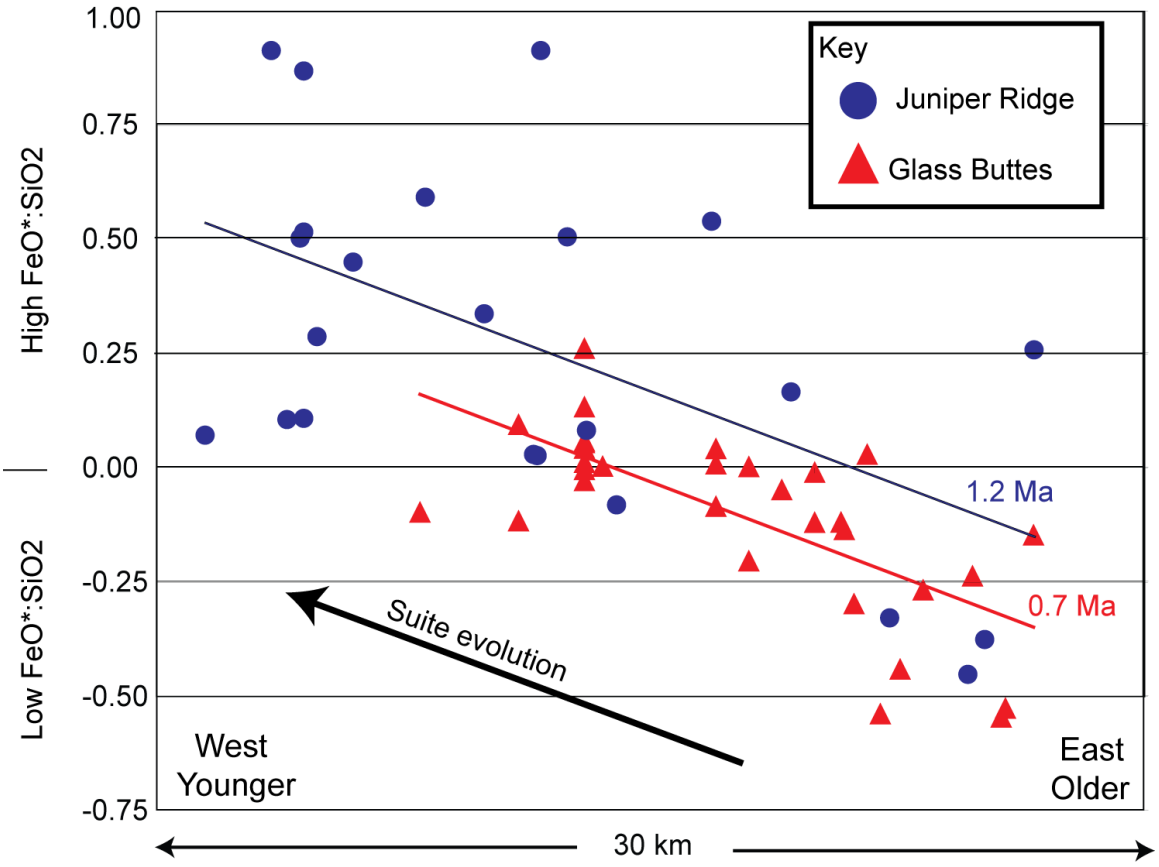

Figure 20: Evolution to higher FeO* in time for Juniper Ridge and Glass Buttes. Each evolves to higher FeO* at a given SiO_2 over time, at nearly the same rate. Y-axis is how far above (high FeO*) or below the Fe-line (Figure 12) each sample is at their SiO_2 content. Lines are least squares best fit lines through each data (R^2 = 0.3 for Juniper Ridge and 0.5 for Glass Buttes) set and length of the line is proportional to the duration of volcanism for each suite. The overall trend for the HLP (excluding peralkaline samples) shows a similar trend (Figure 21).

Figure 21: Spatial separation of low and high FeO* samples. Hillshade DEM of the HLP – NWBR showing low FeO* at given silica compositions are prevalent in the NWBR. More variability in the eastern HLP in FeO* content gives way to higher FeO* contents as the crust becomes more mafic through time due to intraplated basaltic magmas and mafic residuum from partial melting (basaltification) of the crust, resulting in high FeO* at given silica further west, similarly to individual suites (Figure 20). Proposed or known tuff sources given by dashed circles. The HLP has a higher basaltic flux and therefore heat flux into the crust, resulting in the different compositions for rhyolites.

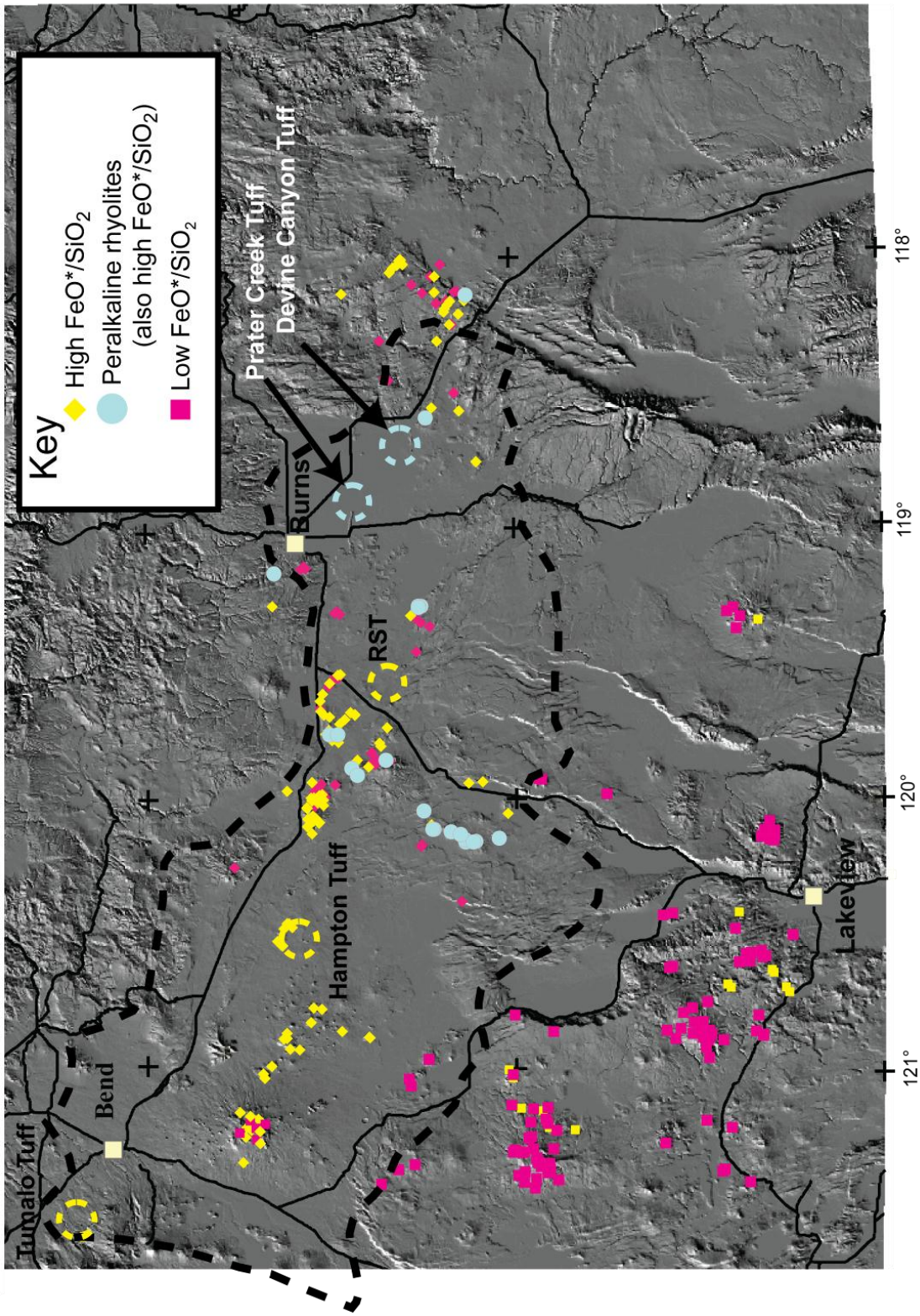
Key
High FeO*/SiO2
Peralkaline rhyolites
(also high FeO*/SiO2)
Low FeO*/SiO2
Prater Creek Tuff
Devine Canyon Tuff
Burns
RST
Hampton Tuff
Tumalo Tuff
Bend
Lakeview
118°
119°
120°
121°

Figure 21:

Figure 22: Resolving asthenopheric flow and plate motion to create the HLP volcanic trend. A: Four time slices at 10.5 Ma (Duck Butte), 7.1 Ma (RST), 3.9 Ma (Frederick Butte and Hampton Tuff) and 0 Ma (Newberry Volcano, present day) showing the positions of subsequent eruptions with the motion of the North American Plate (26 km/Ma). Colors for eruptions from previous time slices are muted. Inset B shows simplified geologic map of the HLP with the four episode discussed (compare to Figure 4D). Surface expression of HLP rhyolitic volcanism moves WNW at ~33 km/Ma as shown in inset C (after Jordan et al, 2004) but the rate slows at ~ 4 Ma (see text). The four episodes discussed are plotted (NB = Newberry Volcano). Dotted box in A indicates where volcanism would plot if the HLP volcanic trend rate had remained at 33 km/Ma, approximately 25 km south of South Sister Volcano (SS) in the Cascades. D: Histogram showing shear wave splitting (SKS phases) delay times for the HLP (Long, et al. 2009) with black arrow from this data. Figure is to scale indicating westward asthenopheric flow rate is generally uniform, averaging 53 km/Ma from 10.5 to 4 Ma.

Figure 22:

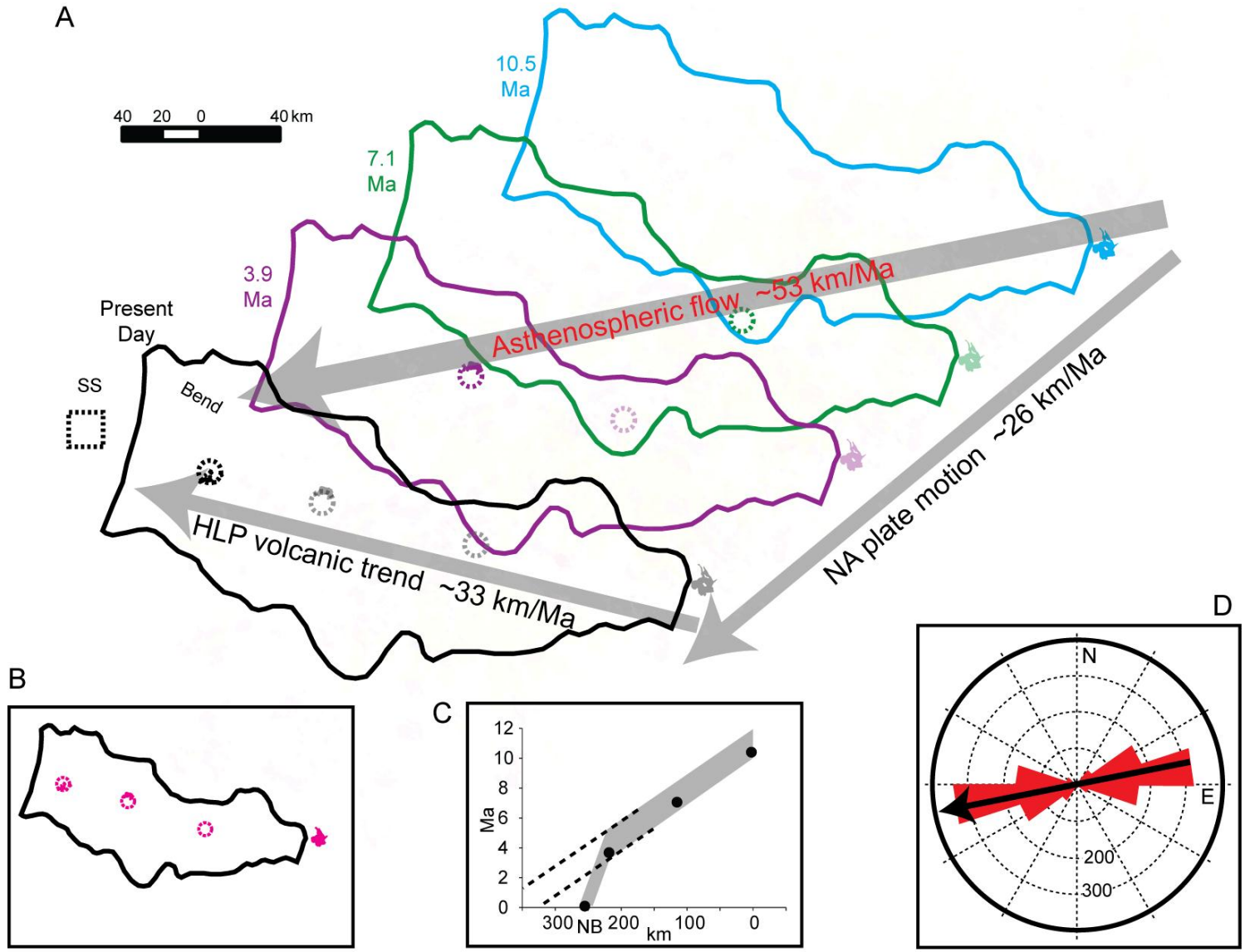
A
40 20 0 40 km
10.5 Ma
7.1 Ma
3.9 Ma
Present Day
SS
Bend
Asthenospheric flow ~53 km/Ma
NA plate motion ~26 km/Ma
HLP volcanic trend ~33 km/Ma
B
C
12
10
8
6
4
2
0
Ma
300 NB 200 km 100 0
D
N
E
200
300

TABLES:

Table 1: Representative whole rock major and trace element compositions of rhyolites from the HLP and NWBR. For methods used, see text, Appendix 2 and references. Date key as follows: *italicized* are from this work (see Table 2); **emboldened** from Jordan et al., 2004; single asterisk (*) K-Ar data from Fiebelkorn et al., 1983; (**) are inferred from field relations and dated samples. Errors for ^{40}Ar-^{39}Ar dates are at 1 standard deviation. Latitude and longitude (NAD 1927) given to appropriate significant digits, asterisk (*) is inferred vent location. Location gives position of the sample, either in the physiographic HLP or NWBR (Figure 1, 21). Affinity is the position of the sample with regards to the Fe-Line (Figure 12) where thol. = tholeiitic indicating the sample has high FeO* at a given SiO_2, like the SRP or Iceland and calk-alk. = calk-alkaline indicating the sample plots below the Fe-line, like most Cascades samples. All major elements normalized to 100% anhydrous, with pre-normalized totals (PNT) given.

Standard errors on precision for compositions are given at 95% confidence interval, calculated from t-distributions, compiled from duplicate analyses and given in either weight percent or ppm (XRF, n = 4 and ICP, n = 7 except Y and REE, n = 6). Very low concentrations of some analytes (e.g., Ba, Sr) may have smaller errors than stated. This error is applicable to "silicic" (generally > ~ 60 wt. % SiO_2) MTF and KCS samples and can be generally applied to other samples analyzed by the same methods (See Appendix 1 and Appendix 2). For a more detailed treatment of errors and errors for other methods not covered here, see Appendix 1. For values, significant digits indicate the level of precision, except where reduced due to alternative, less precise methods or larger uncertainties in some of the published work. Blank values indicate that the analyte was not analyzed and zero values indicate the analyte was below detection limit. Additional sources include: RST (Streck and Grunder, 1997), Juniper Ridge (MacLean, 1994), Duck Creek Butte (Johnson and Grunder, 2000). See Appendix 1 and Electronic Data Supplement for more data.

Sample No	RT173H	RT173A	MTF 07-10	HP-91-10	JR-91-13	MTF 07-12	JR-92-56	JJ 92-1
age	**7.093**	**7.093**	*9.63*	**7.096**	5.8**	4.0	**6.90**	**10.50**
error	**0.015**	**0.015**	*0.03*	**0.015**		0.4*	**0.02**	**0.03**
Lat	43.33*	43.33*	43.4538	43.1776	43.480	43.6198	43.477	43.1711
Long	119.5*	119.5*	118.1844	120.119	119.751	120.4635	119.533	118.1514
location	HLP	HLP	HLP	HLP	HLP	HLP	HLP	HLP
style	tuff	tuff	tuff	dome	dome	dome	dome	dome
affinity	thol	thol	thol	thol	thol	thol	thol	calc-alk
local name	RST A	RST E	DCT	Horse Mt.	Juniper Rdg.	Frederick B.	Juniper Rdg.	Duck Creek B.
SiO2	77.74	75.87	76.54	76.49	77.19	68.24	73.92	70.19
TiO2	0.11	0.16	0.198	0.202	0.07	0.760	0.21	0.55
Al2O3	11.97	12.50	10.85	10.43	12.16	14.65	13.40	14.51
FeO*	0.78	2.01	2.80	3.25	1.09	4.55	2.17	3.15
MnO	0.08	0.10	0.056	0.101	0.03	0.103	0.09	0.07
MgO	0.05	0.01	0.08	0.00	0.02	1.29	0.08	0.80
CaO	0.26	0.54	0.26	0.18	0.83	3.31	0.51	2.18
Na2O	3.46	4.19	3.71	4.83	3.96	4.19	4.96	3.59
K2O	5.53	4.60	5.49	4.50	4.64	2.71	4.63	4.79
P2O5	0.02	0.02	0.013	0.020	0.01	0.19	0.02	0.18
PNT	99.51	99.26	96.32	99.11	99.56	99.51	99.48	96.46
Rb	122	62	134	123	105	66.1	109	115
Ba	39	2030	36.5	175	332	890	1170	1630
Sr	2.1	22.5	6.1	0.5	12.5	193	8	283
Zr	175	474	1160	733	207	233	513	242
Nb	39.4	26.8	80.5	40.7	21.8	10.5	27.3	22
Y	100	77	144	108	87.5	45.5	61.2	30
Pb	20.0	13.1	31.0	28.5	17.7	9.9	15.4	
Zn	88	120	234	191	106	64	86	
V	0	4	2	0	2	60	0	
Cu	1	4	6	5	4	13	6	
Ni	14	10	0	14	13	1	9	
Cr	0	0	2	2	2	9	0	6
Sc	3.9	4.5	1.1	0.8	0.8	13	6.9	6.2
Ga	17.6	19.0	27.3	22.6	19.0	16.8	17.8	
Cs	4.48	2.33	4.42	5.8	3.49	2.57	4.86	3.28
U	4.94	2.68	5.7	4.6	4.11	2.84	4.17	4.62
Th	9.5	5.7	14.0	13.3	8.8	6.9	9.4	10.4
Hf	7.1	11.2	25.6	17.1	7.9	6.5	12.4	5.5
Ta	2.16	1.36	4.97	2.3	1.31	0.83	1.55	1.20
La	19.9	51.9	90	62	20.2	26.0	36.2	34.2
Ce	49	120	188	139	54	50	80	62
Pr			23.8			7.3		
Nd	28	61	93	68	29.3	30.5	36.7	26.5
Sm	9.6	13.6	22.5	16.2	10.8	7.5	8.0	5.2
Eu	0.65	2.6	0.72	1.37	0.62	1.79	1.13	1.16
Gd			23.1			7.7		
Tb	2.22	2.16	4.1	2.86	2.06	1.34	1.51	0.77
Dy			26.7			8.4		
Ho			5.6			1.74		
Er			16.0			4.9		
Tm			2.37			0.72		
Yb	10.5	8.0	15.2	11	9.2	4.6	6.8	3.33
Lu	1.61	1.24	2.39	1.58	1.24	0.73	0.99	0.44
Sb	1.6	1.1		2.5	0.8		0.7	0.7
As	4.4	4.2		14.6	4.4		3.1	1.5
Co	0.1	0.1		0.2	0.2		0.4	4.6

Sample No	JR-92-54	MTF 07-49	MTF 07-58	MTF 07-29	MTF 07-30	MTF 07-14	Std error
age	6.9**	*5.17*	*8.96*	*8.05*	*6.87*	*5.67*	95%
error		*0.05*	*0.03*	*0.02*	*0.04*	*0.08*	confidence
Lat	43.483	42.4307	42.3013	42.3242	42.3072	43.0103	interval
Long	119.548	121.3598	120.1561	120.5787	120.6293	121.0304	wt % or ppm
location	HLP	NWBR	NWBR	NWBR	NWBR	NWBR	
style	dome	dome	dome	dome	dome	dome	(see Appendix 1
affinity	calc-alk	calc-alk	calc-alk	calc-alk	thol	thol	for more detail
local name	Juniper Rdg.	Bug B.	Drakes Peak	Cox Flat	Cougar Peak	Hagar Mt.	regarding errors)
SiO2	72.75	70.84	72.12	76.71	75.60	66.19	0.06
TiO2	0.32	0.468	0.305	0.061	0.187	0.93	0.003
Al2O3	14.33	15.46	14.81	13.46	13.27	15.17	< 0.03
FeO*	1.93	2.31	2.29	0.49	1.36	5.31	0.07
MnO	0.04	0.065	0.064	0.070	0.032	0.130	0.005
MgO	0.57	0.26	0.21	0.05	0.16	1.04	0.02
CaO	1.76	1.36	1.69	0.84	1.09	2.93	< 0.02
Na2O	3.75	5.95	3.86	3.57	3.67	4.57	< 0.02
K2O	4.48	3.18	4.54	4.75	4.58	3.41	< 0.01
P2O5	0.07	0.123	0.121	0.008	0.058	0.33	< 0.01
PNT	99.44	99.53	98.53	97.08	99.04	99.12	
Rb	114	47.1	61.7	142	107	102	0.35
Ba	1220	1010	1720	46.6	870	1020	12.7
Sr	122	191	251	27.3	145	239	1.0
Zr	251	241	154	59	108	291	1.3
Nb	12.2	8.8	6.5	10.9	8.2	11.1	0.15
Y	26	26.5	15.9	15.7	14.7	39.0	0.2
Pb	12.1	11.7	16.1	26.9	19.2	12.3	0.15
Zn	36	47	44	23	34	79	1.7
V	18	21	25	0	13	59	1
Cu	8	3	12	0	6	15	1.5
Ni	6	0	0	0	0	0	
Cr	4	2	3	1	3	4	0.5
Sc	4.8	6.2	4.1	3.0	2.7	14	0.4
Ga	14.0	19.4	15.6	16.9	14.2	18.8	0.5
Cs	5.47	0.71	0.98	5.24	3.64	2.07	0.02
U	4.70	1.69	1.30	5.0	4.20	5.2	0.02
Th	10.9	4.3	4.1	8.6	10.9	12.9	0.08
Hf	6.5	6.7	4.18	3.20	3.55	7.7	0.06
Ta	0.94	0.57	0.54	1.23	0.87	0.79	0.01
La	22.5	22.2	33.8	9.8	29.0	26.6	0.42
Ce	47	45	56	17.8	50	58	0.60
Pr		6.0	5.9	2.07	5.3	7.3	0.09
Nd	19.9	23.5	20.0	7.3	17.9	30.5	0.37
Sm	3.67	5.1	3.55	1.71	3.15	7.2	0.09
Eu	0.71	1.17	0.91	0.20	0.49	1.92	0.01
Gd		4.42	2.93	1.69	2.59	7.1	0.06
Tb	0.62	0.74	0.46	0.31	0.41	1.18	0.02
Dy		4.71	2.81	2.08	2.47	7.3	0.08
Ho		1.00	0.58	0.47	0.52	1.54	0.01
Er		2.92	1.67	1.51	1.52	4.3	0.05
Tm		0.47	0.26	0.27	0.25	0.64	0.01
Yb	2.98	3.12	1.78	2.00	1.67	4.1	0.05
Lu	0.49	0.50	0.30	0.35	0.28	0.67	0.01
Sb	0.8						
As	3.1						
Co	2.9						

Table 2: New age determinations from this study. In all cases, the plateau age and inverse isochron age are within 2σ of each other and the plateau age is preferred. WR = whole rock mini-core, san = sanidine mineral separate, bt = biotite mineral separate, plag = plagioclase series mineral separates with whole rock K_2O values given. See Figure 5 for age spectra from each sample and Electronic Data Supplement for Excel sheets and original .age files (ArArCalc files).

Sample	Local name	Age type	wt. % K2O if WR	**Accepted (plateau) age**	2 sigma Error	2 sigma percent	% radio-genic Ar 40	Reverse isochron age	2 sigma error
MTF 07-04	Glass Buttes "A"	WR	4.20	**5.79**	0.04	0.75	98.49	5.74	0.11
MTF 07-05	Glass Buttes "E"	WR	4.48	**6.49**	0.05	0.80	100	6.49	0.06
MTF 07-38	North Connelly Hills	WR	3.72	**5.59**	0.05	0.86	77.7	5.59	0.07
MTF 07-16	Cougar Mt (Lake Co.)	WR	3.82	**4.34**	0.05	1.08	99.59	3.92	0.58
MTF 07-10	Devine Canyon Tuff	san		**9.63**	0.05	0.55	94.93	9.61	0.06
KCS 06-06	Alkali Buttes	san		**7.26**	0.05	0.66	100	7.25	0.05
MTF 07-49	Bug Butte (top)	plag		**5.17**	0.09	1.65	98.57	5.10	0.10
MTF 07-37	Spodue Mt (top)	plag		**5.77**	0.07	1.19	100	5.81	0.12
MTF 07-58	Drake Peak (Trf)	plag		**8.96**	0.06	0.64	95.84	8.95	0.13
MTF 07-52	Quartz Mountain Pass	bt		**6.79**	0.04	0.58	80.32	6.81	0.08
MTF 07-30	Cougar Peak (top)	plag		**6.87**	0.07	1.06	55.55	6.94	0.08
MTF 07-29	Dome south of Cox Flat	san		**8.05**	0.04	0.52	99.84	8.07	0.06
MTF 07-14	Hagar Mountain (top)	plag		**5.67**	0.16	2.83	100	5.73	0.28
MTF 07-53	Fergason Mountain	plag		**6.16**	0.04	0.62	99.66	6.16	0.06
MTF 07-34	Bald Butte	san		**17.53**	0.08	0.45	97.12	17.54	0.10
MTF 07-26	Drum Hill	plag		**17.30**	0.09	0.53	98.71	17.33	0.11
MTF 07-57	Twenty Mile Creek	san		**15.03**	0.08	0.56	100	15.04	0.09
MTF 07-02	Pine Mountain	WR	2.75	**6.25**	0.03	0.52	43.67	6.25	0.04

Table 3: Estimated volumes for the different episodes of volcanism expressed in the < 12 Ma HLP and NWBR. Additional volumes of the Deschutes and some Newberry related flows extend outside the physiographic HLP and NWBR and are not included here. Total eruptive volumes considered for this study (see text) are 1,000 – 1,250 km^3 of basaltic, 950 – 1,250 km^3 of rhyolitic and ~ 100 km^3 of intermediate composition volcanics.

Location	Minimum (cubic km)	Maximum (cubic km)
Deschutes Formation	negligible	100
This study, 12 - 0 Ma HLP and NWBR	2,000	2,500
Newberry related, including basalts	800	1,000
Total	2,800	3,600

Table 4: Phenocryst assemblage detail from this work. SiO_2 content is given to help cross reference samples in Table 1 or Appendix 1. Aph = aphyric, with an asterisk (*) indicating very few phenocrysts are present; diseq. texture indicates if disequilibrium textures are either X = limited but present, XX = prevalent, or XXX = pervasive; type is the type of sample that was examined where wr = whole rock and ts = thin section. For phases, qtz = quartz, alk feld = alkali feldspar (Na or K), plag = plagioclase (generally andesine or more calcic), cpx = clinopyroxene, opx = orthopyroxene, fa = fayalite, amph = amphibole, bt = biotite, op = opaque minerals where X = very uncommon or not present in all samples from that location, XX = sparse, but generally present, XXX = commonplace. Where left blank, phase was not observed. For whole rock determination, phenocryst and disequilibrium texture evaluation may not be complete, especially for dark colored phase in dark samples. While no disequilibrium textures were observed in NWBR samples, most only contain a whole rock characterization and such textures are prevalent in the literature (Appendix 4).

Samples from the HLP													
	SiO2	aph*	diseq.	type	qtz	alk	plag	cpx	opx	fa	amph	bt	op
			texture			feld				(ol)			
MTF 07-04	77.42	X		wr									
MTF 07-05	77.30	X		wr									
MTF 07-06	73.49			ts		XXX	XXX				XXX	XXX	XX
MTF 07-08	74.51	X		wr									
MTF 07-09	74.93	X		wr									
MTF 07-11	76.01			wr			X				XXX	XXX	
MTF 07-16	77.08	X		wr									
MTF 07-32	75.51	X		wr									
MTF 07-39	69.03			wr			XXX	X	X		X	X	
KCS-06-06	71.83			wr		XXX							
HP-91-2	74.45	X*		wr			XX						
HP-91-3	73.46			wr		XXX	XXX				XXX	XXX	XX
HP-91-4	73.42			wr		XXX	XXX				XXX	XXX	XX
HP-91-5	74.34			ts		X	XXX					XXX	XX
HP-91-10	76.49	X		ts									
HP-91-11	75.02			ts		XXX	XXX				XX	XXX	XX
HP-92-3	76.79			wr	X	XXX	X	XX					
HP-92-4	76.80			wr	X	XXX	X	XX					
HP-92-7	76.69			ts	XXX	XXX	XXX	XXX		XXX			XX
HP-92-8B	68.06		XX	ts	XXX		XXX	XXX		X			XX
HP-92-9	77.45			wr	X	X	X						
HP-92-9/2	77.46			wr	X	X	X						
HP-92-10	77.14	X*		ts	XX	XX	XX				XX		
HP-93-2	77.67			ts	XXX	XXX	X				XX		XX
HP-93-3	77.55			ts	XXX	XXX					XX		XX
HP-93-4	75.95	X*		wr	X								
HP-93-5	75.39			ts			XXX	XXX	XX	XXX			XX
HP-93-6	70.52		XX	ts			XXX		XXX				XX
HP-93-8	70.98		XXX	ts			XXX	XX	XXX	XXX			XX
HP-93-10	77.25			wr	XXX	XXX			X				
HP-93-11	76.93			ts	XXX	XXX		X		X	X		XX

Table 4 continued:

	SiO2	aph*	diseq. texture	type	qtz	alk feld	plag	cpx	opx	fa (ol)	amph	bt	op
HP-93-12	73.69		X	ts		X	XXX	XXX		XX			XX
HP-93-13C	77.56	X*		ts	XX	XX							XX
HP-93-14C	85.52	X*		ts				XX					XX
HP-93-15	76.28			wr		XXX	X				X	XXX	
HP-93-16	77.93			ts	XXX	XXX	XXX						XX
HP-93-19	75.12	X*	X	ts	XX	XX	XX	X			XX		XX
HP-93-20	76.77	X		wr									
HP-93-21	71.72			ts		XXX	XXX	XX		XX			XX
HP-93-25	76.16			ts	XXX	XXX		XXX					XX
HP-93-28	76.29	X*		ts			XX		XX			XX	XX
HP-93-30	67.40		X	ts			XXX	XXX	XX	XX			XX
HP-93-32	75.67	X*		ts	XX	XX		XX		XX			XX
HP-93-34	75.13			ts	XXX	XXX	XX	XXX		X			XX
HP-93-37A	70.76		XX	ts		XXX	XXX	XXX	XXX	XXX			XX
HP-93-39	64.87			wr			XXX	XXX	X				
HP-93-40	70.23		XXX	ts			XXX	X	XXX		XXXX		XX
HP-93-43	76.15			wr	X	X	XXX						
HP-93-44	74.51			ts		XXX	XXX	XXX					XX
HP-93-45	76.27			ts		XXX	XXX	XX	XXX			XXX	XX
DO-93-12	76.75	X*		ts	XX						XX		XX
DO-93-13	71.88		X	ts			XXX	XXX		XXX			XX
DO-93-15	76.78	X*		ts				XX					
DO-93-16	76.52	X		wr									
DO-93-18	71.67			ts			XX						XX
DO-93-19	70.16		XXX	ts			XXX						XX
DO-93-4	71.58	X*		wr			XX						
DO-93-7	71.67		X	ts			XXX	XXX	XXX	XX			XX
DO-93-8	71.69		X	ts			XXX	XXX	XXX	XXX			XX
ER-93-1	75.10			ts		XXX	XX	XXX		XXX			XX
ER-93-3	74.52			ts		XXX	XXX	XXX	X	XXX			XX
ER-93-6	74.40	X		wr									
41BJ95	75.17	X		ts									
BB-92-1	74.34	X		wr									
BB-92-18	76.71	X		wr									
BB-92-22	76.91	X		wr									
BB-92-25	77.00	X		wr									
BB-92-28	70.50			wr	X	X	XX	X	X				
BB-92-29	67.28			wr			XX	X	X				
BB-92-6	74.32	X		wr									
BB-92-9	70.63			wr	X	X	XX	X	X				

Table 4 continued:

Samples from the NWBR													
	SiO2	aph*	diseq.	type	qtz	alk	plag	cpx	opx	fa	amph	bt	op
			texture			feld				(ol)			
MTF 07-14	66.19			ts			XXX	XXX	XXX				XXX
MTF 07-18	71.91			wr			XXX				XX	XX	
MTF 07-20	76.63	X		wr									
MTF 07-25	76.48	X		wr									
MTF 07-27a	77.17	X*		wr		X					X	X	
MTF 07-28	76.70	X		wr									
MTF 07-29	76.71	X*		wr			X					X	
MTF 07-30	75.60			wr			XXX				XX	XXX	
MTF 07-37	68.93			wr			XXX	X	X		X	X	
MTF 07-38	69.77	X*		wr							XX		
MTF 07-40	72.40			ts			XX				XXX	XX	XXX
MTF 07-41	67.98			wr			XX				X	X	
MTF 07-42	73.30			ts			XXX						XXX
MTF 07-47	70.90			wr			XXX				XX		
MTF 07-48	70.34			wr			XXX				XXX		
MTF 07-49	70.84			wr			XXX				XXX		
MTF 07-50	71.24			wr			XXX						
MTF 07-51	77.85			wr		XX	X				XXX	XXX	
MTF 07-52	74.25			wr			XXX				XXX	XXX	
MTF 07-53	71.98			wr		XX	XX				XXX	X	
MTF 07-56	77.61	X*		wr							X	X	
MTF 07-58	72.12			wr			XXX					XX	
KCS-05-14	75.87			wr			XXX				XX	XXX	
KCS-05-15	74.88	X		wr									
KCS-05-28	64.24			wr			XX	X	X		XX		
KCS-05-29	64.79	X*		wr				X	X		X		
KCS-05-46	74.86	X		wr									
KCS-06-15	67.39			wr			XXX				XXX		
KCS-06-16*	67.24	X*		wr			X						
KCS-06-35A	72.71			wr			XXX				XXX	XXX	
KCS-06-35B	71.88			wr			XXX				XXX	XXX	
KCS-06-37	73.15			wr			XXX				XXX	XXX	

CHAPTER 3:

Isotopic (O, Sr, Nd, Pb, Hf) Geochemistry of Age-progressive Rhyolites from the High Lava Plains and Northwest Basin and Range, Oregon: Petrogenesis and Implications for Crustal Modification in an Intracontinental System

ABSTRACT:

Understanding continental crustal formation and modification is paramount to the development of whole Earth geochemical reference models. While these processes are generally understood at convergent margins, less is known about anorogenic settings. Here we apply 35 whole rock Sr, Nd, Pb and Hf isotopic analyses coupled with $\delta^{18}O_{(melt)}$ values and major and trace element compositions to determine rhyolite petrogenesis in the bimodal High Lava Plains (HLP) and northwestern-most Basin and Range (NWBR) Province in eastern and central Oregon. Disregarded

The HLP – NWBR, together with the Snake River Plain and the Columbia River Basalts, is one of the largest Cenozoic volcanic provinces in the world. In this area where mafic crust is predominant, the early stages of crustal modification are evident, in which a more silicic upper crust is separated from a mafic lower crust. The bulk of the rhyolites in this system are produced by partial melts of crustal mafic protoliths, likely recently emplaced mantle-derived basaltic magmas emplaced. While there is some evidence of minor assimilation of earlier Cenozoic volcanic products, wholesale anatexis or even non-trivial amounts of older, accreted terranes and associated plutons is precluded. There is also isotopic and geochemical evidence in the basalts of a change, both spatially and temporally, in the mantle input to the system.

INTRODUCTION:

The origin and evolution of the continental crust, and how its structure and composition have changed though time, have a direct effect on models describing the evolution of the Earth, including mass balance and planetary accretion models (e.g., Taylor and McLennan, 1995; Rudnick and Gao, 2005). During successive melting and segregation events, the continental crust becomes a low density, increasingly isolated geochemical reservoir that is not subducted back into the mantle. This further enhances the crust's significance on whole earth geochemical models, especially for many incompatible elements. Understanding the mechanisms for crustal formation and modification is a key part of understanding Earth evolution and geochemical reference models.

A number of intracrustal differentiation processes are important in the evolution and stabilization of the continental crust, generally producing a more silicic upper crust and a more mafic lower crust through time. Silicic crust formation is substantial at convergent plate margins, and "zone refining" (Lundstrom, 2009) from open-system processes results in considerable segregation of the crust with the most important regime for crustal formation and modification being in continental arcs (Lee et al., 2007). While some of these processes are complex (e.g. open-system processes such as mixing-assimilation-storage-homogenization - MASH; Hildreth and Moorbath, 1988, 1991 and polybaric episodes of varying amounts of magma recharge, crustal assimilation or melting and minor fractional crystallization - RAFC; Bohrson and Spera, 2001, Spera and Bohrson, 2001) the application of these processes are generally well understood (e.g. Hildreth, 2007; de Silva and Gosnold, 2007). In tectonically thickened, orogenic intracontinental regions, partial melting of deeply buried sedimentary or metasedimentary rock can also compositionally stratify the crust (e.g. the Himalayas: Searle et al., 2010).

Anorogenic environments can also produce compositionally stratified crust and often are driven by an increase in thermal input and/or material from the mantle (e.g. Nekvasil et al., 2000). These anorogenic volcanic rocks are termed "A-type" and they are commonly bimodal, with a peralkaline silicic component containing anhydrous mineral phases (Loiselle and Wones, 1979) and a ferrobasalt or tholeiitic mafic component (e.g. Nekvasil et al., 2000). These include over-thickened mafic proto-continent volcanic piles associated with hotspots, such as Iceland (Gunnarson, et al., 1998; Martin, et al., 2008) and maybe some oceanic plateaus (e.g. Kerguelen: Frey et al., 2000; Wrangellia: Richards, et al., 1991). A-type volcanic rocks also occur in places where there is limited opportunity for interaction between mantle-derived magmas or where crustal extension results in plate thinning and mantle melting. In many of these within-plate, often bimodal systems, multiple petrogenetic hypotheses exist for the silicic magmas (cf. Ethiopian Rift: Peccerillo et al., 2003, Rooney et al., 2007; Snake River Plain, Idaho: Christiansen and McCurry, 2008, Bonnichsen et al., 2008).

The High Lava Plains (HLP) of east-central Oregon and the northwestern-most Basin and Range (NWBR) located in south-central Oregon, together with the Snake

River Plain (SRP) of Idaho (Figure 1) represent an archetypal example of an anorogenic or A-type magmatic province. We can use rhyolite formation and the resultant crustal modifications in the SRP for comparison with the HLP – NWBR. One key difference between the SRP and the HLP – NWBR is that the SRP crustal differentiation processes are taking place in previously differentiated, old (> 2 Ga Wyoming-aged) cratonic crust while the HLP – NWBR volcanism occurs in relatively young (< 250 Ma), mafic accreted terranes, west of the 0.706 $^{87}Sr/^{86}Sr$ line (Figure 1).

Whole rock geochemical mass balance and isotopic constraints on the petrogenesis of the voluminous, age-progressive rhyolites of the SRP indicate that a majority of their volume is derived from partial melts of recently emplaced, mantle-derived mafic rocks or cumulates from mafic differentiation (intra-plating) (Christiansen and McCurry, 2008; McCurry and Rodgers, 2009). In brief, partial melts of the mantle reach a point of neutral buoyancy and stall in the middle crust. MASH processes hybridize parts of the middle crust and fractional melts of this mostly mantle-derived crust result in a parental rhyolite or rhyodacite. Further melt evolution occurs by fractional crystallization and possible ingestion of the upper-most crust results in much of the rhyolite erupted from the large calderas of the SRP (McCurry and Rodgers, 2009; Bindeman et al., 2007). Due to the radiogenic ingrowth, cratonic crustal isotope ratios create significant leverage in mass balance calculations and produce a model detailing crustal modification, particularly with respect to Sr and Nd isotopes (cf. Figure 7 and Figure 8 of McCurry and Rodgers, 2009).

While there is a general consensus that many A-type rhyolites are formed by silicic partial melts of mafic crust coupled with fractional crystallization and potentially minor upper crust assimilation (e.g. HLP, Streck, 2002; SRP, McCurry and Rodgers, 2009; Iceland, Jonasson, 1994; Jonasson, 2007; Lacasse et al., 2007; Martin and Sigmarsson, 2007), some rhyolites might have been produced by protracted fractional crystallization of basaltic parents. These include some rhyolites from Iceland (e.g. Ljosufjoll and Snaefellsjokull: Martin and Sigmarsson, 2007; Oraefajokull: Selbekk and Tronnes, 2007; Austurhorn: Furman et al., 1992) and the non-age-progressive Quaternary rhyolites of the SRP (e.g. Big Southern Butte, Cedar Butte, East Butte, McCurry et al.,

2008; Savov et al., 2009). Furthermore, experimental fractional crystallization studies show that A-type rhyolites can be made from basaltic parent magmas (McCurry et al., 2008; Whitaker et al., 2008; Nekvasil et al., 2000). Fractional crystallization of a low silica rhyolite to produce a high silica rhyolite can obscure the true lineage of a rhyolite (Streck and Grunder, 2008; Frost et al., 2001). Without *a priori* knowledge of the liquid line of decent, an example of which is found in the Cedar Butte – Craters of the Moon trend in the SRP (McCurry et al., 2008), isotopic analyses play a critical role in determining the petrogenesis of rhyolites and thus the mass balance of magmatic system and attendant effects on crustal modification.

In central and eastern Oregon, late Miocene and younger volcanism is the surface manifestation of deeper-seated tectonic and magmatic processes that operate on lithospheric and asthenospheric scales. The timing or eruption and composition of these volcanic rocks give us a record of the dynamics and components of the crust-mantle system that generate and modify continental crust in an anorogenic setting. A study of the silicic rocks in the HLP – NWBR region, with comparative data from the SRP, will delineate which crustal modification processes are dominant, and how the crust has been differentiated.

In this work, we use radiogenic and stable isotopes (Sr, Nd, Pb, Hf, O) to examine the upper mantle and crustal components involved in rhyolite genesis from the HLP and NWBR. In the HLP (relative to the NWBR), there is a greater flux of mantle-derived basaltic magma into the crust, resulting in more partial melt and a hotter regime, despite the crust becoming more mafic. Results generally preclude the strong influence of any sedimentary sources from the upper crust, but do indicate small additions of Cenozoic volcanics to some samples. Some rhyolites show minor additions of a contaminant, likelt terrigenous marine sediments similar to those found in the current-day Astoria Fan oceanic sediments off the Oregon coast (Columbia River drainage), likely from the lower- to mid-crustal partial melt source regions. We frame these results in the context of anorogenic volcanism and the formation and distillation of a more silicic upper crust from a mafic lower crust.

The High Lava Plains and Northwest Basin and Range:

This work focuses on the HLP and NWBR of Oregon (Figure 2), exclusive of the Newberry Volcano shield. The volcanic rocks considered here, together with the Columbia River Basalts (CRBs), Steens Basalts and the Yellowstone – SRP systems, are part of the largest Cenozoic volcanic province in the world (cf. Smith and Luedke, 1984). Prior to ~19 Ma, this Cenozoic province was constructed of volcanic rocks ranging in a continuum from mafic to silicic compositions; during the emplacement of the CRBs, the province was primarily mafic, and over the past 12 to 14 Ma, the basalt-rhyolite bimodal SRP and HLP compositions have dominated, with the SRP containing at least ten times the eruptive volume of the HLP - NWBR. The < 12 Ma silicic rocks of the bimodal HLP – NWBR are part of a single, age-progressive volcanic province (cf. Figure 15, Chapter 2) while the basalts and basaltic andesites show no such age relationship, but may display episodes of increased volcanic volume (Jordan et al., 2004). The province is strongly bimodal as less than five percent of the late Miocene and younger rocks have intermediate (57 – 69 Wt. % SiO_2) compositions, the bulk of which are within the NWBR (Chapter 2).

Ford (Chapter 2) distinguishes a number of compositional trends in < 12 Ma rhyolites. When separated by physiographic province (HLP and NWBR, Figure 2) the HLP contains the majority of high silica rhyolites (> 75 wt. % SiO_2), nearly all of the peralkaline compositions and contains higher FeO* at a given silica content (cf. Figures 6, 7 and 12 in Chapter 2) whereas the NWBR contains a higher number of rocks of intermediate composition. Additionally, the HLP has a much greater volume of rhyolite, primarily due to three voluminous tuffs sourced there. There are also some east to west changes in composition, including a westward increase in Na_2O and decrease in K_2O for both the HLP and NWBR (cf. Figure 13, Chapter 2) and a westward increase in Zr/Nb ratio in the HLP, but not for the NWBR (cf. Figure 14, Chapter 2). Because this is an east – west, age-progressive volcanic province, these spatial trends are also temporal trends. Finally, rhyolites from the extreme eastern part of the HLP (Duck Butte Eruptive Center, DBEC) are displaced with regards to many trace elements compared to other

rhyolites of the province, including higher Rb, Ba, Sr, Cr, U, and Th and slightly lower HFSE contents.

Two additional episodes of volcanism occurred on the western margin of the < 12 Ma HLP – NWBR study area but we exclude them from this work. Within the Cascade Arc volcanic province (Figure 2), the 7 – 6 Ma Deschutes Formation (Taylor, 1981; Sherrod et al., 2004) produced at least two rhyolites (e.g. Pine Mountain, Chapter 2) that crop out within the HLP. The < 0.6 Ma Newberry Volcano lies within the physiographic HLP but is considered a rear-arc Cascade volcano (Donnelly-Nolan et al., 2008). Unlike older volcanism, described below, it sits atop HLP and NWBR volcanism and is excluded from our discussion.

The Crust of the HLP – NWBR:

The crust underlying the HLP – NWBR includes Cenozoic volcanic rocks and basin and eolian deposits including volcaniclastic sediments (e.g. Clarno, John Day and middle Miocene volcanics). Beneath these deposits are Mesozoic to Paleozoic mafic accreted terranes and plutons (e.g. Saleeby and Busby-Spera, 1992; Wyld, 2006; Allan and Barnes, 2006). The composition of these terranes and some plutons will be detailed later in the discussion (and Appendix 6), but the crust that underlies this area, and most of Oregon, are accreted terranes and are more mafic and much younger than the crust of the craton to the east (0.706 line of Kistler and Peterson, 1978). One of the consequences of dealing with young and broadly mafic crust is that the isotopic ratios of radionuclides with long half-lives have not had time to evolve to levels that would clearly implicate crust involvement in magma production, as they might in a cratonic setting (cf. DePaolo, 1981). We will interpret O isotopes to help determine crustal involvement. Attempting to solve the involvement of young, mafic crust in the petrogenesis of rhyolites is a main tenant of this work and has implications for crustal compositional stratification.

ANALYTICAL PROCEDURES:

Sample Selection:

For this study, we chose samples to achieve spatial and temporal coverage of the HLP and NWBR. While the emphasis is on silicic samples < 12 Ma, some samples from outside this 12 - 0 Ma window were selected in order to see if there was any discernible change in isotopic systematics over time. Additionally, some samples were targeted based upon low-Sr abundances reported in previous work (e.g. MacLean, 1994; Walker, 1981; Ambroz, 1997). The reason for these choices is that if there is a crustal influence on the petrogenesis of the rhyolites, it might best be manifested in samples with a low Sr concentration.

Trace Element Geochemistry:

Trace elements given in Table 1 were determined by either isotope dilution (ID) at the Department of Terrestrial Magnetism (DTM) (described below), or ICP-MS or XRF at the Washington State University (WSU) GeoAnalytical Laboratory, following the methods of Knaack et al., 1994 and Johnson et al., 1999. For a complete list of major and trace element results and more detailed information on which analyte was analyzed by each method, see Chapter 2.

Wet Chemistry:

Sr, Nd, Hf and Pb isotopic analyses were performed at DTM and closely follow the analytical procedures described by Carlson, et al. (2006) except as follows. Samples were protected from metal spallation with either thick paper or burlap during initial steel plate and hammer reduction and any pieces showing "hammer marks" were removed. Approximately 100 g was ground to ~ 200 mesh in a Spex alumina mill. Approximately 100 – 200 mg of these powdered samples, depending on the whole rock Sr concentration, were spiked with ^{87}Rb and ^{84}Sr tracers and dissolved in a 2:1 mixture of concentrated HF:HNO_3 (Carlson et al., 2006). After digestion, the samples were dried, re-dissolved in ~1 ml concentrated HNO_3, dried, re-dissolved in HNO_3, dried then finally completely

dissolved in ~6 ml of 4N HCl. Samples were then dried, re-dissolved in 1 ml 0.5N HBr, dried and then re-dissolved in 3 ml of 0.5N HBr in preparation for Pb columns. Pb, Rb, Sr, Nd and Hf were separated using the procedures described in Carlson et al. (2006). Additional separations for Sm, Lu, and U were not performed for these samples. After each column separation, ~0.04 ml (one drop) of concentrated HNO_3 was added to the dry element separate to destroy any organic material. A procedural blank was also produced and followed all of the above steps. Total procedural blanks measured during these analyses were Sr = 306 pg, Rb = 49 pg, Nd = 172 pg, Sm = 112 pg, Hf = 70 pg and Pb = 100 pg.

In addition to the methods described in Carlson et al. (2006) and the modifications above, a Sr "clean-up" column was used to remove any additional cations and purify the sample. The sample was loaded in 2N HNO_3 and passed through ~0.25 ml of Eichrom Sr resin. This resin was then rinsed with 2.0 ml of 2N HNO_3 and the Sr was collected by eluting 2.0 ml of 0.05N HNO_3. This was then dried and one drop of concentrated HNO_3 was added before re-drying.

Instrumentation and Errors:

Isotopic compositions of Rb were measured by inductively coupled plasma mass spectrometry (ICP-MS) statically in Faraday cups on the VG P-54 multi-collector at DTM with instrumental drift and mass fractionation corrected by bracketed standard runs and corrections made for Sr interference by monitoring ^{88}Sr. Sr isotopes were measured by thermal ionization mass spectroscopy (TIMS) on the Thermo-Finnigan Triton using single Re filaments following a procedure similar to that given in Carlson et al. (2006) and errors are reported in Table 1. The ratio used to correct for fractionation was $^{86}Sr/^{88}Sr = 0.1194$ and the $^{87}Sr/^{86}Sr$ obtained for the NIST-987 Sr standard was 0.710249 +/- 0.000022 (2 SD; n = 8) with data reported relative to $^{87}Sr/^{86}Sr = 0.71025$. This external reproducibility precision is usually worse than in run precisions and is the error reported in Table 1 for most samples. For some samples, particularly for low Sr concentration samples, in run precision is less than the external error stated above and for a few samples with extreme Rb/Sr ratios, the error in the age calculation and resultant

uncertainty in radiogenic ingrowth exceeds the external error (see Table 1). Analytical uncertainties for Rb and Sr concentration by ID (from DTM) are estimated at better than 0.5% (2 SD) which is better than errors determined by ICP-MS at WSU which has errors of 1 to 3%, depending upon the concentrations of Rb and Sr (cf. Chapter 2). Concentrations determined at both labs are typically within error of each other except for concentrations of Sr that are near or below the LOD for WSU ICP-MS (less than ~ 10 ppm) and for sample MTF 07-40, which has ID Sr = 141 ppm and ICP-MS Sr = 151 ppm. ID values are used in all calculation.

Nd isotopic compositions were also measured on the Thermo-Finnigan Triton using double Re filaments and static multi-collection similar to the procedure described in Carlson, et al. (2006). A fractionation correction to $^{146}Nd/^{144}Nd = 0.7219$ was applied and results are reported relative to $^{143}Nd/^{144}Nd = 0.511860$ for the La Jolla standard and 0.512117 for JNdi standard. Faraday cups in the Triton were replaced for later runs and thus two different external reproducibility results are reported here and in Table 1. One set resulted in measured La Jolla samples averaging 0.511866 +/- 0.000008 (2 SD; n = 4) with the other set averaging 0.511846 +/- 0.000006 (2 SD; n = 5). One other set of analyses used the JNdi standard, which returned a measured value of 0.5121324 with external errors on JNdi similar to those reported for the La Jolla standard (Carlson et al., 2006). These external errors are greater than the in run precision variations and thus data in Table 1 are reported with the external error. The concentration of Nd and Sm for most samples (cf. Chapter 2) was determined by ICP-MS at WSU and standard errors (precision) are less than 0.5 ppm for Nd and 0.1 ppm for Sm (95% confidence interval) relative to measured values, corresponding to average errors of two percent for both elements. Some other sample compositions are from the literature (see Table 1) and may have slightly greater errors associated with the Nd and Sm measurements but these variations still result in less uncertainty than the external isotopic error quoted above.

Most of the Hf isotopic compositions were measured on the Nu-Instruments high-resolution multi-collector ICP-MS with a subordinate number measured on the VG P54 with potential interference from Yb, Lu, Ta and W monitored. A fractionation correction using $^{179}Hf/^{177}Hf = 0.7325$ was applied and results are reported relative to $^{176}Hf/^{177}Hf =$

0.282160 for the JMC-475 standard. Daily runs of this standard measured during the same analytical sessions averaged 0.282126 +/- 0.000005 (2 SD; n = 14). This external error is generally greater than in run precision and data in Table 1 is reported with this error, except where noted. The precision standard errors for Hf and Lu concentrations determined by ICP-MS (WSU) are 0.06 and 0.01 ppm (95% confidence interval) respectively, corresponding to average errors better than two percent relative to the measured values.

Pb isotopic compositions were measured on the DTM Axiom multi-collector ICP-MS using Tl to correct for mass fractionation. Most samples were run with ^{208}Pb signals of between 3.7 to 7.2 x 10-11 amps except for MTF 07-16 (0.6 x 10-11 amps) and MTF 07-40 (2.1 x 10-11 amps) with ^{205}Tl signals between 1.1 to 3.7 x 10-11 amps with the exception of MTF 07-29 where ^{205}Tl was 0.8 x 10-11 amps. Corrections for mass fractionation are first made using Tl and then by comparison of Tl-spiked NBS981 standards with the values reported for NBS981 by Todt et al. (1996). During the course of these measurements, the average value obtained for NBS981 Pb was: ^{206}Pb/^{204}Pb: ^{207}Pb/^{204}Pb: ^{208}Pb/^{204}Pb = 16.9254 ± 0.0013: 15.4792 ± 0.00016: 36.678 ± 0.004 where the uncertainty is expressed as a 2σ mean of 25 measurements. In all cases, this external reproducibility is less precise than the in run precession for each sample and thus the external precision is used for the errors for the measurements reported in Table 1. U and Pb concentrations were determined by ICP-MS (WSU) and precision standard errors are better than 0.02 ppm (two percent, on average of measured values) for U and 0.15 ppm (just under two percent, on average of measured values) for Pb (2 SD).

Oxygen isotopes analyses were performed using 35W CO_2 laser fluorination technique (Sharp, 1990) at the University of Oregon stable isotope lab and closely follow the methods described in Bindeman et al. (2010). Five aliquots of standard reference material Gore Mountain Garnet (GMG; δ^{18}O = 5.75 ‰; Valley et al., 1995) were analyzed each day together with the unknowns and daily δ^{18}O variability GMG ranged from 5.52 to 5.82 ‰ (–0.23 to +0.07 ‰), in agreement with previous work from this laboratory (Bindeman et al., 2008; 2010). These values were used to adjust the sample measurements for the small day-to-day instrumental drift correction and variability,

yielding the resultant absolute values on the SMOW scale (after Baertschi, 1976). The average precision on standards and duplicate samples is better than 0.1 per mil (‰).

RESULTS:

Overall Results:

A total of 35 whole rock Sr, Nd, Hf, and Pb isotopic compositions on silicic rocks are presented in Table 1 with 31 O isotopic compositions on basalts and rhyolites presented in Table 1 and Table 2. Errors are reported above or, if greater than the external reproducibility precision, are noted in Table 1. Whole rock major and trace element methods, results and sample locations (latitude, longitude) are reported in Chapter 2. That work also contains ^{40}Ar-^{39}Ar age determinations for many samples (see Table 1 caption for details on sample whole rock compositions and ages from other sources). Results for a number of Cenozoic volcanic episodes analyzed in this study are summarized in Table 3, with a focus on the < 12 Ma rhyolites.

Samples analyzed for radiogenic isotopes include dacites and rhyolites ranging from 66 to nearly 78 wt. % SiO_2. Two of the samples are from John Day volcanic rocks, four are from silicic domes that are roughly coeval with Steens Basalt volcanism, 10 are from the age-progressive silicic rocks of the NWBR and 17 are from the age-progressive silicic rocks of the HLP (< 12 Ma). Additionally, we analyzed the likely Deschutes Formation-related Pine Mountain rhyolite and Iron Mountain, a 2.54 Ma dome from the HLP that is substantially younger than age-progressive rhyolites in the same area.

Despite relatively young samples (the oldest in this dataset is 30.4 Ma) measured $^{87}Sr/^{86}Sr$ values have a wide range from 0.70364 to 0.81838 which is partially the result of variable $^{87}Rb/^{86}Sr$ values, some of which exceed 1,000 (with Rb/Sr values approaching 400). When corrected for radiogenic ingrowth, $^{87}Sr/^{86}Sr_{(i)}$ values range from 0.70317 to 0.70689 for < 12 Ma rhyodacites and rhyolites of the HLP and NWBR, both from this work (n = 27, Table 3) and previous reports (Scarberry, 2007, n = 2; Streck and Grunder, 2008, n = 7; Savov et al., 2009, n = 3). The John Day age and middle Miocene silicic

volcanic rocks (n = 6) cover a smaller range, with $^{87}Sr/^{86}Sr_{(i)}$ values from 0.70362 - 0.70440, including previous work (Scarberry 2007, n = 3).

Radiogenic ingrowth is not nearly as great for Nd isotopes, with shifts as great as a half epsilon unit for the oldest samples. The overall range for this (Table 3) and previous works for the various volcanic time periods is $^{143}Nd/^{144}Nd_{(i)}$ = 0.512586 - 0.512935 with corresponding CHUR corrected $\varepsilon Nd_{(i)}$ values of -0.72 to 6.22. The $\varepsilon Nd_{(i)}$ for the > 12 Ma silicic rocks occupy the higher side of this range from 4.74 – 6.22 while the < 12 Ma samples range from a $\varepsilon Nd_{(i)}$ = -0.72 to 5.73.

Lead and hafnium isotopes similarly have limited radiogenic ingrowth and thus initial ratios don't shift much with age corrections for these rhyolites. $^{206}Pb/^{204}Pb_{(i)}$ range from 18.76 – 19.16 and $^{207}Pb/^{204}Pb_{(i)}$ range from 15.569 to 15.622 for both the > 12 Ma and < 12 Ma sets, with the older set more constricted in values (Table 3). $^{208}Pb/^{204}Pb_{(i)}$ ranges from 38.41 to 38.76 for the younger HLP and NWBR silicic rocks while those > 12 Ma range from 38.31 – 38.60. Hafnium isotopes yield a $^{176}Hf/^{177}Hf_{(i)}$ range of 0.282864 – 0.283138 (Table 3) and corresponding CHUR time corrected $\varepsilon Hf_{(i)}$ of 3.48 to 13.11. The older than 12 Ma samples are restricted within in this range from $\varepsilon Hf_{(i)}$ = 5.85 to 12.39.

Oxygen isotopes, representing melt values, are reported for both rhyolites (Table 1) and basalts (Table 2). $\delta^{18}O_{(melt)}$ values on rhyolites > 12 Ma range between 5.74 and 6.99 ‰. Those for the < 12 Ma rhyolites range from 4.86 to 7.48 from this work (Table 3) but Savov et al. (2009) and Roche (1987) report two lower values of 4.4 and 3.9 ‰. Savov et al. (2009) also report 2 higher values, 7.6 and 7.9 ‰. For the basalts (n = 9), $\delta^{18}O_{(melt)}$ values range between 6.01 and 6.38 ‰. Two additional rhyolitic samples were analyzed that are not listed in Table 1. These include KCS 04-10 with a ^{40}Ar-^{39}Ar age of 21.8 Ma and a $\delta^{18}O_{(melt)}$ value of 6.99 ‰ and KCS 06-37 with a ^{40}Ar-^{39}Ar age of 8.6 Ma and a $\delta^{18}O_{(melt)}$ value of 7.18 ‰ (see Scarberry, 2007 for additional isotopic analyses for these samples). The latter data point is plotted on the < 12 Ma figures.

Focusing on the < 12 Ma Rhyolites:

All but two of the < 12 Ma rhyolites with $^{87}Sr/^{86}Sr_{(i)} > 0.7042$ are high silica (> 75 wt. % SiO_2) rhyolites. The exceptions are from Burns Butte (analysis of Streck and Grunder, 2008) and Duck Creek Butte of the DBEC (Figure 3a). But, elevated silica does not always correlate with more elevated radiogenic Sr isotope ratios as high silica rhyolites span the range from lowest to highest $^{87}Sr/^{86}Sr_{(i)}$. Most rhyodacites to moderate silica rhyolites (up to 75 wt. % SiO_2) fall within the narrow range of 0.70361 – 0.70416 for $^{87}Sr/^{86}Sr_{(i)}$. When plotted against Fe-line parameter, we note a great cluster of points, containing both HLP and NWBR that are less than $^{87}Sr/^{86}Sr_{(i)} = 0.7042$ and have a FeO*:SiO_2 of ~-0.3 to 0.6. Most other points are widely scattered, although no points plot at very negative FeO:SiO_2 and high $^{87}Sr/^{86}Sr_{(i)}$ (Figure 3b). The RST (Rattlesnake Tuff) sample compositions seem to follow a curved trend as the system evolved from lower silica dacite pumices through unit E pumice, to high silica RST pumice (unit A). There does not seem to be a strong correlation between peraluminousity and Sr isotopic ratio. There do not appear to be any identifiable trends when comparing Nd, Hf, Pb or O isotopes with SiO_2 or the Fe-line parameter.

DISCUSSION:

Isotopic Inputs to the HLP – NWBR System:

There are two potential inputs involved in rhyolite production: parental basaltic magmas that fractionate to more silicic compositions, and partial melting of crustal sources. For this study area, these partial melts can be of many different affinities, recently intraplated basaltic magmas, a diversity of Cenozoic volcanic rocks (ranging from basalts to rhyolites), volcaniclastics and sediments, accreted oceanic terranes and Mesozoic plutons. Furthermore, the isotopic character from mantle-sourced inputs (e.g. basaltic magmas, or fractionates thereof), may not be constant on the time scales and spatial distributions investigated here. We explore the variable contribution of each of these in greater detail below.

Temporal and Spatial Changes in Mantle Source - Evidence from the Basalts:

Carlson and Hart (1987) show a decrease in FeO*/MgO over time in eastern and central Oregon over the past 16 Ma, including high aluminum olivine tholeiites (HAOT) and Steens Basalts. Our compiled dataset also shows a decrease in FeO*/MgO (or an increase in MgO/(MgO+FeO*) for basalts and basaltic andesites through time in the more narrowly defined HLP (Figure 4), most of which is driven by increases in MgO. There is also a subtle decrease in Zr/Nb ratio through time in HLP basalts and basaltic andesites; Nb data for some of the easternmost and older basalts do not exist so this trend is not as definitive as that for the Fe-Mg relationship. These changing ratios, more evident in the HLP than in the NWBR, indicate that the parental basaltic magmas to this system might be changing through time, indicating hotter basaltic magmas and greater degrees of partial melting of the mantle, a changing asthenospheric source composition over time or interaction with a more depleted mantle lithosphere through time (cf. Carlson and Hart, 1987).

A number of authors have also recognized the spatial variation in isotopic ratios with longitude of HAOT of the western US, which is a trend towards more cratonic (higher $^{87}Sr/^{86}Sr$ ratios and lower $^{143}Nd/^{144}Nd$ ratios) values to the east (Hart, 1985; Leeman, 1982; Jordan, 2001). These authors generally call on an older, more isotopically evolved, lithospheric mantle component, perhaps older to the east, to produce this trend. While there are few data from the NWBR, there is a clear separation between HLP basalts from west and east of ~ 118.75 degrees longitude with the eastern set trending towards cratonic radiogenic isotopes signatures and the western set having less evolved (more MORB-like) isotopes (Figure 5 and Jordan, 2001). When basaltic Sr and Nd isotopes are plotted against age (Figure 6) another interesting trend is seen. At any general location over time, $^{87}Sr/^{86}Sr$ ratios decrease and $^{143}Nd/^{144}Nd$ ratios increase**.** This trend is strongest in the basalts west of 118.75 degrees, which span over about 9 m.y. and is most apparent in the Nd isotopic ratios. For the eastern region basalts, which span over the last 12 m.y., the decreasing trend $^{87}Sr/^{86}Sr$ ratios is not as apparent, but the younger samples do have a more narrowly defined range.

Based on the major, trace, and isotopic compositions, we confirm the established E-W regional change in parental basaltic source and refine this to show that major and trace element trends are more evident when HLP basalts are separated from NWBR basalts. We add that there is a temporal change in parental basaltic source from 12 to 0 Ma in the HLP. Eastern basalts have more variability in isotope geochemistry with higher $^{87}Sr/^{86}Sr$ and lower $^{143}Nd/^{144}Nd$ ratios indicating they contain more of a lithospheric input as shown here and discussed by previous workers (see above). However, over time, both in the eastern and western portions of the HLP, $^{87}Sr/^{86}Sr$ ratios decrease and $^{143}Nd/^{144}Nd$ ratios increase, and this shift is correlated to a change in FeO*/MgO and Zr/Nb ratios. Furthermore, the rate of change between the eastern and western basalts is similar for $^{143}Nd/^{144}Nd$ (Figure 6), and while they show a similar trend, there is too much scatter in $^{87}Sr/^{86}Sr$ of eastern samples to make a similar statement. It seems likely that the isotopic character of the lithospheric mantle has changed over the past ~ 10 m.y., with the $^{87}Sr/^{86}Sr$ ratio dropping by at least ~0.0005 and the $^{143}Nd/^{144}Nd$ ratio increasing by at least ~ 0.0001, corresponding to an increase in $\varepsilon Nd_{(i)}$ of ~ 2.

Evidence of Crustal Inputs into Rhyolites of the HLP and NWBR:

The westward trend of Sr and Nd isotope ratios in basalts is largely mimicked by the rhyolitic samples (Figure 5, Figure 7). Those rhyolites that plot within the basalt field must either be partial melts of crust that has an isotopic signature similar to the basalts, or partial melts or fractionates of the basaltic magmas themselves, or a combination of the two. When plotting $^{143}Nd/^{144}Nd$ vs. $^{87}Sr/^{86}Sr_{(i)}$ ratios (Figure 7), nearly all of the rhyolites plot within the field of basalt data points and only a few samples are displaced to higher $^{87}Sr/^{86}Sr_{(i)}$ ratios, indicating incorporation of older crust. We also plot $\varepsilon Hf_{(i)}$ vs. $\varepsilon Nd_{(i)}$ as a check of the Nd measurements (Figure 8). Most samples parallel the terrestrial array of Vervoort et al. (1999) indicating that Nd and Hf systematics have not been perturbed in these samples, except for potentially one HLP rhyolite that plots above a $\varepsilon Hf_{(i)}$ of 12 (Burns Butte).

Modeling by Streck and Grunder (2008) of the most evolved (high silica, ~ 2 ppm Sr) unit A of the Rattlesnake Tuff (RST) incorporates a small amount of radiogenically

evolved crustal component, thus driving the $^{87}Sr/^{86}Sr_{(i)}$ ratio straight up in Figure 5, away from the basalts. This shift in $^{87}Sr/^{86}Sr_{(i)}$ ratios obviates the need for incorporation of at least small amounts of crust with radiogenic Sr in nine or ten samples (Figure 5). This can happen in two ways: 1) addition of likely upper-crustal components into a "parental rhyolite" (e.g. Streck and Grunder, 2008), or 2) mixing and hybridization (MASH) of likely mid- to upper-crustal components with primitive basaltic magmas followed later by partial melting of this hybrid protolith (e.g. McCurry and Rodgers, 2009). While all of the rhyolite samples that have elevated $^{87}Sr/^{86}Sr_{(i)}$ ratios contain < ~60 ppm Sr, some other samples with low total Sr have basalt-like Sr isotopic ratios, including some with < 1 ppm Sr, suggesting that not all HLP rhyolites incorporate crust that is elevated in radiogenic Sr.

Other isotopic data shows evidence of crustal involvement in rhyolite petrogenesis. The Pb isotopic system, in particular, the $^{207}Pb/^{204}Pb$ vs. $^{206}Pb/^{204}Pb$ system (Figure 9) shows that some rhyolite samples have higher $^{207}Pb/^{204}Pb$ and $^{206}Pb/^{204}Pb$ than the basalts, indicating a crustal influence in this system. The stable element Oxygen (O) system can also show different types of crustal incorporation (Figure 10). Convecting meteoric waters can lower the $\delta^{18}O$ of the crustal rocks while ophiolites, granites and sedimentary materials are generally enriched in ^{18}O relative to mantle values (Hoefs, 2009). Thus, in a $^{87}Sr/^{86}Sr_{(i)}$ vs. $\delta^{18}O$ plot (Figure 10), rhyolites that are lower in $\delta^{18}O$ than mantle-sourced basaltic magmas likely have a lineage that contains meteoric water altered crust. Those that are about 1 ‰ above the basalts might have derived their O isotope signature solely through fraction crystallization or could be re-melts of mafic protoliths with a similar $\delta^{18}O$, and these scenarios will be discussed later. When plotted against $^{87}Sr/^{86}Sr_{(i)}$, we can further determine if the crust involved was "mafic crust" or crust without radiogenically evolved Sr isotopes, or a "mixed crust" where some silicic, sedimentary or other isotopically evolved (high $^{87}Sr/^{86}Sr_{(i)}$) material is required (see Figure 10).

In summary, many rhyolites show isotopic evidence of crustal involvement, whether it be assimilation of crustal material, as seen in the Pb and Sr isotopes, or possibly partial melts of meteorically altered parental rocks, as seen in the low $\delta^{18}O$

rhyolites. The rhyolites that have $\delta^{18}O$ about 1 ‰ above regional basalts but similar Sr isotopic signatures may include some partial melts of crustal materials with elevated $\delta^{18}O$ signatures but "basalt-like" Sr isotopes, or could be a result of fractional crystallization, and we will examine these two options later in this work. We will next discuss possible crustal assimilants and then which of these was involved in the petrogenesis of the HLP and NWBR rhyolites.

Isotopic State of the Crust:

This next section explores what is known about the crust that lies beneath the thin veneer of < 12 Ma volcanic rocks of the HLP – NWBR. We go into some detail regarding the Cenozoic crustal components of the HLP – NWBR, as some of this information is presented in this work for the first time. Based on analogs from the Blue and Klamath Mountains, the pre-Cenozoic crust under the HLP – NWBR is generally comprised of accreted terranes, plutons and metamorphosed sediments and are covered briefly here, and in more detail in Appendix 6 and references therein. Appendix 6 also contains isotopic ranges for many potential inputs into the HLP – NWBR system as well as some surrounding provinces.

Sources of Crustal Contamination Part 1 - The Cenozoic and Upper-most Crust:

There are three major episodes of Cenozoic volcanic activity in the region that pre-date the < 12 Ma HLP – NWBR volcanic rocks, including the Clarno Formation, John Day Formation and Steens Basalts and broadly coeval rhyolites. These volcanic rocks, along with intercalated sediments and volcaniclastics, are presumed to make up an appreciable volume of the upper-most crust in the HLP – NWBR. Energy exploration drill holes (Popenow, 1961; Newton et al., 1962) are consistent with recent geophysical data (Cox, 2011) and indicate that Cenozoic intercalated volcanics and sediments are greater than six km thick in the Harney Basin (eastern HLP, cf. Figure 3, Chapter 2) and greater than three km thick in many other places. The HLP and NWBR province covers an area of ~50,000 km^2, and this equates to a volume of Cenozoic upper-most crust of

~150,000 km^3, assuming an average of 3 km thickness over the study area, of Cenozoic sediments, volcaniclastics and volcanics.

The oldest of these episodes produced the 54 – 40 Ma calk-alkaline, primarily intermediate composition Clarno volcanic rocks and associated volcaniclastics which crop out to the north and west in the Blue Mountains Terrane (Figure 2) to thicknesses > 1800 m (Walker and Robinson, 1990; Bestland and Retallack, 1994a). While not exposed in the HLP – NWBR, such rocks likely extend sub-surface from the north, and may be present in large volumes especially in the northern and western HLP. We assign a maximum crustal volume of 50,000 km^3 for the Clarno Formation but this may be as little as 10,000 km^3. Isotopic compositions for mafic rocks of the Clarno (Bromley, 2011) fall within the range of mafic samples from the HLP – NWBR (see Appendix 6).

The 37 – 20 Ma John Day Formation consists generally of tuffaceous sediments, volcaniclastics, localized basalt flows, intermediate to rhyolitic centers and some wide-reaching ash-flow tuffs, reaching thicknesses in excess of 1,000 m (Robinson et al., 1990; Bestland and Retallack, 1994b). The volcaniclastics are predominantly of intermediate composition and related to arc, calk-alkaline volcanism that was widely distributed from central Oregon vents, westward to the western Cascades (McBirney, 1978; Robinson et al., 1990). Single vent complexes have been known to produce in excess of 500 km^3 of ash flow tuff, just north of the study area (Crooked Creek Caldera, McClaughry et al., 2009). Localized basalt to rhyolite eruptions also occurred throughout central Oregon at this time and in the study area, as demonstrated by the Coleman Hills (22 – 21 Ma; Scarberry, et al., 2010), Rabbit Hills (22.3 – 20.3 Ma; Scarberry, 2007), Hart Mountain (~26.4 Ma; Mathis, 1993) and Hampton Butte (~30.4 Ma; Iademarco, 2009), as well as other localities (cf. Figure 4, Chapter 2). Much of this John Day episode is exposed either along the northern margins of the HLP or by extensional faults in the NWBR and southern HLP. John Day rocks presumably underlie the younger volcanic sequences of the central HLP where not exposed. The rhyolites exposed along the northern margin of the HLP, such as Hampton Butte, Bear Creek Butte and the 28.3 +/- 1.0 Ma (K-Ar) Powell Buttes (Evans and Brown, 1981), located in the northwest corner of the HLP, are similar in age and composition and have been ascribed to the John Day Formation. The

crustal contribution from Oligocene to early Miocene John Day Formation is at least 10,000 km^3 and may be in excess of 50,000 km^3 in the HLP – NWBR. Isotopic compositions from John Day silicic rocks that crop out in the HLP – NWBR are presented here (Table 1) and in Scarberry (2007) while mafic samples from this period are from north of the HLP (Bromley 2011) and are presented in Appendix 6. These samples produce a possible mixing end member in the $^{143}Nd/^{144}Nd$ vs. $^{87}Sr/^{86}Sr_{(i)}$ and $^{207}Pb/^{204}Pb$ vs. $^{206}Pb/^{204}Pb$ system, which is further discussed below.

A third episode of volcanism occurred just prior to or coeval with the emplacement of the 16.6 to 15.5 Ma Steens Basalt (Brueseke et al., 2007). Isolated silicic domes are exposed as kipukas both within the HLP (e.g. 15.6 Ma Horsehead Mountain, 15.7 Ma Little Juniper Mountain, and 15.3 Ma Jackass Butte, Jordan et al., 2004) and NWBR (e.g. 17.3 Ma Drum Hill and 17.5 Ma Bald Butte, cf. Figure 4, Chapter 2). It is likely that some middle Miocene domes have been completely covered over by younger, < 12 Ma volcanic rocks.

The aerially extensive Steens Basalt stretches into Idaho, Nevada and northern California and is estimated to cover 65,000 km^2 (Carlson and Hart, 1987), and while younger volcanic rocks overlie much of the Steens Basalt, thicknesses over one kilometer are exposed by Basin and Range faulting. Carlson and Hart (1988) conservatively estimate the volume of the Steens Basalt to be 60,000 km^3, approximately half of which occurs this study area. Thus, a considerable portion, as much as 30,000 km^3 of the volume of Cenozoic uppermost crust and volcanic rocks, is Steens Basalt within the study area. The volume of basalts and rhyolites that lies outside the study area defined in Figure 2 is not considered here. Additionally, the primarily basaltic middle Miocene Strawberry Volcanics and various ash-flow tuffs (e.g. Sucker Creek, Littlefield, Dinner Creek: Walker and MacLeod, 1991) may underlie the extreme northeastern corner of the HLP, resulting in a small volume addition. The total volume contribution from this ~19-15 Ma period is at least 35,000 km^3, the vast majority of which is Steens Basalt. Isotopic compositions for silicic rocks of this period are from this study (Table 1) and mafic samples are primarily from the Steens Basalts (see Appendix 6; Calrson and Hart, 1987). As with the Clarno Formation, isotopic ratios generally plot within the range defined by

the HLP – NWBR samples for Pb isotopes but some silicic samples have more radiogenic Sr isotopes.

The formations and volcanic episodes described above are only minimally exposed in the HLP – NWBR but presumably they compose the vast majority of the upper-most crust beneath the region. At an absolute minimum, these volcanic episodes represent > 70,000 km^3 of volcanic rocks and related sediments, the majority of which would be mantle-derived Steens Basalt (Carlson and Hart, 1988). The maximum contribution is potentially > 150,000 km^3 and dwarfs the volume of the < 12 Ma volcanic rocks, which total ≤ 2,500 km^3 (Chapter 2). Undoubtedly, these older volcanics are linked to a substantially larger volume that is lodged in the crust as stalled, crystallized basaltic magmas (intraplated basaltic magmas) and derivatives of fractional crystallization (cumulates and differentiated rocks) (cf. Carlson and Hart, 1987). Such a long period of intense volcanism from the Eocene into the middle Miocene certainly modified the crust in this region, and although much of the evidence for these prior volcanic episodes are exposed only at the margins of the present day HLP – NWBR, it is likely they have modified the crust under the HLP-NWBR as well.

Sources of Crustal Contamination Part 2 - The Mesozoic Middle to Upper Crust:

There are nearly no pre-Cenozoic crustal rocks exposed in the HLP and NWBR, but there are three accreted terranes that likely underlie the area or may have made up part of the crust before magmatic modification: 1) the Devonian – Cretaceous accreted supra-subduction zone formed terranes and associated later plutons of the Klamath Mountains province in southwestern Oregon and northwestern California (Irwin and Wooden, 1999; review by Allen and Barnes, 2006 and sources therein), 2) the Devonian – Cretaceous accreted terranes and plutons of the Blue Mountains province of northeastern Oregon (Wyld et al., 2006; Schwartz et al., 2010) and 3) Cretaceous-age plutons in the Pine Forest and Pueblo Mountains of northwestern Nevada and southeastern Oregon (Figure 2), which might have genetic connections to the Blue Mountains and Klamath plutons, respectively (Wyld and Wright, 2001).

Rocks that make up the Klamath Mountains have been studied in detail (e.g. Snoke and Barnes, 2006) but much less information is available for the other crustal components that likely underlie the HLP and NWBR. In appendix 6, we give ranges for the isotopic compositions of some of the Mesozoic crustal components that potentially underlie the HLP – NWBR, including some Klamath and Blue Mountain plutons, metasedimentary rocks, and the Josephine Ophiolite. We also summarize the petrogenesis of silicic plutons which are partial melts associated with the Klamath Terrane. These plutons are generally formed by partial melts and isotope signatures generally preclude that they are involved in the production of HLP – NWBR silicic rocks.

Mixing of Crustal Reservoirs and Basalts or Parental Rhyolites:

We next examine two systems to explore potential crustal mixing end members. We delineate two generalized starting compositions for this section, a basalt (such as those erupted on the HLP – NWBR) and a "parental" rhyolite, which would be a low to medium silica rhyolite (70 – 74 wt % SiO_2) with "basalt-like" radiogenic isotopes, produced either by fractional crystallization or partial melting. In the $^{143}Nd/^{144}Nd$ vs. $^{87}Sr/^{86}Sr_{(i)}$ system, we have shown that many of the basalts and rhyolites are isotopically similar and, in the eastern sections, basalts and rhyolites have similarly higher $^{87}Sr/^{86}Sr_{(i)}$ and lower $^{143}Nd/^{144}Nd$ values (Figure 5, Figure 7). However, there are some rhyolites that are displaced from the basalts. Figure 11 shows potential $^{143}Nd/^{144}Nd$ and $^{87}Sr/^{86}Sr_{(i)}$ crustal reservoirs that, when mixed the isotopic signature of a parental rhyolite or isotopically similar basalts, could yield the outliers. In this figure, the fields indicate measured (current day) isotopic values for most reservoirs. For the John Day and middle Miocene silicic fields, measured values have been time corrected to 7 Ma (the eruption time of the RST) while such a correction has little effect on the older (e.g. Klamath or Blue Mountains) isotope ratios or current-day sediment isotope ratios, which have very low Rb/Sr ratios. This correction for the John Day and middle Miocene fields only affects the Sr isotopic values and thus does not change the general shape of these fields relative to HLP – NWBR samples.

From examination of Figure 11, we see that two samples, Wagontire Mountain from the HLP and south Cox Flat from the NWBR, plot along hypothetical mixing lines from the HLP – NWBR field to the John Day or middle Miocene fields. From Figure 5, another sample from northeast Cox Flat is also high in $^{87}Sr/^{86}Sr_{(i)}$ as is Cougar Mountain from the HLP, and the Sr and Nd isotopic systematics in these samples could also be explained by the addition of crust with greater concentrations of radiogenic Sr and Nd (resulting in both higher $^{143}Nd/^{144}Nd$ and $^{87}Sr/^{86}Sr_{(i)}$), although this is difficult to see given the scale on Figure 11. Finally, the array of data representing the RST (Streck and Grunder, 2008) mimics the above pattern. The mafic inclusion and dacitic mixed pumices have a similar isotopic signature to HLP basalts, while the least evolved rhyolite (E) has slightly higher $^{87}Sr/^{86}Sr_{(i)}$ and the most evolved rhyolite (A) is higher still (Figure 5, Figure 11). One key point though, is that the $^{143}Nd/^{144}Nd$ ratio appears to get *more* radiogenic with evolution. This is possible only with the addition of Cenozoic silicic rocks and not any other potential mixing component.

Finally, one sample, Burns Butte from the HLP, may plot along similar mixing lines as those described above. We feel that its petrogenesis is likely similar to the 5 systems described above, namely minor assimilation of Cenozoic silicic rocks but that one of two issues cause it to plot to lower $^{143}Nd/^{144}Nd$. Either, 1) the parental rhyolite (or basalt) for this 7.7 Ma sample had higher $^{87}Sr/^{86}Sr_{(i)}$ and lower $^{143}Nd/^{144}Nd$ isotopic composition, and this would be in line with eastern samples (both basalts and older rhyolites) having a higher $^{87}Sr/^{86}Sr_{(i)}$ (cf. Figure 5) or 2) the Nd systematics of this sample are somehow upset, based on Figure 8, and the fact that this is the only sample that plots appreciably off the terrestrial array of Vervoort et al. (1999).

In a similar fashion we explore potential mixing end members in the $^{207}Pb/^{204}Pb$ vs. $^{206}Pb/^{204}Pb$ system (Figure 12). While we did not have the dataset to explore the Pb isotopic regime for the Klamath and Blue Mountains, based upon our above assessment of Nd and Sr isotopes, we believe these to be unlikely contaminants for the HLP – NWBR rhyolites. In the $^{207}Pb/^{204}Pb$ vs. $^{206}Pb/^{204}Pb$ system, the John Day silicic rocks again plot to more radiogenic values (Figure 12). Middle Miocene samples, however, plot directly underneath the HLP – NWBR samples, and they are not shown in Figure 12.

Two samples plot along this John Day array, including Quartz Mountain from the HLP and Hagar Mountain from the NWBR, and thus John Day silicic rocks or Tyee-like sediments (see below) could impart the Pb isotopic signature seen in these samples. If this is the case, one might expect to see some shift in Sr isotopes as well. Indeed, Quartz Mountain plots marginally higher than basalts in $^{87}Sr/^{86}Sr_{(i)}$ at 0.70441 (Figure 5), although Hagar Mountain shows no discernible shift in Sr isotopes. All of the samples discussed in the Sr section above that show a larger shift in $^{87}Sr/^{86}Sr_{(i)}$ also have Sr concentrations below 35 ppm while Quartz Mountain, which only shows a subtle shift, is 60 ppm and Hagar Mountain, with no shift in $^{87}Sr/^{86}Sr_{(i)}$ as compared to local basalts, has > 200 ppm Sr, thus limiting any increase in $^{87}Sr/^{86}Sr$ due to assimilation of lower Sr concentration John Day silicic rocks.

The Tyee Formation, an Eocene sedimentary formation generally located in the Coast Range of Oregon (plotted with a "T" in Figure 12, after Church, 1976), has the proper Pb isotopes to be a potential mixing component for these two samples. But, this formation, which likely got its isotopic signal from the Idaho Batholith (Heller et al., 1985), does not have the required Sr and Nd isotope ratios to be a contaminant (Figure 11) for these samples. The amount of contamination from a Tyee-like isotopic source required to impart the Pb isotopic ratios in these samples would result in a significant shift in the Sr and Nd isotope ratios. Conrey et al., (2001) suggest that due to low Pb concentrations in parental basaltic magmas that all mafic lavas could have crustal Pb contamination in the central Cascades. This may also be true in the HLP – NWBR but some rhyolites are clearly elevated above the basalts in the $^{207}Pb/^{204}Pb$ vs. $^{206}Pb/^{204}Pb$ system (Figure 12). It is possible that these samples inherited some Pb from one crustal contaminant and Sr from another, as discussed below.

In addition to Quartz and Hagar Mountains, at least five rhyolites and the RST plot to slightly higher $^{207}Pb/^{204}Pb$ than do the corresponding basalts (Figure 9, Figure 12). An argument can be made that this might indicate the assimilation of some contaminant, similar to the isotopic makeup of that found in the Astoria Fan, in to a parental (lower silica) rhyolite or during the evolution from a parental (lower silica) to high silica rhyolite. We do not believe this is the case based on the following argument. First, the

high Sr concentration of these potential contaminants, coupled with reasonably high $^{87}Sr/^{86}Sr$ ratios would likely result in high $^{87}Sr/^{86}Sr_{(i)}$ in the rhyolites, especially those with lower Sr concentrations, but we do not observe this. The DCT and Indian Creek Butte, both of which have high ^{207}Pb and low total Sr (6 and 18 ppm respectively) are not displaced to higher $^{87}Sr/^{86}Sr$ ratios compared to local basalts (Figure 5, Figure 7). Secondly, the Nd isotopic ratios for those rhyolitic samples that do show increased $^{87}Sr/^{86}Sr_{(i)}$ are inconsistent with addition of a Astoria Fan or Tyee-like contaminant, with the exception of Burns Butte (see above). Finally, the RST (green field, Figure 12) shows no difference in Pb isotopic ratios between member E and A, despite showing differences in Sr and Nd isotope compositions of these genetically related magmas (Figure 5 and Figure 11).

We favor a two-stage contamination model. Small amounts of a contaminant, a terrigenous marine sediments similar to that found in the Astoria Fan, are incorporated in the partial melt of the basalt source region for some HLP rhyolites and the RST and this achieves the high ^{207}Pb signature seen in some samples. We do not see any NWBR rhyolites with only high ^{207}Pb and this is consistent with a greater flux of basaltic magma into the crust in the HLP, resulting in a hotter regime and increased potential for partial melt. There may also be a mantle lithospheric contribution to the overall high ^{207}Pb values measured in the basaltic rocks.

There is also an upper-crustal contaminant in some rhyolites, which is added to the parental (lower silica) rhyolite produced by the partial melt, or while this parental rhyolite is fractionating to produce a high-silica rhyolite. Two rhyolites (Quartz and Hagar Mountains) show elevated ^{206}Pb, which is consistent with contamination of a small amount of John Day-like upper-crustal signature in these higher Sr concentration rhyolites. Some low-Sr rhyolites show elevated $^{87}Sr/^{86}Sr_{(i)}$ but also have more radiogenic $^{143}Nd/^{144}Nd$ (e.g. RST, Cox Flat), again consistent with assimilation of small amounts of John Day-like crust and inconsistent with other possible assimilants. This upper-crustal addition is possible both in the HLP and NWBR and in some cases (RST and maybe Burns Butte) there is minor contribution at both stages.

Partial Melting of Mafic Protoliths: Isotopic Constraints:

Oxygen isotopes also help to determine possible protoliths for partial melting that forms the bulk of the rhyolites in the HLP – NWBR. Eight of the 25 $\delta^{18}O_{(melt)}$ values for rhyolites are below those for regional basalts (Figure 10), indicating that meteoric water-affected crust is the protolith for partial melting. Such rhyolites cannot be formed solely by fractional crystallization of basalt. Due to this shift to lower $\delta^{18}O$ values, O isotope values cannot eliminate those protoliths that have similar Nd, Sr, and Pb isotopic values from being a protolith for those eight samples. Indeed, nearly all mafic crustal rocks are still potential protoliths, including < 12 Ma basalts, other Cenozoic mafic volcanic rocks, ophiolites (e.g. Josephine), Mesozoic mafic intrusives, some metaplutonics, and even some silicic plutons without strongly evolved (high $^{87}Sr/^{86}Sr$ and low $^{143}Nd/^{144}Nd$) isotope ratios (Appendix 6), as long as their O isotopic signature has been affected by meteoric waters.

For those rhyolites that are approximately 0.8 to 1.4 ‰ above the basalts in $\delta^{18}O$ (see boxes in Figure 13), there are three possible explanations. These include: 1) incorporation of a contaminant with Pb isotopes similar to the Astoria Fan, likely during the partial melting phase, 2) increases in $\delta^{18}O_{(melt)}$ due to non-modal partial melting of a mafic protolith to form parental rhyolites, fractional crystallization (either from parental rhyolites to high silica rhyolites or from parental basalt to rhyolites, e.g. the extreme fractional crystallization of McCurry et al., 2008), or both, and 3) melting of a crustal protolith with a homogeneous $\delta^{18}O$ that approximates that of the rhyolites.

The first of the possible ways to increase $\delta^{18}O$ is also used to increase Pb isotopic ratios for some samples, namely the addition of a contaminant (similar to terrigenous marine sediments) with an isotopic signature similar to the Astoria Fan. In two component mixing models, using a hypothetical mafic protolith similar to basalts from the HLP - NWBR, approximately 1 to 10 % terrigenous marine sediment contaminant is needed to match the Pb isotopic data for the high ^{207}Pb rhyolites, depending on if one chooses the least or most radiogenic end member for the sediments and depending on the initial Pb isotopic composition of the starting basalt (Figure 14). With an estimated $\delta^{18}O$

of 20 ‰ in the contaminant (pelagic clays ranging from 15 – 25 ‰; cf. Eiler, 2001) and 6.2 ‰ in the basalt or mafic source rock, the resulting $\delta^{18}O$ of the partial melt closely matches that of the rhyolites with ~4 to 7 % addition of the contaminant (PbM mixing line, Figure 13), similar to what is needed to shift the Pb isotopes as well. The current day $^{87}Sr/^{86}Sr$ ratio for cratonic sediments (Astoria Fan) can be approximated by the modern day Columbia River (Goldstein and Jacobsen, 1988) but values for past sediments are certainly higher due to a greater percentage of Proterozoic material deposited during large discharge events (Prytulak et al., 2006), as is evidenced in the Tyee Formation values (Figure 11, Heller et al., 1985). While addition of a contaminant similar to Astoria Fan sediments also shift the Nd and Sr isotopes, it is not enough to eliminate this as a scenario (Figure 15; Table 4) where a low percentage of contamination is added to the partial melting of a mafic protolith with relatively high Sr concentrations.

As discussed earlier, this contaminant addition must happen during the partial melting phase. If a parental rhyolite (higher in total Pb concentration than a basalt would be) is used for the starting composition, the minimum amount required is at least 10 to 15% of the highest ^{207}Pb and ^{206}Pb Astoria Fan sediment (used as a proxy for terrigenous marine sediments) to get the Pb isotopic signature of the high ^{207}Pb rhyolites (Figure 14). This results in $\delta^{18}O_{(melt)}$ values well over 8 ‰ and unreasonable Nd and Sr isotopes as well (Figure 14 and Figure 15; Table 4). While these models do not show the full range of possible outcomes, they are representative and dictate the timing of assimilation. Small percentages (1 -7 %) of a contaminant like the Astoria Fan added during partial melting can increase the $\delta^{18}O$ to nearly observed levels (Figure 13), produce the increase in radiogenic Pb for some samples (Quart Mountain and Hagar Mountain require a John Day-like contaminant) and not perturb the Sr and Nd isotopic systems enough to fall outside what is observed.

The second mechanism relies on either fractional crystallization or non-modal partial melting to get the increase in $\delta^{18}O_{(melt)}$ from basalts to rhyolites (Figure 13). Previous workers have noticed an increase of approximately 1 ‰ in $\delta^{18}O_{(melt)}$ in suites believed to be produced by fractional crystallization from basalt to rhyolite (e.g. Chivas

et al., 1982; Muehlenbachs and Byerly, 1982). Other workers, in both natural systems (e.g. Harris et al., 2000) or using forward-step MELTS modeling (Bindeman et al., 2004) have indicated that only 0.3 – 0.4 ‰ increase is expected with fractionation from basalt to rhyolite. In our results, we see an increase of 0.2 – 0.3 ‰ in $\delta^{18}O_{(melt)}$ from low to high silica rhyolites (increasing from 71 to 77 wt. % SiO_2) and this may be related to fractional crystallization. For the RST, Streck and Grunder (1997) show that fractional crystallization of about 50% of least-evolved unit E can produce most-evolved unit A. Using their calculations of non-modal fractionating phases (64% feldspar – generally oligoclase to anorthoclase, 32 % quartz and 4 % magnetite) and $\Delta^{18}O$(mineral – melt) values calculated from Bindeman and Valley (2003), the increase in $\delta^{18}O_{(melt)}$ would be ~0.14 ‰. For the RST system, the increase in $\delta^{18}O_{(melt)}$ by the fractionation of feldspars is essentially canceled by the decrease caused by fractionation of quartz and thus the small amount of magnetite fractionation strongly controls the oxygen isotope systematics. Magnetite crystallization and fractionation also causes an increase in increase $\delta^{18}O$ for HLP high silica rhyolites that are produced by the fractional crystallization of low silica rhyolites, but fractionation of plagioclase and alkali feldspars from samples that do not fractionate much quartz would also cause an increase (cf. Table 4, Chapter 2). We do not see this increase represented by the RST data in Figure 13 because only unit C of the RST was measured for oxygen isotopes (Streck and Grunder, 2008).

Partial melting can also increase $\delta^{18}O$. In our simplified and *ad hoc* model, we examined the non-modal dehydration (no water added) melting of composition 478 of Beard and Lofgren (1991) at 3 kb and 900ºC. This starting composition is similar to Wilson Butte of the HLP and partial melting (19%) produced a high iron, ~73 wt. % SiO_2 rhyolite melt, albeit more tonalitic (low K) than HLP – NWBR rhyolites. We applied $\Delta^{18}O$(mineral – melt) values calculated from Bindeman and Valley (2003) and Bindeman et al. (2004) to the phase assemblage produced by this non-modal partial melt (9 quartz + 33 amphibole + 5 plagioclase = 2 magnetite + 25 pyroxene + 19 melt; Beard and Lofgren, 1991) and calculated an increase slightly less than 0.4 ‰ in $\delta^{18}O$. It is an open question if fractional crystallization alone can produce the increase in $\delta^{18}O_{(melt)}$ we see but it seems

highly unlikely that partial melting alone can cover the entire gap in oxygen isotopes between basalts and rhyolites.

Finally, one last way to produce the O isotope signature measured in the rhyolites is to melt a protolith with a similar isotopic signature. This would preclude wholesale melting of many of the Mesozoic protoliths as many of them have $\delta^{18}O > 8$ ‰ (Appendix 6). Another issue is the apparent homogeneity of the rhyolites that cluster between 6.8 and 7.0 ‰ (that is, not including the rhyolites that have meteoric water involvement, cf. Figure 10, Figure 13). There is not a spatial or temporal shift in O isotopes in the rhyolites from across the HLP - NWBR. This means that a large area of the crust under central and eastern Oregon, which is composed of a mélange of accreted terranes, including ophiolites and sea floor deposits with widely variable O isotopic signatures, would have to become homogenized prior to partially melting to produce the fairly uniform $\delta^{18}O$ we see in the HLP – NWBR rhyolites and we feel that is an unlikely scenario.

Our favored model includes the partial melt of recently emplaced late Miocene and younger basaltic magmas, which may have been amphibolitized from water given off by the crystallizing, stalled basaltic magmas. Some of these solidified basalts were affected by meteoric waters to obtain the low $\delta^{18}O$ signature and many contain a few percent of marine sediment, or a similar contaminant. This, coupled with a few tenths of a per mil increase from partial melting can produce the Pb and O isotopic signatures seen in the low silica rhyolites. Fractionation to high silica rhyolites pushes the $\delta^{18}O_{(melt)}$ up a few more tenths of a per mil and in some cases (e.g. RST, Cox Flat), upper crustal contamination from John Day silicic rocks, or possibly middle Miocene rocks yields the elevated Sr isotopes seen in some samples. We favor partial melts of recent basalts over other Cenozoic basalts for two reasons: 1) the energetics of partial melting already hot, recent basalts are more favorable (e.g. Christiansen and McCurry, 2008; Chapter 4) and 2) many ^{206}Pb isotopes for HLP – NWBR rhyolites are lower than potential Oligocene and older mafic protoliths but not lower than middle Miocene and < 12 Ma basalts (Figure 12).

There does not seem to be a correlation between Fe-line (cf. Figure 12, Chapter 2) and low $\delta^{18}O$ signature or other isotopic ratios that indicates crustal contamination. Some samples from the HLP that have a low FeO* at a given silica have low $\delta^{18}O$ (e.g. Round Top Butte, Burns Butte) while others have a "normal" $\delta^{18}O$ (e.g. Palomino Butte, Iron Mountain). Likewise, high FeO* at a given silica samples can have either a low (Devine Canyon Tuff, Horse Mountain) or normal (Hampton Tuff, Glass Buttes) $\delta^{18}O$ signature (Figure 10).

Slight depletion of the middle REE (rare earth elements) is common in both HLP and NWBR samples and does not seem correlated to isotopic composition. This indicates that amphibole is involved in either partial melting or as a crystallizing phase. During partial melting, if the crustal protolith of a low silica rhyolite contains residual amphibole, then the resultant partial melt would show depletion in the middle REE but if the amphibole phase is melted completely, then no depletion would be expected. If AFC (assimilation and fractional crystallization) is occurring and amphibole is a crystallizing phase, depletion in middle REE will also result. This slight depletion (most pronounced in Ho and Er) becomes difficult or impossible to distinguish as low silica rhyolites differentiate to high silica rhyolites and other workers (e.g. Streck and Grunder, 2008) this fractional can obscure the true lineage of a rhyolite.

CONCLUSIONS:

The < 12 Ma age-progressive rhyolites from the HLP and NWBR have $^{87}Sr/^{86}Sr_{(i)}$ values that range from 0.70317 to 0.70689 and most are similar to local basalts (Figures 5, 7, 10). A few samples have Sr isotope ratios above those of the basalts and we believe this is due to small degrees of contamination from Oligocene (John Day) to middle Miocene silicic volcanic rocks. These volcanics and volcaniclastic sediments are likely not evenly distributed over the HLP – NWBR area, but could average as much as 1000 m in thickness (with a corresponding total volume of up to 50,000 km^3) and locally could be much thicker. These volcanics could now be multiple km deep in the HLP due to basinal

downwarping, based upon the dips of ignimbrite sheets at the northern margins of the HLP (cf. Chapter 2).

In Pb isotope space, $^{206}Pb/^{204}Pb_{(i)}$ ranges from 18.76 – 19.16 and $^{207}Pb/^{204}Pb_{(i)}$ ranges from 15.57 to 15.62 for the < 12 Ma rhyolites. Some rhyolites are only marginally displaced above the Pb isotopes for local basalts (Figure 9) and we attribute this to small amounts, likely 2 to 7 %, of a contaminant added during partial melting in the lower to middle crust. This contaminant, which are terrigenous marine sediments that are isotopically similar to that in the Astoria Fan, has Proterozoic craton isotope signatures and is likely part of the mélange of accreted terranes that make up the crust of much of Oregon. This signal is not enough to perturb the Sr and Nd isotopic systematics of the system but can raise the radiogenic Pb signature to match what we observe. Additionally, this increases the $\delta^{18}O_{(melt)}$ of the parental rhyolite a few tenths of a per mil. Two rhyolites plot off in an array that suggests the assimilation of a significant amount of John Day silicic volcanic rocks (Figure 12). The Tyee Formation is precluded for these two samples based on the Nd and Sr isotopes ratios and the large amounts of contaminant required.

O isotopes for basalts in this work yield a $\delta^{18}O_{(melt)}$ of 6.0 – 6.4 ‰ and the rhyolites from this work and previous work (Savov et al., 2009; Roche, 1987) are 3.9 – 7.9 ‰. Eight rhyolites have $\delta^{18}O_{(melt)}$ values less than the basalts indicating petrogenesis from a source which has been altered by meteoric water. The remaining rhyolites are generally 0.8 to 1.4 ‰ higher than the basalts. This increase could be due either to fractional crystallization alone or, more likely, to a combination of processes. These include incorporation of a small percentage of a contaminant isotopically similar to Astoria Fan sediments with a high $\delta^{18}O$ in the lower or middle crust where partial melting is occurring, some increase in $\delta^{18}O$ due to non-modal partial melting, and some fractional crystallization, especially to go from low silica rhyolite to high silica rhyolite, likely in the upper crust. Each of these processes is capable of adding 0.1 to 1.0 ‰ to the $\delta^{18}O$ signature of the resulting melt. Partial melts of most Mesozoic rocks are precluded because of their variable and high $^{87}Sr/^{86}Sr_{(m)}$ and $\delta^{18}O$ signature and the likelihood that

these accreted terranes are heterogeneous with respect to O isotopes, especially on the spatial scale of the HLP – NWBR, while most < 12 Ma rhyolites (excluding the low $\delta^{18}O_{(melt)}$ rhyolites) show little variation in O isotope space.

Hafnium isotopes yield a $^{176}Hf/^{177}Hf_{(i)}$ range of 0.282864 – 0.283138 (Table 3) with corresponding CHUR time corrected $\varepsilon Hf_{(i)}$ of 3.48 to 13.11. With the exception of one sample, samples plot along the terrestrial array of Vervoort et al. (1999) indicating that Nd and Hf systematics are not decoupled and we generally prefer to use the more precise Nd isotope ratios (Figure 8).

Nd isotopes help to constrain the upper crustal contaminant and $^{143}Nd/^{144}Nd$ ratios range from 0.512586 – 0.512922 for time corrected (initial) values, corresponding to $\varepsilon Nd_{(i)}$ of -0.71 to 5.73. This contaminant must have a $^{143}Nd/^{144}Nd$ ratio equal to or greater than the HLP – NWBR rhyolites and also have more radiogenic Sr isotopes. The only assimilants that could accomplish this are the middle Miocene or John Day aged (Oligocene) silicic rocks. We believe the John Day rocks to be the more likely assimilant as they are implicated as a mixing component in Pb isotope space for some samples and are thought to be much more widespread than the middle Miocene (Steens-aged) silicic rocks. Additionally, flexural downwarping of the crust, likely due to magmatic addition, could place the John Day aged silicic rocks deep enough in the crust to be a possible contaminant. Overall, there are much less data on the Tertiary silicic rocks in central and eastern Oregon and the possibility that middle Miocene or Clarno samples with the appropriate isotopic signature to be a mixing end member cannot be completely ruled out.

We also note both a spatial and temporal shift in Nd and Sr isotopes in the basalts of the HLP – NWBR (Figure 5, Figure 6). This spatial shift has been noted region-wide (Hart, 1985; Leeman, 1982; Jordan, 2001) and ascribed to an old, perhaps cratonic-influenced lithosphere that lies to the east, and we see a similar trend in the HLP proper. We also see a temporal shift in the basaltic isotopes, with younger basalts having lower $^{87}Sr/^{86}Sr$ and higher $^{143}Nd/^{144}Nd$ ratios, maybe indicating a shift in the mantle input. Major and trace elements also indicate that there might be greater degrees of partial melting in the mantle and that these melts are hotter. Younger, hotter basalts have less radiogenic Sr while younger rhyolites have constant or increasingly radiogenic

compositions (cf. Figure 5 and Figure 6, west is younger for rhyolites), which indicates that there is increasing upper crustal component in the western rhyolites. This is consistent with our model of building heat through time (thermal maturation) in the HLP, resulting in an increase in $FeO^*:SiO_2$, a tendency towards anhydrous phase assemblages (cf. Chapter 2).

In the HLP, we see crustal differentiation in an intracontinental system. The increased heat flow that drives this crustal differentiation is a result of asthenopheric counterflow and upwelling around the subducting Juan de Fuca plate, not a hot spot or plate thinning as in a rift. This differentiation is rapid, mobilizing a silicic partial melt from sub-solidus, recently intraplated mantle-sourced basaltic magmas and leaving behind a more mafic cumulate. Unlike in the SRP, there is no evidence of hybridization of recent mantle derived basaltic magmas and older crustal protoliths in the middle crust, only evidence of the addition of a few percent of a component that isotopically resembles marine sediments.

REFERENCES:

Allen, C. M and Barnes, C. G, 2006, Ages and some cryptic sources of Mesozoic plutonic rocks in the Klamath Mountains, California and Oregon, in Snoke, A. W. and Barnes, C. G., eds., Geological studies in the Klamath Mountains province, California and Oregon; a volume in honor of William P. Irwin: Geological Society of America Special Paper 410, p. 223-245.

Ambroz, J. A.,1997, Characterization of archaeologically significant obsidian sources in Oregon by neutron activation analysis: University of Missouri MS Thesis, 199 p.

Baertschi, P., 1976, Absolute 18O content of standard mean ocean water: Earth and Planetary Science Letters, v. 31, p. 341-344.

Bacon, C. R., Bruggman, P. E., Christiansen, R. L., Clynne, M. A., Donnelly-Nolan, J. M. and Hildreth, W., 1997, Primitive magmas at five Cascade volcanic fields: Melts from hot, heterogeneous sub-arc mantle: The Canadian Mineralogist, v. 35, p. 397-423.

Bacon, C. R., Gunn, S. H., Lanphere, M. A and Wooden, J. L., 1994, Multiple isotopic components in Quaternary volcanic rocks of the Cascades Arc near Crater Lake, Oregon: J. of Petrology, v. 35, p. 1521-1556.

Beard, J. S. and Lofgren, G. E., 1991, Dehydration melting and water-saturated melting of basaltic and andesitic greenstones and amphibolites: Journal of Petrology, v. 32, p. 365-401.

Bestland, E. A., and Retallack, G. J., 1994a, Geology and paleoenvironments of the Clarno Unit, John Day Fossil Beds National Monument, Oregon: U.S. National Park System, Open File Report, 160 p.

Bestland, E. A. and Retallack, G. J., 1994b, Geology and paleoenvironments of the Painted Hills Unit, John Day Fossil Beds National Monument, Oregon: U.S. National Park System, Open File Report, 211 p.

Bindeman, I. N. and Valley, J. W., 2003, Rapid generation of both high- and low $\delta^{18}O$, large-volume silicic magmas at the Timber Mountain/Oasis Valley caldera complex, Nevada: GSA Bulletin, v. 115, p. 581-595.

Bindeman, I. N., Ponomareva, V. V., Bailey, J. C., Valley, J. W., 2004, Volcanic arc of Kamchatka: a province with high-delta O-18 magma sources and large-scale O-18/O-16 depletion of the upper crust: Geochimica et Cosmochimica Acta v. 68, p. 841-865.

Bindeman, I. N., Leonov, V. L., Izbekov, P. E., Ponomareva, V. V., Watts, K. E., Shipley, N. K., Perepelov, A. B., Bazanova, L.I., Jicha, B. R., Singer, B. S., Schmitt, A. K., Portnyagin, M. V. and Chen, C. H., 2010, Large-volume silicic volcanism in Kamchatka: Ar–Ar and U–Pb ages, isotopic, and geochemical characteristics of major pre-Holocene caldera-forming eruptions: J. Volcanology and Geothermal Research, v. 189, p. 57-80.

Bindeman, I., Gurenko, A., Sigmarsson, O. and Chaussidon, M., 2008, Oxygen isotope heterogeneity and disequilibria of olivine crystals in large volume Holocene basalts from Iceland: Evidence for magmatic diggestion and erosion of Pleistocene hyaloclastites: Geochimica et Cosmochimica Acta, v. 72, p. 4397-4420.

Bindeman, I., Watts, K. E., Schmitt, A. K., Morgan, L. A., and Shanks, P. W. C., 2007, Voluminous low $\delta^{18}O$ magmas in the late Miocene Heise volcanic field, Idaho: Implications for the fate of Yellowstone hotspot calderas: Geology, v. 35, p. 1019-1022.

Bohrson,W. A. and Spera, F. J., 2001, Energy-constrained open-system magmatic processes II: Application of energy-constrained assimilation-fractional crystallization (EC-AFC) model to magmatic systems: J. of Petrology, v.42, p. 1019-1041.

Bonnichsen, B., Leeman, W. P., Honjo, N., W. C., McIntosh, and Godchaux, M. M., 2008, Miocene silicic volcanism in southwestern Idaho: geochronology, geochemistry, and evolution of the central Snake River Plain: Bulletin of Volcanology, v. 70, no. 3, p. 315-342.

Bowen, G. J. and Revenaugh J., 2003, Interpolating the isotopic composition of modern meteoric precipitation: Water Resources Research, v. 39, 1299, 13 p.

Bromley, S. A., 2011, Evolution and inheritance of Cascadia sub-arc mantle reservoirs: Oregon State University MS Thesis, 192 p.

Brueseke, M. E., Heizler, M. T., Hart, W. K. and Mertzman, S. A., 2007, Distribution and geochronology of Oregon Plateau (U.S.A.) flood basalt volcanism: The Steens Basalt revisited: J. of Volcanology and Geothermal Research, v. 161, p. 187-214.

Carlson, R. W., Czamanske, G., Fedorenko, V., and Ilupin, I., 2006, A comparison of Siberian meimechites and kimberlites: Implications for the source of high-Mg alkalic magmas and flood basalts: Geochemistry Geophysics Geosystems, v. 7, no. 11, Nov 21, 2006.

Carlson, R. W. and Hart, W. K., 1987, Crustal Genesis on the Oregon Plateau: J. of Geophysical Research, v. 92, p. 6191-6206.

Carlson, R. W. and Hart, W. K., 1988, Flood basalt volcanism in the Pacific Northwestern United States, in: Macdougall, J.D., ed., Continental Flood Basalts: Kluwer, Dordecht, p. 35-62.

Chivas, A. R., Andrew, A. S., Sinha, A. K., and O'Neil J. R., 1982, Geochemistry of a Pliocene-Pleistocene ocean-arc pluton complex, Guadalcanal: Nature, v. 300, p. 139-143.

Christiansen, E. H. and McCurry, M., 2008, Contrasting origins of Cenozoic silicic volcanic rocks from the western Cordillera of the United States: Bulletin of Volcanology, v. 70, no. 3, p. 251-267.

Church, S. E., 1976, The Cascade Mountains revisited: A re-evaluation in light of new lead isotopic data: Earth and Planetary Science Letters, v. 29, p. 175-188.

Conrey,R. M., Hooper, P. R., Larson, P. B., Chesley, J. and Ruiz, J., 2001, Trace element and isotopic evidence for two types of crustal melting beneath a High Cascade volcanic center, Mt. Jefferson, Oregon: Contributions to Mineralogy and Petrology, v. 141, p. 710-732.

Cox, C., 2011, A Controlled- Source Seismic and Gravity Study of the High Lava Plains (HLP): University of Oklahoma MS Thesis, 110 p.

DeMets, C., Gordon, R. G., Argus, D. F. and Stein, S., 1994, Effect of recent revisions to the geomagnetic reversal time scale on estimate of current plate motions: Geophysical Research Letters, v. 21, no. 20, p. 2191-2194.

DePaolo, D. J., 1981, Trace element and isotopic effects of combined wallrock assimilation and fractional crystallization: Earth and Plaetary Science Letters, v. 53, p. 189-292.

de Silva, S. L. and Gosnold, W. D., 2007, Episodic construction of batholiths: Insights from the spatiotemporal development of an ignimbrite flare-up: J.of Volcanology and Geothermal Research, v. 167, p. 320-335.

Dicken, S. N., 1950, Oregon Geography: First Preliminary Edition: Ann Arbor, MI, Edwards Brothers, 104 p.

Donnelly-Nolan, J. M., 1998, Abrupt shift in $\delta^{18}O$ values at Medicine Lake Volcano (California, USA): Bulletin of Volcanology, v. 59, p. 529-536.

Donnelly-Nolan, J. M., Grove, T. L., Lanphere, M. A., Champion, D. E. and Ramsey, D. W., 2008, Eruptive history and tectonic setting of Medicine Lake Volcano, a large rear-arc volcano in the southern Cascades: J. of Volcanology and Geothermal Research, v. 177, p. 313-328.

Eiler, J. M., 2001, Oxygen isotope variations of basaltic lavas and upper mantle rocks, in Valley, J. W. and Cole, D. R., eds., Stable Isotope Geochemistry: Reviews in Mineralogy and Geochemistry, v. 43, p. 319-364.

Evans, S. H. and Brown, F. H., 1981, Summary of potassium/argon dating – 1981: Department of Energy, Division of Geothermal Energy ID-12079-45, 29 p.

Fiebelkorn, R. B., Walker, G. W., MacLeod, N. S., McKee, E. H., and Smith, J. G., 1983, Index to K-Ar determinations for the state of Oregon: Isochron Weast, no. 37, p. 3-60.

Frey F.A., Coffin M.F., Wallace P.J., Weis D., Zhao X., Wise S.W., Jr., Wahnert V., Teagle D.A.H., Saccocia P.J., Reusch D.N., Pringle M.S., Nicolaysen K.E., Neal C.R., Müller D.R., Moore C.L., Mahoney J.J., Keszthelyi L., Inokuchi H., Duncan R.A., Delius H., Damuth J.E., Damasceno D., Coxall H.K., Borre M.K., Boehm F., Barling J., Arndt N.T. and Antretter M., 2000, Origin and Evolution of a Submarine Large Igneous Province: The Kerguelen Plateau and Broken Ridge, Southern Indian Ocean: Earth and Planetary Science Letters, v. 176, p. 73-89.

Frost, B. R., Barnes, C. B., Collins, W. J., Arculus, R. J., Ellis, D. J. and Frost, C. D., 2001, A geochemical classification for granitic rocks: J. of Petrology, v. 42, p. 2033-2048.

Furman, T., Frey, F. A., Meyer, P. S., 1992, Petrogenesis of evolved basalts and rhyolites at Austurhorn, southeastern Iceland: the role of Fractional Crystallization: J. of Petrology, v. 33, p. 1405-1445.

Goldstein, S. J. and Jacobsen, S. B., 1988, Nd and Sr isotopic systematics of river water suspended material: implications for crustal evolution: Earth and Planetary Science Letters, v. 87, p. 249-265.

Graham, D. W., Reid, M. R., Jordan, B. T., Grunder, A. L., Leeman, W. P., and Lupton, J. E., 2009, Mantle source provinces beneath the Northwestern USA delimited by helium isotopes in young basalts: J. of Volcanology and Geothermal Research, v. 188, p. 128-140.

Grove, T. L., Donnelly-Nolan, J. M. and Housh, T., 1997, Magmatic processes that generated the rhyolite of Glass Mountain, Medicine Lake volcano, N. California: Contributions to Mineralogy and Petrology, v. 127, p. 205-223.

Gunnarsson, B., Marsh, B. D. and Taylor, H. P., 1998, Generation of Icelandic rhyolites: silicic lavas from the Torfajokull central volcano: J. of Volcanology and Geothermal Research, v. 83, p. 1-45.

Hanan, B. B. and Graham, D. W., 1996, Lead and Helium isotope evidence from oceanic basalts for a common deep source of mantle plumes: Science, v. 272, p. 991-995.

Hanan, B. B., Shervais, J. W. and Vetter, S. K., 2008, Yellowstone plume-continental lithosphere interaction beneath the Snake River Plain: Geology, v. 36, p. 51-54.

Harmon, R. S. and Hoefs, J. 1995, Oxygen isotope heterogeneity of the mantle deduced from global ^{18}O systematics of basalts from different geotectonic settings: Contributions to Mineralogy and Petrology, v. 120, p. 95-114.

Harris, C., Smith, H. S. and le Roex, A. P., 2000, Oxygen isotope composition of phenocrysts from Tristan da Cunha and Gough Island lavas: Variation with fractional crystallization and evidence for assimilation: Contributions to Mineralogy and Petrology, v. 138, p. 164-175.

Hart, S. R., 1984a, The DUPAL anomaly: A large scale isotopic anomaly in the southern hemisphere: Nature, v. 309, p. 753-756.

Hart, W. K., 1985, Chemical and isotopic evidence for mixing between depleted and enriched mantle, northwestern USA: Geochimica et Cosmochimica Acta, v. 49, p. 131-144.

Hegner, E. and Tatsumoto, M., 1987, Pb, Sr, and Nd isotopes in basalts and sulfides from the Juan de Fuca Ridge: J. of Geophysical Research, v. 92, p. 11380-11386.

Heller, P. L., Peterman, Z. E., O'Neil, J. R. and Shafiqullah, M., 1985, Isotopic province of sandstones from the Eocene Tyee Formation, Oregon Coast Range: Geological Society of America Bulletin, v. 96, p. 770-780.

Hildreth, W., 2007, Quaternary magmatism in the Cascades – geologic perspectives: US Geological Survey Professional Paper 1744, 125 p.

Hildreth, W., and Moorbath, S., 1988, Crustal contributions to arc magmatism in the Andes of central Chile: Contributions to Mineralogy and Petrology, v. 98, p. 455-489.

Hildreth, W., and Moorbath, S., 1991, Reply to comment on "Crustal contributions to arc magmatism in the Andes of central Chile" by W. Hildreth and S. Moorbath: Contributions to Mineralogy and Petrology, v. 108, p. 247-252.

Hoefs, J., 2009, Stable isotope geochemistry: Springer-Verlag, Berlin, Germany, 288p.

Iademarco, M. J., 2009, Volcanism and faulting along the northern margin of Oregon's High Lava Plains: Hampton Butte to Dry Mountain: Oregon State University MS Thesis, 141 p.

Irwin, W. P. and Wooden, J. L., 1999, Plutons and accretionary episodes of the Klamath Mountains, California and Oregon: U. S. Geological Survey Open File Report 99-374, 1 sheet.

Ito, E., White, W. M. and Gopel, C., 1987, The O, Sr, Nd and Pb isotope geochemistry of MORB: Chemical Geology, v. 62, p. 157-176.

Jicha, B. R., Hart, G. L., Johnson, C. M., Hildreth, W., Beard, B. L., Shirey, S. B. and Valley, J. W., 2009, Isotopic and trace element constraints on the petrogenesis of lavas from the Mount Adams volcanic field, Washington: Contributions to Mineralogy and Petrology, v. 157, p. 189-207.

Johnson, D. M., Hooper, P. R. and Conrey, R. M., 1999, XRF analysis of rocks and minerals for major and trace elements on a single low dilution Li-tetraborate fused bead: Advances in X-ray analysis, v. 41, p. 843-867.

Johnson, J. A., and Grunder, A. L., 2000, The making of intermediate composition magma in a bimodal suite: Duck Butte Eruptive Center, Oregon, USA: J. of Volcanology and Geothermal Research, v. 95, p. 175-195.

Jonasson, K., 1994, Rhyolite volcanism in the Krafla central volcano, north-east Iceland: Bulletin of Volcanology, v. 56, p. 516-528.

Jonasson, K., 2007, Silicic volcanism in Iceland: Composition and distribution within the active volcanic zones: J. of Geodynamics, v. 43, p. 101-117.

Jordan, B. T., 2001, Basaltic volcanism and tectonics of the High Lava Plains, southeastern Oregon: Oregon State University PhD thesis, 218 p.

Jordan, B. T., Grunder, A. L., Duncan, R. A., and Deino, A. L., 2004, Geochronology of age-progressive volcanism of the Oregon High Lava Plains: Implications for the plume interpretation of Yellowstone: J of Geophysical Research, v. 109, issue B10, p. 1-19.

Kinzler, R. J., Donnelly-Nolan, J. M. and Grove, T. L., 2000, Late Holocene hydrous mafic magmatism at the Paint Pot Crater and Callahan flow, Medicine Lake Volcano, N. California and the influence of H2O in the generation of silicic magmas: Contributions to Mineralogy and Petrology, v. 138, p. 1-16.

Kistler, R. W. and Peterson, Z. E., 1978, Reconstruction of crustal blocks of California on the basis of initial strontium isotopic compositions of Mesozoic granitic rocks: USGS Professional Paper 1071, 17 p.

Knaack, C., Cornelius, S. B., and Hooper, P. R., 1994, Trace element analyses of rocks and minerals by ICP-MS: Washington State University, open file report, http://www.sees.wsu.edu/Geolab/note/icpms.html, checked 11/22/11.

Lacasse, C., Sigurdsson, H., Carey, S. N., Jóhannesson, H., Thomas, L. E., Rogers, N. W., 2007, Bimodal volcanism at the Katla subglacial caldera, Iceland: insight into the geochemistry and petrogenesis of rhyolitic magmas: Bulletin of Volcanology, v. 69, p. 373-399.

Lee, C. –T. A., Morton, D. M., Kistler, R. W. and Baird, A. K., 2007, Petrology and tectonics of Phanerozoic continent formation: From island arcs to accretion and continental arc magmatism: Earth and Planetary Science Letters, v. 263, p. 370-387.

Leeman, W. P., 1982, Tectonic and magmatic significance of strontium isotope variations in Cenozoic volcanic rocks from the western United States: Geological Society of America Bulletin, v. 93, p. 487-503.

Leeman, W. P., Smith, D. R., Hildreth, W., Palacz, Z. and Rogers, N., 1990, Compositional diversity of late Cenozoic basalts in a transect across the southern Washington Cascades: Implications for subduction zone magmatism: J. of Geophysical Research, v. 95, p. 19561-19582.

Loiselle, M. C. and Wones, D. S., 1979, Characteristics and origins of anorogenic granites: Geological Society of America Program with Abstracts, v. 11, p. 468.

Lundstrom, C., 2009, Hypothesis for the origin of convergent margin granitoids and Earth's continental crust by thermal migration zone refining: Geochemica et Cosmochemica Acta, v. 73, p. 5709-5729.

MacLean, J. W., 1994, Geology and geochemistry of Juniper Ridge, Horsehead Mountain and Burns Butte: implications for the petrogenesis of silicic magma on the High Lava Plains, southeastern Oregon: Oregon State University MS Thesis, 141 p.

MacLeod, N. S., Sherrod, D. R., Chitwood, L. A. and Jensen, R. A., 1995, Geologic Map of Newberry Volcano, Deschutes, Klamath, and Lake Counties: Oregon, USGS Miscellaneous Investigations Series Map I-2455, scale 1:62,500 and 1:24,00.

Martin, E., Martin, H. and Sigmarsson, O., 2008, Could Iceland be a modern analogue for the Earth's early continental crust?: Terra Nova, v. 20, p. 463-468.

Martin, E. and Sigmarsson O., 2007, Crustal thermal state and origin of silicic magma in Iceland: the case of Torfajokull, Ljosufjoll and Snaefellsjokull volcanoes: Contributions to Mineralogy and Petrology, v. 153, p. 593-605.

Mathis, A. C., 1993, Geology and petrology of a 26-Ma trachybasalt to peralkaline rhyolite suite exposed at Hart Mountain, Oregon: Oregon State University MS thesis, 141 p.

McBirney, A. R., 1978, Volcanic evolutions of the Cascade Range: Annual Review of Earth and Planetary Sciences, v. 6, p. 437-456.

McClaughry, J. D., Ferns, M. L., Gordon, C. L. and Patridge, K. A., 2009, Field trip guide to the Oligocene Crooked River caldera: Central Oregon's Supervolcano, Crook, Deschutes, and Jefferson Counties, Oregon: Oregon Geology, v. 69, p. 25-44.

McCurry, M., Hayden, K. P., Morse, L. H. and Mertzman, S., 2008, Genesis of post-hotspot, A-type rhyolite of the Eastern Snake River Plain volcanic filed by extreme fractional crystallization of olivine tholeiite: Bulletin of Volcanology, v. 70, p. 361-383.

McCurry, M. and Rodgers, D. W., 2009, Mass transfer along the Yellowstone hotspot track I: petrologic constraints on the volume of mantle-derived magma: J. of Volcanology and Geothermal Research, v. 188, p. 86-98.

Muehlenbachs, K. and Byerly, G., 1982, 18O enrichment of silicic magmas caused by crystal fractionation at the Galapagos spreading center: Contributions to Mineralogy and Petrology, v.79, p. 76-79.

Nekvasil, H., Simon, A., and Lindsley, D. H., 2000, Crystal fractionation and the evolution of intra-plate hy-normative igneous suites: Insights from their feldspars: J. of Petrology, v. 41, p. 1743-1757.

Newton, V. C., Corcoran, R. E. and Deacon, R. J., 1962, Oregon, still without oil, offers favorable pay areas, in Petroleum Exploration in Oregon: Oregon Department of Geology and Mineral Industries Miscellaneous Paper No. 9, p. 1-5.

Peccerillo, A., Barberio, M. R., Yirgu, G., Ayalew, D., Barberi, M. and Wu, T. W., 2003, Relationships between mafic and acid peralkaline magmatism in continental rift settings: a petrological, geochemical and isotopic study of the Gedemsa volcano, central Ethiopian Rift: J. of Petrology v. 44, p. 2003–2032.

Pezzopane, S. K. and Weldon, R. J., 1993, Tectonic role of active faulting in central Oregon: Tectonics, v. 12, p. 1140-1169.

Popenoe, H. L., 1961, Developments in west coast area in 1960; Bulletin of the American Association of Petroleum Geologists, v. 45, p. 959-973.

Prytulak, J., Vervoort, J. D., Plank, T., and Yu, C., 2006, Astoria Fan sediments, DSDP site 174, Cascadia Basin: Hf-Nd-Pb constraints on province and outburst flooding: Chemical Geology, v. 233, p. 276-292.

Richards, M. A., Jones, D. L., Duncan, R. A. and DePaolo, D. J., 1991, A mantle plume initiation model for the Wrangellia Flood Basalt and other oceanic plateaus: Science, v. 254, p. 263-267.

Robinson, P. T., Walker, G. W. and McKee, E. H., 1990, Eocene (?), Oligocene, and lower Miocene rocks of the Blue Mountains Region: US Geological Survey Professional Paper, 1437, p. 29-62.

Roche, R. L., 1987, Stratigraphic and geochemical evolution of the Glass Buttes Complex, Oregon: Portland State University MS Thesis, 99 p.

Rooney, T., Furman, T., Bastow, I., Ayalew, D. and Yirgu, G., 2007, Lithospheric modification during crustal extension in the Main Ethiopian Rift: J. of Geophysical Research v. 112, p. B10201.

Rudnick, R. L. and Gao, S., 2005, Composition of the Continental Crust, in Rudnick, R. L., ed., The Crust: Treatise on Geochemistry, Holland, H. D. and Turekian, K. K., eds., v. 3, p. 1-64.

Saleeby, J. B. and Busby-Spera, C., 1992, Early Mesozoic tectonic evolution of the western United States Cordillera, in Burchfiel, B. C., Lipman, P. W. and Zoback, M. L., eds., The Cordilleran orogen: Conterminous United States: Geologic Society of America, v. G-3, p. 107-168.

Saunders, A. D., Norry, M. J., and Tarney, J., 1988, Origin of MORB and chemically depleted mantle reservoirs: trace element constraints: J. of Petrology, Special Lithosphere Issue, p. 415-445.

Savov, I. P., Leeman, W. P., Lee, C. T. A. and Shirey, S. B., 2009, Boron isotopic variations in NW USA rhyolites: Yellowstone, Snake River Plain, Eastern Oregon: J. of Volcanology and Geothermal Research, v. 188, p. 162-172.

Scarberry, K. C., 2007, Extension and volcanism: Tectonic development of the northwestern margin of the Basin and Range Province in southern Oregon: Oregon State University PhD thesis, 168 p.

Scarberry, K. C., Meigs, A., and Grunder, A., 2010, Faulting in a propagating continental rift: Insight from the late Miocene structural development of the Abert Rim fault, southern Oregon, USA: Tectonophysics v. 488, p. 71-86.

Schmidt, M. E., Grunder, A. L. and Rowe, M. C., 2008, Segmentation of the Cascade Arc as indicated by Sr and Nd isotopic variations among diverse primitive basalts: Earth and Planetary Science Letters, v. 266, p. 166-181.

Schwartz, J. J., Snoke, A. W., Frost, C. D., Barnes, C. G., Gromet, L. P. and Johnson, K., 2010, Analysis of the Wallowa-Baker terrane boundary: Implications for tectonic accretion in the Blue Mountains province, northeastern Oregon: Geological Society of America Bulletin, v. 122, p. 517-536.

Searle, M. P., Cottle, J. M., Streule, M.J. and Waters, D. J., 2010, Crustal melt granites and migmatites along the Himalaya: melt source, segregation, transport and granite emplacement mechanisms in Clemens, J.D., Donaldson, C., Frost, C.D., Kisters, A.F.M., Moyen, J.-F., Rushmer, T., and Stevens, G., eds. Sixth Hutton Symposium on the Origin of Granites and Related Rocks: Geological Society of America Special Paper, v. 472, p. 219-233.

Selbekk, R. S. and Tronnes, R. G., 2007, The 1362 AD Oraefajokull eruption, Iceland: Petrology and geochemistry of large-volume homogeneous rhyolite: J. of Volcanology and Geothermal Research, v. 160, p. 42-58.

Sharp, Z. D., 1990, A laser-based microanalytical method for the in situ determination of oxygen isotope ratios of silicates and oxides: Geochemica et Cosmochemica Acta, v. 54, p. 1353-1357.

Sherrod, D. R., Taylor, E. M., Ferns, M. L., Scott, W. E., Conrey, R. M., and Smith, G. A., 2004, Geologic map of the Bend 30- X 60- minute quadrangle, central Oregon: US Geological Survey Geologic Investigations Series I-2683, 48 p.

Shervais, J. W. and Vetter, S. K., 2009, High-K alkali basalts of the Western Snake River Plain (Idaho): Abrupt transition from tholeiitic to mildly alkaline plume-derived basalts: J. of Volcanology and Geothermal Research, v. 188, p. 141-152.

Shoemaker, K. A. and W. K. Hart, 2002, Temporal controls on basalt genesis and evolution on the Owyhee Plateau, Idaho and Oregon, in Bonnichsen, B., White, C. M. and McCurry, M., eds., Tectonic and Magmatic Evolution of the Snake River Plain Volcanic Province: Idaho Geological Survey Bulletin, v. 30, p. 313-328.

Smith, R.L. and Luedke, R.G., 1984, Potentially active volcanic lineaments and loci in western conterminous United States, in, Explosive Volcanism: Inception, Evolution and Hazards, National Research Council, p. 47-66.

Snoke, A. W. and Barnes, C. G., eds., 2006, Geological studies in the Klamath Mountains province, California and Oregon; a volume in honor of William P. Irwin: Geological Society of America Special Paper 410, 505 p. ISBN-13 978-0-8137-2410-2

Spera, F. J. and Bohrson,W. A., 2001, Energy-constrained open-system magmatic processes I: General model and energy-constrained assimilation and fractional crystallization (EC-AFC) Formulation: J. of Petrology, v. 42, p. 999-1018.

Stefano, C. J., 2010, Volatiles, major oxide, trace element and isotope geochemistry in the Snake River Plain and Columbia River Flood Basalts: Implications for the evolution of a continental hotspot: University of Michigan PhD thesis, 191 p.

Streck, M. J., 2002, Partial melting to produce high-silica rhyolites of a young bimodal suite: compositional constraints among rhyolites, basalts, and metamorphic xenoliths from the Harney Basin, Oregon: International J. of Earth Sciences, v. 91, p. 583-593.

Streck, M. J. and Grunder, A. L., 1997, Compositional gradients and gaps in high-silica rhyolites of the Rattlesnake Tuff, Oregon: J. of Petrology, v. 38, p. 133-163.

Streck, M. J. and Grunder, A. L., 2008, Phenocryst-poor rhyolites of bimodal, tholeiitic provinces: the Rattlesnake Tuff and implications for mush extraction models: Bulletin of Volcanology, v. 70, p. 385-401.

Taylor, E. M., 1981, Central High Cascade roadside geology, in Johnston, D. A. and Donnelly-Nolan, J. M., eds., Guides to some volcanic terranes in Washington, Idaho, Oregon, and northern California: US Geological Survey Circular 838, p. 55-83.

Taylor, S. R. and McLennan, S. M., 1995, The geochemical evolution of the continental crust: Reviews in Geophysics, v. 33, p. 241-265.

Todt, W., Cliff, R. A., Hanser, A., Hofmann, A. W., 1996, Evaluation of a 202Pb-205Pb double spike for high-precision lead isotope analysis, in Basu, A and Hart, S. R, eds., Earth Processes: Reading the isotopic code: Geophysical Monograph 95, American Geophysical Union, p. 429-437.

Valley, J. W., Kitchen, N., Kohn, M. J., Neindorf, C. R. and Spicuzza, M. J., 1995, UWG-2, a garnet standard for oxygen isotope ratios: Strategies for high precision and accuracy with laser heating: Geochemica et Cosmochemica Acta, v. 59, p. 5223-5231.

Vervoort, J. D., Patchett, P. J., Blichert-Toft, J. and Albarede, F., 1999, Relationships between Lu-Hf and Sm-Nd isotopic systems in the global sedimentary system: Earth and Planetary Science Letters, v. 168, p. 79-99.

Walker, G. W., 1981, Uranium, thorium, and other metal associations in silicic volcanic complexes of the northern Basin and Range, a preliminary report: USGS Open File Report no 81-1290, 45 p.

Walker, G.W., and MacLeod, N.S., 1991, Geologic map of Oregon: U. S. Geological Survey, scale 1:500,000.

Walker, G. W. and Robinson, P. T., 1990, Paleocene (?), Eocene and Oligocene (?) rocks of the Blue Mountains region, in Walker, G. W., ed., Geology of the Blue Mountains Region of Oregon, Idaho, and Washington: US Geological Survey Professional Paper 1437, p 13-27.

Whitaker, M. L., Nekvasil, H., Lindsley, D. H., McCurry, M., 2008, Can crystallization of olivine tholeiite give rise to potassic rhyolites? – an experimental investigation: Bulletin of Volcanology, v. 70, p. 417-434.

Wyld, S. J. and Wright, J. E., 2001, New evidence for Cretaceous strike-slip faulting in the United States Cordillera and implications for terrane-displacement, deformation patterns, and plutonism, American Journal of Science, v. 301, p. 150-181.

Wyld, S. J., Umhoefer, P. J. and Wright, J. E., 2006, Reconstructing northern Cordilleran terranes along known Cretaceous and Cenozoic strike-slip faults: Implications for the Baja British Columbia hypothesis and other models, in Haggart, J.E., Enkin, R. J. and Monger, J. w. H., eds., Paleogeography of the North American Cordillera: Evidence for and against large-scale displacements: Geological Association of Canada Special Paper 46, p. 277-298.

FIGURES:

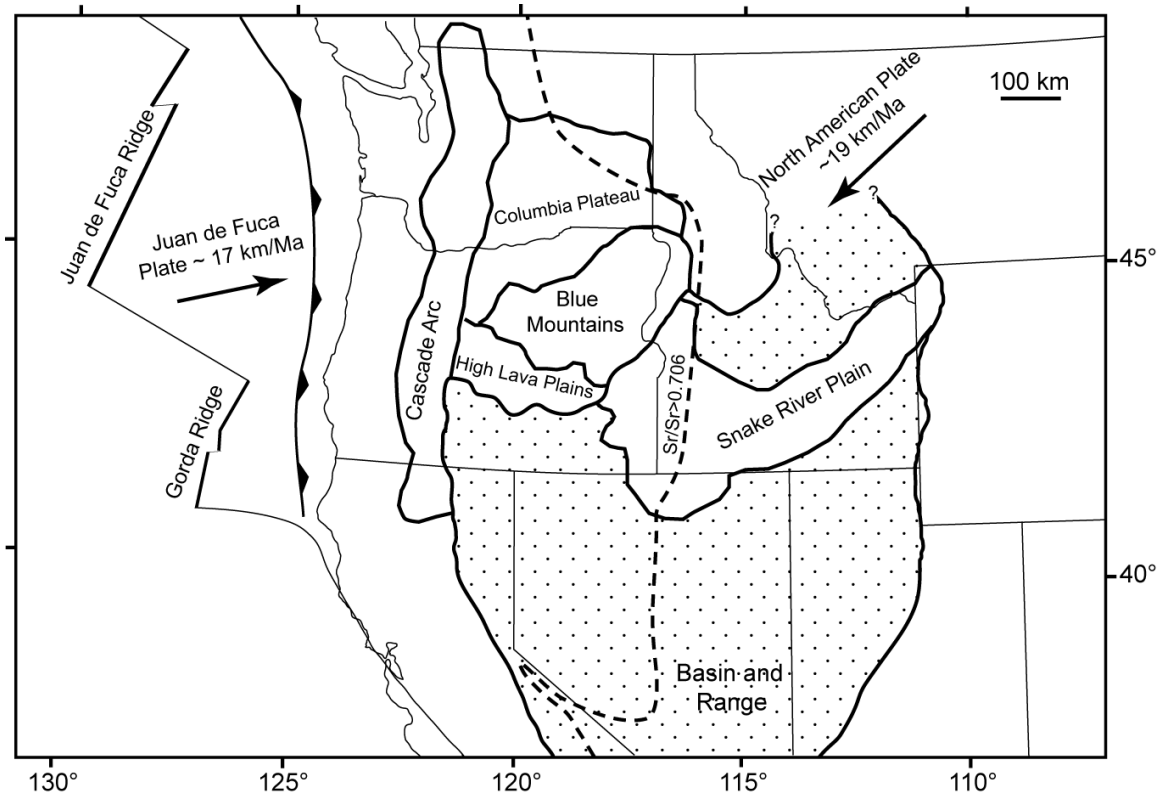

Figure 1: Regional tectonic setting of the High Lava Plains and surrounding provinces. Dashed line indicates approximate position of the $^{87}Sr/^{86}Sr$ 0.706 line (after Kistler and Peterson, 1978), representing the western edge of the Proterozoic or older craton of North America with generally Mesozoic and younger accreted terranes to the west. Stippled region indicates middle Miocene and younger extensional normal faulting (Basin and Range style, after Pezzopane and Weldon, 1993). Arrows give the absolute plate motions and velocities based on models of DeMets, et al., 1994 (no net rotation NUVEL-1A model). Modified after Jordan, et al., 2004.

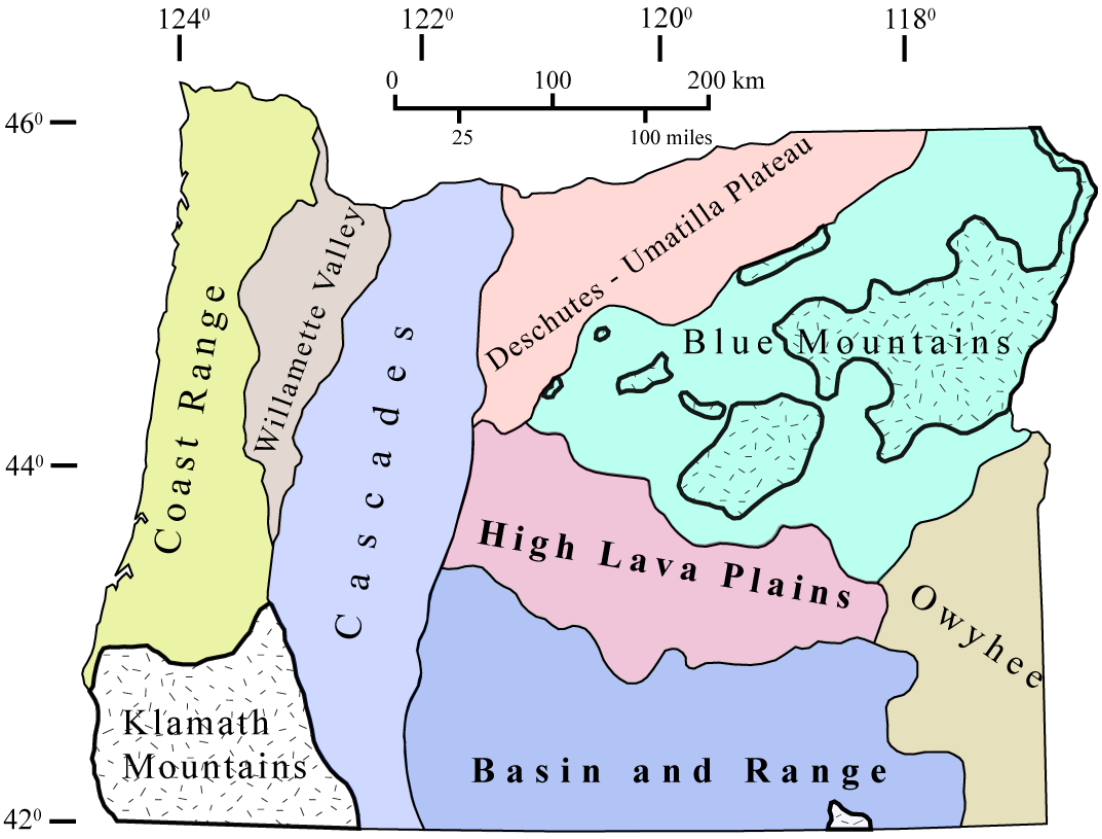

Figure 2: Physiographic provinces of Oregon with HLP and NWBR. The HLP and NWBR are emboldened and the approximate extent of pre-Tertiary outcrops is outlined and with a stipple pattern (adapted after Dicken, 1950; MacLeod, et. al., 1995; Walker and MacLeod, 1991). Study area approximated by the extent of the HLP and NWBR provinces.

Figure 3: Rhyolite classification vs. $^{87}Sr/^{86}Sr_{(i)}$ A) SiO_2 and B) $(FeO^*:SiO_2)_n$ (the normalized Fe-line of Ford, Chapter 2; cf. Figure 12 in Chapter 2). This parameter is the amount above (represented by negative values which equal high iron) or below (positive values, equating to low iron) the Fe-line for rhyodacites and rhyolites of the HLP and NWBR. All rhyolite data from Table 1 (n = 29) except as follows: marked with an "x" (n = 3) and RST (Streck and Grunder, 2008); marked with an "*" (n = 3, Savov, et al., 2009) and marked with a dot (n = 2, Scarberry, 2007). Green arrow marks suite evolution of the RST from dacite pumice (I) to unit E to unit A (highest in SiO_2). DB indicates low silica point from DBEC in the extreme eastern HLP and DCT is the Devine Canyon Tuff. Error bars are present only where the error is greater than the symbol size (see Table 1).

Figure 3A:

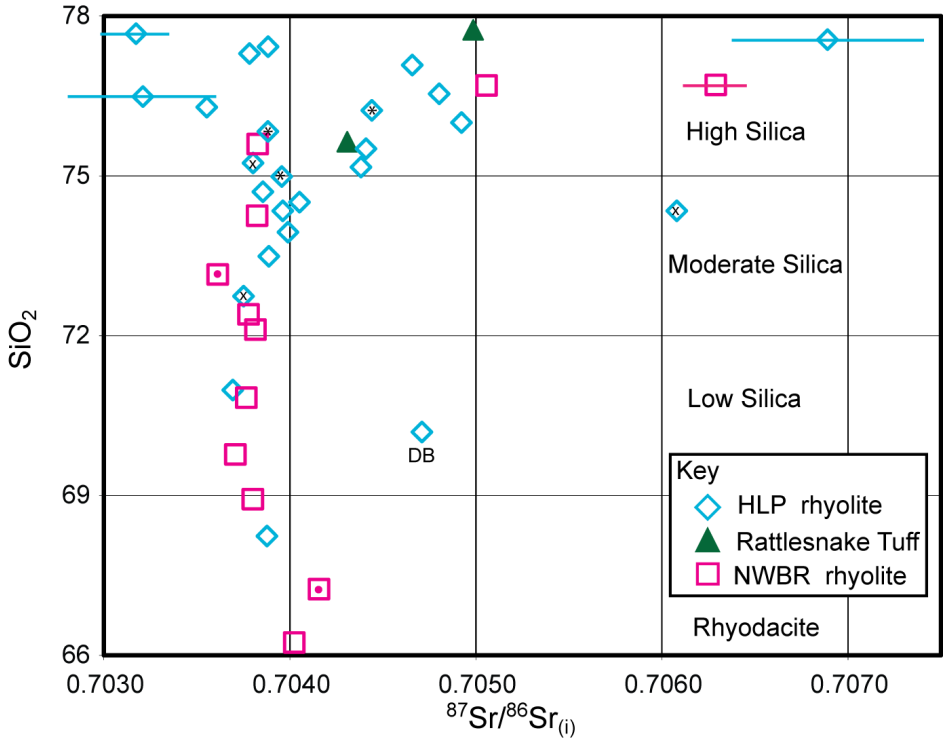

Figure 3B:

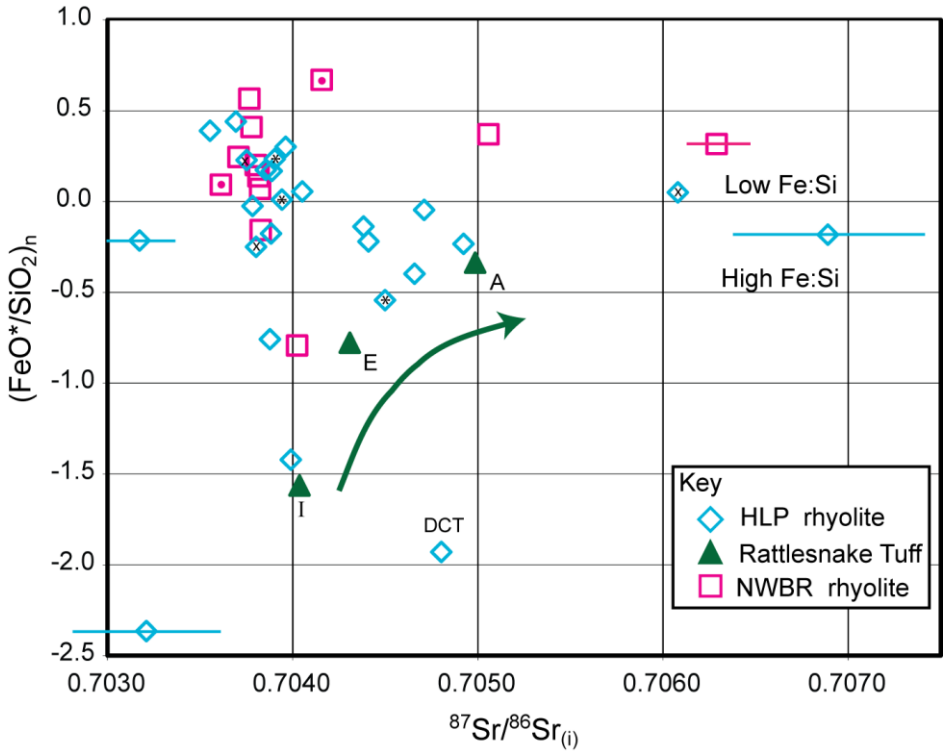

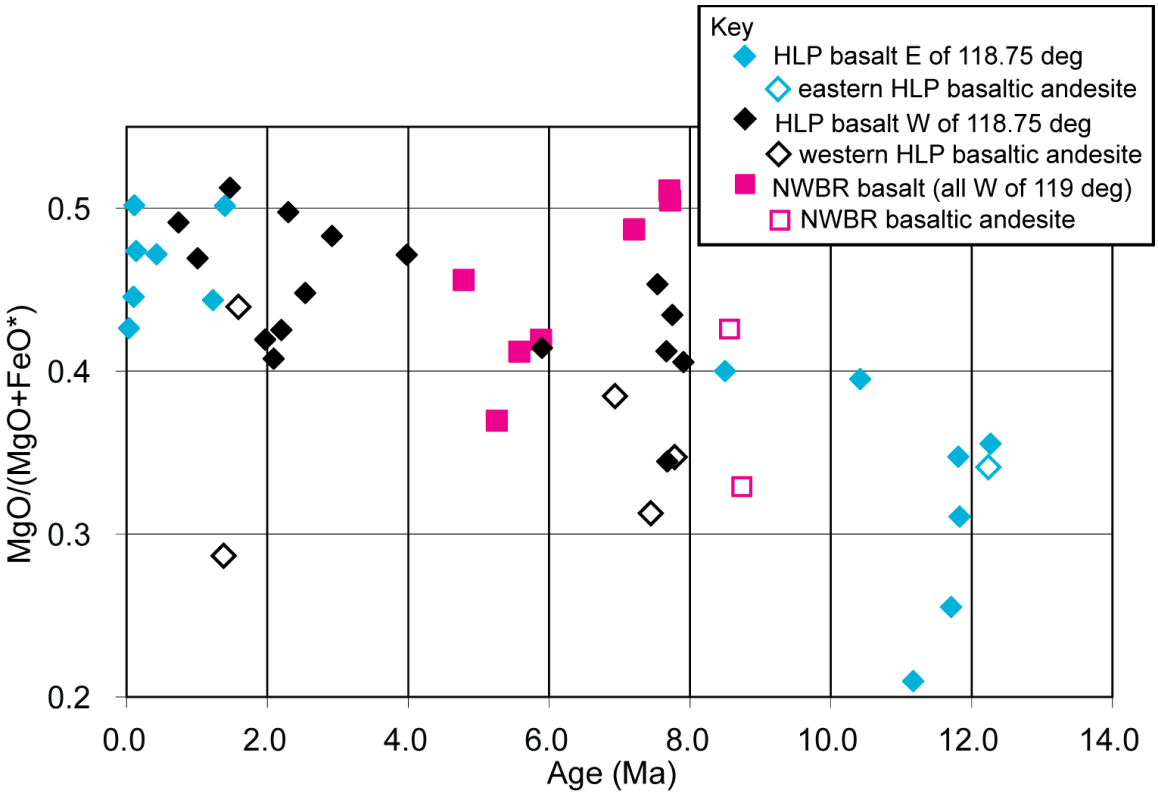

Figure 4: MgO/(MgO+FeO*) vs. age for HLP basalts and basaltic andesites. For both eastern samples and western samples (HLP), MgO/(MgO+FeO*) (wt. %) ratio increases through time. The vast majority of the age measurements are better than ±0.15 m.y. with a few points at ± 10%. Data is from Jordan et al., 2004; Carlson and Hart, 1987; Stefano, 2010; Iademarco, 2009 and Scarberry, 2007.

Figure 5: Spatial Sr isotopic variations. East-west variation in initial Sr isotopic concentrations ($^{87}Sr/^{86}Sr_{(i)}$) for < 12 Ma basalts and rhyolites of the HLP and NWBR. Bold "N" marks the Big Obsidian Flow of Newberry Volcano (Savov et al., 2009) and bar represents the range in $^{87}Sr/^{86}Sr_{(i)}$ isotopes from the Central Cascades with MCT including Medicine Lake, Crater Lake and Three Sisters (Grove et al., 1997, Kinzler et al., 2000, Bacon, et al., 1994, 1997 and Schmidt, et al., 2008) and JHA including Mt. Jefferson, Mt. Hood and Mt. Adams (Leeman et al., 1990; Conrey et al., 2001; Jicha et al., 2009 Koleszar, pers com). DC is the Holocene Diamond Craters (with black outlined symbols) and bars on the right indicate the range for the Holocene Jordan Craters (JC), just east of the study area (Shoemaker and Hart, 2002) and Quaternary Snake River Plain (SRP) basalts in Idaho (after Shervais and Vetter, 2009). All rhyolite data from Table 1 (n = 29) except as noted in Figure 3. Basalt data form the following: Jordan, 2001 and Graham et al., 2009 (NWBR and HLP basalts, n = 16); Streck and Grunder, 2008 (HLP basalts, n = 4); Scarberry, 2007 (NWBR basalts, n = 2); Stefano, 2010 ("eastern" HLP basalts, n = 4); Hart, 1985, and Carlson and Hart, 1987 ("eastern" HLP basalts, n = 9). Error bars are present only where the error is greater than the symbol size (see Table 1).

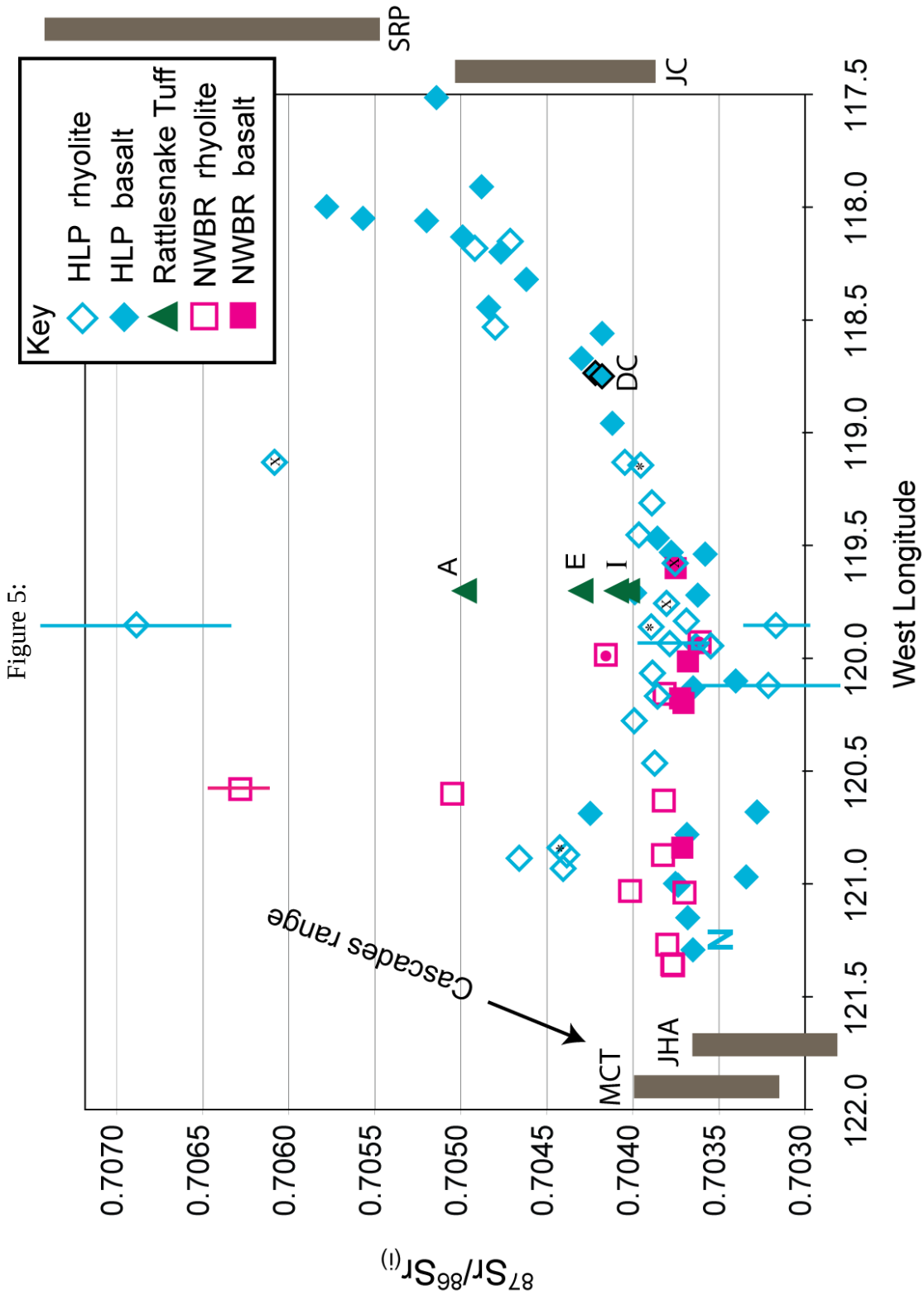
Key
HLP rhyolite
HLP basalt
Rattlesnake Tuff
NWBR rhyolite
NWBR basalt
SRP
JC
DC
A
E
I
N
MCT
JHA
Cascades range
87Sr/86Sr(i)
West Longitude
0.7070
0.7065
0.7060
0.7055
0.7050
0.7045
0.7040
0.7035
0.7030
122.0
121.5
121.0
120.5
120.0
119.5
119.0
118.5
118.0
117.5

Figure 5:

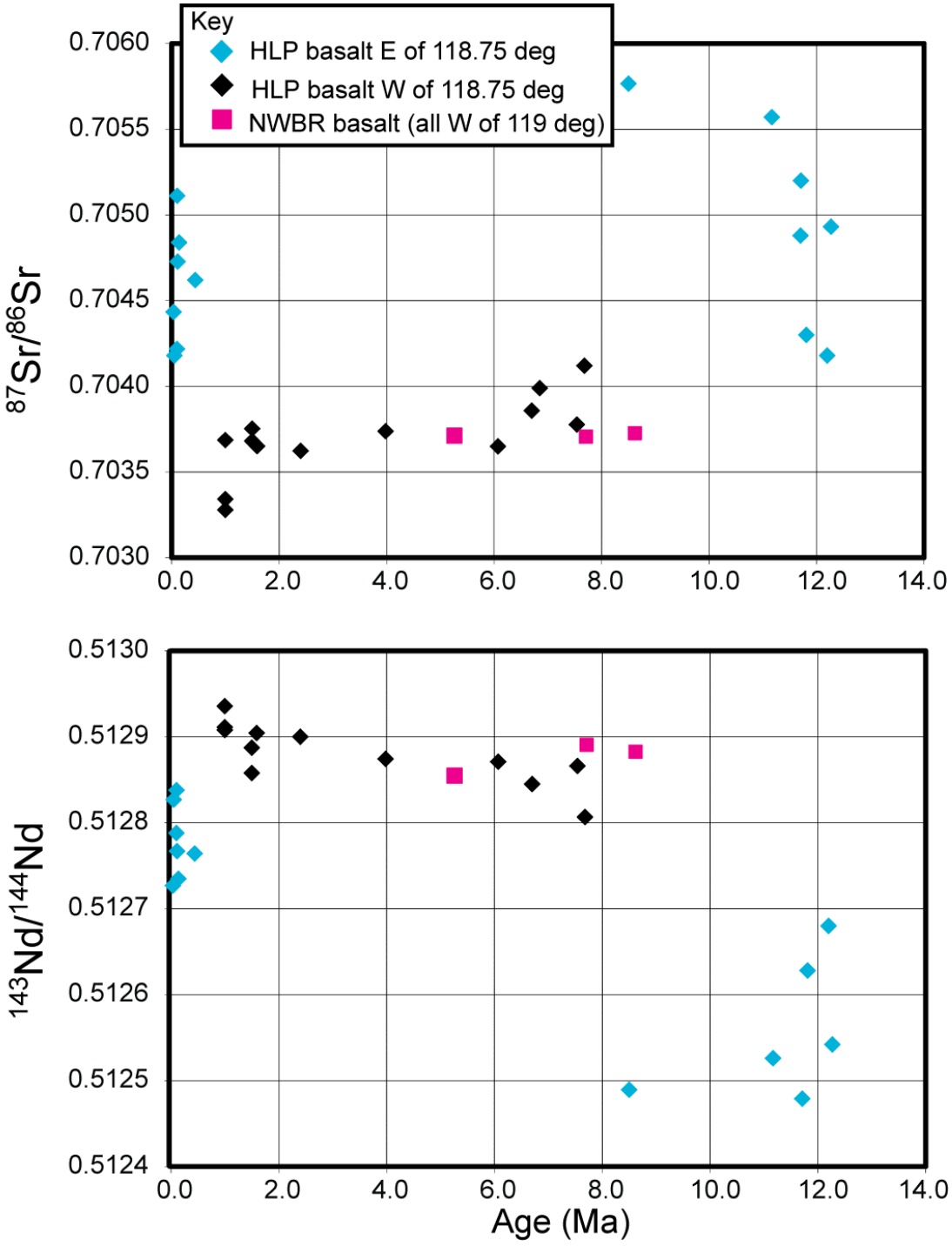

Figure 6: $^{87}Sr/^{86}Sr$ and $^{143}Nd/^{144}Nd$ vs. age for < 12 Ma basalts of the HLP and NWBR. Both data the east of 118.75º and west of 118.75º data sets show marked changes, becoming less radiogenic over time. See figure 5 for Holocene Jordan Craters data range. Data primarily from Jordan, 2001; Streck and Grunder, 2008; Iademarco, 2009; Scarberry, 2007; Hart, 1985; Carlson and Hart, 1987 and Stefano, 2010.

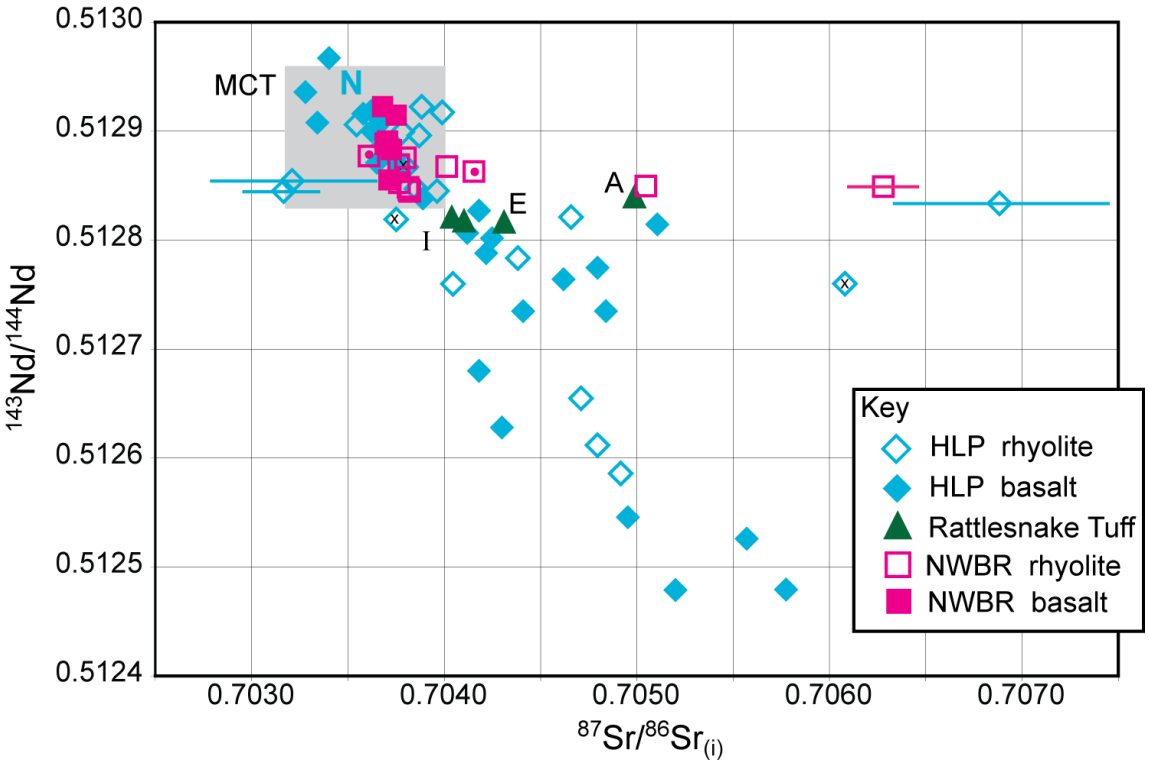

Figure 7: $^{143}Nd/^{144}Nd$ vs. $^{87}Sr/^{86}Sr_{(i)}$ for < 12 Ma basalts and rhyolites of the HLP and NWBR. Key, symbols and sources are similar to those in Figure 3 and Figure 5 with MCT (Cascades) range represented by a light grey box. Note the evolution of the RST from dacite pumice (I) to unit E to unit A (highest in SiO_2).

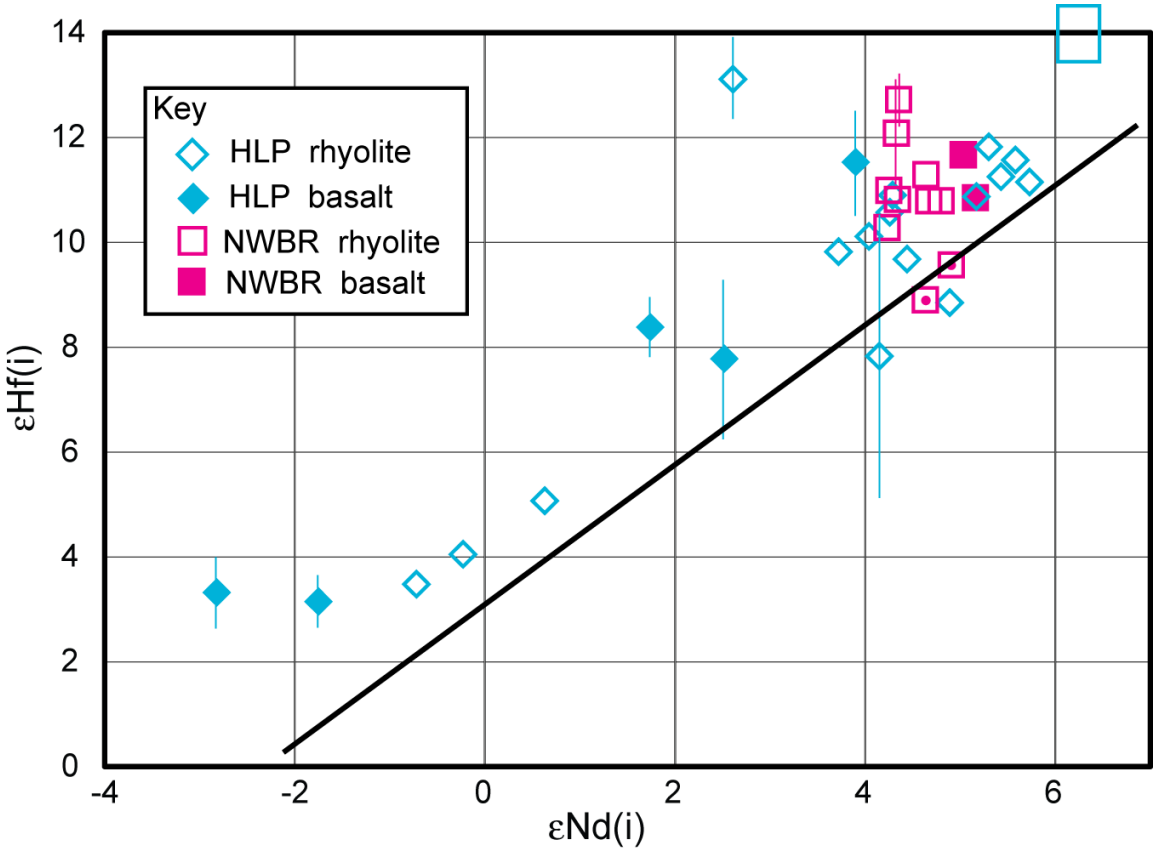

Figure 8: $\varepsilon Hf_{(i)}$ vs. $\varepsilon Nd_{(i)}$ for < 12 Ma basalts and rhyolites of the HLP and NWBR. Key, symbols and sources are similar to Figure 3 and Figure 5 except that all HLP basalts and Picture Gorge Basalts (larger blue box) are from Stefano (2010). Error bars are given only where larger than the symbol. Five rhyolites yielded low voltages when measured for Hf and four of these have error greater than the symbol size. Errors on Scarberry (2007) samples are unknown (rhyolites with dots, two basalts from the NWBR). Line is the "terrestrial array" of Vervoort, et al. (1999).

Figure 9: A) $^{207}Pb/^{204}Pb$ vs. $^{206}Pb/^{204}Pb$ diagram for basalts and rhyolites of the HLP and NWBR. Key, symbols and sources are similar to those in Figure 3 and Figure 5. The large arrow indicates pelagic sediments or continental crust addition (Appendix 6; Prytulak, et al., 2006) and the Northern Hemisphere Reference Line (NHRL) from Hart (1984a) is given. Figure 9B shows a histogram of $^{207}Pb/^{204}Pb$ data from Figure 9A for basalts and rhyolites of the HLP with filled boxes representing the number of basalts and open boxes the number of rhyolites. Rhyolites extend to higher $^{207}Pb/^{204}Pb$ ratios.

Figure 9A:

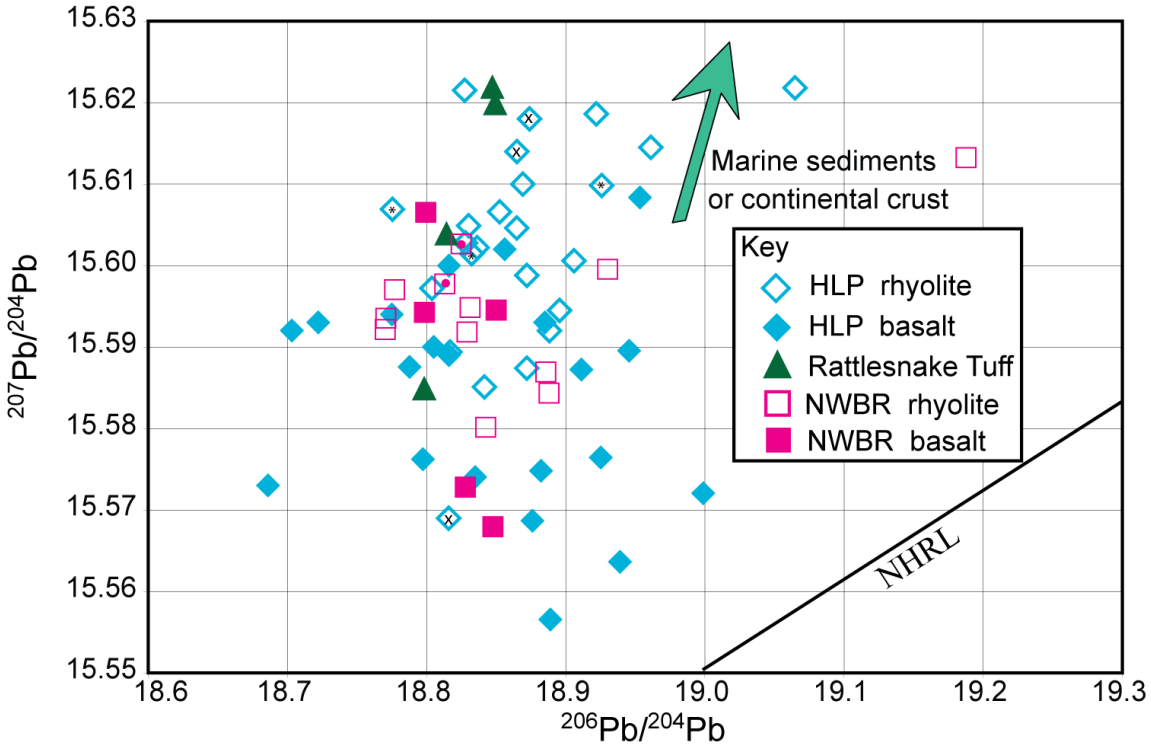

Figure 9B:

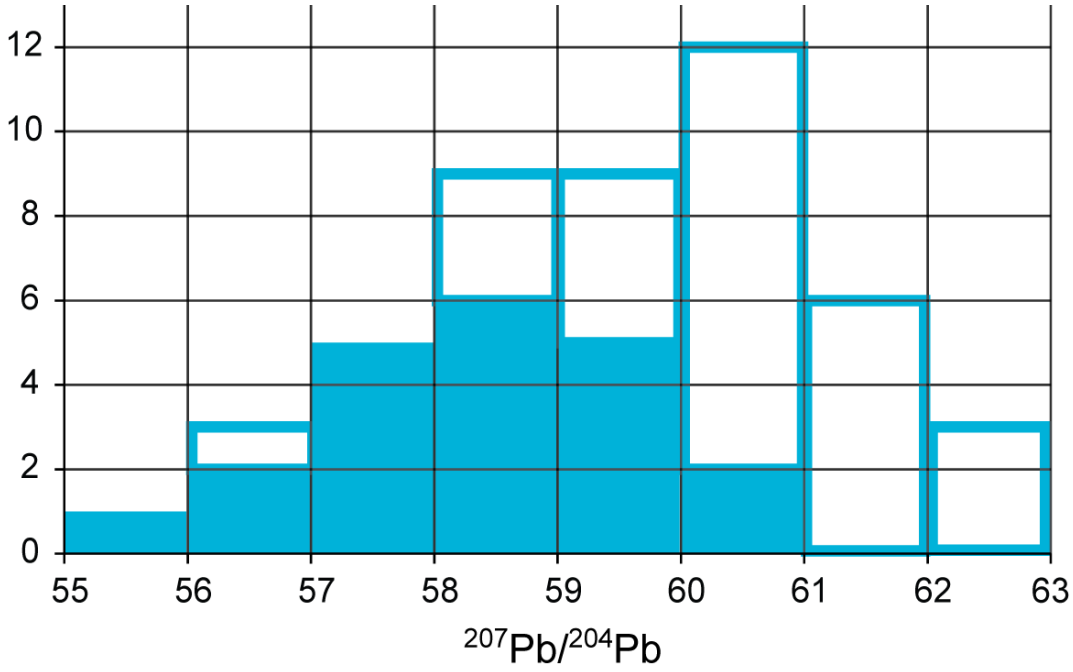

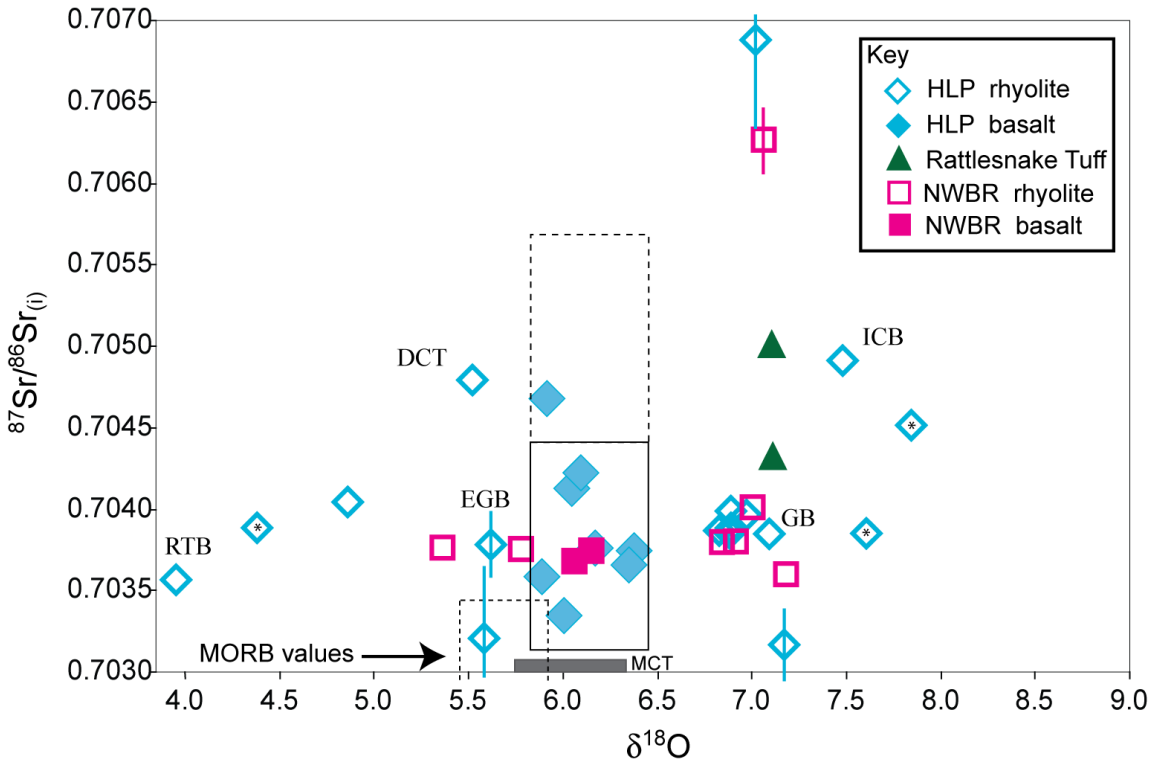

Figure 10: $^{87}Sr/^{86}Sr_{(i)}$ vs. $\delta^{18}O_{(melt)}$ for < 12 Ma basalts and rhyolites of the HLP and NWBR. Key, symbols and sources are similar to those in Figure 3 and Figure 5 except that $\delta^{18}O_{(melt)}$ values for Medicine Lake from Donnelly-Nolan (1998). MORB values from compilation of Saunders et al. (1988) and Harmon and Hoefs (1995). Solid box roughly outlines the field of basalts from the western HLP while dashed box likely outlines basalts from the eastern HLP, but there is only one oxygen isotope composition from these basalts. ICB = Indian Creek Butte and DCT = Devine Canyon Tuff, both of which are from the eastern HLP and have Sr isotope ratios similar to local basalts (cf. Figure 5). All $\delta^{18}O$ from Table 1 and Table 2 except RTB = Round Top Butte, GB = Glass Buttes, EGB = East glass buttes $\delta^{18}O$ from Roche (1987), and asterisk points (n = 3) from Savov et al., 2009. Many rhyolites are ~ 1‰ higher than the basalts, with similar Sr isotopic ratios but many rhyolites also have a $\delta^{18}O$ lower than basalts (see text).

Figure 11: $^{143}Nd/^{144}Nd$ vs. $^{87}Sr/^{86}Sr_{(i)}$ diagram for the study area with fields of potential input with symbols similar to Figure 3. The large area of overlap of basalts and rhyolites of the HLP – NWBR from Figure 7 is now shown as a field and only outliers are shown with individual fields. Green bar represents evolution of RST (I to E to A – see Figure 7). Eolian and Columbia River sediments represent current day values but the Astoria Fan contains a mixture of more recent source rocks and those from the Proterozoic Belt Supergroup (Prytulak et al., 2006), which would result in extremely high $^{87}Sr/^{86}Sr_{(m)}$ values, as indicated by arrows. Large "T" are two whole rock samples from the Tyee Formation (Heller et al., 1985). For the John Day and middle Miocene silicic fields, measured values for Sr isotopes have been time corrected to 7 Ma but such a correction has little effect on the older (e.g. Klamath or Blue Mountains) isotope ratios or current-day sediment isotope ratios and these fields are measured (not age corrected) isotopic ratios. Details on references for fields of potential mixing end members are given in Appendix 6.

Figure 11:

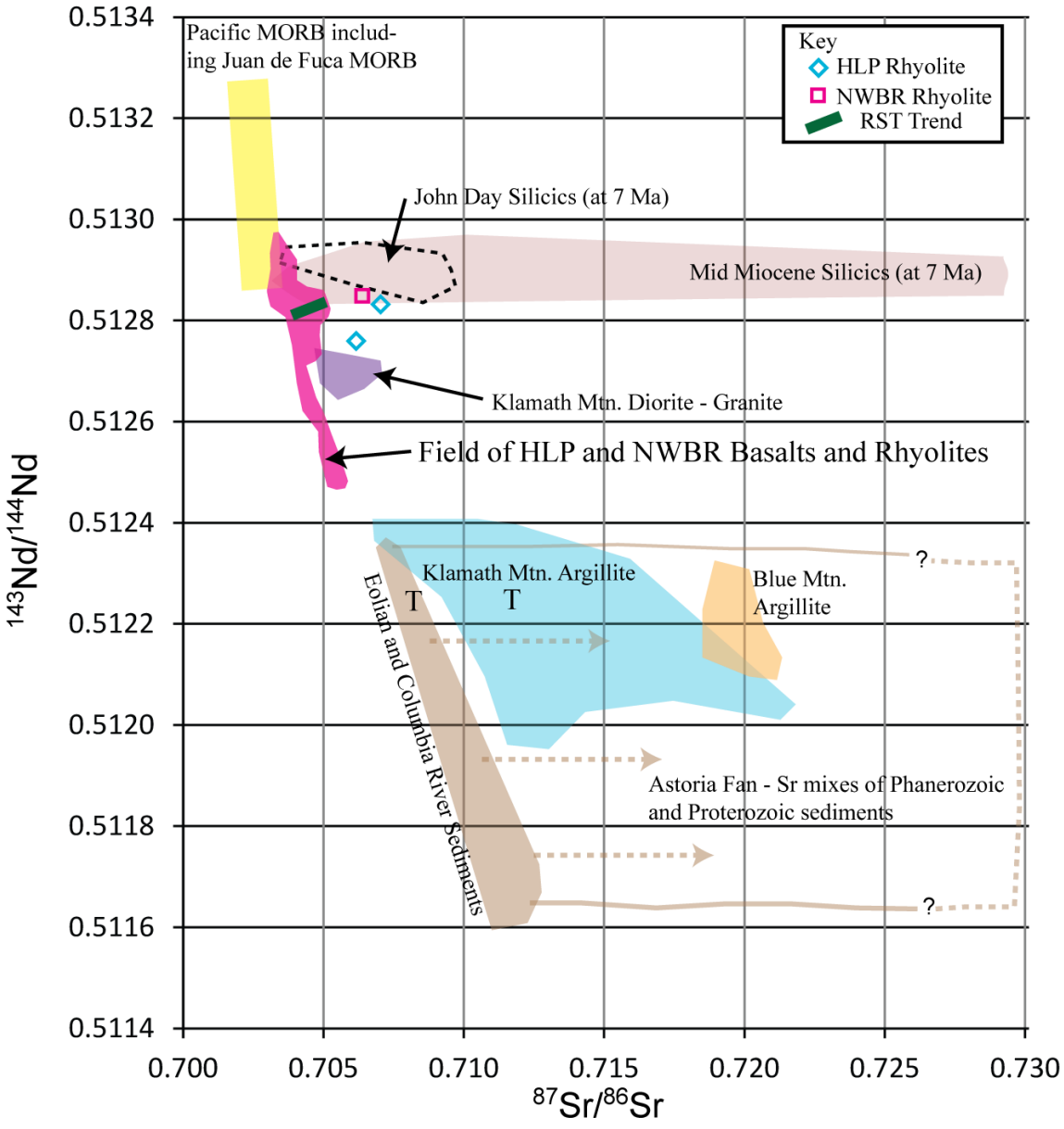
Pacific MORB including Juan de Fuca MORB
Key
HLP Rhyolite
NWBR Rhyolite
RST Trend
John Day Silicics (at 7 Ma)
Mid Miocene Silicics (at 7 Ma)
Klamath Mtn. Diorite - Granite
Field of HLP and NWBR Basalts and Rhyolites
Klamath Mtn. Argillite
Blue Mtn. Argillite
Eolian and Columbia River Sediments
Astoria Fan - Sr mixes of Phanerozoic and Proterozoic sediments
?
?
0.5134
0.5132
0.5130
0.5128
0.5126
0.5124
0.5122
0.5120
0.5118
0.5116
0.5114
143Nd/144Nd
0.700
0.705
0.710
0.715
0.720
0.725
0.730
87Sr/86Sr

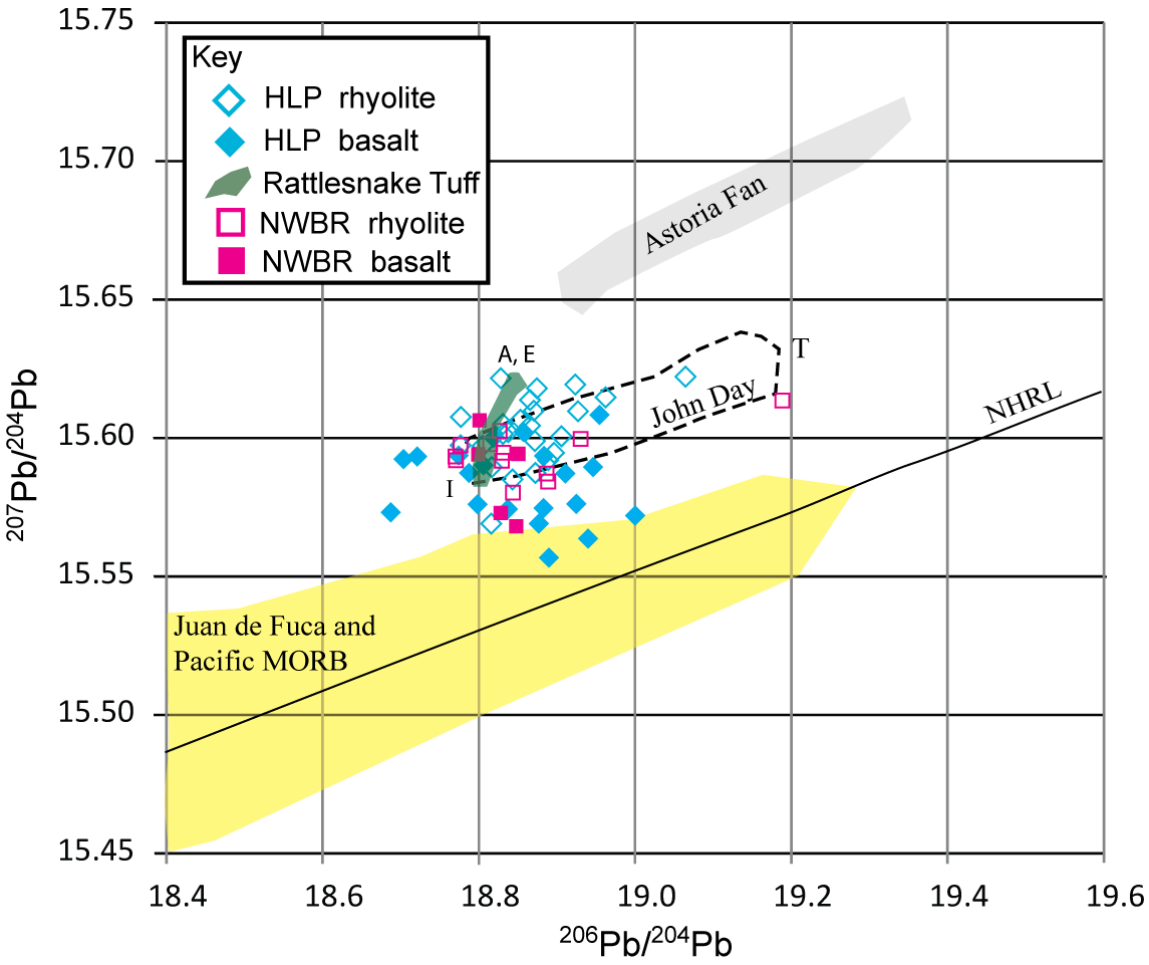

Figure 12: $^{207}Pb/^{204}Pb$ vs. $^{206}Pb/^{204}Pb$ diagram for the study area with fields of potential input. Symbols and references as in Figure 9 except RST is given as a field, with units A and E being the most radiogenic and nearly identical and inclusions in the tuff (I) the least. Large "T" is position of sediments from the Eocene Tyee Formation (see text; Church, 1976). John Day field is for both mafic and silicic volcanic rocks from this study (Table 1) and Bromley (2011). Middle Miocene samples would plot directly underneath the HLP – NWBR samples and are not shown. Astoria Fan data are from Prytulak et al. (2006) and MORB from Hanan and Graham (1996), Hanan et al. (2008), Hegner and Tatsumoto (1987), and Ito et al. (1987), See Appendix 6.

Figure 13: Mixing lines superimposed on a simplified version of Figure 10. Key, symbols and sources are similar to those in Figure 3, 5 and 10. Mixing lines are as follows with tic marks indicating increments of 1 % or 5 % mixing: mafic crust + meteoric water line is a mix of basalt or basalt-like crust ($\delta^{18}O$ = 6.2 ‰) and estimated regional meteoric water ($\delta^{18}O$ = -14 ‰; Bowen and Revenaugh, 2003); PbM is a similar mixing line used for the Pb isotopes (Figure 14) using basaltic crust ($\delta^{18}O$ = 6.2 ‰ and $^{87}Sr/^{86}Sr$ = 0.7035) and terrigenous marine sediments (Astoria fan-like contaminant - estimated $\delta^{18}O$ = 20 ‰ and $^{87}Sr/^{86}Sr$ = 0.71161). PM / FC is the approximated per mil increase due to non-modal partial melting and fractional crystallization for this system (see text). Three AFC lines are plotted, with tic marks at 5 % intervals indicating the percentage of magma remaining. RST is the AFC line with unit E (Streck and Grunder, 2008) and a John Day sample ($\delta^{18}O$ = 7 ‰ and $^{87}Sr/^{86}Sr$ = 0.708) with Sr isotopes corrected to 7 Ma and oxygen isotope fractionation based on model in the text. Results to form RST unit A are similar to those found in Streck and Grunder (2008), needing a low ratio of assimilant to fractional crystallization (0.05 in this case) and about 50% fractionation. Model AFC1 is AFC from basaltic crust with John Day contaminant using the same 0.05 (very low) ratio and oxygen isotope fractionation based on Bindeman et al. (2004). Model AFC2 is similar to AFC1 but uses a much higher ratio of assimilant to fractional crystallization (0.5). This much higher ration is appropriate due to higher temperature expected in this model over the RST model.

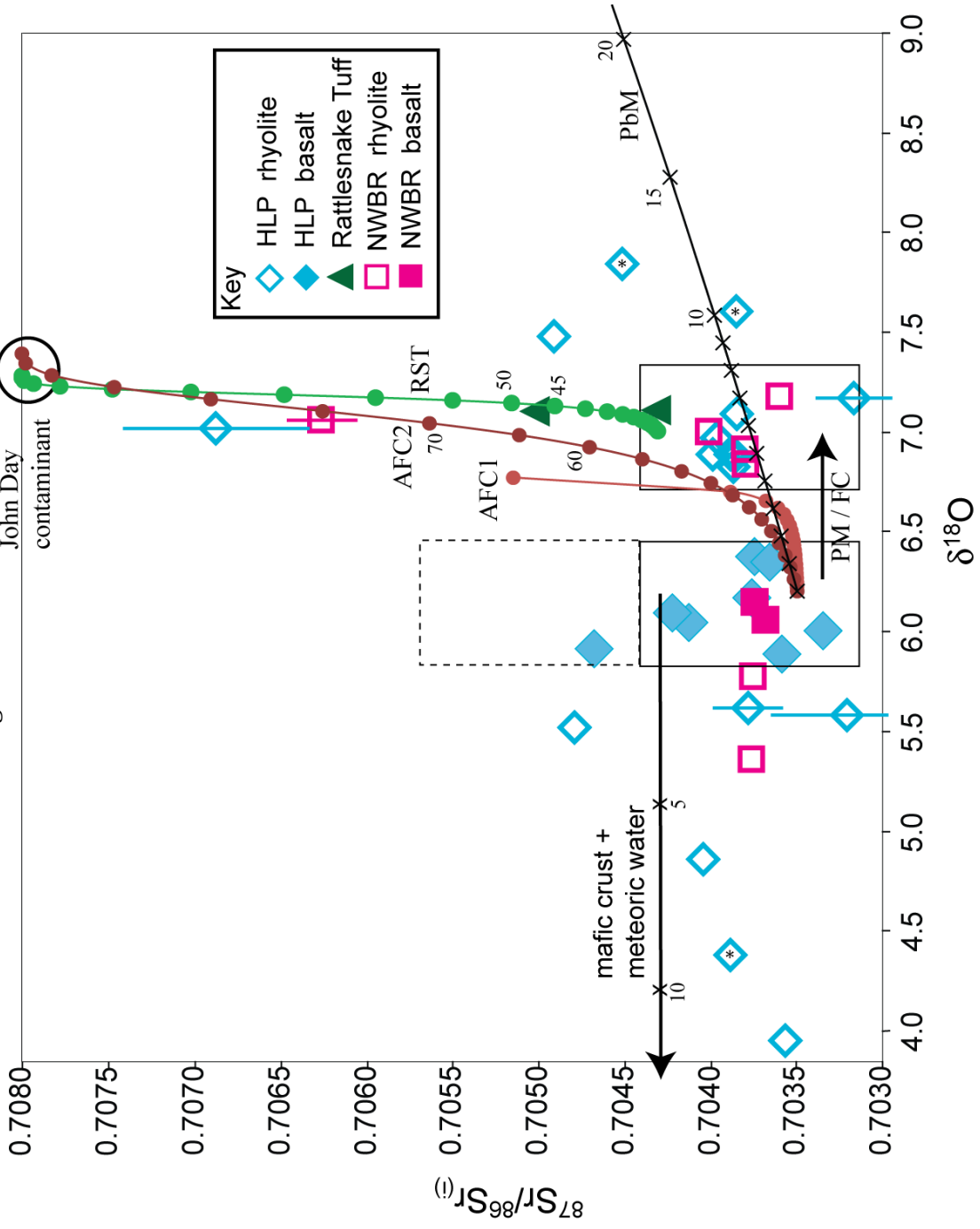
Key
HLP rhyolite
HLP basalt
Rattlesnake Tuff
NWBR rhyolite
NWBR basalt
John Day
contaminant
RST
AFC2
AFC1
PbM
PM / FC
mafic crust +
meteoric water
$^{87}Sr/^{86}Sr_{(i)}$
$\delta^{18}O$

Figure 13:

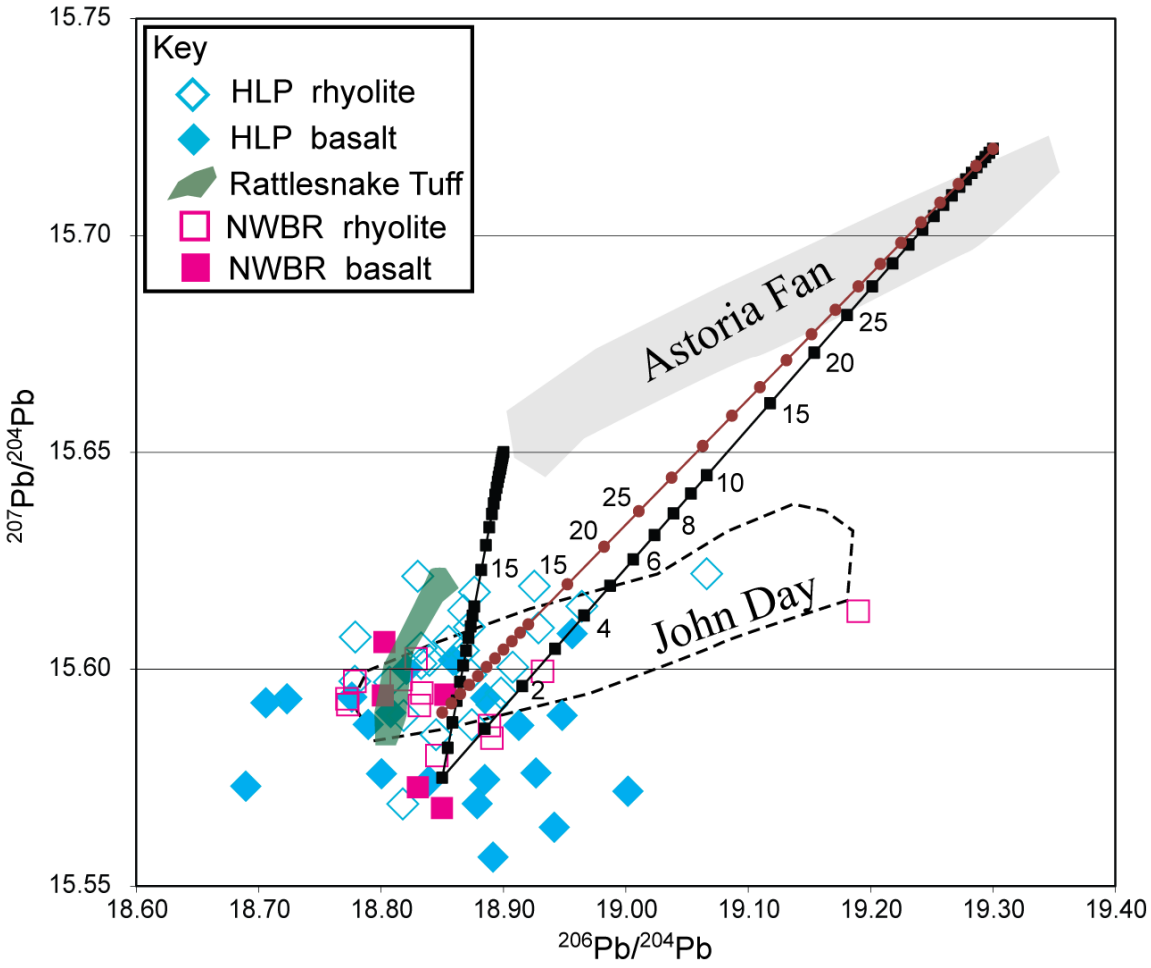

Figure 14: Mixing lines superimposed on a simplified version of Figure 12. Black boxes and lines are mixing lines between a hypothetical HLP-like basalt and low and high radiogenic Pb Astoria Fan end members. Brown circles and line are a mixing line between a parental rhyolite and the Astoria Fan. Numbers indicate the percentage of assimilant, by increments of 1 % up to 10 % and then by increments of 5 %. See text and Table 4 for more information.

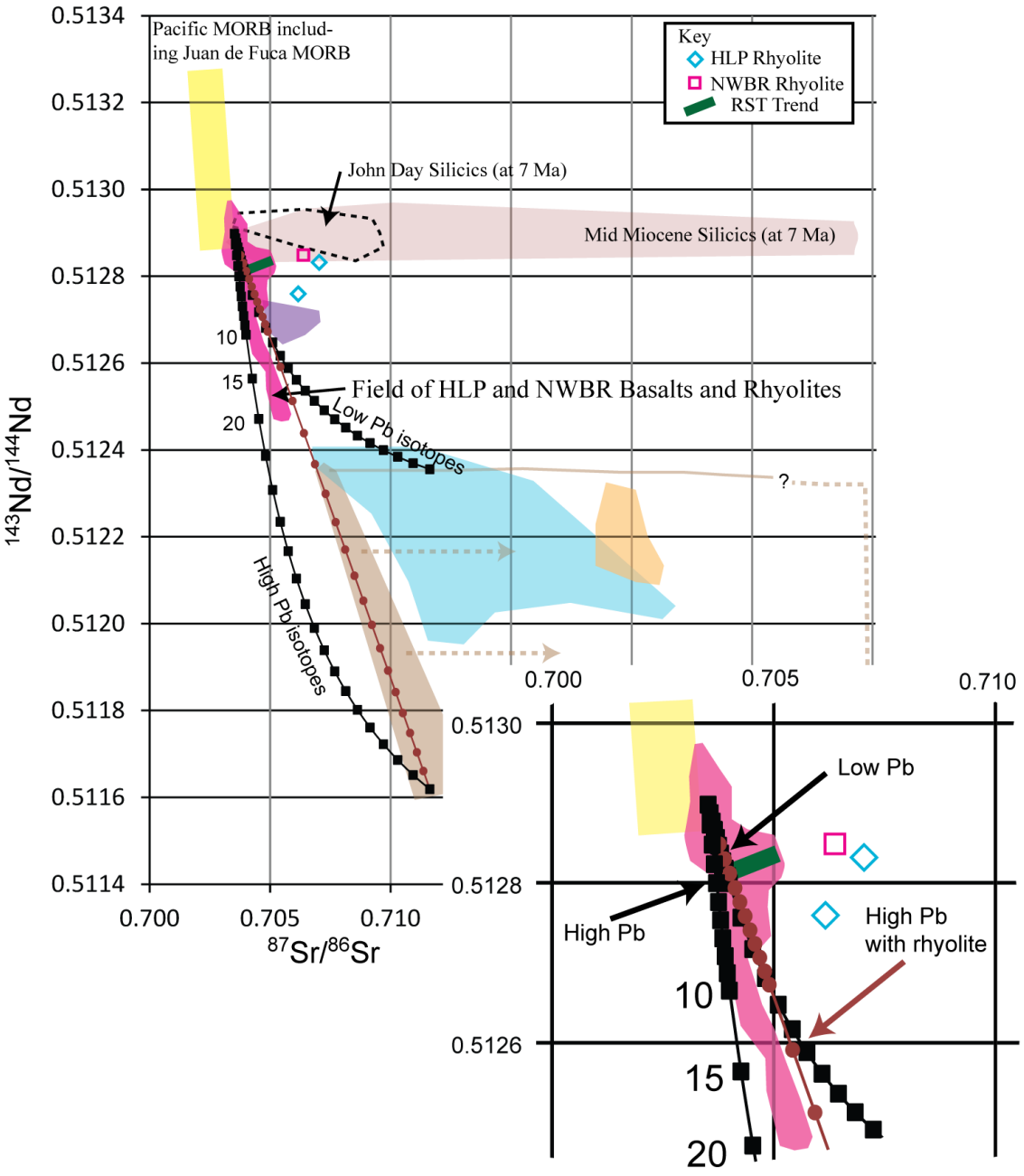

Figure 15: Mixing lines superimposed on a simplified version of Figure 11. These are the same mixing lines from Figure 14 applied to the Sr and Nd isotopic system. Figure is simplified from Figure 11 and inset focuses in on the region of interest. Black or brown arrows point at the percentage of assimilant mentioned in the text and given in Table 4.

TABLES:

Table 1: Isotopic compositions from the HLP and NWBR. Ages determined by Ar-Ar method except as noted and errors on ages is given at the 1-σ confidence with sources as follows: MTF: Ford (Chapter 2); BJ: Jordan et al (2004); MI: Iademarco (2009); RBF: Fiebelkorn et al (1983) compilation (K-Ar ages). Superscripts as follows: *a*: Likely age, estimated at 7.2 Ma based on Ar-Ar results of HP 93-13c but another sample from nearly the same location yielded an age of 15.1 Ma which would time correct the $^{87}Sr/^{86}Sr(i)$ downward by 0.000178, the $^{208}Pb/^{204}Pb$ (i) by 0.044 and the $^{206}Pb/^{204}Pb$ (i) by 0.025; *b*: estimated age based on similar sample MTF 07-29 located 5 km away and of similar morphology and composition; *c*: average of three K-Ar dates; *d*: estimated date based on spatial bracketing of rhyolite domes which are 6.49 and 7.18 Ma. For isotope ratios, (m) = measured and (i) = time corrected or initial using given ages. All 2σ errors on $^{87}Sr/^{86}Sr$ (m) are 0.000022 external errors except where reported, italics: measured error; bold: error based on 2σ age error (leading zeros omitted). Standards for Nd measurements are further discussed in the text. All 2σ errors on $^{176}Hf/^{177}Hf$ (m) are 0.000005 external errors except where reported (leading zeros omitted). Oxygen isotopes are given relative to the SMOW scale in per mil and are +/- 0.1 ‰. Oxygen isotopes marked with an asterisk (*) are from Roche (1987). Rb and Sr are from ID while other trace elements are from whole rock composition with references as follows: 1: Ford (Chapter 2), 2: Iademarco (2009) and 3: Johnson and Grunder (2000).

Table 1:

Sample	MTF 07-02	MTF 07-04	MTF 07-05	MTF 07-06	MTF 07-08	MTF 07-10	MTF 07-12
Age (Ma)	6.25	5.79	6.49	6.35	7.68	9.63	4.0
Age error (1-s)	0.02	0.02	0.03	0.03	0.04	0.03	0.4
age reference	MTF	MTF	MTF	BJ	BJ	MTF	RBF K-Ar
Rb (ppm)	69.6	82.7	123	111	115	136	65.3
Sr (ppm)	246	21.6	1.43	204	26.7	5.19	190
87Rb/86Sr	0.8172	11.08	248.7	1.577	12.43	75.97	0.9946
87Sr/86Sr (m)	0.703879	0.704794	0.726706	0.704029	0.705408	0.715193	0.703934
error (if > 22)		*23*	**212**			**65**	
87Sr/86Sr (i)	0.703806	0.703883	0.703783	0.703887	0.704052	0.704803	0.703878
Sm (ppm)	3.03	6.41	7.61	3.86	6.30	22.45	7.50
Nd (ppm)	15.24	25.61	22.23	18.72	31.01	93.36	30.46
147Sm/144Nd	0.1203	0.1512	0.2070	0.1095	0.1228	0.1454	0.1488
143Nd/144Nd (m)	0.512869	0.512928	0.512908		0.512766	0.512621	0.512900
1433Nd/144Nd (i)	0.512864	0.512922	0.512899		0.512760	0.512612	0.512896
ENd (0)	4.55	5.70	5.31		2.54	-0.29	5.15
ENd (i)	4.61	5.73	5.30		2.61	-0.23	5.17
Nd standard	La Jolla	JNdi	JNdi		La Jolla	La Jolla	La Jolla
Tdm (Ga)	0.53	0.65	5.37		0.72	1.26	0.69
Lu (ppm)	0.25	0.89	1.24	0.45	0.77	2.39	0.73
Hf (ppm)	3.91	4.06	4.34	4.52	7.92	25.63	6.45
176Lu/177Hf	0.0092	0.0312	0.0405	0.0142	0.0138	0.0132	0.0161
176Hf/177Hf (m)	0.283070	0.283087	0.283107	0.283065	0.283140	0.282883	0.283078
176Hf/177Hf (i)	0.283069	0.283084	0.283102	0.283063	0.283138	0.282881	0.283077
error (if > 5)		7	6	12	22		
Ehf (0)	10.54	11.14	11.85	10.36	13.01	3.93	10.82
Ehf (I)	10.64	11.15	11.82	10.44	13.11	4.05	10.87
Tdm (Ga)	0.41	1.42	-8.05	0.50	0.34	0.86	0.51
U (ppm)	2.46	3.45	6.76	3.62	4.08	5.71	2.84
Pb (ppm)	10.68	14.94	17.67	16.80	15.75	30.97	9.89
238U/204Pb	14.58	14.65	24.27	13.67	16.47	11.74	18.23
206Pb/204Pb (m)	18.817	18.841	18.872	18.837	18.853	18.827	18.906
207Pb/204Pb (m)	15.591	15.585	15.587	15.602	15.607	15.622	15.601
208Pb/204Pb (m)	38.447	38.432	38.441	38.499	38.601	38.772	38.546
206Pb/204Pb (i)	18.803	18.828	18.848	18.823	18.833	18.810	18.895
207Pb/204Pb (i)	15.591	15.585	15.586	15.602	15.606	15.621	15.600
208Pb/204Pb (i)	38.419	38.414	38.412	38.482	38.575	38.760	38.521
del18O (magma)		7.1 *	5.6 *	6.89	4.86	5.52	6.83
Trace reference	1	1	1	1	1	1	1

Table 1 continued:

Sample	MTF 07-14	MTF 07-16	MTF 07-26	MTF 07-28	MTF 07-29	MTF 07-30	MTF 07-32
Age (Ma)	5.67	4.34	17.30	8	8.05	6.87	1.13
Age error (1-s)	0.08	0.03	0.05	0.2	0.02	0.04	0.05
age reference	MTF	MTF	MTF	estimate[b]	MTF	MTF	RBF K-Ar
Rb (ppm)	103	91.6	152	132	141	106	129
Sr (ppm)	240	33.3	15.3	20.0	26.1	143	59.5
87Rb/86Sr	1.246	7.958	28.85	19.04	15.67	2.148	6.262
87Sr/86Sr (m)	0.704124	0.705149	0.710772	0.707220	0.708081	0.704037	0.704510
error (if > 22)			**41**	*58*	*180*		
87Sr/86Sr (i)	0.704024	0.704659	0.703684	0.705057	0.706290	0.703827	0.704410
Sm (ppm)	7.16	6.92	5.01	1.46	1.71	3.15	5.78
Nd (ppm)	30.53	24.30	26.60	5.69	7.25	17.87	24.94
147Sm/144Nd	0.1418	0.1722	0.1139	0.1553	0.1422	0.1066	0.1233
143Nd/144Nd (m)	0.512872	0.512826	0.512896	0.512857	0.512856	0.512850	
1433Nd/144Nd (i)	0.512867	0.512821	0.512883	0.512849	0.512849	0.512845	
ENd (0)	4.60	3.71	5.07	4.31	4.29	4.17	
ENd (i)	4.64	3.72	5.25	4.35	4.35	4.25	
Nd standard	La Jolla	JNdi	La Jolla	La Jolla	La Jolla	La Jolla	
Tdm (Ga)	0.68	1.32	0.46	0.87	0.72	0.49	
Lu (ppm)	0.67	0.88	0.39	0.35	0.35	0.28	0.70
Hf (ppm)	7.72	5.16	6.27	3.06	3.20	3.55	5.69
176Lu/177Hf	0.0122	0.0242	0.0089	0.0161	0.0155	0.0113	0.0175
176Hf/177Hf (m)	0.283089	0.283049	0.283023	0.283129	0.283111	0.283080	0.283032
176Hf/177Hf (i)	0.283088	0.283047	0.283020	0.283127	0.283109	0.283079	0.283032
error (if > 5)	8	7		14	28	10	
Ehf (0)	11.21	9.80	8.88	12.63	11.99	10.89	9.19
Ehf (I)	11.29	9.82	9.15	12.72	12.08	10.99	9.21
Tdm (Ga)	0.42	0.89	0.49	0.40	0.43	0.42	0.66
U (ppm)	5.15	3.01	6.38	5.07	4.98	4.20	4.60
Pb (ppm)	12.30	16.33	18.09	26.96	26.91	19.16	18.00
238U/204Pb	26.81	11.71	22.44	11.92	11.72	13.90	16.32
206Pb/204Pb (m)	19.188	18.888	18.962	18.771	18.771	18.832	19.065
207Pb/204Pb (m)	15.613	15.592	15.593	15.594	15.592	15.595	15.622
208Pb/204Pb (m)	38.748	38.527	38.586	38.423	38.421	38.480	38.718
206Pb/204Pb (i)	19.164	18.881	18.901	18.756	18.756	18.817	19.062
207Pb/204Pb (i)	15.612	15.592	15.591	15.593	15.591	15.594	15.622
208Pb/204Pb (i)	38.707	38.517	38.515	38.411	38.409	38.464	38.715
del18O (magma)	7.00		5.74		7.06	6.89	
Trace reference	1	1	1	1	1	1	1

Table 1 continued:

Sample	MTF 07-34	MTF07-37	MTF 07-38	MTF 07-40	MTF 07-49	MTF 07-52	MTF 07-58
Age (Ma)	17.53	5.77	5.59	5	5.17	6.79	8.96
Age error (1-s)	0.04	0.04	0.03	0.7	0.05	0.02	0.03
age reference	MTF	MTF	MTF	RBF K-Ar[c]	MTF	MTF	MTF
Rb (ppm)	292	77.4	80.6	101	47.6	105	62.6
Sr (ppm)	5.24	274	188	141	185	199	241
87Rb/86Sr	161.8	0.8179	1.243	2.073	0.7458	1.529	0.7493
87Sr/86Sr (m)	0.744686	0.703868	0.703806	0.703925	0.703821	0.703972	0.703911
error (if > 22)	**184**						
87Sr/86Sr (i)	0.704401	0.703801	0.703707	0.703778	0.703766	0.703825	0.703816
Sm (ppm)	2.18	7.51	6.41	6.03	5.10	3.35	3.55
Nd (ppm)	9.87	33.51	31.80	28.88	23.46	18.15	20.05
147Sm/144Nd	0.1333	0.1354	0.1218	0.1262	0.1315	0.1117	0.1070
143Nd/144Nd (m)	0.512893	0.512880	0.512892	0.512856	0.512873	0.512849	0.512854
1433Nd/144Nd (i)	0.512878	0.512875	0.512888	0.512852	0.512869	0.512844	0.512848
ENd (0)	5.01	4.76	4.99	4.29	4.62	4.15	4.25
ENd (i)	5.15	4.80	5.05	4.34	4.67	4.23	4.36
Nd standard	La Jolla	La Jolla	La Jolla	La Jolla	La Jolla	La Jolla	La Jolla
Tdm (Ga)	0.57	0.61	0.50	0.59	0.60	0.52	0.49
Lu (ppm)	0.50	0.63	0.68	0.57	0.50	0.29	0.30
Hf (ppm)	43.09	6.37	8.32	6.69	6.71	3.60	4.18
176Lu/177Hf	0.0016	0.0141	0.0110	0.0121	0.0106	0.0115	0.0097
176Hf/177Hf (m)	0.283006	0.283075		0.283076	0.283075	0.283060	
176Hf/177Hf (i)	0.283005	0.283073		0.283075	0.283074	0.283059	
error (if > 5)				8		6	
Ehf (0)	8.28	10.72		10.75	10.72	10.18	
Ehf (I)	8.64	10.79		10.82	10.79	10.28	
Tdm (Ga)	0.42	0.48		0.44	0.42	0.46	
U (ppm)	3.58	4.17	2.38	3.11	1.69	3.81	1.30
Pb (ppm)	26.35	16.08	14.68	14.74	11.68	19.19	16.15
238U/204Pb	8.64	16.49	10.31	13.38	9.18	12.57	5.10
206Pb/204Pb (m)	18.955	18.930	18.886	18.888	18.843	18.829	18.777
207Pb/204Pb (m)	15.602	15.600	15.587	15.584	15.580	15.592	15.597
208Pb/204Pb (m)	38.621	38.570	38.495	38.485	38.444	38.460	38.438
206Pb/204Pb (i)	18.931	18.916	18.877	18.878	18.835	18.816	18.770
207Pb/204Pb (i)	15.600	15.599	15.586	15.584	15.580	15.591	15.597
208Pb/204Pb (i)	38.602	38.550	38.482	38.471	38.431	38.445	38.428
del18O (magma)	6.62			5.36	5.78		6.84
Trace reference	1	1	1	1	1	1	1

Table 1 continued:

Sample	HP 91-5	HP 91-7	HP 91-10	HP 91-11	HP 91-14	HP 93-2	HP 93-8[a]
Age (Ma)	2.89	15.65	7.096	6.90	15.63	7.177	7.2
Age error (1-s)	0.08	0.04	0.015	0.02	0.03	0.014	
age reference	BJ	BJ	BJ	BJ	BJ	BJ	estimate[a]
Rb (ppm)	115	84.0	123	97.6	97.5	127	86.6
Sr (ppm)	214	249	0.35	222	201	0.75	157
87Rb/86Sr	1.553	0.9758	1012	1.269	1.401	490.1	1.592
87Sr/86Sr (m)	0.704026	0.703869	0.805171	0.703979	0.704078	0.753124	0.703856
error (if > 22)			**432**			*134* / ***195***	
87Sr/86Sr (i)	0.703962	0.703652	0.703210	0.703855	0.703767	0.703173	0.703693
Sm (ppm)	2.19	7.03	16.16	2.16	7.05	8.24	6.17
Nd (ppm)	13.50	33.10	68.40	12.00	29.67	29.10	31.60
147Sm/144Nd	0.0981	0.1284	0.1428	0.1090	0.1436	0.1712	0.1180
143Nd/144Nd (m)	0.512847	0.512948	0.512861	0.512852	0.512930	0.512853	0.512883
1433Nd/144Nd (i)	0.512845	0.512935	0.512854	0.512847	0.512915	0.512845	0.512877
ENd (0)	4.12	6.09	4.39	4.21	5.74	4.23	4.82
ENd (i)	4.15	6.22	4.44	4.29	5.84	4.26	4.89
Nd standard	La Jolla	La Jolla	JNdi	La Jolla	La Jolla	La Jolla	JNdi
Tdm (Ga)	0.46	0.44	0.71	0.50	0.58	1.20	0.50
Lu (ppm)	0.21	0.46	1.58	0.18	0.64	1.60	0.52
Hf (ppm)	3.10	7.90	17.10	3.12	7.11	6.76	8.15
176Lu/177Hf	0.0096	0.0083	0.0131	0.0084	0.0128	0.0336	0.0091
176Hf/177Hf (m)	0.282992	0.283057	0.283043	0.283077	0.283031	0.283071	0.283019
176Hf/177Hf (i)	0.282991	0.283055	0.283041	0.283076	0.283027	0.283067	0.283018
error (if > 5)	76		6	6	7		
Ehf (0)	7.78	10.08	9.58	10.79	9.16	10.57	8.73
Ehf (I)	7.83	10.34	9.68	10.90	9.37	10.57	8.85
Tdm (Ga)	0.56	0.42	0.53	0.39	0.55	2.17	0.50
U (ppm)	4.40	3.90	4.60	3.39	3.78	4.32	3.74
Pb (ppm)	16.80	15.90	28.50	14.43	13.70	22.00	12.00
238U/204Pb	16.62	15.58	10.25	14.89	17.56	12.46	19.79
206Pb/204Pb (m)	18.865	18.891	18.872	18.804	18.916	18.828	18.869
207Pb/204Pb (m)	15.605	15.604	15.599	15.597	15.610	15.603	15.610
208Pb/204Pb (m)	38.506	38.523	38.529	38.443	38.554	38.494	38.513
206Pb/204Pb (i)	18.857	18.853	18.861	18.788	18.874	18.814	18.847
207Pb/204Pb (i)	15.604	15.602	15.598	15.596	15.608	15.602	15.609
208Pb/204Pb (i)	38.497	38.473	38.520	38.420	38.488	38.481	38.474
del18O (magma)	6.97		5.58	6.88	6.93	7.17	
Trace reference	1	1	1	1	1	1	1

Table 1 continued:

Sample	HP 93-13c	HP 93-28	HTB 05-01	HTB 06-13	HTB 07-01	JJ 92-1	JJ 92-5
Age (Ma)	7.171	6.8	30.39	28.63	3.80	10.50	10.38
Age error (1-s)	0.018	0.4	0.13	0.17	0.08	0.03	0.03
age reference	BJ	estimate[d]	MI	MI	MI	BJ	BJ
Rb (ppm)	131	127	53.2	14.9	69.8	124	164
Sr (ppm)	0.35	30.7	382	927	89.9	254	29.8
87Rb/86Sr	1095	11.95	0.4021	0.0465	2.246	1.408	15.89
87Sr/86Sr (m)	0.818384	0.704711	0.703715	0.703638	0.704111	0.704920	0.707265
error (if > 22)	**560**	**68**					
87Sr/86Sr (i)	0.706890	0.703554	0.703541	0.703619	0.703990	0.704710	0.704923
Sm (ppm)	9.10	3.98	3.46	1.95	10.49	5.24	7.24
Nd (ppm)	31.40	17.00	16.40	9.79	41.37	26.46	32.59
147Sm/144Nd	0.1752	0.1415	0.1274	0.1204	0.1533	0.1197	0.1343
143Nd/144Nd (m)	0.512842	0.512912	0.512909	0.512935	0.512921	0.512663	0.512595
1433Nd/144Nd (i)	0.512834	0.512906	0.512884	0.512912	0.512917	0.512655	0.512586
ENd (0)	4.02	5.38	5.33	5.83	5.56	0.53	-0.80
ENd (i)	4.04	5.43	5.59	6.11	5.58	0.63	-0.72
Nd standard	La Jolla	La Jolla	La Jolla	La Jolla	La Jolla	La Jolla	La Jolla
Tdm (Ga)	1.36	0.60	0.51	0.43	0.69	0.86	1.14
Lu (ppm)	1.69	0.58	0.28	0.09	1.31	0.44	0.70
Hf (ppm)	7.23	3.23	3.81	2.04	10.90	5.48	4.72
176Lu/177Hf	0.0332	0.0255	0.0103	0.0066	0.0171	0.0114	0.0211
176Hf/177Hf (m)	0.283058	0.283089	0.283005	0.283108	0.283098	0.282911	0.282868
176Hf/177Hf (i)	0.283054	0.283086	0.282999	0.283104	0.283097	0.282909	0.282864
error (if > 5)	6	10	10	68			
Ehf (0)	10.11	11.21	8.24	11.88	11.53	4.92	3.39
Ehf (I)	10.11	11.25	8.70	12.39	11.57	5.07	3.48
Tdm (Ga)	2.13	0.82	0.55	0.32	0.49	0.75	1.26
U (ppm)	4.43	4.75	1.91	0.82	2.76	4.62	6.18
Pb (ppm)	22.00	17.00	8.39	8.44	13.11		
238U/204Pb	12.77	17.70	14.49	6.18	13.35		
206Pb/204Pb (m)	18.830	18.817	18.916	18.806	18.896	18.961	18.922
207Pb/204Pb (m)	15.605	15.589	15.585	15.586	15.595	15.615	15.619
208Pb/204Pb (m)	38.497	38.431	38.483	38.413	38.524	38.670	38.755
206Pb/204Pb (i)	18.816	18.798	18.848	18.778	18.888		
207Pb/204Pb (i)	15.604	15.589	15.582	15.584	15.594		
208Pb/204Pb (i)	38.483	38.408	38.311	38.345	38.512		
del18O (magma)	7.02	3.9 *		6.66	6.89		7.48
Trace reference	1	1	2	2	2	3	3

Table 2: Oxygen isotopic compositions for basalts in this study. References for select radiogenic isotopes are as follows, 1: Jordan et al. (2004), 2: Jordan (2001), 3: Graham et al. (2009), 4: Streck and Grunder, (2008), 5: Scarberry (2007). Q for age indicates Quaternary and less than sign indicates age based on stratigraphic relationship. Precision on $\delta^{18}O$ is better than 0.1 ‰.

Sample	HLP-98-33	21-WHLP-97	8-WHLP-97	30-WHLP-98	HLP-98-38	43-WHLP-98	JR-92-53	HLP-98-22	KCS-05-21
reference	1,2,3	1,2,3	1,2,3	1,2,3	2,3	2,3	4	2	5
general location	HLP	HLP	HLP	HLP	HLP	HLP	HLP	NWBR	NWBR
approx. age	7.7	Q	4.0	1.6	0.1	1.5	5.7	< 6	8.6
Latitude	43.057	43.749	43.928	43.554	43.080	43.724	43.485	42.676	42.773
Longitude	118.958	120.968	121.005	121.292	118.736	120.998	119.538	120.012	120.176
SiO_2	48.27	49.16	49.37	53.49	47.62	49.98	48.19	48.01	52.55
$^{87}Sr/^{86}Sr$ (m)	0.704120	0.703342	0.703738	0.703651	0.704218	0.703753	0.70366	0.703680	0.70374
$^{143}Nd/^{144}Nd$ (m)	0.512807	0.512908	0.512874	0.512904	0.512788	0.512858	0.512916	0.512922	0.512890
$^{206}Pb/^{204}Pb$ (m)	18.889	18.925	18.835	18.939	18.876		18.805	18.799	18.8
$^{207}Pb/^{204}Pb$ (m)	15.557	15.576	15.574	15.564	15.569		15.590	15.594	15.6065
$^{208}Pb/^{204}Pb$ (m)	38.470	38.487	38.439	38.512	38.623		38.438	38.470	38.6714
$\delta\ ^{18}O$ (magma)	6.05	6.01	6.38	6.35	6.10	6.17	5.89	6.06	6.15

Table 3: Summary table of isotopic ranges for rhyolitic samples from this study. See text for more information on the general age or location of these samples. N = generally the number of radiogenic isotope samples for each age or location, although in some cases, not all isotopes were analyzed for. $\delta^{18}O$ is of the melt. See Table 1 for complete data.

General Age or Location*	HLP rhyolites	NWBR rhyolite	Irom Mountain	Deschutes Formation	Steens-aged rhyolites	John Day-aged rhyolites
Age Range (Ma)	12 - 0	12 - 5	2.54	7 - 6	18 - 15	37 - 20
n**	17	10	1	1	4	2
$^{87}Sr/^{86}Sr(i)$	0.70317 - 0.70689	0.70371 - 0.70629	0.703962	0.703806	0.70365 - 0.70440	0.70354 - 0.70362
$^{143}Nd/^{144}Nd(i)$	0.512586 - 0.512922	0.512844 - 0.512888	0.512845	0.512864	0.512878 - 0.512935	0.512884 - 0.512912
e_{Nd} (i)	-0.72 - 5.73	4.23 - 5.05	4.15	4.57	5.15 - 6.22	5.59 - 6.11
$^{206}Pb/^{204}Pb(i)$	18.79 - 19.06	18.76 - 19.16	18.86	18.80	18.85 - 18.93	18.78 - 18.85
$^{207}Pb/^{204}Pb(i)$	15.585 - 15.622	15.580 - 15.612	15.604	15.591	15.591 - 15.608	15.582 - 15.584
$^{208}Pb/^{204}Pb(i)$	38.41 - 38.76	38.41 - 38.71	38.50	38.42	38.47 - 38.60	38.31 - 38.34
$^{176}Hf/^{177}Hf(i)$	0.28286 - 0.28314	0.28306 - 0.28313	0.282991	0.283069	0.28301 - 0.28306	0.28300 - 0.28310
δ 18 O	4.86 - 7.48	5.36 - 7.18	6.97	na	5.74 - 6.93	6.66 - 6.99

Table 4: Representative mixing models described in the text. HLP basalt is a hypothetical basalt with near-average chemical and isotopic characteristics. "Parental" rhyolite is very similar to JR 92-48 (MacLean, 1994; Streck and Grunder, 2008) and approximates the average low to mid-silica rhyolite. High and low Pb seds are Astoria Fan results from Prytulak et al (2006) with $^{87}Sr/^{86}Sr$ estimated from the modern-day Columbia River (Goldstein and Jacobsen, 1988) and $\delta^{18}O$ from pelagic clays ranging from 15 – 25 ‰ (cf. Eiler, 2001). See text and table in Appendix 6.

Starting compositions		$^{87}Sr/^{86}Sr$	Sr ppm	$^{143}Nd/^{144}Nd$	Nd ppm	$^{206}Pb/^{204}Pb$	$^{207}Pb/^{204}Pb$	Pb ppm	δ18O
A	HLP basalt	0.70350	400	0.51290	15	18.850	15.575	3	6.0
B	"parental" rhyolite	0.70375	150	0.51285	20	18.850	15.590	15	6.9
	Assimilants:								
X	Low Pb seds	0.71161	227	0.512356	30	18.900	15.650	25	20
Y	High Pb seds	0.71161	227	0.511617	30	19.300	15.720	25	20
	Results:								
	90A + 10 X	0.70393		0.512801		18.874	15.611		7.4
	96A + 4 Y	0.70369		0.512825		18.966	15.612		6.6
	90 B + 10 Y	0.70488		0.512674		18.920	15.610		8.2

CHAPTER 4:

The Formation of Stratified Crust and Production of Rhyolites in Bimodal Volcanic Suites

ABSTRACT:

Crustal modification and magma flux play a critical role in determining the style of volcanism in continental regions. In the Cascades volcanic arc (Pacific Northwest of the US), a high mantle-derived flux of basaltic magmas penetrated and pervasively modified crust, resulting in a continuum of rock compositions. In the High Lava Plains (HLP) of central and eastern Oregon, a relatively unmodified mafic crust has produced bimodal volcanism as mantle-derived magmatic flux waxed and waned through time. Age-progressive rhyolites have resulted from mafic crustal partial melts that are produced by a focusing of mantle partial melting. This mantle melting is a result of the interplay of North American Plate motion and the roll back and steepening of the subducting Cascadia slab. Mantle-sourced magma flux progressively modified the crust and gravitationally stratified it into seismically identifiable lower and upper crustal seismic reflectors. In the northwestern Basin and Range (NWBR) of southern Oregon, a lower overall mantle-derived flux, coupled with more extension in the crust resulted in a "mini-MASH" model where small crustal reprocessing zones were established and fractional crystallization coupled with mixing and recharge created intermediate compositions. In this region, there is less modification of the crust and less segregation into dense lower crustal and less dense upper crustal regions.

INTRODUCTION:

First, a review of key conclusions from Chapter 2 and Chapter 3 is given and these are used to evaluate previous models for volcanism in the HLP – NWBR. We then link some of our findings and extant petrologic models for volcanism to recent crustal geophysical models, forming a new model of crustal densification and stratification that is used to explain geochemical data and the crustal seismic and density profiles. We review other bimodal volcanic and tectonic settings and discuss how our findings fit into this framework. Finally, we present a conceptual model for the role of the flux of basaltic magmas from the underlying mantle in driving silicic volcanism in the HLP.

SUMMARY OF KEY RESULTS:

The rhyolitic rocks of the bimodal HLP and NWBR are part of a single, age-progressive volcanic trend (cf. Figure 15, Chapter 2) that has been active over the past 12 million years, continuing in the HLP until the present at Newberry Caldera. There is a transfer and reorganization of crustal stresses to the axis of the active arc by the formation of the Cascades graben (Smith et al., 1987; Conrey et al., 1997). This stress transfer may have terminated volcanic activity in the NWBR and led to waning of rhyolitic volcanic activity in the HLP < 4 Ma as the opening of the Cascades graben progressed northward, accommodating strain. The HLP – NWBR volcanic trend, which has moved N20ºW at ~ 33 km/Ma, is in apparent contrast to the southwestward movement of the North American plate. But, very large seismic anisotropies (SKS phases), indicative of strong asthenopheric flow (Long et al., 2009), coupled with plate motion vectors combine to resolve the HLP – NWBR trend (cf. Figure 22, Chapter 2).

There are subtle but identifiable differences in geochemical composition and phase assemblages between the rhyolites of the HLP and NWBR, while the basalt compositions are similar in the two provinces. About 25% of rhyolitic samples are aphyric. Among those with phenocrysts, hydrous phases are much more prevalent in NWBR rhyolites whereas anhydrous Fe-rich assemblages, containing hedenbergite ± fayalite, are more common in HLP rhyolites. Many HLP rhyolites are higher in FeO* at a given SiO_2 concentration than NWBR rhyolites and many samples have higher absolute concentrations of FeO*, SiO_2, TiO_2, high field strength elements (HFSE) and rare earth elements (REE) but lower Pb and Sr (cf. Figures 8, 9, 11 and 12 in Chapter 2). Overall, there is more chemical diversity in HLP rhyolites, including peralkaline compositions. Our geochemical arguments from Chapter 2 generally favor partial melts of amphibolite to form low silica HLP rhyolites and assimilation – fractional crystallization (AFC) processes to form NWBR rhyolites. High silica rhyolites are then generally produced by crystal fractionation of low silica rhyolites (cf. Streck and Grunder, 2008).

In the HLP, across the province as a whole, and over any one area that has protracted rhyolitic volcanism (e.g. Juniper Ridge, Glass Buttes), there is an increase in FeO* at a given silica. This is likely due to two factors. First, the source area for the

partial melt became more mafic over time, likely due to intraplated basalt and the dense residuum left behind by partial melting, a process we term "basaltification". This partial melt source area became progressively more mafic and refractory but also hotter with continuing flux of basaltic magmas from the mantle. The second factor is related to the partial melting. Experimental melts of basalt and amphibolite are quite variable depending upon starting compositions and intensive variables. But, for the assumed conditions of amphibolite stability under the HLP, incrementally larger degrees of partial melting, while lower in overall silica content, produce higher FeO* to SiO_2 ratios in the melts (Sisson et al., 2005; Beard and Lofgren, 1991). These two processes combined to both increase the FeO* at a given silica for long-lived systems and create the voluminous, high FeO* ignimbrites, which are unknown in the NWBR.

Based on isotopic compositions (Sr, Nd, and Pb; Chapter 3), low silica "parental" rhyolites of the HLP are partial melts of recently intraplated basaltic magmas which are likely amphibolitized in the lower or middle crust. Water to produce the amphibolites comes from the crystallization of stalled basaltic magmas. During partial melting, in some samples, a few percent of a contaminant, terrigenous marine sediments in accreted terranes (Prytulak et al., 2006), is assimilated to produce the Pb isotopic signature in some of the rhyolites (cf. Figure 14, Chapter 3). Some of these parental rhyolites stall in the upper crust, where they differentiate and some assimilate a few percent of upper-crustal Cenozoic volcanics (cf. Figure 11, Chapter 3). Combinations of the above processes, coupled with meteoric water alteration of some of the protoliths can create the oxygen isotopic signature in these rhyolites. Of the 23 identifiably unique silicic centers which have radiogenic isotope measurements from the HLP, about half (12) have an isotopic signature indicative of minor crustal assimilation, totaling no more than 10% of the overall protolith. In contrast, only 3 of the 11 NWBR centers show evidence of crustal interaction in the radiogenic isotopes (Table 1). An additional 3 samples from the HLP and 2 samples from the NWBR have oxygen isotopes that indicate a meteoric water influence but do not otherwise have a crustal isotopic signature (Table 1).

DISCUSSION AND SYNTHESIS:

Previous Models Used to Explain HLP – NWBR Volcanism:

While all of the following models have their merits and some of our conclusions are drawn from them, none fully capture the interplay between basalt and rhyolite magmatism. They do not address the subtle differences in composition between the HLP and NWBR rhyolites nor the change in compositions, especially FeO* at a given SiO_2 value over time in the HLP. We first discuss some previous models, most of which focused on the basaltic magmas and then present a unifying model.

A) Carlson and Hart (1987) suggest that the westward younging HLP – NWBR rhyolite trend may result from the clockwise rotation of the Klamath and Cascades terranes (Wells et al., 1998), as a result of the northwestern migration of the Mendocino Triple Junction (Atwater and Stock, 1998). This mechanism would result in a wedge-shaped time transgressive pattern to rhyolitic eruptions where the propagation rate would be faster in southern Oregon and slower in central Oregon, along the Brothers Fault Zone. Using available paleomagnetic data, Carlson and Hart (1987) suggested that significant extension, maybe up to 50%, had occurred in the HLP – NWBR over the past 14 Ma. More recent work (e.g. Wells and Heller, 1988) indicate that extension near the current day southern border of Oregon was < 17% and along the "Steens section", covering the area similar to our NWBR, was only 6 – 10%. Extension lessens to the north and may be < 1% in the HLP, where it also contains a significant amount of shear (Trench, 2008). Such low rates of extension are unlikely to create enough crustal thinning to result in the decompression required to produce basaltic magmas in the upper mantle (McKenzie and Bickle, 1988; Langmuir et al., 1992). Also the rhyolite propagation rate is similar or slower in southern Oregon, especially from 5 to 7 Ma, and the age range may not span the entire 12 m.y. over which this southern section of Oregon was extended (cf. Figure 15, Chapter 2). The wedge-shaped opening also does not explain the episodic increases or pulses in basaltic output (Jordan et al., 2004).

B) Draper (1991) suggests that a plume head, entrained in the asthenopheric counterflow of the subducting Juan de Fuca plate, spread out over time, thus younger (5-7 Ma) silicic volcanics have a wider distribution than the older (7-12 Ma) volcanics. As this plume spread over time, volume is also diminished. Draper also invokes the plume head as a heat source, via basaltic magmas, to create anatectic rhyolites in the region and, hense, the eastern basalts would be hotter than western basalts. Jordan et al. (2004) have shown that basaltic eruptions are not age-progressive so the onset of basaltic volcanism does not follow the westward migration of a plume head. Additionally, the basalts trend to higher MgO in time, so that younger basalts are hotter than older basalts, in contrast to Draper's model (cf. Figure 4, Chapter 3). Basalts also do not have a He isotopic signature indicative of plume involvement (Graham et al., 2009). This model does not support the shortening of the isochrons, indicating less widespread silicic volcanism in the HLP region with ages less than 4 Ma, which are located only in the central-western part of the HLP physiographic region, or the large volumes of silicic magma at Newberry Volcano, located at the western end of the HLP age trend.

C) Jordan et al (2004), with extensive ^{40}Ar-^{39}Ar dating, further refined the positions of the isochrons, removing some of the sharp bends in previous isochron models (Macleod, et al, 1976) but allowing a 2 m.y. duration of volcanism at each isochron. They liken the trend in ages to flow from a circular plume head material along the slope of a westward thinning lithosphere, creating age-progressive volcanism that waned to the west as flow "up the lithospheric slope" decreased. Extant transtension provided magma pathways to the surface, thus producing volcanism in the NWBR as well. While satisfying in many ways, the model does not seem to address a number of key points. It does not explain the non-age-progressive nature of the basalts, which erupt continuously over the past 12 Ma in the region. While it does provide a thermal argument for the voluminous HLP volcanism (both a basalt pulse and large rhyolite ignimbrites) from 7 – 10 Ma, it does not explain why the NWBR, which had significantly more extension, did not have as much or more volcanism at this time. It also misses the apparent increase in spatial distribution for the 5 to 7.5 Ma rhyolites, generally located in the north-westernmost Basin and

Range. That said, our work and some of its conclusion do draw on many of the tenets forth by Jordan et al. (2004).

D) Other models (Christiansen, 1993; Christiansen et al., 2002) draw isochrons similar to those in Chapter 3 and Jordan et al. (2004) for the age-progressive rhyolites. The Christiansen model relies on progressive northwesterly extension in the NWBR and Brothers Fault Zone (BFZ), in the HLP, to generate crustal melting and the rhyolitic trend. As discussed in Jordan et al. (2004) and demonstrated by Trench (2008), the BFZ has been active over at least the past 8 Ma in the HLP. Also, as mentioned above, the extension (or transtension) is not enough to generate decompression partial melts in the mantle under the HLP without involving other processes.

A Unifying Model:

Our preferred model attempts to link all of the observations made in previous chapters (Chapter 2 and 3). We call on asthenopheric counterflow and resultant upwelling created by the Cascadia slab rollback, steepening, and down-dip motion (Druken et al. 2011) as the process that creates partial melts in the mantle, and the interplay of this flow with North American plate motion to form the HLP – NWBR trend. This eliminates the need for any plume head involvement, and the complications that might arise from it such as variable plume – lithospheric interaction or flow rates (Jordan et al., 2004) or the fact that He isotopes do not indicate any plume involvement in the HLP basalts (Graham et al., 2009). But, we concur that such a large and impactful event that happened in the mid-Miocene, very near the HLP – NWBR, played at least some role in crustal modification in eastern areas or otherwise may contribute to very early volcanism in the HLP and NWBR.

Along with extensional stresses, at least some magmatism appears to have been transferred from the HLP – NWBR to the Cascades as the Cascades graben opened. Onset and geographical expansion of extensional tectonics in Oregon follows the pattern of Basin and Range growth at the margins of the province (e.g. Christiansen and Yeats, 1992) and the bulk of mafic volcanism occurs at these opening margins (Fitton et al.

1991). The opening of the Cascades graben accommodates strain from the margins of the extending northwest Basin and Range. This may effectively shut off rhyolitic volcanism in the NWBR at ~ 5 Ma and may be causing the reduction of volcanism in the HLP starting at nearly the same time. Additionally, the highest density of volcanic vents in the Oregon Cascades and very young (< 40 ka) silicic centers are found in the Three Sisters Volcanic Field (Guffanti and Weaver, 1986; Schmidt and Grunder, 2011), which is at the intersection of the HLP trend and the Cascades graben (cf. Figure 22, Chapter 2). In contrast, to the south, there is a paucity of Quaternary vents (especially south of Mt. McLoughlin to the Mt. Shasta region) but this "gap is rich in Pliocene mafic centers" (Hildreth, 2007). This may be a manifestation of the southern portion of the Cascades graben opening earlier than northern portions, transferring a locus of volcanism from the NWBR to the Cascades Arc.

In terms of the flux of magmas from the mantle to the crust and related heat flux, and using eruptive volume as a crude proxy, the Cascades have a much greater flux with ~ 6,400 km^3 of eruptive products in the Quaternary alone (Hildreth, 2007), much greater than the adjacent HLP – NWBR over the past 12 Ma. Furthermore, we believe that the HLP has a greater flux than the NWBR, based on the presence of voluminous tuffs and unquantified but apparently larger volumes of basalt. This forms the resulting relationship in terms of both thermal and material flux from the mantle: the Cascades Arc >> HLP > NWBR. These differences in flux, coupled with the tectonic regime have created the differences observed in both the style and composition of the eruptions as described below.

The Cascades Arc, Very High Flux:

We provide a simplified summary of Cascade Arc volcanism petrogenesis which is key to helping explain our overall model and the reader is referred to Hildreth (2007) for a thorough and comprehensive discussion. The Cascades Arc is predominantly basalt and basaltic andesite (McBirney, 1978, Sherrod and Smith, 2000, Hildreth, 2007 and sources therein). This, along with isotopic studies indicates that much of the arc has either a direct mantle source or contains remelted crustal material that had a mantle

source (Schmidt and Grunder, 2009; Hildreth, 2007). At the Three Sisters volcanic center, the area where the HLP trend and Cascades Arc intersect, basalt is more common than in other places in Oregon in the arc and rhyolites are also comparatively common (Schmidt and Grunder, 2009; Hildreth, 2007). Many arc intermediate-composition samples are a result of melting, assimilation, storage and homogenization or MASH processes (Hildreth and Moorbath, 1988, 1991). Thick volcanic piles develop over time and become a plexus of residuum, differentiates, intrusions, and plutons that are reworked and modified via partial melting, magma mixing, fractionation and crystallization to produce intermediate to silicic volcanics. Rarely, basalt and basaltic andesite magmas may traverse this complex crustal plumbing system relatively unaltered but most often they are unable to penetrate this hot zone. Basaltic magmas may also sidestep the pile to produce satellite vents.

There is often not a strong radiogenic $^{87}Sr/^{86}Sr$ signature in MASH-produced Quaternary Cascade silicic rocks (cf. Figure 29 of Hildreth, 2007); the isotopic compositions of silicic rocks are similar to most mafic rocks. Some of the reasons given for this are that young (Mesozoic and younger) accretionary arc-like and oceanic terraness provide little leverage to change the isotopic composition of more recent volcanics that might interact with the crust. We face a similar issue in the underpinnings of the HLP – NWBR in central and eastern Oregon, but we still see some evidence of elevated $^{87}Sr/^{86}Sr$ and $^{207}Pb/^{204}Pb$, especially in the HLP (cf. Figures 5 and 9, Chapter 3). Another reason for little separation between basalts and evolved rocks in the Cascades is that the young, thick volcanic piles involved in the MASH processes are largely from mantle derived melts, including their associated differentiates and reworked plutons which do not differ (isotopically) from the volcanic rocks they produce. In a few places (e.g. Mt. Lassen) there is evidence of mixing with older crust that has an isotopic signature different from the mantle-derived magmas (Bullen and Clynne, 1990).

The HLP, Moderate to Low Flux:

Volcanism in the HLP obliquely cuts the BFZ. This zone of northwest-striking normal faults with offsets of less than 10 m (Lawrence, 1976) is partially formed by

horsetail structures emanating from extending Basin and Range faults, but also shows evidence of independent transtension over at least the past 8 m.y. (Meigs et al., 2009, Trench, 2008). The BFZ is therefore akin to a leaky transform fault, and this is responsible for the basaltic eruptions that do not show any age-progressive nature across the HLP. In other words, some basaltic lavas have been able to erupt throughout the 12 m.y. history of the HLP due to this leaky transform (Grunder and Meigs, 2009).

Eruptions in the HLP are ultimately driven by a flux (heat and material) out of the mantle, created by decompression partial melts produced by upwelling and counterflow, as described above. We believe this flux is greater in the HLP than in the NWBR from 10 – 5 Ma due to the geometry of the subducting Cascadia slab of the Juan de Fuca plate, creating a more intense area of partial melt in the mantle under the HLP. The slab dip is currently steeper to the south and continues to steepen from south to north (Xue and Allen, 2007; Burgette et al., 2009), which would result in stronger asthenopheric counterflow and therefore upwelling under the HLP compared to the NWBR. As discussed earlier, volcanic flux since 5 Ma is also impacted by the unzipping of the Cascades graben from south to north.

While the leaky transform (BFZ) allows some mafic magmas to traverse the crust, some basaltic melts stalled in the crust. MELTS modeling (Ghiorso and Sack, 1995; Asimow and Ghiorso, 1988) of the average primitive basalt of Jordan (2001) with 0.2 wt. % water indicate that densities range from 2.68 g/cc at 1 kb to 2.78 g/cc at 9 kb. Raising the water contents to 0.5 or 0.8 wt. % slightly reduces these densities by 0.02 to 0.05 g/cc. This range in water content, with a preference for the lower end, is suggested by Till et al. (in preparation) for primitive high alumina olivine tholeiites (HAOT) in the HLP and is similar to that suggested for HAOT at Medicine Lake volcano (Sisson and Grove, 1993). We use a density of 2.8 g/cc for mantle-derived basaltic magmas for our models and calculations.

Basaltic magmas can differentiate in the upper crust to basaltic andesites. MELTS modeling by Jordan (2001) indicated that fractional crystallization of primitive basalt with assimilation of a low silica rhyolite at pressures between 1.5 and 3 kb could form the evolved basalts, but higher pressures could not. Our modeling shows that many

of the evolved basalts can be formed via fractional crystallization of primitive basalt without assimilation, with water contents between 0.2 and 0.5 wt. %, but lower pressures are favored, generally < 2 kb. Thus, petrogenetic modeling suggests primitive basalts stalled in the crust between 1 and 3 kb (~ 3.5 to 11 km depth) where evolved basalts are formed by FC ± A processes, with the potential assimilant being an HLP-style low silica rhyolite (Jordan model).

This creates some minor problems in reconciling the petrologic data with the seismic refraction crustal structure models. Both models of the western HLP by Catchings and Mooney (1988) and Cox (2011) yield a mid-crustal density of ~ 2.75 g/cc with a change to 2.64 or 2.5 g/cc at about 6 to 7 km depth (Figure 1). This change in density could cause primitive basalt to reach neutral buoyancy and stall, producing a basaltic sill or plexus of sills, where it could differentiate to basaltic andesite. This is consistent with the petrologic models. But any stalled (crystallized) basalts will have a density of ~ 2.8 g/cc and differentiation of primitive basalt like those modeled above leaves a fractionation residuum averaging 2.95 g/cc or more. Thus, if there was substantial intraplating and differentiation of basaltic melts at this shallow level, we would expect to see this in the crustal structure inferred from geophysical studies. This appears to be the case in the Steens region where mid-crustal densities are higher compared to surrounding areas (Cox, 2011) and petrogenetic models indicate as much as 50,000 km^3 of basalt and residuum has been added to the crust (Carlson and Hart, 1987), forming a dense layer akin to the mid-crustal sill in the Snake River Plain (McQuarrie and Rodgers, 1998).

Both geophysical models also show a strong density contrast between a lower crust at 2.9 g/cc and mid-crust at ~ 2.75 g/cc, although at different depths (pressures). In both cases, primitive basalt could reach neutral buoyancy at this density transition (if magma over pressures are insufficient to overcome the strength of the crust) and fractionate to form the denser residuum and become part of the 2.9 g/cc layer. But, the petrologic models indicate that pressures of 5 or 6.5 kb are inconsistent with phase assemblages required to produce evolved basalts (Jordan, 2001). This leaves two possibilities:

1) Basaltic magmas are emplaced in the mid to lower crust. More petrogenetic modeling of the basalts, with different parameters, is required to be able to produce evolved basaltic andesite composition from this deeper crustal reservoir. Both crystallized basalts and residuum from fractional crystallization to form evolved compositions could be represented by the 2.9 g/cc layer.

2) Mafic magmas stall to create intraplated basalts at two levels, maybe depending on slight compositional differences or on the state of transtension in the region. Intraplated basaltic magmas in the mid to lower crust produce a "hot zone" and are the sources of the partial melts that produce low silica rhyolites. The basalts emplaced in the shallow crustal reservoir differentiate to form basaltic andesites and the amount of residuum generated in the western HLP could not be detected by the seismic refraction studies. The total volume of erupted basaltic andesites over the entire HLP (based on total volume of basalts presented in Chapter 2 and geochemical classifications from Jordan et al., 2004) is ~ 250 km^3. Based on MELTS modeling, formation of basaltic andesite from primitive basalt yields ~ 1:1 ratio of cumulates to magma. This would yield a cumulate layer, if distributed evenly under the HLP of ~ 10 m, which, if distributed over a couple of kilometers (thickness) of crust, is likely not resolvable with the geophysics.

This second scenario favored and presented in a generic HLP model in Figure 2. In this model, some basaltic magmas stall in the lower crust, where over time, they build heat and are able to partially melt the crust to produce low silica rhyolites. Some basaltic magmas stall in the upper crust, where they fractionally crystallize to form basaltic andesites. Some basaltic magmas, depending on the state of transtension in the crust, do not stall in the crust and erupt to the surface. In this scenario, we might occasionally find some evolved basalts with elevated $^{87}Sr/^{86}Sr$ isotope ratios as they assimilate small portions of upper crustal material. We would also expect not to see any changes in $^{207}Pb/^{204}Pb$ isotopic ratios as the basalts are not stored in the lower crust and therefore cannot obtain the elevated Pb isotopic signature that comes from this region and is present in the rhyolites (Chapter 3). This is in fact, what we observe in the isotope geochemistry.

Regardless of where precisely the mantle-derived melts stall in the crust, as more and more intraplated basaltic magmas differentiate, the original crust becomes more dense. Additionally, as heat builds, some partial melts are extracted from this area of the crust to form low silica rhyolites, and the resultant residuum also makes the crust slightly more dense, and higher in FeO*. These two processes result in a more refractory, higher FeO* crust that we have termed "basaltification". Progressive injection and heating by basaltic magmas increases the FeO* at a given SiO_2 of the rhyolitic partial melts, as we have seen both province-wide and in loci of sustained volcanism (e.g. Juniper Ridge, Glass Buttes) (cf. Figure 20 and 21, Chapter 2).

In some cases, there is enough heating in the lower crust not only to re-mobilize recently intraplated, frozen basaltic magmas, but also to heat and partially melt (assimilate) some of the regional crust (Table 1). Our isotopic work (Chapter 3) indicates that assimilation of a few percent of a contaminant from within the accreted terranes, similar to terrigenous marine sediments deposited in the Astoria fan (Prytulak et al., 2006), could increase the $^{207}Pb/^{204}Pb$ ratios without noticeably perturbing the other isotopic ratios. We believe this partial melting to be taking place in the mid to lower crust, where the 2.75 to 2.9 g/cc density transition takes place. We do not identify any increase in $^{207}Pb/^{204}Pb$ between basalts and basaltic andesites (evolved basalts).

The partial melt of the recently intraplated basaltic magmas, some of which may be amphibolitized by the water given off by crystallization of the basaltic magmas, is a low silica rhyolite (e.g. Beard and Lofgren, 1991; Sisson, et al., 2005) that could buoyantly rise in the crust until either manifesting as volcanism, or stalling out to form an upper crustal magma chamber. This likely happens in the shallow levels of the crust (4 – 8 km deep) where there is a change in density from 2.5 to 2.7 g/cc (Cox, 2011). Some of the low silica rhyolites that stall at this level differentiate to form high silica rhyolites before eruption. In some cases, these upper crustal chambers can assimilate small amounts of crustal material. A subset of seven rhyolites from Table 1 show an increase in $^{87}Sr/^{86}Sr$ compared to local basalts (cf. Figure 5, Chapter 3), which we propose to come from minor assimilation of previous Cenozoic silicic volcanism (Figure 15, Chapter 3). Six of the seven centers with elevated $^{87}Sr/^{86}Sr$ ratios are high silica rhyolites (cf. Figure

3, Chapter 3). Thus, in our preferred model, low silica rhyolite forms by partial melt of amphibolized basalt in the mid to lower crust. Differentiation of this low silica rhyolite to form high silica rhyolite takes place in the upper crust (Figure 2). Intermediate (andesites and dacites) compositions are rare in the HLP and where they do exist, many appear to be mixes of basaltic andesite and rhyolite, although a few lie along basalt – rhyolite mixing lines (cf. Figure 9, Chapter 2). Our model has fractional crystallization of both basaltic magmas to form basaltic andesites and low silica rhyolitic magmas to form high silica rhyolites in the same area in the crust, which may explain why most of the intermediate mixed compositions lie along basaltic andesite – rhyolite mixing lines.

The residuum from the differentiation of the low silica rhyolites would have a density close to that modeled for the mid crust at 2.67 to 2.8 g/cc, comprised largely of plagioclase and other feldspars. Some rhyolitic magmas may fail to erupt at all, and produce granite (~ 2.65 g/cc). This would produce a crystalline "granite-like" layer in the upper crust which may be represented by the 2.5 g/cc layer in the Cox (2011) gravity models. There are some areas of "faster material" in the vicinity of the Harney Basin (density = 2.8 g/cc; Cox, 2011), likely equating to a more dense residuum left behind by either fractionating large amounts of low silica rhyolite to form the high silica rhyolite of the voluminous tuffs (e.g. Rattlesnake Tuff) or from basalt that forms the root zone of the associated large magma chamber, as described below and in Streck and Grunder (1997).

Figure 3 shows crustal modification though time in the HLP. This model is loosely analogous to an east to west transect, but more appropriately illustrates how crust at any one location changes through time. In the early stages (Time 1), there is not a well-developed lower crust. This is not unexpected as the young, accreted terranes that make up the crust in this region have not differentiated into the commonly found upper and lower crustal components so common in older continental settings (e.g. Peng and Humphreys, 1998). For these models, we use the term lower crust to describe that portion of the crust below the ~2.9 g/cc boundary (Figure 1). Any pre-existing lower crust would be from previous crustal processing, maybe during the Clarno, John Day, or Steens volcanic episodes, as discussed in Chapter 2. A low flux of mafic magmas formed by intensified mantle counterflow (upwelling) and decompression melting in the mantle

may stall in the lower crust, but some erupt to the surface depending on the regional transtensional state.

In Time 2, there is an increase in flux of basalt to the lower crust, a result of mantle counterflow due to the rollback and gradual steepening of the Cascadia slab. This increased flux migrates from east to west in time, based on the resolution of the asthenopheric flow and plate motion vectors (Figure 22, Chapter 2). When crustal stress conditions are favorable, there could be a pulse of basalt activity (e.g. ~ 7.5 Ma; Jordan et al., 2004). The lower crust (2.9 g/cc zone) grows primarily due to basalt injection and formation of residuum from partial melting of the lower crust. Time 2 also shows basaltic andesite formation in the upper crust, at the base of the low density sediments and volcanics (Figure 2).

At Time 3, we have accumulated so much basalt in the lower crust that the sensible and latent heat has built to the point where partial melting is possible. This creates a feedback whereas the hot, ductile lower crust now prevents basaltic magmas from penetrating and reaching the surface. These zones of partial melt yield low silica rhyolites which then coalesce and buoyantly rise to the base of the sediments or occasionally erupt. In some cases, Pb isotopes indicate that a few percent of a contaminant with elevated $^{207}Pb/^{204}Pb$ is assimilated (Figure 1), but most of the partially melting material is recently intraplated, and maybe still hot basalts, or amphibolite formed by the water given off by these basalts. Along with the thickening of the lower crustal (2.9 g/cc) zone, we show flexural downwarping of the crust due to the added mass in the crust, resulting in basin formation (e.g. Harney Basin). Basinal sag likely develops at some time after the crustal load is added, after the eruption of the voluminous tuffs, but our cartoon shows it to be coeval for simplicity.

There are three models given for Time 3. In the first panel (3a), as described above, low and high silica rhyolites are generated from an increase in basaltic flux to the lower crust. In 3b, we see the development of another high silica rhyolite, sourced out of a region that has already undergone crustal modification and basaltification. This partial melt of a more mafic crust would be a rhyolite with a higher FeO* at a given silica, as exemplified at Juniper Ridge and Glass Buttes (cf. Figure 20, Chapter 2). We show a

high silica rhyolite being formed, but the low silica rhyolite could erupt if crustal stresses were favorable. In some cases, in the upper crust, the rhyolitic magmas assimilate a few percent of Cenozoic silicic volcanics to get slightly elevated $^{87}Sr/^{86}Sr$ ratios (Chapter 3) (Figure 1).

Time slice 3c (Figure 3) shows the development of a large ignimbrite system, similar to the Rattlesnake Tuff. Its development is similar to dome systems, but the zone of partial melt, and maybe the flux of basalt, is greater. The large upper crustal magma chamber is able to assimilate a few percent of Cenozoic silicic rocks and becomes stratified before eruption (cf. Streck and Grunder, 1997, 2008). Such a large chamber of low density rhyolitic magmas would not permit basaltic magmas to pass, creating a mafic root zone beneath the upper crustal chamber, and might result in the 2.8 g/cc layer in the upper crust of the Harney Basin (cf. Figure 10 of Streck and Grunder, 1999).

The thin zone of underplated basalts or, more likely, residuum shown at the crust-mantle boundary might develop as part of the HLP system, or might have been formed by an earlier magmatic event, maybe related to Steens Basalts, as the unit is considerably thicker in that area (Figure 1). This dense zone between the mantle and crust (underplated crust) could form if the lower crust became soft, due to high flux and partial melting, and decoupled from the mantle, thus inhibiting basalt transfer across this boundary (Fyfe, 1993). It could also represent the residuum from partial melting.

By Time 4, the influx of basaltic magma that drives this system has moved to the west, and the lower crust has cooled. This again allows basaltic magmas to penetrate all the way to the surface. Time 5 shows the development of the one post age-progressive rhyolite dome, the 2.54 Ma Iron Mountain. In this scenario, heat flux into the lower crust is not necessarily higher, but enough basalt is put into one region in the lower crust to create some partial melt and a low silica rhyolite. By this point there is only small-scale mass addition to the crust and crustal flexure has ceased.

The NWBR, Low or Very Low Flux:

The AFC processes coupled with potential mafic replenishment and magma mixing (cf. RAFC of Bohrson and Spera, 2001; Spera and Bohrson, 2001) thought to

produce the NWBR silicic samples is largely based on the bulk rock geochemistry which includes many more intermediate samples (57 – 69 wt. % SiO_2) than the HLP. Many of these intermediate sample compositions cannot be produced by fractional crystallization or mixing alone (cf. Al_2O_3, Na_2O, Sr, Figures 8 and 9, Chapter 2) and many contain phenocrysts that are resorbed, sieve-textured and inclusion rich (Chapter 2; Wells, 1979; Hering, 1981). While not explicitly required for the formation of these silicic magmas, recharge and mixing cannot be excluded either. Examination of Table 1 shows that there is *not* a strong Mesozoic or Tertiary crustal signature in NWBR dacites and rhyolites, as represented by the isotopic compositions. Thus the "A" of AFC must primarily be of recently intraplated mantle-derived material.

For our (R)AFC model (Figure 4), pods of melt form within a small hot zone or crust processing zone of intraplated basaltic magmas instead of the crustal-scale volcanic piles found in arc settings. Within these small pods of partial melt, storage resulting in fractional crystallization and even some recharge and mixing of magmas are akin to a "mini-MASH" model. The continuum of compositions seen in the NWBR can only be produced by melting, mixing and fractional crystallization occurring at the same place in the crust, not at multiple levels as in the HLP.

As described above, flux of basaltic magmas into the NWBR is lower than that for the HLP. Also, due to the greater amounts of extension in the NWBR, basaltic magmas are less likely to stall in the crust and create large partial melt zones. The geophysical model by Cox (2011) and resultant crustal density models (Figure 5) show a less dense mid to lower crust (at 2.85 g/cc) in the NWBR of Oregon (our study area), indicating less mafic addition and basaltification has occurred in this area. The density and thickness of the lower crust continues to decrease to the south in NV, where Basin and Range extension is greater still. We still see the WNW trend of migrating rhyolitic centers because there is still an increase in flux from the mantle, just like in the HLP, but it is not as large. Rhyolite formation by partial melt in the lower crust, similar to that for the HLP, is not expressly precluded and indeed, some rhyolites are likely formed in that way in the NWBR.

Implications for Bimodal Volcanism in Other Provinces:

Our model for the HLP has implications for bimodal volcanism in many similar volcanic provinces. Two such provinces, Iceland and the Snake River Plain (SRP) of Idaho, are bimodal basalt - rhyolite systems where there are multiple petrogenetic models for the rhyolites (Christiansen and McCurry, 2008; Bonnichsen et al., 2008; McCurry and Rodgers, 2009; Furman et al., 1992; Jonasson, 1994) (see petrogenetic summaries in Appendix 5). Other places where bimodal volcanism occurs on primarily mafic crust, precluding rhyolite petrogenesis by melting of a silicic protolith, include the Izu-Bonin Arc (Tamura, et al., 2009), the Kerguelen Plateau (Frey et al., 2000), the Galapagos Islands (Geist et al., 1995) and Hawaii (Shamberger and Hammer, 2006).

For the age-progressive large ignimbrite-forming rhyolites of the SRP (and Yellowstone system), a consensus is building around a partial melting model. There, intraplated mantle-derived basaltic magmas in the mid to upper crust hybridize with local, silicic, Archean crustal rocks and then partially melt in a MASH-like zone to produce low silica rhyolites which then fractionate in shallow magma chambers to produce the high silica rhyolitic ignimbrites (McCurry and Rodgers, 2009). In this model, the intraplated basalt and partial melting in the mid to upper crust is similar to our basaltification in the lower crust. In both cases, basalts are being emplaced and partial melts are being removed, leaving the crust more dense, and in the case of the SRP, producing the mid-crustal sill (Peng and Humphreys, 1998). In the SRP model, the basaltic magmas stall at shallower levels in the crust because the lower crust is already very dense; it is “mature” lower crust which has undergone multiple distillations in the past, unlike the crust of the HLP which is young and only beginning stratification.

The McCurry and Rodgers (2009) model invokes 20 – 30% partial melting of a dioritic hybrid source to produce the low silica rhyolites, but small degrees of partial melt of recently intraplated, amphibolitized basalts coupled with anatexis of the old, silicic crust would produce similar results. This model would be very similar to that which we propose for the HLP, namely remobilization or partial melts of recently intraplated, potentially amphibolitized basalts coupled with anatexis of crust. In our case, the crust would be amphibolitic facies accreted terranes, which can contain a few percent of a

contaminant similar to terrigenous marine sediments to balance the Pb isotopes (Chapter 3) and in the SRP this would be the Archean crust. Some samples from the HLP show slight depletions of the mid- to heavy rare earth elements (REE) including Ho and Er and steady to declining Sr/Y values (cf. Figure 19, Chapter 2) indicating that partial melting of amphibolite is involved in the petrogenesis of the rhyolites. Unfortunately, very few of the over 500 whole rock geochemical analyses from the SRP contain Y or the mid- to heavy REE. With those data, we would be able to distinguish between partial melting of a dioritic hybrid (without amphibole) and partial melting of recently intraplated, amphibolitized basalts coupled with crustal anatexis.

Quaternary rhyolite domes of the SRP (e.g. McCurry et al., 2008) may be produced by extreme fractional crystallization of mantle derived basaltic magmas. McCurry et al. (2008) come to this conclusion mostly based on the continuum of chemistry demonstrated by Cedar Butte and Craters of the Moon sequence, coupled with the Whitaker et al. (2008) experiments that show a continuous liquid line of descent from an SRP olivine tholeiite to rhyolite, albeit with low potassium. While we agree that this is compelling and a likely possibility for Cedar Butte, for other Quaternary SRP domes (e.g. Big Southern Butte; the Blackfoot Volcanic Field), our model of continued modification of the crust (by basaltification) could also produce these rhyolites. Indeed, Big Southern Butte has slightly elevated $^{87}Sr/^{86}Sr$ isotopic ratios, not unlike some rhyolites of the HLP, which could come from assimilation of some of the recent (~ 10 Ma) SRP ignimbrite, or more likely, the unerupted or plutonic crustal equivalent. Emplacement of basaltic magmas in the crust has continued in the SRP since the age-progressive rhyolites were produced, making the mid-crust more mafic. Additionally, $\delta^{18}O$ values for these rhyolites are very similar to local basalts (Ford, unpublished; Savov et al., 2009), not what one would expect from extreme fractional crystallization (see discussion in Chapter 3).

The Icelandic province shows strong similarities to the HLP. There is no silicic crust to hybridize with basalts so partial melts must be produced from either recently intraplated basalts or amphibolitized basalts (or both). The geochemistry bears this out as some rhyolites show slight depletions in the mid to heavy REE and declining Sr/Y values

(cf. Figure 19, Chapter 2). It is important to point out that a lack of depletion in Ho or Er (a flat mid to heavy REE curve) does not indicate that amphibolite was not involved in the partial melt; such depletion only occurs if there is amphibole in the residuum, not if the amphibolite was completely melted.

Some authors point to protracted fractional crystallization as a mechanism to produce rhyolites in Iceland (e.g. Furman et al., 1992; Martin and Sigmarsson, 2007). There is a paucity of "true intermediate magmas" lying along the liquid line of decent in Iceland, but they are reported (Jonasson, 2005). We cannot discount the possibility that extreme fractional crystallization plays a role in the petrogenesis of some rhyolites from Iceland, but believe that crustal modification model for the HLP would also be applicable to the petrogenesis of these rhyolites. Many intermediate compositions in Iceland are the result of magma mixing (see Chapter 2 and petrogenetic summaries in Appendix 5).

The apparent lack of intermediate magmas, other than by binary mixing, in the HLP, coupled with the slight change in chemistry over time (to higher FeO* at a given SiO_2) and the evidence that amphibolite partial melt is involved in many samples indicates that partial melting of an increasing more mafic crust (basaltification) is the primary genesis for HLP rhyolites. The formation of rhyolites by extensive fractional crystallization from basalt all the way to rhyolite is very rare and potentially absent in the three systems discussed above (HLP, SRP and Iceland). Our model is capable of producing the bulk of the rhyolites observed in these systems, except for the Cedar Butte – Craters of the Moon sequence of the SRP, and capable of producing bimodal assemblages in areas with a predominately mafic crust.

Basaltic Flux to the Crust:

In this section we briefly detail the methodology in determining the total mantle-derived addition required to create the rhyolites of the HLP and provide a rudimentary quantification. The maximum thickness (a unit thickness added per unit area, used as proxy for mass) contribution to the HLP crust is estimated based on erupted volume and thermal constraints. The following maximum estimates are used for the HLP: a uniform thickness of 50 m of high silica rhyolite over the HLP (1250 km^3 dispersed over 25,000

km^2), 50 m thickness of mafic volcanic rocks over that same area, and a 1:1 ratio of basalts to basaltic andesites. For this model, all low silica rhyolites are produced by partial melting in the lower crust and we use a 50% fractionation factor to go from low silica rhyolites to high silica rhyolites (MacLean, 1994; Streck and Grunder, 1997). We use a 50% fractionation factor to go from basalts to basaltic andesites (Jordan et al., 2004, Ford, unpublished). We present these results as a unit thickness (m) per square meter of crust, in other words, how much crustal addition results from the observed volcanism.

Mass (Unit Volume) Added by Erupted Basalts:

The total mass added by the erupted basalts would be a uniform thickness of basalt (density = 2.8 g/cc) of 75 m. This includes the surface expression of 25 m of basalt and 25 m of basaltic andesite and adds 25 m of cumulate from basalt fractionation left in the upper crust (1:1 ratio) (Figure 6). This is a maximum value based on the eruptive volume, as total basaltic andesite volumes are closer to 250 km^3, and this does not include any basalts or basaltic andesites that are lodged in the crust and do not have a surface expression. This mass is negligible compared to that required to drive the silicic volcanism.

Mass (Unit Volume) Added by Erupted Rhyolites:

This calculation has considerable uncertainty associated with it and parameters are chosen to produce a reasonable maximum mass (unit thickness of basalts) required to create a thickness of 50 m per m^2 (per unit area) of erupted high silica rhyolite. A significant unknown is the fraction of the rhyolite magma chamber that erupted, with estimates ranging between 10% (Shaw, 1985) and nearly 100% (Wilson et al., 2006). We choose a low, but reasonable value of 20% of the magma chamber erupted (again, looking to maximize basalt contribution) which results in a total of 250 m of high silica rhyolite, of which 50 m erupts.

The amount of fractionation required to go from low silica rhyolite to high silica rhyolite is also variable, but simple mass balance suggests a fractionation factor of ~ 50%, similar to that shown by Streck and Grunder (1997) for the Rattlesnake Tuff. For

the peralkaline rhyolites, this factor is larger. These parameters result in 500 m (uniform thickness) of "parental" low silica rhyolite, 450 m of which is emplaced in the upper crust as unerupted high silica rhyolites, cumulates from fractionation and unextruded upper crustal granite (Figure 6). This assumes that all silicic bodies produce an eruptive unit, which is almost certainly not the case. Many likely lodge in the crust to become granites and we cannot quantify this based on eruptive volumes. The granites and cumulates formed by crystal fractionation are imaged by the geophysics and modeled as the 2.5 g/cc layer (Figures 1 and 2).

The melt fraction of basalt or amphibolite required to produce the 500 m (unit thickness) of parental low silica rhyolites is also quite variable. Experiments by Sisson et al. (2005) and Beard and Lofgren (1991) indicate that a melt fraction of 10 to 15% can produce low silica rhyolites similar to those from the HLP. Using the lower constraint (again, to maximize mantle basaltic input), these partial melts must be extracted from a 5,000 m thickness of mafic crust (Figure 6), leaving a slightly more dense residue, which would make up part of the 2.9 g/cc layer in the lower crust (Figures 1 and 2).

Using methods and constants including sensible and latent heat, similar to Grunder (1995) and Guffanti et al (1996), the amount of mantle-derived basalt needed to heat this thickness of lower crust to the liquidus is ~2,500 m (per m^2) if the crust starts at 400ºC and about half that if this amount in the lower crust is already fairly warm (600ºC starting temperature). The amount of basalt needed to partially melt the near liquidus crust to ~ 10% is additional 930 m (per m^2). This assumes that only the crust that is required to produce the low silica rhyolites is heated and that all of the melt is extracted. Thus, based on the eruptive volume (all as high silica rhyolites), a very modest chamber eruption factor, an appropriate amount of fractionation, and the lower end of literature-based partial melting constraints in a cool (400ºC) crust, the volume of mantle-derived magmas to produce the rhyolites is about 3.5 km (unit thickness, per square meter of crust), not including those rhyolites that don't produce a volcanic expression and using the assumption that crustal melting is 100% efficient (Figure 6). This results in a ratio of ~70:1 basaltic influx to erupted high silica rhyolites.

This total flux could be inflated to as much as 6 km of basalt equivalent, depending on the efficiency of removing partial melts, and we consider this an absolute maximum for this system. Using parameters that are more similar to what we see on the surface and that would limit basalt requirements (30 m of high silica rhyolite and 10 m of low silica rhyolite, 30% eruptability, 50% fractional crystallization to make high silica rhyolites, a warm (600ºC) crust and 15% partial melting) yields about 750 m of basalt, or less than 20:1 basalt influx to erupted rhyolite. This seems to be at or near the minimum required to drive this system. The addition of 1 to 6 km (unit thickness) of mantle-derived basaltic magma is consistent with what we observe in the geophysical models.

CONCLUSIONS:

The interplay between flux of mantle-derived basaltic magmas and crustal extension helps determine the style of volcanism in an area with mafic crust. In zones of high flux, crustal-scale MASH zones are produced as basaltic liquids are unable to traverse the thermally weakened crustal column. In places with low flux and moderate extension, there is not enough thermal flux to the crust to create crustal partial melts. Where there is moderate flux and low extension, bimodal vocalism forms as some basaltic magmas can traverse the crust but many have insufficient buoyancy and magma overpressure to overcome crustal strength. These basaltic magmas stall in the crust and can begin to partially melt this crust, which creates a feedback where more basalt is entrapped. These partial melts evolve to higher FeO* at a given silica as there is more melt extraction and basalt injection. Thus, basaltification and the stratification of juvenile crust develops.

The models we have developed are internally consistent and adhere to geochemical, petrological, and geophysical constraints on the HLP and NWBR system. The models address the age-progressive nature of the both the HLP and NWBR, while explaining the difference in volumes between the two provinces. They can also explain the different styles of volcanism but allow for some flexibility, depending on the state of transtension in the crust. Additionally, the models satisfy the following observations: 1) the creation of a more dense lower crust, 2) the creation of a silicic crystal residuum in

the upper-most crust, 3) the dearth of intermediate compositions in the HLP, 4) the creation of a bimodal assemblage in the HLP, 5) the isotopic composition of the rhyolites, with a greater crustal component in the HLP, 6) the increase in FeO* at a given silica at any long-lived center or over the HLP province as a whole, 7) the underplated crust in areas with the greatest flux (Harney Basin), 8) (potentially) the addition of enough mass to create basinal sag in the Harney Basin, 9) the elimination for the need of a plume source of any kind for the HLP volcanism, 10) the explanation of the existence of one post age progression (Iron Mountain) rhyolite, and 11) the production of large ignimbrites in the HLP but not the NWBR.

REFERENCES:

Asimow, P. D. and Ghiorso, M. S., 1998, Algorithmic Modifications Extending MELTS to Calculate Subsolidus Phase Relations: American Mineralogist, v. 83, p. 1127-1131.

Atwater, T and Stock, J, 1998, Pacific-North America plate tectonics of the southwestern United States, an update: International Geological Review, v. 40, p. 375-402.

Beard, J. S. and Lofgren, G. E., 1991, Dehydration melting and water-saturated melting of basaltic and andesitic greenstones and amphibolites at 1, 3, and 6.9 kb: J. of Petrology, v. 32, p. 365-401.

Bohrson,W. A. and Spera, F. J., 2001, Energy-constrained open-system magmatic processes II: Application of energy-constrained assimilation-fractional crystallization (EC-AFC) model to magmatic systems: J. of Petrology, v.42, p. 1019-1041.

Bonnichsen, B., Leeman, W. P., Honjo, N., W. C., McIntosh, and Godchaux, M. M., 2008, Miocene silicic volcanism in southwestern Idaho: geochronology, geochemistry, and evolution of the central Snake River Plain: Bulletin of Volcanology, v. 70, no. 3, p. 315-342.

Bullen, T. D. and Clynne, M. A., 1990, Trace element and isotopic constraints on magmatic evolution of the Lassen Volcanic Center: J. of Geophysical Research, v. 95, p. 19671-19691.

Burgette, R. J., Weldon, R. J. and Schmidt, D. A., 2009, Interseismic uplift rates for western Oregon and the along-strike variation in locking on the Cascadia subduction zone, J. of Geophysical Research, v. 114, B01408, p. 1 – 24.

Carlson, R. W. and Hart, W. K., 1987, Crustal Genesis on the Oregon Plateau: J. of Geophysical Research, v. 92, p. 6191-6206.

Catchings, R. D. and Mooney, W. D., 1988, Crustal structure of east central Oregon: Relation between Newberry Volcano and regional crustal structure: J. of Geophysical Research, v. 93, p. 10081-10094.

Christiansen, E. H. and McCurry, M., 2008, Contrasting origins of Cenozoic silicic volcanic rocks from the western Cordillera of the United States: Bulletin of Volcanology, v. 70, no. 3, p. 251-267.

Christiansen, R.L., and Yeats, R.L., 1992, Post-Laramide geology of the U.S. Cordillerian region: in Burchfiel, B.C., Lipman, P.W., and Zoback, M.L., eds., The Cordillerian Orogen: Conterminous U.S.: Boulder, CO, Geological Society of America, Geology of North America: v. G-3, p. 261–406.

Christiansen, R.L., 1993, The Yellowstone hot spot: Deep mantle plume or upper mantle melting anomaly?: EOS, Transactions of the American Geophysical Union, v. 76, p. 602.

Christiansen, R.L., Foulger, G.R., and Evans, J.R., 2002, Upper-mantle origin of the Yellowstone hotspot: Geological Society of America Bulletin, v. 114, p. 1245-1256.

Conrey, R. M., Sherrod, D. R., Hooper, P. R. and Swanson, D. A., 1997, Diverse primitive magmas in the Cascade Arc, northern Oregon and southern Washington: Canadian Mineralogist, v. 35, no. 2, p. 367-496.

Cox, C., 2011, A Controlled- Source Seismic and Gravity Study of the High Lava Plains (HLP): University of Oklahoma MS Thesis, 110 p.

Draper, D. S., 1991, Late Cenozoic bimodal magmatism in the northern Basin and Range Province of southeastern Oregon: J. of Volcanology and Geophysical Research, v. 47, p. 299-328.

Druken, K. A., Long, M. D. and Kincaid, C., 2011, Patterns in seismic anisotropy driven by rollback subduction beneath the High Lava Plains: Geophysical Research Letters, v. 38, L13310, p. 1-6.

Fitton, J. G., James, D. and Leeman, W. P., 1991, Basic magmatism associated with Late Cenozoic extension in the western United States – compositional variations in space and time: J. of Geophysical Research, v. 96, p. 13693-13711.

Frey F.A., Coffin M.F., Wallace P.J., Weis D., Zhao X., Wise S.W., Jr., Wahnert V., Teagle D.A.H., Saccocia P.J., Reusch D.N., Pringle M.S., Nicolaysen K.E., Neal C.R., Müller D.R., Moore C.L., Mahoney J.J., Keszthelyi L., Inokuchi H., Duncan R.A., Delius H., Damuth J.E., Damasceno D., Coxall H.K., Borre M.K., Boehm F., Barling J., Arndt N.T. and Antretter M., 2000, Origin and Evolution of a Submarine Large Igneous Province: The Kerguelen Plateau and Broken Ridge, Southern Indian Ocean: Earth and Planetary Science Letters, v. 176, p. 73-89.

Furman, T., Frey, F. A., Meyer, P. S., 1992, Petrogenesis of evolved basalts and rhyolites at Austurhorn, southeastern Iceland: the role of Fractional Crystallization: J. of Petrology, v. 33, p. 1405-1445.

Fyfe, W. S., 1993, Hot spots, magma underplating, and modification of continental crust: Canadian J. of Earth Sciences, v. 30, p. 908-913.

Geist, D., Howard, K. A. and Larson, P., 1995, The generation of oceanic rhyolites by crystal fractionation – The basalt-rhyolite association at Volcan Alcedo, Galapagos Archipelago: J. of Petrology, v. 36, p. 965-982.

Ghiorso, M. S. and Sack, R. O., 1995, Chemical Mass Transfer in Magmatic Processes IV: A Revised and Internally Consistent Thermodynamic Model for the Interpolation and Extrapolation of Liquid-Solid Equilibria in Magmatic Systems at Elevated Temperatures and Pressures: Contributions to Mineralogy and Petrology, v. 119, p. 197-212.

Graham, D. W., Reid, M. R., Jordan, B. T., Grunder, A. L., Leeman, W. P., and Lupton, J. E.,2009, Mantle source provinces beneath the Northwestern USA delimited by helium isotopes in young basalts: J. of Volcanology and Geothermal Research, v. 188, p. 128-140.

Grunder, A. L. and Meigs, A., 2009, Volcanic and structural setting of the High Lava Plains, an intracontinental transform zone in the northwestern USA: Geological Society of America Abstracts with Programs, Vol. 41, No. 7, p. 572.

Grunder, A. L., 1995, Material and thermal roles of basalt in crustal magmatism: Case study from eastern Nevada: Geology, v. 23, p. 952-956.

Guffanto, M., Clynne, M. A. and Muffler, L. J. P., 1996, Thermal and mass implications of magmatic evolution in the Lassen volcanic region, California, and minimum constraints on basalt influx to the lower crust: J. of Geophysical Research, v. 101, p. 3003-3013.

Guffanti, M. and Weaver, G. S., 1988), Distribution of Late Cenozoic volcanic vents in the Cascade Range: Volcanic arc segmentation and regional tectonic considerations: J. of Geophysical Research, v. 93, p. 6513 – 6529.

Hering, C. W., 1981, Geology and petrology of the Yamsay Mountain Complex, south-c entral Oregon: A study of bimodal volcanism: University of Oregon PhD thesis, 189 p.

Hildreth, W., 2007, Quaternary magmatism in the Cascades – geologic perspectives: US Geological Survey Professional Paper 1744, 125p.

Hildreth, W., and Moorbath, S., 1988, Crustal contributions to arc magmatism in the Andes of central Chile: Contributions to Mineralogy and Petrology, v. 98, p. 455-489.

Hildreth, W., and Moorbath, S., 1991, Reply to comment on "Crustal contributions to arc magmatism in the Andes of central Chile" by W. Hildreth and S. Moorbath: Contributions to Mineralogy and Petrology, v. 108, p. 247-252.

Jonasson, K., 1994, Rhyolite volcanism in the Krafla central volcano, north-east Iceland: Bulletin of Volcanology, v. 56, p. 516-528.

Jonasson, K., 2005, Magmatic evolution of the Heidarsporour Ridge, NE-Iceland: J. of Volcanology and Geothermal Research, v. 147, p. 109-124.

Jordan, B. T., 2001, Basaltic volcanism and tectonics of the High Lava Plains, southeastern Oregon: Oregon State University PhD thesis, 218p.

Jordan, B. T., Grunder, A. L., Duncan, R. A., and Deino, A. L., 2004, Geochronology of age-progressive volcanism of the Oregon High Lava Plains: Implications for the plume interpretation of Yellowstone: J of Geophysical Research, v. 109, issue B10, p. 1-19.

Langmuir, C. H., Klein, E. M. and Plank, T., 1992, Petrological Systematics of Mid-Ocean Ridge Basalts: Constraints on Melt Generation Beneath Ocean Ridges: AGU Monograph, v. 71, p. 183-280.

Long, M. D., Gao, H., Klaus, A., Wagner, L. S., Fouch, M. J., James, D. E., and Humphreys, E., 2009, Shear wave splitting and the pattern of mantle flow beneath eastern Oregon: Earth and Planetary Science Letters, v. 288, p. 359-369.

MacLeod, N. S., Walker, G. W. and McKee, E. H., 1976, Geothermal significance of eastward increase in age of upper Cenozoic rhyolitic domes in southeastern Oregon, Second United Symposium on the development and use of geothermal resources, Proceedings v. 1, p. 465-474.

Martin, E. and Sigmarsson O., 2007, Crustal thermal state and origin of silicic magma in Iceland: the case of Torfajokull, Ljosufjoll and Snaefellsjokull volcanoes: Contributions to Mineralogy and Petrology, v. 153, p. 593-605.

MacLean, J. W., 1994, Geology and geochemistry of Juniper Ridge, Horsehead Mountain and Burns Butte: implications for the petrogenesis of silicic magma on the High Lava Plains, southeastern Oregon: Oregon State University MS Thesis, 141 p.

McBirney, A. R., 1978, Volcanic evolutions of the Cascade Range: Annual Review of Earth and Planetary Sciences, v. 6, p. 437-456.

McCurry, M. and Rodgers, D. W., 2009, Mass transfer along the Yellowstone hotspot track 1: Petrologic constraints on the volume of mantle-derived magma: J. of Volcanology and Geothermal Research, v. 188, p. 86-98.

McCurry, M., Hayden, K. P., Morse, L. H. and Mertzman, S., 2008, Genesis of post-hotspot, A-type rhyolite of the Eastern Snake River Plain volcanic filed by extreme fractional crystallization of olivine tholeiite: Bulletin of Volcanology, v. 70, p. 361-383.

McKenzie, D. and Bickle, M. J., 1988, The volume and composition of melt generated by extension of the lithosphere: J. of Petrology, v. 29, p. 625-679.

McQuarrie, N. and Rodgers, D. W., 1998, Subsidence of a volcanic basin by flexure and lower crustal flow: The eastern Snake River Plain, Idaho: Tectonics, v. 17, no. 2, p. 203-220.

Meigs, A., Scarberry, K., Grunder, A., Carlson, R., Ford, M. T., Fouch, M., Grove, T., Hart, W. K., Iademarco, M., Jordan, B., Milliard, J., Streck, M., Trench, D. and Weldon, R., 2009, Geological and geophysical perspectives on the magmatic and tectonic development, High Lava Plains and northwest Basin and Range, in O'Connor, J.E., Dorsey, R.J. and Madin, I.P., eds., Volcanoes to Vineyards: Geologic Field Trips through the Dynamic Landscape of the Pacific Northwest: Geological Society of America Field Guide 15, p. 435-470.

Peng, X, and Humphreys, E. D., 1998, Crustal velocity structure across the eastern Snake River Plain and the Yellowstone swell: J. of Geophysical Research, v. 103, p. 7171-7186.

Prytulak, J., Vervoort, J. D., Plank, T., and Yu, C., 2006, Astoria Fan sediments, DSDP site 174, Cascadia Basin: Hf-Nd-Pb constraints on province and outburst flooding: Chemical Geology, v. 233, p. 276-292.

Savov, I. P., Leeman, W. P., Lee, C. T. A. and Shirey, S. B., 2009, Boron isotopic variations in NW USA rhyolites: Yellowstone, Snake River Plain, Eastern Oregon: J. of Volcanology and Geothermal Research, v. 188, p. 162-172.

Schmidt, M. E. and Grunder, A. L., 2009, The evolution of North Sister: A volcano shaped by extension and ice in the central Oregon Cascades Arc: Geological Society of America Bulletin, v. 121, p. 643-662.

Schmidt, M. E. and Grunder, A. L., 2011, Deep mafic roots to arc volcanoes: Mafic recharge and differentiation of basaltic andesite at North Sister Volcano, Oregon Cascades: J. of Petrology, v. 52, p. 603-641.

Shamberger, P. J. and Hammer, J. E., 2006, Leucocratic and gabbroic xenoliths from Hualalai Volcano, Hawaii: J. of Petrology, v. 47, p. 1785-1808.

Shaw, H.R., 1985, Links between magma-tectonic rate balances, plutonism and volcanism: J. of Geophysical Research, v. 90, p.11275–11288.

Sherrod, D. R. and Smith, J. G., 2000, Geologic map of upper Eocene to Holocene volcanic and related rocks of the Cascades Range, Oregon: U.S. Geological Survey Map I-2569, scale 1:500,000; pamphlet 17 p.

Sisson, T.W. and Grove, T. L., 1993. Experimental investigations of the role of H_2O in calc-alkaline differentiation and subduction zone magmatism: Contributions to Mineralogy and Petrology, v. 113, p. 143-166.

Sisson, T. W., Ratajeski, K., Hankins, W. B., Glazner, A. F., 2005, Voluminous granitic magmas from common basaltic sources: Contributions to Mineralogy and Petrology, v. 148, p. 635-661.

Smith, G. A., Snee, L. W., and Taylor, E. M., 1987, Stratigraphic, sedimentologic, and petrologic record of the late Miocene subsidence of the Oregon High Cascades: Geology, v. 15, p. 389-392.

Spera, F. J. and Bohrson,W. A., 2001, Energy-constrained open-system magmatic processes I: General model and energy-constrained assimilation and fractional crystallization (EC-AFC) Formulation: J. of Petrology, v. 42, p. 999-1018.

Streck, M. J. and Grunder, A. L., 1997, Compositional gradients and gaps in high-silica rhyolites of the Rattlesnake Tuff, Oregon: J. of Petrology, v. 38, p. 133-163.

Streck, M. J. and Grunder, A. L., 1999, Enrichment of basalt and mixing of dacite in the rootzone of a large rhyolitic chamber: inclusions and pumices from the Rattle Snake Tuff, Oregon: Contributions to Mineralogy and Petrology, v. 136, p. 193-212.

Streck, M. J. and Grunder, A. L., 2008, Phenocryst-poor rhyolites of bimodal, tholeiitic provinces: the Rattlesnake Tuff and implications for mush extraction models: Bulletin of Volcanology, v. 70, p. 385-401.

Tamura, Y., Gill, J. B., Tollstruo, D., Kawabayta, H., Shukuno, H., Chang, Q., Miyazaki, T., Takahashi, T., Hirahara, Y., Kodaira, S., Ishizuka, O., Suzuki, T., Kido, Y., Fiske, R. S. and Tatsumi, Y., 2009, Silicic magmas in the Izu-Bonin oceanic arc and implications for crustal evolution: J. of Petrology, v. 50, p. 685-723.

Till, C. B., Grove, T. L., Carlson, R. W., Donnelly-Nolan, J. M., Fouch, M., Wagner, L., Hanson-Hedgecock, S., Hot Adiabatic Decompression Melting Near the Lithosphere-Astheosphere Boundary below southern Oregon and northern California: In preparation for G-cubed special volume.

Trench, D., 2008, The Termination of the Basin and Range Province into a Clockwise Rotating Region of Transtension and Volcanism, Central Oregon: Oregon State University MS thesis, 71 p.

Wells, R. E., 1979, Drake Peak – A structurally complex rhyolite center in southeastern Oregon: US Geological Survey Professional Paper 1124, p. E1-E16.

Wells, R. E., Weaver, C. S. and Blakely, R. J., 1998, Fore arc migration in Cascadia and its neotectonic significance: Geology, v. 26, p. 759-762.

Wells, R. E. and Heller, P. L., 1988, The relative contribution of accretion, shear, and extension to Cenozoic tectonic rotation in the Pacific Northwest: Geological Society of American Bulletin, v. 100, p. 325-338.

Whitaker, M. L., Nekvasil, H., Lindsley, D. H., McCurry, M., 2008, Can crystallization of olivine tholeiite give rise to potassic rhyolites? – an experimental investigation: Bulletin of Volcanology, v. 70, p. 417-434.

Wilson, C. J. N., Blake, S., Charlier, B. L. A. and Sutton, A.N., 2006, The 26.5 ka Oruanui eruption, Taupo Volcano, New Zealand: development, characteristics and evacuation of a large rhyolitic magma body: J. of Petrology, v. 47, p. 35–69.

Xue, M and Allen, R. M., 2007, The fate of the Juan de Fuca plate: Implications for a Yellowstone plume head: Earth and Planetary Science Letters, v. 264, p. 266-276.

FIGURES:

Figure 1: Density model (west to east) for the HLP. Density model constrained by seismic refraction data from west to east of the HLP, Steens area, Owyhee Plateau and into westernmost southern Idaho. Modified slightly from Cox (2011).

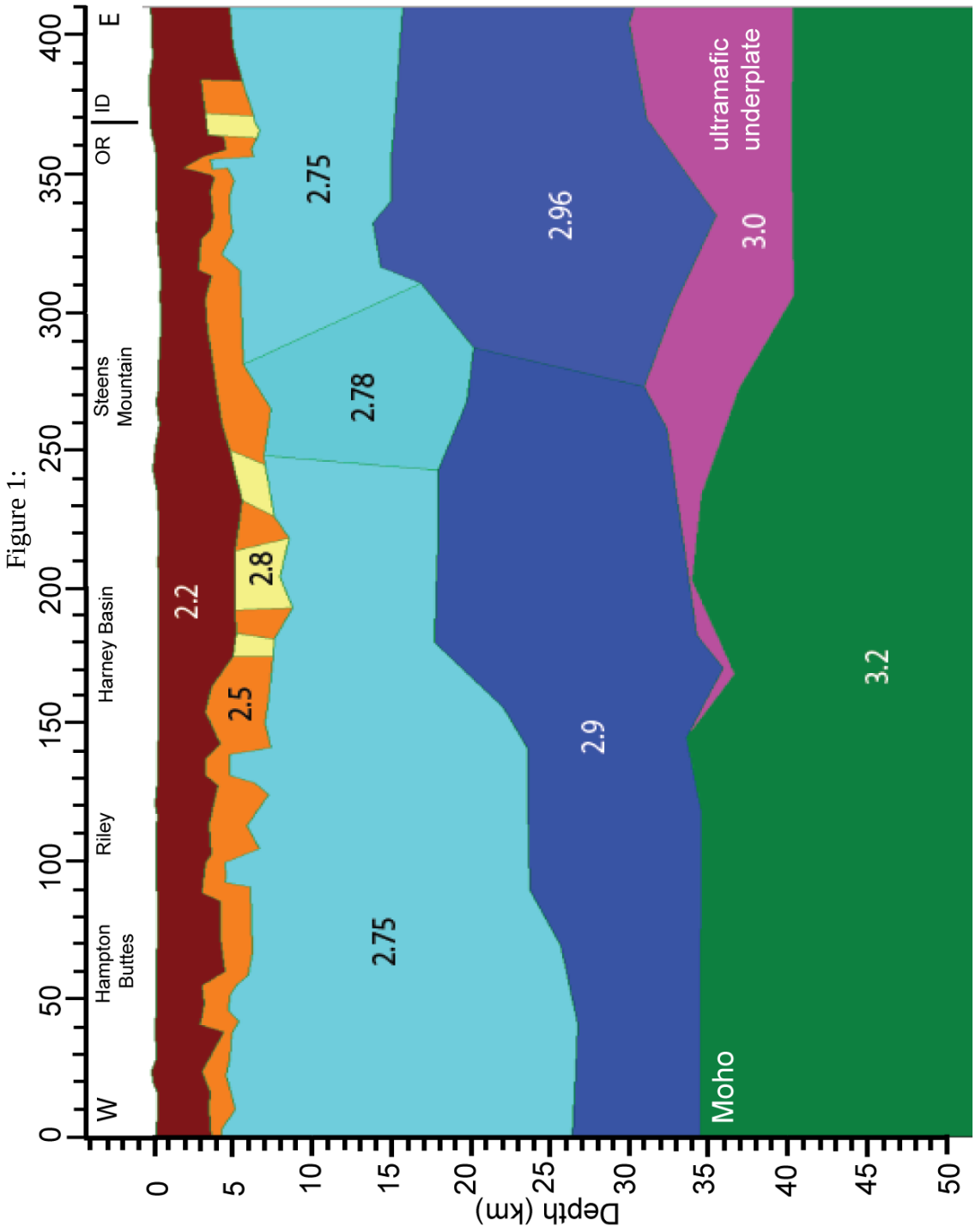
W
Hampton Buttes
Riley
Harney Basin
Steens Mountain
OR
ID
E
0
50
100
150
200
250
300
350
400
Depth (km)
0
5
10
15
20
25
30
35
40
45
50
2.2
2.5
2.8
2.75
2.78
2.75
2.9
2.96
3.0
3.2
ultramafic underplate
Moho

Figure 1:

Figure 2: Generalized petrogenetic cartoon model for the HLP. Model shows intraplated basaltic magmas in the lower crust, partial melting of lower crustal amphibolite or recently intraplated basaltic magmas to form low silica rhyolites and fractionation in upper crustal chambers to make high silica rhyolites. The model in the Harney Basin area shows a highly diagrammatized Rattlesnake Tuff formation. Small curved lines with arrows indicate assimilation of a few percent of crustal rocks to get more radiogenic $^{207}Pb/^{204}Pb$ or $^{87}Sr/^{86}Sr$ isotope ratios (see text for discussion). Intermediate rocks are mixes of basaltic andesite (or rarely basalt) and rhyolite. The crust – mantle boundary at ~ 35 km, the lower crust and upper to middle crust is separated by the dashed line and the upper crustal magma chambers are 5 to 8 km deep.

Figure 2:

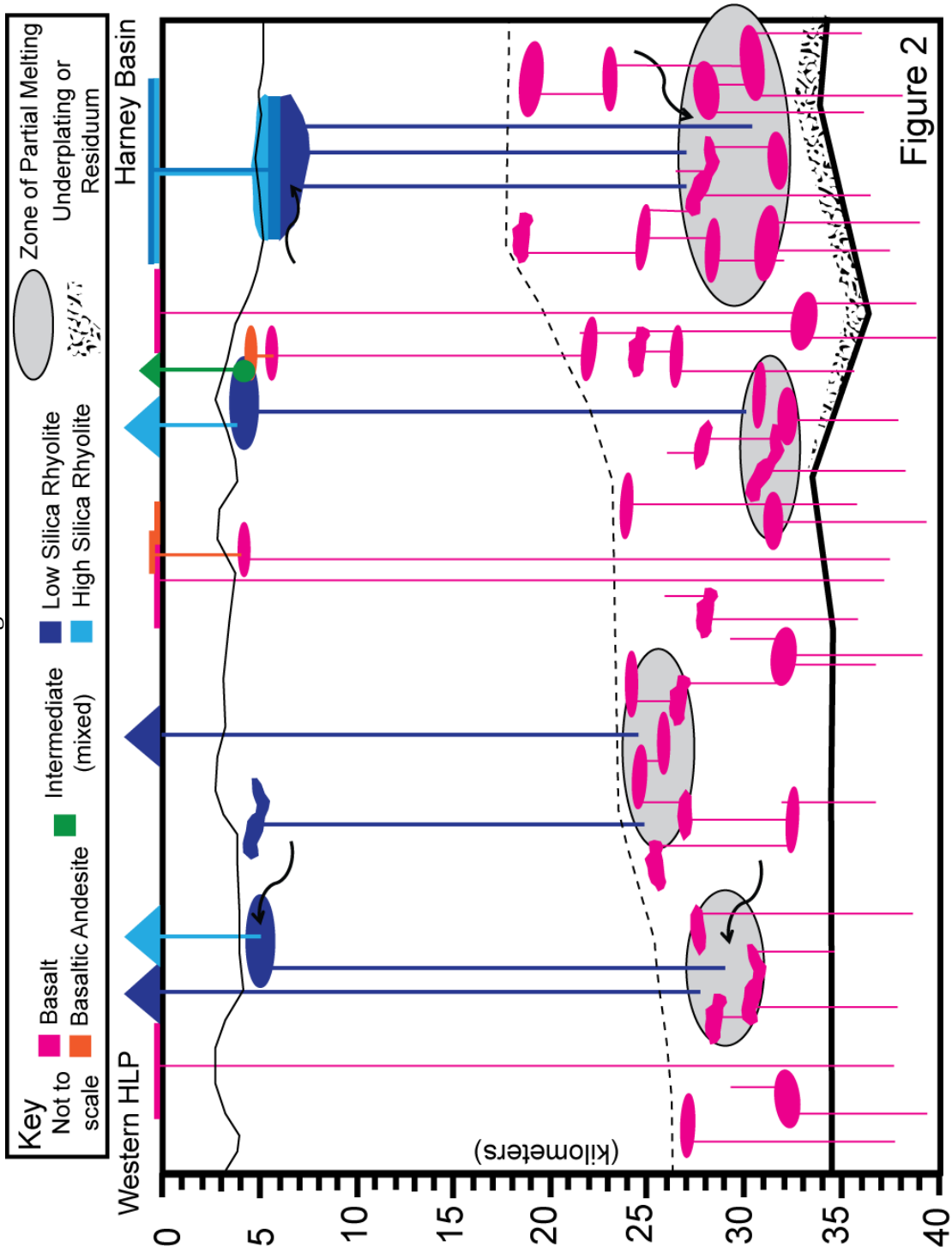
Key
Not to scale
Basalt
Basaltic Andesite
Intermediate (mixed)
Low Silica Rhyolite
High Silica Rhyolite
Zone of Partial Melting
Underplating or Residuum
Western HLP
Harney Basin
(kilometers)
0
5
10
15
20
25
30
35
40
Figure 2

Figure 3: Crustal evolution through time model for HLP development. Model shows modification of lower crust from intraplated basaltic magmas and partial melting (basaltification), thickening of the higher density lower crust though time, an increase in basaltic flux to create a hot zone that can produce partial melts, potential basinal sag in the upper crust and thickening of basin fill (2 – 5 km deep), slight deepening of the crust – mantle boundary as mass is transferred to the crust, emplacement of some basalts and low silica rhyolites in upper crustal chambers (5 – 8 km deep) where they can differentiate, progressive enrichment of FeO* at a given silica content in areas of prolonged activity, resumption of basaltic magmas being able to get to the surface after the hot zone cools, and development of unusual late-stage rhyolites in the HLP. See text for further discussion. Symbols are as in Figure 2.

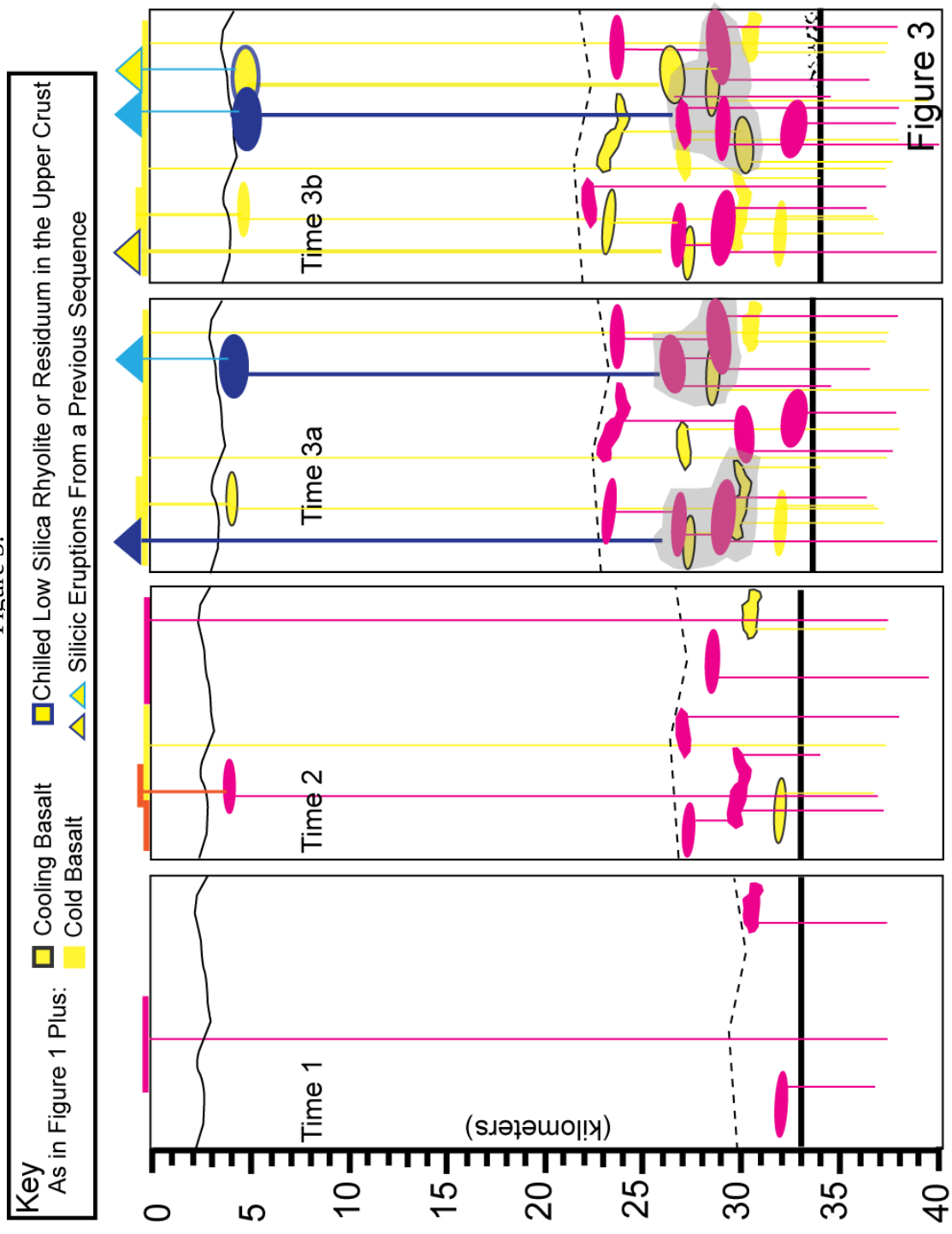
Key
As in Figure 1 Plus:
Cooling Basalt
Cold Basalt
Chilled Low Silica Rhyolite or Residuum in the Upper Crust
Silicic Eruptions From a Previous Sequence
Time 1
Time 2
Time 3a
Time 3b
(kilometers)
0
5
10
15
20
25
30
35
40
Figure 3

Figure 3:

Figure 3 continued:

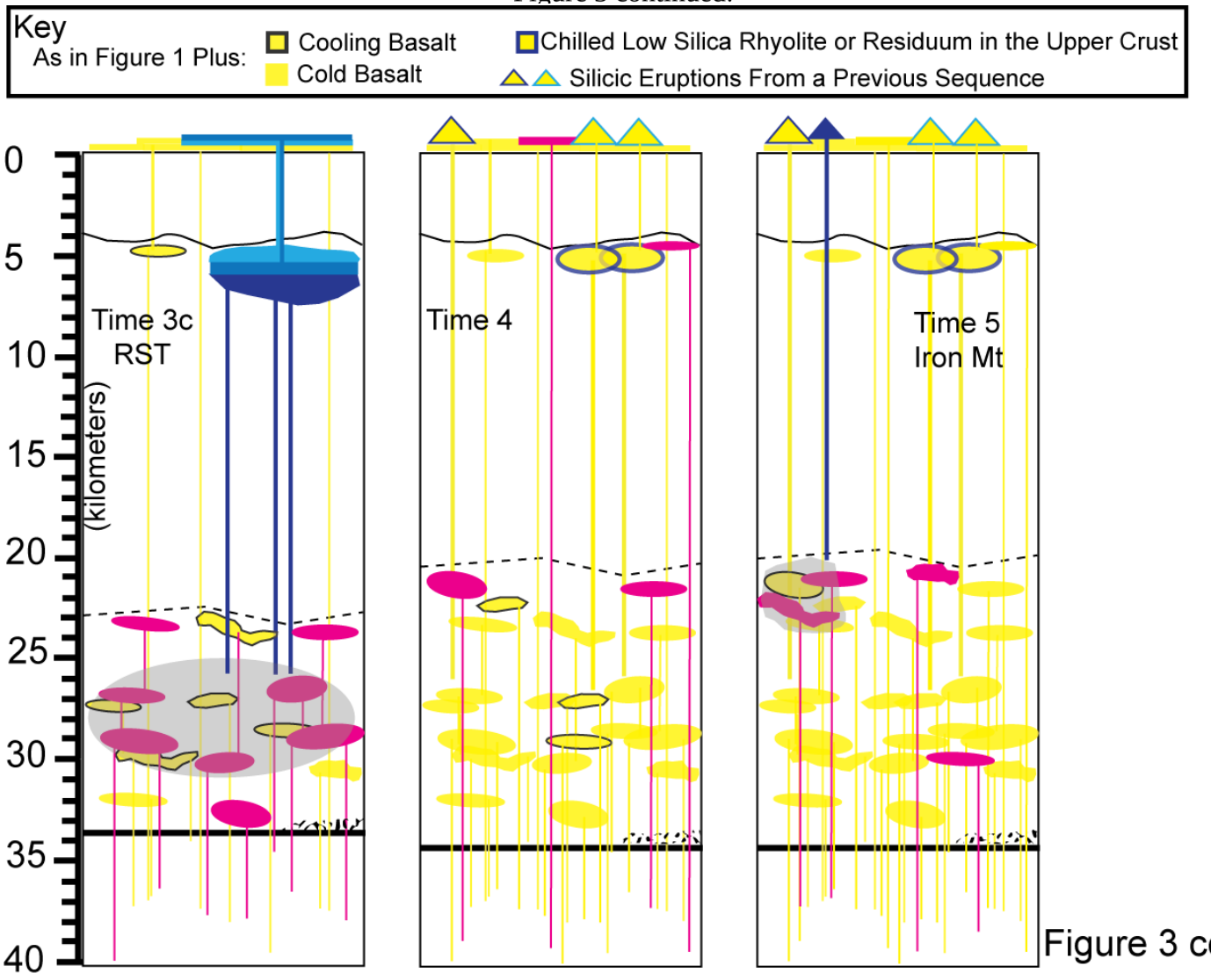

Figure 3 cont.

Figure 4: Generalized petrogenetic cartoon model for the NWBR. Model shows less intraplating of basaltic magmas into a lower crust that is not as dense as the HLP crust (Figure 5). Greater crustal extension allows basaltic magmas to traverse the crust effectively, but there is a lower basaltic flux than in the HLP. Pods of melts (shown vastly oversized), coupled with potential recharge, mixing and fractional crystallization create a "mini-MASH" zone where a continuum of composition can result. Formation of rhyolites may come from fractional crystallization of an intermediate melt (as shown), but some rhyolites might be formed by partial melting in the lower crust, as shown in the HLP model. Isotopes (Table 1) indicate that there is not much interaction with crust that has substantially different isotopic signature than the parental basalts. NV B & R is Basin and Range in Nevada, HB is the Harney Basin. Symbols are as in Figure 2.

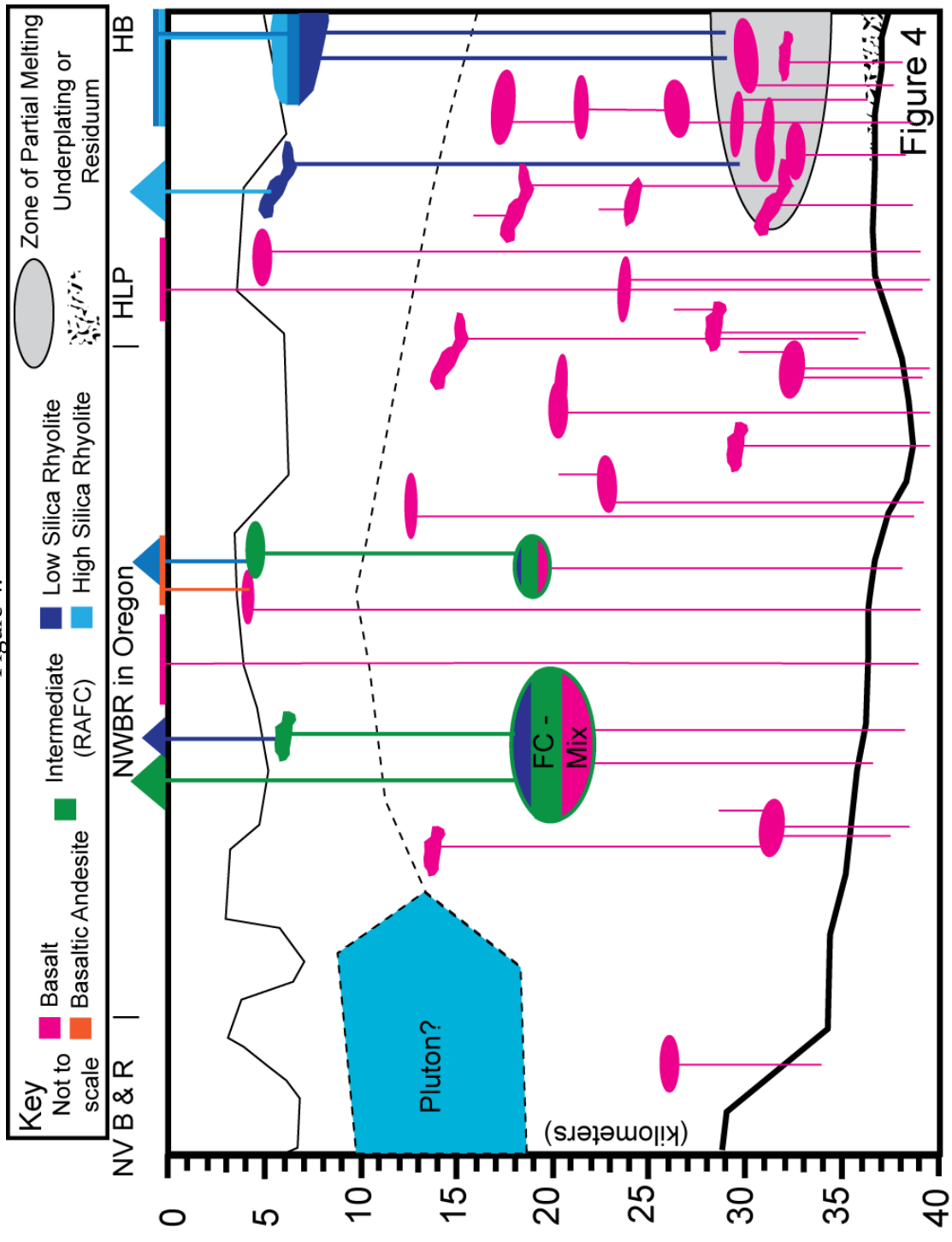
Key
Not to scale
Basalt
Basaltic Andesite
Intermediate (RAFC)
Low Silica Rhyolite
High Silica Rhyolite
Zone of Partial Melting
Underplating or Residuum
NV B & R
NWBR in Oregon
HLP
HB
Pluton?
FC - Mix
(kilometers)
0
5
10
15
20
25
30
35
40
Figure 4

Figure 4:

Figure 5: Density model (south to north) for the NWBR. Density model constrained by seismic refraction data from south to north of the Nevada Basin and Range, NWBR (in Oregon), the HLP and into the Blue Mountains. Modified slightly from Cox (2011).

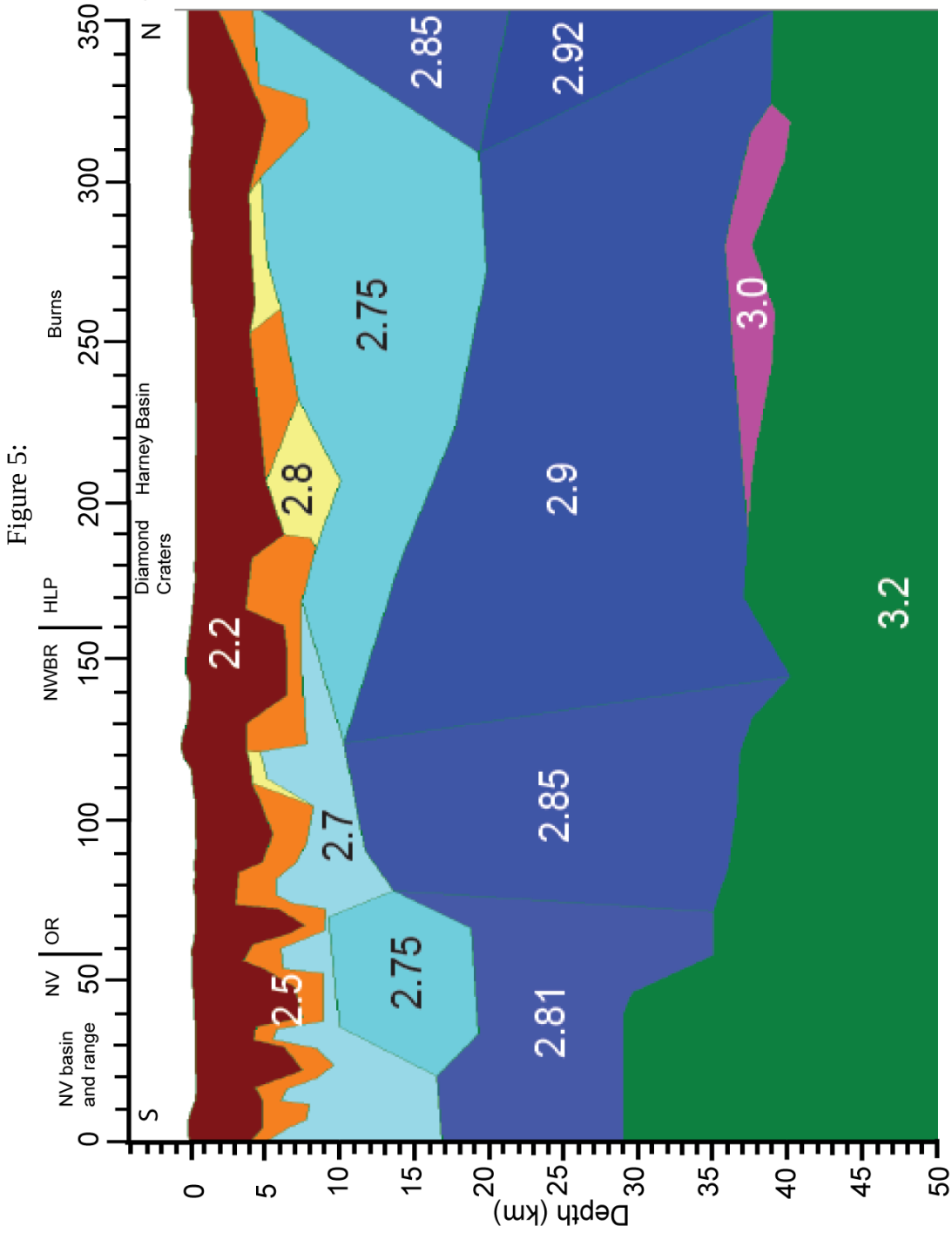
S
N
NV basin and range
NV
OR
NWBR
HLP
Burns
Diamond Craters
Harney Basin
0
50
100
150
200
250
300
350
Depth (km)
0
5
10
15
20
25
30
35
40
45
50
2.2
2.5
2.75
2.7
2.8
2.75
2.85
2.92
2.81
2.85
2.9
3.0
3.2

Figure 5:

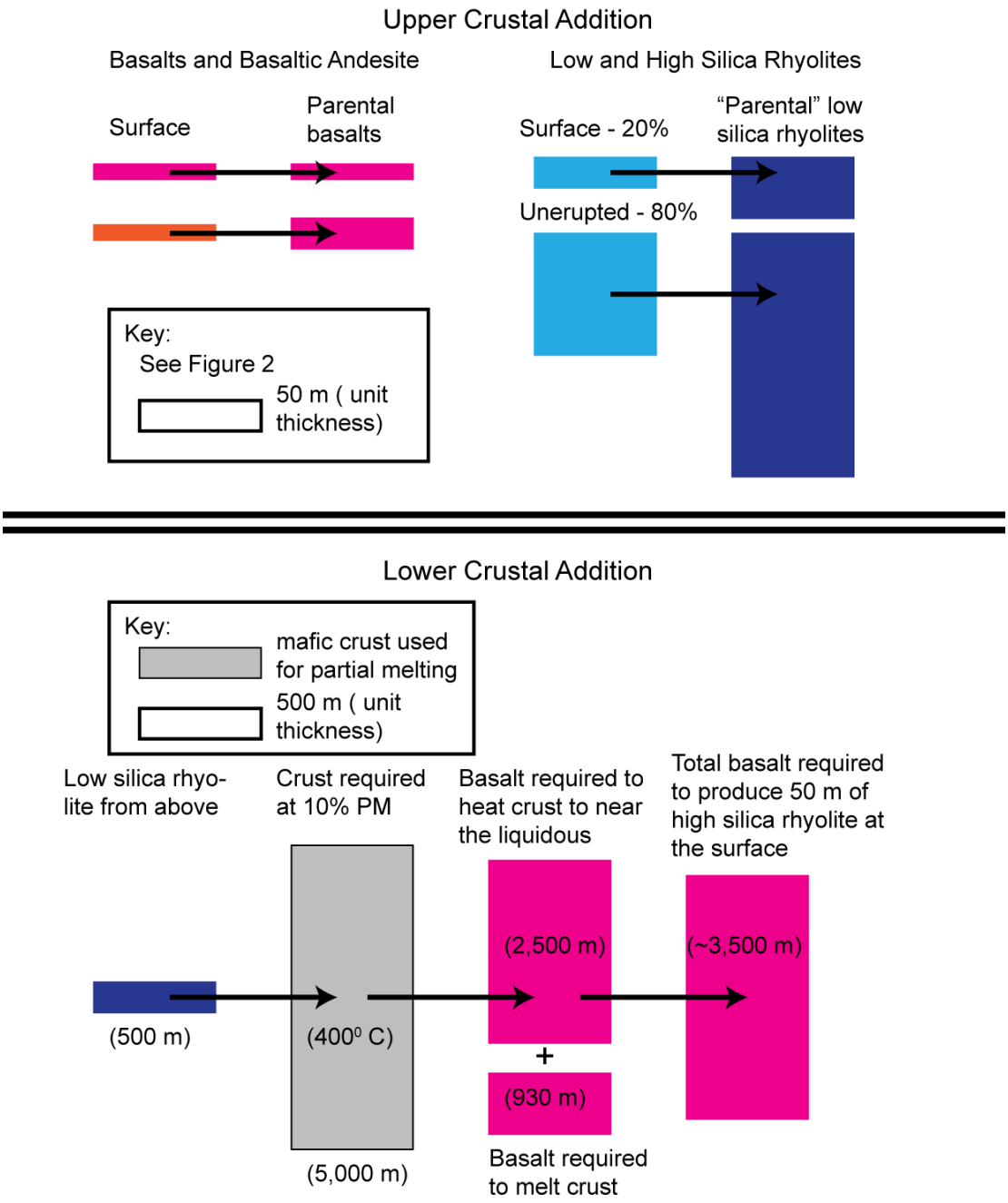

Figure 6: Schematic of required crustal addition calculation. Upper crustal addition includes 50 m of basalt and basaltic andesite (50% fractionation factor) and 50 m of erupted high silica rhyolite, 20% eruption factor and 50% fractionation factor to go from low to high silica rhyolites. Lower crustal addition shows the amount of basalt required to partially melt mafic crust to around 10% to produce low silica rhyolite, assuming that all melt is extracted. Colors are similar to those used in Figure 2. Note change in scale from upper crustal to lower crustal sections. See text for more details.

TABLES:

Table 1: Crustal factors in the HLP and NWBR. The table shows that there is a crustal signature in more HLP samples than in NWBR samples. Within the HLP, the high FeO* at a given silica rhyolites more often contain a crustal isotope signature than those with lower FeO* at a given silica. This could be indicative of more heat being added to the system, resulting in partial melts of crustal rocks in addition to remobilization of recently intraplated basaltic magmas. This would be more likely to happen in an area where basaltification is occurring or had occurred and the crust is more mafic, but also hotter.

	HLP	NWBR
Crustal signatures (Sr, Pb +/- meteoric water)	12	3
No observed crustal factors based on radiogenic isotopes	11	8
Meteoric water (low δ18O) signature only	3	2

Within the HLP:	High Fe/Si	Low Fe/Si	Total HLP
Crustal signatures (Sr, Pb +/- meteoric water)	10	2	12
No observed crustal factors based on radiogenic isotopes	5	6	11
Meteoric water (low δ18O) signature only	2	1	3

BIBLIOGRAPHY:

Allen, C. M and Barnes, C. G, 2006, Ages and some cryptic sources of Mesozoic plutonic rocks in the Klamath Mountains, California and Oregon, in Snoke, A. W. and Barnes, C. G., eds., Geological studies in the Klamath Mountains province, California and Oregon; a volume in honor of William P. Irwin: Geological Society of America Special Paper 410, p. 223-245.

Ambroz, J. A.,1997, Characterization of archaeologically significant obsidian sources in Oregon by neutron activation analysis: University of Missouri MS Thesis, 199 p.

Annen, C., Blundy, J. D. and Sparks, R. S. J., 2006, The genesis of intermediate and silicic magmas in deep crustal hot zones: J. of Petrology, v. 47, p. 505-539.

Asimow, P. D. and Ghiorso, M. S., 1998, Algorithmic Modifications Extending MELTS to Calculate Subsolidus Phase Relations: American Mineralogist, v. 83, p. 1127-1131.

Atwater, T and Stock, J, 1998, Pacific-North America plate tectonics of the southwestern United States, an update: International Geological Review, v. 40, p. 375-402.

Baertschi, P., 1976, Absolute 18O content of standard mean ocean water: Earth and Planetary Science Letters, v. 31, p. 341-344.

Bachmann, O., Miller, C. F. and de Silva, S. L., 2007, The volcanic–plutonic connection as a stage for understanding crustal magmatism: J. of Volcanology and Geothermal Research, v. 167, p. 1-23.

Bachmann, O. and Bergantz, G.W., 2004, On the origin of crystal-poor rhyolites: extracted from batholithic crystal mushes: J of Petrology v. 45, p. 1565–1582.

Bacon, C. R., Bruggman, P. E., Christiansen, R. L., Clynne, M. A., Donnelly-Nolan, J. M., and Hildreth, W., 1997, Primitive magmas at five Cascade volcanic fields; melts from hot, heterogeneous sub-arc mantle: Canadian Mineralogist, v. 35, no. 2, p. 397-423.

Bacon, C. R., Gunn, S. H., Lanphere, M. A and Wooden, J. L., 1994, Multiple isotopic components in Quaternary volcanic rocks of the Cascades Arc near Crater Lake, Oregon: J. of Petrology, v. 35, p. 1521-1556.

Bacon, C. R. and Druitt, T. H., 1988, Compositional evolution of the zoned calcalkaline magma chamber of Mount Mazama, Crater Lake, Oregon: Contributions to Mineralogy and Petrology, v. 98, p. 224-256.

Barnes, C. G., Petersen, S. W., Kistler, R. W., Prestvik, T. and Sundvoll, B., 1992, Tectonic implications of isotopic variation among Jurassic and Early Cretaceous plutons, Klamath Mountains: Geological Society of America Bulletin, v. 104, p. 117-126.

Barnes, C. G., Petersen, S. W., Kistler, R. W., Murray, R., Kays, M. A., 1996, Source and tectonic implications of tonalite-trondhjemite magmatism in the Klamath Mountains: Contributions to Mineralogy and Petrology, v. 123, p. 40-60.

Barnes, C. G., Mars, E. V., Swapp, S. and Frost, C. D., 2006A, Petrology and geochemistry of the Middle Jurassic Ironside Mountain Batholith; evolution of potassic magmas in a primitive arc setting, in Snoke, A. W. and Barnes, C. G., eds., Geological studies in the Klamath Mountains province, California and Oregon; a volume in honor of William P. Irwin: Geological Society of America Special Paper 410, p. 199-221.

Barnes, C. G., Snoke, A. W., Harper, G. D., Frost, C. D., McFadden, R. R., Bushey, J. C. and Barnes, M. A. W., 2006B, Arc plutonism following regional thrusting; petrology and geochemistry of syn- and post-Nevadan plutons in the Siskiyou Mountains, Klamath Mountains province, California, in Snoke, A. W. and Barnes, C. G., eds., Geological studies in the Klamath Mountains province, California and Oregon; a volume in honor of William P. Irwin: Geological Society of America Special Paper 410, p. 357-376.

Bailey, D. G. and Conrey, R. M., 1992, Common parent magma for Miocene to Holocene mafic volcanism in the northwestern United States: Geology, v. 20, p. 1131-1134.

Beard, J. S. and Lofgren, G. E., 1991, Dehydration melting and water-saturated melting of basaltic and andesitic greenstones and amphibolites at 1, 3, and 6.9 kb: J. of Petrology, v. 32, p. 365-401.

Beard, J. S., Abitz, R. J. and Lofgren, G. E., 1993, Experimental melting of crustal xenoliths from Kilbourne Hole, New Mexico and implications for the contamination and genesis of magmas: Contributions to Mineralogy and Petrology, v. 115, p. 88-102.

Beard, J. S., Lofgren, G. E., Sinha, A. K. and Tollo, R. P., 1994, Partial melting of apatite-bearing charnockite, granulite, and diorite: melt compositions, restite mineralogy, and petrologic implications: J. of Geophysical Research, v. 99, p. 21591-21603.

Berri, D. A., 1982, Geology and hydrothermal alteration of Glass Buttes, Southeast, Oregon: Portland State University MS Thesis, 125p.

Bestland, E. A. and Retallack, G. J., 1994, Geology and paleoenvironments of the Painted Hills Unit, John Day Fossil Beds National Monument, Oregon: U.S. National Park System, Open File Report, 211 p.

Bestland, E. A., and Retallack, G. J., 1994, Geology and paleoenvironments of the Clarno Unit, John Day Fossil Beds National Monument, Oregon: U.S. National Park System, Open File Report, 160 p.

Bindeman, I. N. and Valley, J. W., 2003, Rapid generation of both high- and low $\delta^{18}O$, large-volume silicic magmas at the Timber Mountain/Oasis Valley caldera complex, Nevada: GSA Bulletin, v. 115, p. 581-595.

Bindeman, I. N., Ponomareva, V. V., Bailey, J. C., Valley, J. W., 2004, Volcanic arc of Kamchatka: a province with high-delta O-18 magma sources and large-scale O-18/O-16 depletion of the upper crust: Geochimica et Cosmochimica Acta v. 68, p. 841-865.

Bindeman, I. N., Leonov, V. L., Izbekov, P. E., Ponomareva, V. V., Watts, K. E., Shipley, N. K., Perepelov, A. B., Bazanova, L.I., Jicha, B. R., Singer, B. S., Schmitt, A. K., Portnyagin, M. V. and Chen, C. H., 2010, Large-volume silicic volcanism in Kamchatka: Ar–Ar and U–Pb ages, isotopic, and geochemical characteristics of major pre-Holocene caldera-forming eruptions: J. Volcanology and Geothermal Research, v. 189, p. 57-80.

Bindeman, I., Gurenko, A., Sigmarsson, O. and Chaussidon, M., 2008, Oxygen isotope heterogeneity and disequilibria of olivine crystals in large volume Holocene basalts from Iceland: Evidence for magmatic diggestion and erosion of Pleistocene hyaloclastites: Geochimica et Cosmochimica Acta, v. 72, p. 4397-4420.

Bindeman, I., Watts, K. E., Schmitt, A. K., Morgan, L. A., and Shanks, P. W. C., 2007, Voluminous low $\delta^{18}O$ magmas in the late Miocene Heise volcanic field, Idaho: Implications for the fate of Yellowstone hotspot calderas: Geology, v. 35, p. 1019-1022.

Bindeman, I. N., Fu, B., Kita, N. T., Valley, J. W., 2008, Origin and evolution of silicic magmatism at Yellowstone based on ion microprobe analysis of isotopically zoned zircons: J. of Petrology, v. 49, p. 163-193.

Bohrson,W. A. and Spera, F. J., 2001, Energy-constrained open-system magmatic processes II: Application of energy-constrained assimilation-fractional crystallization (EC-AFC) model to magmatic systems: J. of Petrology, v.42, p. 1019-1041.

Bonnichsen, B., Leeman, W. P., Honjo, N., W. C., McIntosh, and Godchaux, M. M., 2008, Miocene silicic volcanism in southwestern Idaho: geochronology, geochemistry, and evolution of the central Snake River Plain: Bulletin of Volcanology, v. 70, no. 3, p. 315-342.

Boroughs, S. Wolff, J., Bonnichsen, B., Godchaux, M., Larson, P., 2005, Large volume, low $-\delta^{18}O$ rhyolites of the central Snake River Plain, Idaho, USA: Geology, v. 33, p. 821-824.

Bowen, G. J. and Revenaugh J., 2003, Interpolating the isotopic composition of modern meteoric precipitation: Water Resources Research, v. 39, 1299, 13 p.

Bowen, N.L., 1928, The evolution of igneous rocks: Dover, NewYork, 332 p.

Brikowski, T. H., 1983, Geology and petrology of Gearhart Mountain: A study of calc-alkaline volcanism east of the Cascades in Oregon: University of Oregon PhD thesis, 157 p.

Bromley, S. A., 2011, Evolution and inheritance of Cascadia sub-arc mantle reservoirs: Oregon State University MS Thesis, 192 p.

Brown, D. E., McLean, G. D. and Black, G. L., 1980, Preliminary geology and geothermal resource potential of the southern Harney Basin, Oregon: Oregon Department of Geology and Mineral Industries Open File Report O-80-07, 90 p.

Brueseke, M. E., Heizler, M. T., Hart, W. K. and Mertzman, S. A., 2007, Distribution and geochronology of Oregon Plateau (U.S.A.) flood basalt volcanism: The Steens Basalt revisited: J. of Volcanology and Geothermal Research, v. 161, p. 187-214.

Bullen, T. D. and Clynne, M. A., 1990, Trace element and isotopic constraints on magmatic evolution of the Lassen Volcanic Center: J. of Geophysical Research, v. 95, p. 19671-19691.

Burgette, R. J., Weldon, R. J. and Schmidt, D. A., 2009, Interseismic uplift rates for western Oregon and the along-strike variation in locking on the Cascadia subduction zone, J. of Geophysical Research, v. 114, B01408, p. 1 – 24.

Bushey, J. C., Snoke, A. W., Barnes, C. G. and Frost, C. D., 2006, Geology of the Bear Mountain intrusive complex, Klamath Mountains, California, in Snoke, A. W. and Barnes, C. G., eds., Geological studies in the Klamath Mountains province, California and Oregon; a volume in honor of William P. Irwin: Geological Society of America Special Paper 410, p. 287-315.

Camp, V. E. and Ross, M. E, 2004, Mantle dynamics and genesis of mafic magmatism in the intermontane Pacific Northwest, J. of Geophysical Research, v. 109, B08204, doi:10.1029/2003JB002838.

Camp, V. E., Ross, M. E. and Hanson, W. E., 2003, Genesis of flood basalts and Basin and Range volcanic rocks from Steens Mountain to the Malheur River Gorge, Oregon: Geological Society of America Bulletin, v. 115, p. 105-128.

Carlson, R. W., Hart, W. K. and Grove, T. L., 2009, Cenozoic basaltic volcanism in the Pacific Northwest: Geological Society of America Abstracts with Programs, v. 41, p. 571

Carlson, R. W. and Hart, W. K., 1988, Flood basalt volcanism in the Pacific Northwestern United States, in: Macdougall, J.D., ed., Continental Flood Basalts: Kluwer, Dordecht, p. 35-62.

Carlson, R. W., Czamanske, G., Fedorenko, V., and Ilupin, I., 2006, A comparison of Siberian meimechites and kimberlites: Implications for the source of high-Mg alkalic magmas and flood basalts: Geochemistry Geophysics Geosystems, v. 7, no. 11, Nov 21, 2006.

Carlson, R. W. and Hart, W. K., 1987, Crustal Genesis on the Oregon Plateau: J. of Geophysical Research, v. 92, p. 6191-6206.

Carlson, R. W., Lugmair, G.W., and Macdougall, J. D., 1981, Columbia River volcanism: the question of mantle heterogeneity or crustal contamination: Geochimica et Cosmochimica Acta, v. 45, p. 2483-2499.

Catchings, R. D. and Mooney, W. D., 1988, Crustal structure of east central Oregon: Relation between Newberry Volcano and regional crustal structure: J. of Geophysical Research, v. 93, p. 10081-10094.

Chappell, B. W. and White, A. J. R., 1974, Two contrasting granite types: Pacific Geology, v. 8, p. 173-174.

Chivas, A. R., Andrew, A. S., Sinha, A. K., and O'Neil J. R., 1982, Geochemistry of a Pliocene-Pleistocene ocean-arc pluton complex, Guadalcanal: Nature, v. 300, p. 139-143.

Christiansen, E. H. and McCurry, M., 2008, Contrasting origins of Cenozoic silicic volcanic rocks from the western Cordillera of the United States: Bulletin of Volcanology, v. 70, no. 3, p. 251-267.

Christiansen, R.L., and Yeats, R.L., 1992, Post-Laramide geology of the U.S. Cordillerian region: in Burchfiel, B.C., Lipman, P.W., and Zoback, M.L., eds., The Cordillerian Orogen: Conterminous U.S.: Boulder, CO, Geological Society of America, Geology of North America: v. G-3, p. 261–406.

Christiansen, R.L., 1993, The Yellowstone hot spot: Deep mantle plume or upper mantle melting anomaly?: EOS, Transactions of the American Geophysical Union, v. 76, p. 602.

Christiansen, R.L., Foulger, G.R., and Evans, J.R., 2002, Upper-mantle origin of the Yellowstone hotspot: Geological Society of America Bulletin, v. 114, p. 1245-1256.

Church, S. E., 1976, The Cascade Mountains revisited: A re-evaluation in light of new lead isotopic data: Earth and Planetary Science Letters, v. 29, p. 175-188.

Conrey,R. M., Hooper, P. R., Larson, P. B., Chesley, J. and Ruiz, J., 2001, Trace element and isotopic evidence for two types of crustal melting beneath a High Cascade volcanic center, Mt. Jefferson, Oregon: Contributions to Mineralogy and Petrology, v. 141, p. 710-732.

Conrey, R. M., Sherrod, D. R., Hooper, P. R. and Swanson, D. A., 1997, Diverse primitive magmas in the Cascade Arc, northern Oregon and southern Washington: Canadian Mineralogist, v. 35, no. 2, p. 367-496.

Cox, C., 2011, A Controlled- Source Seismic and Gravity Study of the High Lava Plains (HLP): University of Oklahoma MS Thesis, 110 p.

DeMets, C., Gordon, R. G., Argus, D. F. and Stein, S., 1994, Effect of recent revisions to the geomagnetic reversal time scale on estimate of current plate motions: Geophysical Research Letters, v. 21, no. 20, p. 2191-2194.

DePaolo, D. J., 1981, Trace element and isotopic effects of combined wallrock assimilation and fractional crystallization: Earth and Plaetary Science Letters, v. 53, p. 189-292.

de Silva, S. L. and Gosnold, W. D., 2007, Episodic construction of batholiths: Insights from the spatiotemporal development of an ignimbrite flare-up: J.of Volcanology and Geothermal Research, v. 167, p. 320-335.

Dicken, S. N., 1950, Oregon Geography: First Preliminary Edition: Ann Arbor, MI, Edwards Brothers, 104 p.

Donnelly-Nolan, J. M., 1998, Abrupt shift in $\delta^{18}O$ values at Medicine Lake Volcano (California, USA): Bulletin of Volcanology, v. 59, p. 529-536.

Donnelly-Nolan, J. M., Grove, T. L., Lanphere, M. A., Champion, D. E. and Ramsey, D. W., 2008, Eruptive history and tectonic setting of Medicine Lake Volcano, a large rear-arc volcano in the southern Cascades: J. of Volcanology and Geothermal Research, v. 177, p. 313-328.

Donnelly-Nolan, J. M., Champion, D. E., Miller, C. D., Grove, T. L. and Trimble, D. A, 1990, Post-11,000-year volcanism at Medicine Lake Volcano, Cascade Range, northern California: J. of Geothermal Research, v. 95, no. B12, p. 19693-19704.

Draper, D. S., 1991, Late Cenozoic bimodal magmatism in the northern Basin and Range Province of southeastern Oregon: J. of Volcanology and Geothermal Research, v. 47, p. 299-328.

Druken, K. A., Long, M. D. and Kincaid, C., 2011, Patterns in seismic anisotropy driven by rollback subduction beneath the High Lava Plains: Geophysical Research Letters, v. 38, L13310, p. 1-6.

Duncan, R. A. and Hogan, L. G., 1994, Radiometric dating of young MORB using the ^{40}Ar-^{39}Ar incremental heating method: Geophysical Reasearch Letters, v. 21, p. 1927-1930.

Duncan, R. A. and Keller, R. A., 2004, Radiometric ages for basement rocks from the Emperor Seamounts, ODP Leg 197: Geochemistry, Geophysics, Geosystems, v. 5, Q08L03.

Duncan, R. A., Hooper, P. R., Rehacek, J., Marsh, J. S. and Duncan, A. R., 1997, The timing and duration of the Karoo igneous event, southern Gondwana: J. of Geophysical Research, v. 102, p. 18127-18138.

Eiler, J. M., 2001, Oxygen isotope variations of basaltic lavas and upper mantle rocks, in Valley, J. W. and Cole, D. R., eds., Stable Isotope Geochemistry: Reviews in Mineralogy and Geochemistry, v. 43, p. 319-364.

Evans, S. H. and Brown, F. H., 1981, Summary of potassium/argon dating – 1981: Department of Energy, Division of Geothermal Energy ID-12079-45, 29 p.

Ewart, A. and Griffin, W. L., 1994, Application of proton-microprobe data to trace-element portioning in volcanic rocks: Chemical Geology, v. 117, p. 251-284.

Fenneman, N. M., 1916, Physiographic divisions of the United States: Annals of the Association of American Geographers, v. 6, p. 19-98.

Fiebelkorn, R. B., Walker, G. W., MacLeod, N. S., McKee, E. H., and Smith, J. G., 1983, Index to K-Ar determinations for the state of Oregon: Isochron Weast, no. 37, p. 3-60.

Fitton, J. G., James, D. and Leeman, W. P., 1991, Basaltic Magmatism associated with late Cenozoic extension in the western United States: Compositional variations in space and time: J. of Geophysical Research, v. 96, p. 13693-13711.

Ford, M. T., 2005, The petrogenesis of Quaternay rhyolite domes in the bimodal Blackfoot Volcanic Field, southeastern Idaho: Idaho State University MS thesis, 133p.

Ford, M. T., Carlson, R. W. and Grunder, A. L., 2009, Isotopic Compositional Changes Across Space, Time, and Bulk Rock Composition in the High Lava Plains and Northwestern Basin and Range, Oregon: Geological Society of America Abstracts with Programs, v. 41, p. 571.

Frey F.A., Coffin M.F., Wallace P.J., Weis D., Zhao X., Wise S.W., Jr., Wahnert V., Teagle D.A.H., Saccocia P.J., Reusch D.N., Pringle M.S., Nicolaysen K.E., Neal C.R., Müller D.R., Moore C.L., Mahoney J.J., Keszthelyi L., Inokuchi H., Duncan R.A., Delius H., Damuth J.E., Damasceno D., Coxall H.K., Borre M.K., Boehm F., Barling J., Arndt N.T. and Antretter M., 2000, Origin and Evolution of a Submarine Large Igneous Province: The Kerguelen Plateau and Broken Ridge, Southern Indian Ocean: Earth and Planetary Science Letters, v. 176, p. 73-89.

Frost, C. D., Barnes, C. G, and Snoke, A. W., 2006, Nd and Sr isotopic data from argillaceous rocks of the Galice Fromation and Rattlesnake Creek terrane, Klamath Mountains: Evidence for the input of Precambrian sources, in Snoke, A. W. and Barnes, C. G., eds., Geological studies in the Klamath Mountains province, California and Oregon; a volume in honor of William P. Irwin: Geological Society of America Special Paper 410, p. 103-120.

Frost, B. R., Barnes, C. G., Collins, W. J., Arculus, R. J., Ellis, D. J. and Frost C. D., 2001, A geochemical classification for granitic rocks: J. of Petrology, v. 42, p. 2033-2048.

Furman, T., Frey, F. A., Meyer, P. S., 1992, Petrogenesis of evolved basalts and rhyolites at Austurhorn, southeastern Iceland: the role of Fractional Crystallization: J. of Petrology, v. 33, p. 1405-1445.

Fyfe, W. S., 1993, Hot spots, magma underplating, and modification of continental crust: Canadian J. of Earth Sciences, v. 30, p. 908-913.

Geist, D., Howard, K. A. and Larson, P., 1995, The generation of oceanic rhyolites by crystal fractionation – The basalt-rhyolite association at Volcan Alcedo, Galapagos Archipelago: J. of Petrology, v. 36, p. 965-982.

Ghiorso, M. S. and Sack, R. O., 1995, Chemical Mass Transfer in Magmatic Processes IV: A Revised and Internally Consistent Thermodynamic Model for the Interpolation and Extrapolation of Liquid-Solid Equilibria in Magmatic Systems at Elevated Temperatures and Pressures: Contributions to Mineralogy and Petrology, v. 119, p. 197-212.

Goldstein, S. J. and Jacobsen, S. B., 1987, The Nd and Sr isotopic systematics of river-water dissolved material: implications for the sources of Nd and Sr in seawater: Chemical Geology, v. 66, p. 245-272.

Goldstein, S. J. and Jacobsen, S. B., 1988, Nd and Sr isotopic systematics of river water suspended material: implications for crustal evolution: Earth and Planetary Science Letters, v. 87, p. 249-265.

Graham, D. W., Reid, M. R., Jordan, B. T., Grunder, A. L., Leeman, W. P., and Lupton, J. E., 2009, Mantle source provinces beneath the Northwestern USA delimited by helium isotopes in young basalts: J. of Volcanology and Geothermal Research, v. 188, p. 128-140.

Green, R. C., 1973, Petrology of the welded tuff of Devine Canyon, southeastern Oregon: US Geological Survey Professional Paper 797, p. 1-26.

Gripp, A. E. and Gordon, R. G., 2002, Young tracks of hotspots and current plate velocities: Geophysics Journal International, v. 150, p. 321-361.

Grove, T. L., Donnelly-Nolan, J. M. and Housh, T., 1997, Magmatic processes that generated the rhyolite of Glass Mountain, Medicine Lake volcano, N. California: Contributions to Mineralogy and Petrology, v. 127, p. 205-223.

Grunder, A. L. and Meigs, A., 2009, Volcanic and structural setting of the High Lava Plains, an intracontinental transform zone in the northwestern USA: Geological Society of America Abstracts with Programs, Vol. 41, No. 7, p. 572.

Grunder, A. L., 1995, Material and thermal roles of basalt in crustal magmatism: Case study from eastern Nevada: Geology, v. 23, p. 952-956.

Guffanto, M., Clynne, M. A. and Muffler, L. J. P., 1996, Thermal and mass implications of magmatic evolution in the Lassen volcanic region, California, and minimum constraints on basalt influx to the lower crust: J. of Geophysical Research, v. 101, p. 3003-3013.

Guffanti, M. and Weaver, G. S., 1988), Distribution of Late Cenozoic volcanic vents in the Cascade Range: Volcanic arc segmentation and regional tectonic considerations: J. of Geophysical Research, v. 93, p. 6513 – 6529.

Gunnarsson, B., Marsh, B. D. and Taylor, H. P., 1998, Generation of Icelandic rhyolites: silicic lavas from the Torfajokull central volcano: J. of Volcanology and Geothermal Research, v. 83, p. 1-45

Hampton, E.R., 1964, Geologic factors that control the occurrence and availability of groundwater in the Fort Rock Basin, Lake County, Oregon: U.S. Geological Survey Professional Paper 383-B, p. B1-B29.

Hanan, B. B. and Graham, D. W., 1996, Lead and Helium isotope evidence from oceanic basalts for a common deep source of mantle plumes: Science, v. 272, p. 991-995.

Hanan, B. B., Shervais, J. W. and Vetter, S. K., 2008, Yellowstone plume-continental lithosphere interaction beneath the Snake River Plain: Geology, v. 36, p. 51-54.

Harmon, R. S. and Hoefs, J. 1995, Oxygen isotope heterogeneity of the mantle deduced from global ^{18}O systematics of basalts from different geotectonic settings: Contributions to Mineralogy and Petrology, v. 120, p. 95-114.

Harper, G. D., Bowman, J. R., and Kuhns, R., 1988, A field, chemical, and stable isotope study of subseafloor metamorphism of the Josephine Ophiolite, California - Oregon: J. of Geophysical Research, v. 93, p. 4625-4656.

Harper, G. D., Saleeby, J. B. and Heizler, M., 1994, Formation and emplacement of the Josephine ophiolite and the Nevadan orogeny in the Klamath Mountains, California-Oregon: U/Pb zircon and $^{40}Ar/^{39}Ar$ geochronology: J. of Geophysical Research, v. 99, issue B3, p. 4293-4321.

Harris, C., Smith, H. S. and le Roex, A. P., 2000, Oxygen isotope composition of phenocrysts from Tristan da Cunha and Gough Island lavas: Variation with fractional crystallization and evidence for assimilation: Contributions to Mineralogy and Petrology, v. 138, p. 164-175.

Hart, S. R., 1984a, The DUPAL anomaly: A large scale isotopic anomaly in the southern hemisphere: Nature, v. 309, p. 753-756.

Hart, W. K. and Mertzman, S. A., 1983, Late Cenozoic volcanic stratigraphy of the Jordan Valley area, southeastern Oregon: Oregon Geology (Ore Bin), v. 45, p. 15-19.

Hart, W. K., Aronson, J. L., and Mertzman, S. A., 1984, Areal distribution and age of low-K, high-alumina olivine tholeiite magma in the northwestern Great Basin: Geological Society of America Bulletin, v. 95, p. 186-195.

Hart, W. K., Carlson, R. W., and Shirey, S. B., 1997, Radiogenic Os in primitive basalts from the northwestern U. S. A.: Implications for petrogenesis: Earth and Planetary Science Letters, v. 150, p. 103-116.

Hart, W. K., 1985, Chemical and isotopic evidence for mixing between depleted and enriched mantle, northwestern USA: Geochimica et Cosmochimica Acta, v. 49, p. 131-144.

Heiken, G., 1978, Plinian-type eruptions in the Medicine Lake highland, California, and the nature of the underlying magma: J. of Volcanology and Geothermal Research, v. 4, p. 375-402.

Hegner, E. and Tatsumoto, M., 1987, Pb, Sr, and Nd isotopes in basalts and sulfides from the Juan de Fuca Ridge: J. of Geophysical Research, v. 92, p. 11380-11386.

Heller, P. L., Peterman, Z. E., O'Neil, J. R. and Shafiqullah, M., 1985, Isotopic province of sandstones from the Eocene Tyee Formation, Oregon Coast Range: Geological Society of America Bulletin, v. 96, p. 770-780.

Hering, C. W., 1981, Geology and petrology of the Yamsay Mountain Complex, south-central Oregon: A study of bimodal volcanism: University of Oregon PhD thesis, 189 p.

Higgins, M. W., 1973, Petrology of Newberry Volcano, central Oregon: Geological Society of America Bulletin, v. 84, no. 2, p. 455-488.

Hildreth, W., 1981, Gradients in silicic magma chambers: Implications for lithospheric magmatism: J. of Geophysical Research, v. 86, is. B11, p. 153-192.

Hildreth, W., 2007, Quaternary magmatism in the Cascades – geologic perspectives: US Geological Survey Professional Paper 1744, 125 p.

Hildreth, W., and Moorbath, S., 1988, Crustal contributions to arc magmatism in the Andes of central Chile: Contributions to Mineralogy and Petrology, v. 98, p. 455-489.

Hildreth, W., and Moorbath, S., 1991, Reply to comment on "Crustal contributions to arc magmatism in the Andes of central Chile" by W. Hildreth and S. Moorbath: Contributions to Mineralogy and Petrology, v. 108, p. 247-252.

Hoefs, J., 2009, Stable isotope geochemistry: Springer-Verlag, Berlin, Germany, 288p.

Hooper, P. R., Binger, G. B. and Lees, K. R., 2002, Ages of the Steens and Columbia River flood basalts and their relationship to extension-related calc-alkalic volcanism in eastern Oregon: Geological Society of America Bulletin, v. 114, p. 43-50.

Hooper, P.R. and Hawkesworth, C.J., 1993, Isotopic and geochemical constraints on the origin and evolution of the Columbia River basalt: J. of Petrology, v. 34, p. 1203-1246.

Hughes, S. S. and Taylor, E. M., 1986, Geochemistry, petrogenesis, and tectonic implications of central High Cascade mafic platform lavas, Geological Society of America Bulletin, v. 97, p. 1024-1036

Hughes, S. S., McCurry, M. and Geist, D. J., 2002, Geochemical correlations and implications for the magmatic evolution of basalt flow groups at the Idaho National Engineering and Environmental Laboratory, in Link, P. K. and Mink, L. L., eds., Geology, Hydrogeology, and Environmental Remediation: Idaho National Engineering and Environmental Laboratory, Eastern Snake River Plain, Idaho: Geological Society of America Special Paper 353, p. 151-173.

Humphreys, E. D., Dueker, K. G., Schutt, D. L. and Smith, R. B., 2000, Beneath Yellowstone: Evaluating plume and nonplume models using teleseismic data: GSA Today, v. 10, p. 1-7.

Huppert, H. E. and Sparks, R. S. J., 1988, The generation of granitic magmas by intrusion of basalt into continental crust: J. of Petrology, v. 29, p. 599 – 634.

Iademarco, M. J., 2009, Volcanism and faulting along the northern margin of Oregon's High Lava Plains: Hampton Butte to Dry Mountain: Oregon State University MS thesis, 141 p.

Irwin, W. P. and Wooden, J. L., 1999, Plutons and accretionary episodes of the Klamath Mountains, California and Oregon: U. S. Geological Survey Open File Report 99-374, 1 sheet.

Ito, E., White, W. M. and Gopel, C., 1987, The O, Sr, Nd and Pb isotope geochemistry of MORB: Chemical Geology, v. 62, p. 157-176.

Jackson, M. D., Cheadle, M. J. and Atherton, M. P., 2003, Quantitative modeling of granitic melt generation and segregation in the continental crust: J. of Geophysical Research, v. 108, no. 2332. DOI: 10.1029/2001JB001050

Jakobsson, S. P., Jonasson, K., Sigurdsson, I. A., 2008, The three igneous rock series of Iceland: Jokull, v. 58, p. 117-138.

Jensen, R. A., 2006, Roadside guide to the geology and history of Newberry Volcano, 4th ed., CenOreGeoPub, Bend, OR, 182 p.

Jensen, R. A., Donnelly-Nolan, J. M. and Mckay, D., 2009, A field guide to Newberry Volcano, Oregon. In O'Connor, J. E., Dorsey, R. J. and Madin, I. P., eds., Volcanoes to Vineyards: Geologic Field Trips Through the Dynamic Landscape of the Pacific Northwest: Geological Society of America Field Guide 15, p. 53-79.

Jicha, B. R., Hart, G. L., Johnson, C. M., Hildreth, W., Beard, B. L., Shirey, S. B. and Valley, J. W., 2009, Isotopic and trace element constraints on the petrogenesis of lavas from the Mount Adams volcanic field, Washington: Contributions to Mineralogy and Petrology, v. 157, p. 189-207.

Johnson, D. M., Hooper, P. R. and Conrey, R. M., 1999, XRF analysis of rocks and minerals for major and trace elements on a single low dilution Li-tetraborate fused bead: Advances in X-ray analysis, v. 41, p. 843-867.

Johnson, J. A., 1995, Geologic evolution of the Duck Creek Butte eruptive center, High Lava Plains, southeastern Oregon: Oregon State University MS thesis, 151 p.

Johnson, J. A., 1998, Geologic map of the Frederick Butte volcanic center, Deschutes and Lake counties, south-central Oregon: USGS Open File Report 98-208, scale 1:40,000.

Johnson, J. A., and Grunder, A. L., 2000, The making of intermediate composition magma in a bimodal suite: Duck Butte Eruptive Center, Oregon, USA: J. of Volcanology and Geothermal Research, v. 95, p. 175-195.

Johnson, K. E., and Ciancanelli, E. V., 1984, Geothermal exploration at Glass Buttes, Oregon: Oregon Geology, v. 46, p. 15-20.

Johnson, M. J., 1984, Geology, alteration, and mineralization of a silicic volcanic center, Glass Buttes, Oregon: Portland State University MS thesis, 129 p.

Jonasson, K., 2007, Silicic volcanism in Iceland: Composition and distribution within the active volcanic zones: J. of Geodynamics, v. 43, p. 101-117.

Jonasson, K., 2005, Magmatic evolution of the Heidarsporour Ridge, NE-Iceland: J. of Volcanology and Geothermal Research, v. 147, p. 109-124.

Jonasson, K., 1994, Rhyolite volcanism in the Krafla central volcano, north-east Iceland: Bulletin of Volcanology, v. 56, p. 516-528.

Jordan, B. T., 2001, Basaltic volcanism and tectonics of the High Lava Plains, southeastern Oregon: Oregon State University PhD thesis, 218p.

Jordan, B. T., Streck, M. J. and Grunder, A. L., 2002, Bimodal volcanism and tectonism of the High Lava Plains, Oregon in Moore, G. W., ed., Field Guide to Geologic Processes in Cascadia: Oregon Department of Geology and Mineral Industries Special Paper 36, p. 23-46.

Jordan, B. T., Grunder, A. L., Duncan, R. A., and Deino, A. L., 2004, Geochronology of age-progressive volcanism of the Oregon High Lava Plains: Implications for the plume interpretation of Yellowstone: J of Geophysical Research, v. 109, issue B10, p. 1-19.

Kinzler, R. J., Donnelly-Nolan, J. M. and Grove, T. L., 2000, Late Holocene hydrous mafic magmatism at the Paint Pot Crater and Callahan flow, Medicine Lake Volcano, N. California and the influence of H2O in the generation of silicic magmas: Contributions to Mineralogy and Petrology, v. 138, p. 1-16.

Kistler, R. W. and Peterson, Z. E., 1978, Reconstruction of crustal blocks of California on the basis of initial strontium isotopic compositions of Mesozoic granitic rocks: USGS Professional Paper 1071, 17 p.

Knaack, C., Cornelius, S. B., and Hooper, P. R., 1994, Trace element analyses of rocks and minerals by ICP-MS: Washington State University, open file report, www.wsu.edu/~geolab/note/icpms.html, checked 6/30/09.

Koppers, A. A. P., 2002, ArArCalc – software for $^{40}Ar/^{39}Ar$ age calculations: Computers and Geosciences, v.28, p. 605-619.

Kuntz, M. A., Covington, H. R., and Schorr, L. J., 1992, An overview of basaltic volcanism of the eastern Snake River Plain, Idaho. In Link, P. K., Kuntz, M. A., and Platt, L. eds., Regional Geology of eastern Idaho and western Wyoming: Geological Society of America Memoir 179, p. 227-267.

Lacasse, C., Sigurdsson, H., Carey, S. N., Jóhannesson, H., Thomas, L. E., Rogers, N. W., 2007, Bimodal volcanism at the Katla subglacial caldera, Iceland: insight into the geochemistry and petrogenesis of rhyolitic magmas: Bulletin of Volcanology, v. 69, p. 373-399.

Langmuir, C. H., Klein, E. M. and Plank, T., 1992, Petrological Systematics of Mid-Ocean Ridge Basalts: Constraints on Melt Generation Beneath Ocean Ridges: AGU Monograph, v. 71, p. 183-280.

Larson, E. E., 1965, The structure, stratigraphy, and paleomagnetics of the Plush area, southeastern Lake County, Oregon: University of Colorado PhD thesis, 166 p.

Lawrence, R. O., 1976, Strike-slip faulting terminates the Basin and Range province in Oregon: Geological Society of America Bulletin, v. 87, p. 846-850.

Le Bas, M. J., Le Maitre, R. W. and Woolley, A. R., 1992, The construction of the Total Alkali-Silica chemical classification of volcanic rocks: J. of Mineralogy and Petrology, v. 46, No. 1, p. 1-22..

Lee, C. –T. A., Morton, D. M., Kistler, R. W. and Baird, A. K., 2007, Petrology and tectonics of Phanerozoic continent formation: From island arcs to accretion and continental arc magmatism: Earth and Planetary Science Letters, v. 263, p. 370-387.

Leeman, W. P., 1982, Olivine Tholeiites of the Snake River Plain, Idaho, in Bonnichsen, W and Brekenridge, R. M., eds., Cenozoic Geology of Idaho: Bureau of Mines and Geology Bulletin 26, p. 181-191.

Leeman, W. P., 1982, Tectonic and magmatic significance of strontium isotope variations in Cenozoic volcanic rocks from the western United States: Geological Society of America Bulletin, v. 93, p. 487-503.

Leeman, W. P., 1982, Rhyolites of the Snake River Plain – Yellowstone Plateau province, Idaho and Wyoming: A summary of petrogenetic models, in Bonnichsen, W and Brekenridge, R. M., eds., Cenozoic Geology of Idaho: Bureau of Mines and Geology Bulletin 26, p. 203-212.

Leeman, W. P., Menzies, M. A., Matty, D. J., and Embree, G. F., 1985, Strontium, neodymium and lead isotopic compositions of deep crustal xenoliths from the Snake River Plain: evidence for Archean basement: Earth and Planetary Science Letters, v. 75, p. 354-368.

Leeman, W. P., Smith, D. R., Hildreth, W., Palacz, Z. and Rogers, N., 1990, Compositional diversity of late Cenozoic basalts in a transect across the southern Washington Cascades: Implications for subduction zone magmatism: J. of Geophysical Research, v. 95, p. 19561-19582.

Leeman, W. P., Annen,C., Dufek, J., 2008, Snake River Plain-Yellowstone silicic volcanism: implications for magma genesis and magma fluxes: Geological Society of London Special Publication, v. 304, p. 235-259.

Lindsley-Griffin, N., Griffin, J. R., Farmer, J. D., Sivers, E. A., Bruckno, B. and Tozer, M. K., 2006, Ediacaran cyclomedusoids and the paleogeographic setting of the Neoproterozoic-early Paleozoic Yreka and Trinity Terranes, eastern Klamath Mountains, California, in Snoke, A. W. and Barnes, C. G., eds., Geological studies in the Klamath Mountains province, California and Oregon; a volume in honor of William P. Irwin: Geological Society of America Special Paper 410, p. 411-431.

Linneman, S. R., 1990, The petrologic evolution of the Holocene magmatic system of Newberry volcano, central Oregon: University of Wyoming PhD thesis, 293 p.

Lipman, P. W., 1965, Chemical comparison of glassy and crystalline volcanic rocks: U.S. Geological Survey Bulletin 1201-D, p. D1-D24.

Loiselle, M. C. and Wones, D. R., 1979, Characteristics and origin of anorogenic granites: Geological Society of America Abstracts with Programs, v. 11, p. 468.

Long, M. D., Gao, H., Klaus, A., Wagner, L. S., Fouch, M. J., James, D. E., and Humphreys, E., 2009, Shear wave splitting and the pattern of mantle flow beneath eastern Oregon: Earth and Planetary Science Letters, v. 288, p. 359-369.

Luedke, R. G. and Smith, R. L., 1984, Map showing distribution, composition, and age of late Cenozoic volcanic centers in the western conterminous United States: US Geological Survey Miscellaneous Investigations Map I-1523, scale 1:2,500,000.

Lundstrom, C., 2009, Hypothesis for the origin of convergent margin granitoids and Earth's continental crust by thermal migration zone refining: Geochemica et Cosmochemica Acta, v. 73, p. 5709-5729.

MacDonald, R., 1974, Nomenclature and petrochemistry of the peralkaline oversaturated extrusive rocks: Bulletin of Volcanology, v. 38, p. 498-516.

MacLean, J. W., 1994, Geology and geochemistry of Juniper Ridge, Horsehead Mountain and Burns Butte: implications for the petrogenesis of silicic magma on the High Lava Plains, southeastern Oregon: Oregon State University MS Thesis, 141 p.

MacLeod, N. S., Walker, G. W. and McKee, E. H., 1976, Geothermal significance of eastward increase in age of upper Cenozoic rhyolitic domes in southeastern Oregon, Second United Symposium on the development and use of geothermal resources, Proceedings v. 1, p. 465-474.

MacLeod, N. S., Sherrod, D. R., Chitwood, L. A. and Jensen, R. A., 1995, Geologic Map of Newberry Volcano, Deschutes, Klamath, and Lake Counties, Oregon: USGS Miscellaneous Investigations Series Map I-2455, scale 1:62,500 and 1:24,00.

Martin, E. and Sigmarsson O., 2007, Crustal thermal state and origin of silicic magma in Iceland: the case of Torfajokull, Ljosufjoll and Snaefellsjokull volcanoes: Contributions to Mineralogy and Petrology, v. 153, p. 593-605.

Martin, E., Martin, H. and Sigmarsson, O., 2008, Could Iceland be a modern analogue for the Earth's early continental crust?: Terra Nova, v. 20, p. 463-468.

Mathis, A. C., 1993, Geology and petrology of a 26-Ma trachybasalt to peralkaline rhyolite suite exposed at Hart Mountain, Oregon: Oregon State University MS thesis, 141 p.

McBirney, A. R., 1978, Volcanic evolutions of the Cascade Range: Annual Review of Earth and Planetary Sciences, v. 6, p. 437-456.

McClaughry, J. D., Ferns, M. L., Gordon, C. L. and Patridge, K. A., 2009, Field trip guide to the Oligocene Crooked River caldera: Central Oregon's Supervolcano, Crook, Deschutes, and Jefferson Counties, Oregon: Oregon Geology, v. 69, p. 25-44.

McCurry, M. and Rodgers, D. W., 2009, Mass transfer along the Yellowstone hotspot track 1: Petrologic constraints on the volume of mantle-derived magma: J. of Volcanology and Geothermal Research, v. 188, p. 86-98.

McCurry, M., Hackett, W. R. and Hayden, K. P., 1999, Cedar Butte and cogenetic quaternary rhyolite domes of the eastern Snake River Plain, Idaho, in Hughes, S. S. and Thackray, G. D., eds., Guidebook to the Geology of Eastern Idaho: Idaho Museum of Natural History, p. 169-179.

McCurry, M., Hayden, K. P., Morse, L. H. and Mertzman, S., 2008, Genesis of post-hotspot, A-type rhyolite of the Eastern Snake River Plain volcanic filed by extreme fractional crystallization of olivine tholeiite: Bulletin of Volcanology, v. 70, p. 361-383.

McKee, E. H. and Walker, G. W., 1976, Potassium-argon ages of late Cenozoic silicic volcanic rocks, southeastern Oregon: Isochron West, v. 15, p. 37-41.

McKenzie, D. and Bickle, M. J., 1988, The volume and composition of melt generated by extension of the lithosphere: J. of Petrology, v. 29, p. 625-679

McQuarrie, N. and Rodgers, D. W., 1998, Subsidence of a volcanic basin by flexure and lower crustal flow: The eastern Snake River Plain, Idaho: Tectonics, v. 17, no. 2, p. 203-220.

Meigs, A., Scarberry, K., Grunder, A., Carlson, R., Ford, M. T., Fouch, M., Grove, T., Hart, W. K., Iademarco, M., Jordan, B., Milliard, J., Streck, M., Trench, D. and Weldon, R., 2009, Geological and geophysical perspectives on the magmatic and tectonic development, High Lava Plains and northwest Basin and Range, in O'Connor, J.E., Dorsey, R.J. and Madin, I.P., eds., Volcanoes to Vineyards: Geologic Field Trips through the Dynamic Landscape of the Pacific Northwest: Geological Society of America Field Guide 15, p. 435-470.

Miller, C. F., 1985, Are strongly peraluminous magmas derived from pelitic sedimentary sources?: J. of Geology, v. 93, p. 673-689.

Milliard, J., 2010, Two-stage opening of the northwestern Basin and Range in eastern Oregon: Oregon State University MS thesis, **81** p.

Min, K., Mundil, R., Renne, P. R and Ludwig, K. R., 2000, A test for systematic errors in $^{40}Ar/^{39}Ar$ geochronology through comparison with U/Pb analysis of a 1.1-Ga rhyolite: Geochimica et Cosmochimica Acta, v. 64, p. 73-98.

Miyashiro, A., 1974, Volcanic rock series in island arcs and active continental margins: American J. of Science, v. 274, p. 321-355.

Muehlenbachs, K. and Byerly, G., 1982, 18O enrichment of silicic magmas caused by crystal fractionation at the Galapagos spreading center: Contributions to Mineralogy and Petrology, v.79, p. 76-79.

Nakai, S., Halliday, A. N., and Rea, D. K., 1993, Provenance of dust in the Pacific Ocean: Earth and Planetary Science Letters, v. 119, p. 143-157.

Naoum, S. and Tsanis, I. K., 2004, Ranking spatial interpolation techniques using a GIS-based DSS: Global Nest: The International Journal, v. 6, p. 1-20.

Nekvasil, H., Simon, A., and Lindsley, D. H., 2000, Crystal fractionation and the evolution of intra-plate hy-normative igneous suites: Insights from their feldspars: J. of Petrology, v. 41, p. 1743-1757.

Newton, V. C., Corcoran, R. E. and Deacon, R. J., 1962, Oregon, still without oil, offers favorable pay areas, in Petroleum Exploration in Oregon: Oregon Department of Geology and Mineral Industries Miscellaneous Paper No. 9, p. 1-5.

Noble, D. C. and Parker, D. F., 1974, Peralkaline silicic volcanic rocks of the western United States: Bulletin of Volcanology, v. 38, p. 803-827.

O'Brien, P. A., Irving, A. J., McCallum, I. S., and Thirlwall, M. F., 1995, Strontium, neodymium, and lead isotope evidence for the interaction of post-subduction asthenospheric potassic mafic magmas of the Highwood Mountains, Montana, USA, with ancient Wyoming craton lithospheric mantle: Geochimica et Cosmochimica Acta, v. 59, p. 4539-4556.

Otto, B. R. and Hutchison, D. A., 1977, The geology of Jordan Craters, Malheur County, Oregon: The Ore Bin, v. 39, p. 125-140.

Paquette, J., Sigmarsson, O. and Tiepolo, M., 2006, Continental basement under Iceland revealed by old zircons: EOS transactions, American Geophysical Union, v. 52 abstract # V33A-0642.

Parman, S. W and Grove, T. L., 2004, Harzburgite melting with and without H2O: Experimental data and predictive modeling: J. of Geophysical Research, v. 109, is. B2, article number B02201.

Pearce, J. A., 1982, Trace element characteristics of lavas from destructive plate boundaries, in Thorpe, R.S., ed., Andesites: Orogenic andesites and related rocks: Chichester, England, John Wiley and Sons, p. 525-548.

Pearce, J. A. and Parkinson, I. J., 1993, Trace element models for mantle melting: application to volcanic arc petrogenesis, in Prichard, H. M., Alabaster, T., Harris, N. B. W. and Neary, C. R., eds, Magmatic Processes and Plate Tectonics: Special Publication of the Geological Society of London, v. 76, p. 373-403.

Peccerillo, A., Barberio, M. R., Yirgu, G., Ayalew, D., Barberi, M. and Wu, T. W., 2003, Relationships between mafic and acid peralkaline magmatism in continental rift settings: a petrological, geochemical and isotopic study of the Gedemsa volcano, central Ethiopian Rift: J. of Petrology v. 44, p. 2003–2032

Peng, X, and Humphreys, E. D., 1998, Crustal velocity structure across the eastern Snake River Plain and the Yellowstone swell: J. of Geophysical Research, v. 103, p. 7171-7186.

Peterson, N. V., 1959, Preliminary geology of the Lakeview Uranium Area, Oregon: The Ore Bin, v 21, p 11-16.

Pezzopane, S. K. and Weldon, R. J., 1993, Tectonic role of active faulting in central Oregon: Tectonics, v. 12, p. 1140 – 1169.

Pierce, K. L. and Morgan, L. A., 1992, The track of the Yellowstone hotspot: Volcanism, faulting and uplift, in Link, P. K, Kuntz, M. A. and Platt, L. B., eds., Regional Geology of Eastern Idaho and Western Wyoming: Geological Society of America Memoir 179, p. 1-53.

Popenoe, H. L., 1961, Developments in west coast area in 1960; Bulletin of the American Association of Petroleum Geologists, v. 45, p. 959-973.

Prytulak, J., Vervoort, J. D., Plank, T., and Yu, C., 2006, Astoria Fan sediments, DSDP site 174, Cascadia Basin: Hf-Nd-Pb constraints on province and outburst flooding: Chemical Geology, v. 233, p. 276-292.

Raia, F and Spera, F. J., 1997, Simulations of crustal anatexis: Implications for the growth on differentiation of continental crust: J. of Geophysical Research, v. 102, p. 22629-22648.

Ren, M., 2004, Partitioning of Sr, Ba, Rb, Y, and LREE between alkali feldspar and peraluminous silicic magmas: American Mineralogist, v. 89, p. 1290-1303.

Ren, M., Parker, D. F. and White, J. C., 2003, Partitioning of Sr, Ba, Rb, Y, and LREE between plagioclase and peraluminous silicic magmas: American Mineralogist, v. 88, p. 1091-1103.

Renne, P. R., Swisher, C. C., Deino, A. L., Karner, D. B., Owens, T. L. and DePaolo, D. J., 1998, Intercalibration of standards, absolute ages and uncertainties in $^{40}Ar/^{39}Ar$ dating: Chemical Geology, v. 145, p. 117-152.

Richards, M. A., Jones, D. L., Duncan, R. A. and DePaolo, D. J., 1991, A mantle plume initiation model for the Wrangellia Flood Basalt and other oceanic plateaus: Science, v. 254, p. 263-267.

Robinson, P. T., Walker, G. W. and McKee, E. H., 1990, Eocene (?), Oligocene, and lower Miocene rocks of the Blue Mountains Region: US Geological Survey Professional Paper, 1437, p. 29 – 62.

Roche, R. L., 1987, Stratigraphic and geochemical evolution of the Glass Buttes Complex, Oregon: Portland State University MS Thesis, 99p.

Rollinson, H., 1993, Using geochemical data: Evaluation, presentation, interpretation: Longman Group, Essex, England, 352 p.

Rooney, T., Furman, T., Bastow, I., Ayalew, D. and Yirgu, G., 2007, Lithospheric modification during crustal extension in the Main Ethiopian Rift, J. of Geophysical Research v. 112, p. B10201.

Rosenberg, C. L., Medvedev, S. and Handy, M. R., 2007, Effects of melting on faulting and continental deformation, in Handy, M. R., Hirth, G. and Hovius, N, eds., Tectonic faults: Agents of change on a dynamic earth: The MIT Press, Cambridge, MA.

Rubin, K. H., Smith, M. C., Bergmanis, E. C., Perfit, M. R., Sinton, J. M. and Batiza, R., 2001, Geochemical heterogeneity within mid-ocean ridge lava flows: insights into eruption, emplacement and global variations in magma generation: Earth and Planetary Science Letters, v. 188, is. 3-4, p. 349-367.

Rudnick, R. L. and Gao, S., 2005, Composition of the Continental Crust, in Rudnick, R. L., ed., The Crust: Treatise on Geochemistry, Holland, H. D. and Turekian, K. K., eds., v. 3, p. 1-64.

Russell, I. C., 1884, A Geological Reconnaissance in Southern Oregon: US Geological Survey, Annual Report 4, p. 431-464.

Russell, J. K. and Nicholls, J., 1987, Early crystallization history of alkali olivine basalts, Diamond Craters, Oregon: Geochimica et Cosmochimica Acta, v. 51, p. 143-154.

Saleeby, J. B. and Busby-Spera, C., 1992, Early Mesozoic tectonic evolution of the western United States Cordillera, in Burchfiel, B. C., Lipman, P. W. and Zoback, M. L., eds., The Cordilleran orogen: Conterminous United States: Geologic Society of America, v. G-3, p. 107-168.

Saunders, A. D., Norry, M. J., and Tarney, J., 1988, Origin of MORB and chemically depleted mantle reservoirs: trace element constraints: J. of Petrology, Special Lithosphere Issue, p. 415-445.

Savov, I. P., Leeman, W. P., Lee, C-T. A. and Shirey, S. B., 2009, Boron isotopic variations in NW USA rhyolites: Yellowstone, Snake River Plain, Eastern Oregon: J. of Volcanology and Geothermal Research, v. 188, p. 162-172.

Scarberry, K. C., 2007, Extension and volcanism: Tectonic development of the northwestern margin of the Basin and Range Province in southern Oregon: Oregon State University PhD thesis, 168p.

Scarberry, K. C., Meigs, A., and Grunder, A., 2010, Faulting in a propagating continental rift: Insights from the late Miocene structural development of the Abert Rim fault, southern Oregon, USA: Tectonophysics v. 488, p. 71-86.

Schmidt, M. E. and Grunder, A. L., 2011, Deep mafic roots to arc volcanoes: Mafic recharge and differentiation of basaltic andesite at North Sister Volcano, Oregon Cascades: J. of Petrology, v. 52, p. 603-641.

Schmidt, M. E. and Grunder, A. L., 2009, The evolution of North Sister: A volcano shaped by extension and ice in the central Oregon Cascades Arc: Geological Society of America Bulletin, v. 121, p. 643-662.

Schmidt, M. E., Grunder, A. L. and Rowe, M. C., 2008, Segmentation of the Cascade Arc as indicated by Sr and Nd isotopic variations among diverse primitive basalts: Earth and Planetary Science Letters, v. 266, p. 166-181.

Schuessler, J. A.; Schoenberg, R. and Sigmarsson, O, 2009, Iron and lithium isotope systematics of the Hekla volcano, Iceland — Evidence for Fe isotope fractionation during magma differentiation: Chemical Geology, v. 258, p. 78-91.

Schwartz, J. J., Snoke, A. W., Frost, C. D., Barnes, C. G., Gromet, L. P. and Johnson, K., 2010, Analysis of the Wallowa-Baker terrane boundary: Implications for tectonic accretion in the Blue Mountains province, northeastern Oregon: Geological Society of America Bulletin, v. 122, p. 517-536.

Searle, M. P., Cottle, J. M., Streule, M.J. and Waters, D. J., 2010, Crustal melt granites and migmatites along the Himalaya: melt source, segregation, transport and granite emplacement mechanisms in Clemens, J.D., Donaldson, C., Frost, C.D., Kisters, A.F.M., Moyen, J.-F., Rushmer, T., and Stevens, G., eds. Sixth Hutton Symposium on the Origin of Granites and Related Rocks: Geological Society of America Special Paper, v. 472, p. 219-233.

Selbekk, R. S. and Tronnes, R. G., 2007, The 1362 AD Oraefajokull eruption, Iceland: Petrology and geochemistry of large-volume homogeneous rhyolite: J. of Volcanology and Geothermal Research, v. 160, p. 42-58.

Shamberger, P. J. and Hammer, J. E., 2006, Leucocratic and gabbroic xenoliths from Hualalai Volcano, Hawaii: J. of Petrology, v. 47, p. 1785-1808.

Shand, S. J., 1927, Eruptive Rocks: Their Genesis, Composition, Classification and Their Relation to Ore-deposits: Murby, London, 360 p.

Sharp, Z. D., 1990, A laser-based microanalytical method for the in situ determination of oxygen isotope ratios of silicates and oxides: Geochemica et Cosmochemica Acta, v. 54, p. 1353-1357.

Shaw, H. F. and Wasserburg, G. J., 1984, Isotopic constraints on the origin of Appalachian mafic complexes: American Journal of Science, v. 284, p. 319-349.

Shaw, H.R., 1985, Links between magma-tectonic rate balances, plutonism and volcanism: J. of Geophysical Research, v. 90, p.11275–11288.

Shepard, D., 1968, A two-dimensional interpolation function for irregularly-spaced data: Proceedings of the Association of Computing Machinery (ACM) National Conference, p. 517-524.

Sherrod, D. R. and Smith, J. G., 2000, Geologic map of upper Eocene to Holocene volcanic and related rocks of the Cascades Range, Oregon: U.S. Geological Survey Map I-2569, scale 1:500,000; pamphlet 17 p.

Sherrod, D. R., Taylor, E. M., Ferns, M. L., Scott, W. E., Conrey, R. M., and Smith, G. A., 2004, Geologic map of the Bend 30- X 60- minute quadrangle, central Oregon: US Geological Survey Geologic Investigations Series I-2683, 48 p.

Shervais, J. W. and Vetter, S. K., 2009, High-K alkali basalts of the Western Snake River Plain (Idaho): Abrupt transition from tholeiitic to mildly alkaline plume-derived basalts: J. of Volcanology and Geothermal Research, v. 188, p. 141-152.

Shoemaker, K. A. and W. K. Hart, 2002, Temporal controls on basalt genesis and evolution on the Owyhee Plateau, Idaho and Oregon, in Bonnichsen, B., White, C. M. and McCurry, M., eds., Tectonic and Magmatic Evolution of the Snake River Plain Volcanic Province: Idaho Geological Survey Bulletin, v. 30, p. 313-328.

Sigmarsson, O. and Steinthorsson, S., 2007, Origin of Iceland basalts: A review of their petrology and geochemistry: J. of Geodynamics, v. 43, p. 87-100.

Sigmarsson, O., Condomines, M., and Fourcade, S., 1992, A detailed Th, Sr and O isotope study of Hekla: differentiation processes in an Icelandic Volcano: Contributions to Mineralogy and Petrology, v. 112, p. 20-34.

Sigurdsson, H and Sparks, R S J, 1981, Petrology of rhyolitic and mixed magma ejecta from the 1875 eruption of Askja, Iceland: J. of Petrology, v. 22, p. 41-84.

Sisson, T.W. and Grove, T. L., 1993. Experimental investigations of the role of H2O in calc-alkaline differentiation and subduction zone magmatism: Contributions to Mineralogy and Petrology, v. 113, p. 143-166.

Sisson, T.W. and Grove, T. L., 1993. Experimental investigations of the role of H2O in calc-alkaline differentiation and subduction zone magmatism: Contributions to Mineralogy and Petrology, v. 113, p. 143-166.

Sisson, T. W., Ratajeski, K., Hankins, W. B., Glazner, A. F., 2005, Voluminous granitic magmas from common basaltic sources: Contributions to Mineralogy and Petrology, v. 148, p. 635-661.

Smith, G. A., Snee, L. W., and Taylor, E. M., 1987, Stratigraphic, sedimentologic, and petrologic record of the late Miocene subsidence of the Oregon High Cascades: Geology, v. 15, p. 389-392.

Smith, R.L. and Luedke, R.G., 1984, Potentially active volcanic lineaments and loci in western conterminous United States, in, Explosive Volcanism: Inception, Evolution and Hazards, National Research Council, p. 47-66.

Snoke, A. W. and Barnes, C. G., eds., 2006, Geological studies in the Klamath Mountains province, California and Oregon; a volume in honor of William P. Irwin: Geological Society of America Special Paper 410, 505 p. ISBN-13 978-0-8137-2410-2

Spera, F. J. and Bohrson,W. A., 2001, Energy-constrained open-system magmatic processes I: General model and energy-constrained assimilation and fractional crystallization (EC-AFC) Formulation: J. of Petrology, v. 42, p. 999-1018.

Spulber, S. D. and Rutherford, M. J., 1983, The origin of rhyolite and plagiogranite in oceanic crust: An experimental study: J. of Petrology, v. 24, p. 1-25.

Stefano, C. J., 2010, Volatiles, major oxide, trace element and isotope geochemistry in the Snake River Plain and Columbia River Flood Basalts: Implications for the evolution of a continental hotspot: University of Michigan PhD thesis, 191 p.

Steiger, R. H. and Jager, E., 1977, Subcommission on Geochronology – convention on the use of decay constants in geochronology and cosmochronology: Earth and Planetary Science Letters, v. 36, p. 359-363.

Streck, M, J., 2002, Partial melting to produce high-silica rhyolites of a young bimodal suite: compositional constraints among rhyolites, basalts, and metamorphic xenoliths from the Harney Basin, Oregon: International J. of Earth Sciences, v. 91, p. 583-593.

Streck, M. J. and Grunder, A. L., 1995, Crystallization and welding variations in a widespread ignimbrite sheet; the Rattlesnake Tuff, eastern Oregon, USA: Bulletin of Volcanology, v. 57, p. 151-169.

Streck, M. J. and Grunder, A. L., 1997, Compositional gradients and gaps in high-silica rhyolites of the Rattlesnake Tuff, Oregon: J. of Petrology, v. 38, p. 133-163.

Streck, M. J. and Grunder, A. L., 1999, Enrichment of basalt and mixing of dacite in the rootzone of a large rhyolitic chamber: inclusions and pumices from the Rattle Snake Tuff, Oregon: Contributions to Mineralogy and Petrology, v. 136, p. 193-212.

Streck, M. J. and Grunder, A. L., 2008, Phenocryst-poor rhyolites of bimodal, tholeiitic provinces: the Rattlesnake Tuff and implications for mush extraction models: Bulletin of Volcanology, v. 70, p. 385-401.

Suayah, I. B., and Rogers, J. J. W., 1991, Petrology of the lower Tertiary Clarno Formation in north central Oregon: The importance of magma mixing: J. of Geophyisical Research, v. 96, p. 13357-13371.

Sun, S. S. and McDonough, W. F. (1989) Chemical and Isotopic Systematics of oceanic basalts: implications for Mantle Composition and Processes, in Saunders, A. D. and Norry, M. J., eds., Magmatism in the Ocean Basins: Special Publication Geological Society of London, no. 42, p. 313-345.

Sverrisdottir, G., 2007, Hybrid magma generation preceding Plinian silicic eruptions at Hekla, Iceland: Evidence from mineralogy and chemistry of two zoned deposits: Geological Magazine, v. 144, p. 643-659.

Tamura, Y., Gill, J. B., Tollstruo, D., Kawabayta, H., Shukuno, H., Chang, Q., Miyazaki, T., Takahashi, T., Hirahara, Y., Kodaira, S., Ishizuka, O., Suzuki, T., Kido, Y., Fiske, R. S. and Tatsumi, Y., 2009, Silicic magmas in the Izu-Bonin oceanic arc and implications for crustal evolution: J. of Petrology, v. 50, p. 685-723.

Taylor, E. M., 1981, Central High Cascade roadside geology, in Johnston, D. A. and Donnelly-Nolan, J. M., eds., Guides to some volcanic terranes in Washington, Idaho, Oregon, and northern California: US Geological Survey Circular 838, p. 55-83.

Taylor, S. R. and McLennan, S. M., 1995, The geochemical evolution of the continental crust: Reviews in Geophysics, v. 33, p. 241-265.

Till, C. B., Grove, T. L., Carlson, R. W., Donnelly-Nolan, J. M., Fouch, M., Wagner, L., Hanson-Hedgecock, S., Hot Adiabatic Decompression Melting Near the Lithosphere-Astheosphere Boundary below southern Oregon and northern California: In preparation for G-cubed special volume.

Todt, W., Cliff, R. A., Hanser, A., Hofmann, A. W., 1996, Evaluation of a 202Pb-205Pb double spike for high-precision lead isotope analysis, in Basu, A and Hart, S. R, eds., Earth Processes: Reading the isotopic code: Geophysical Monograph 95, American Geophysical Union, p. 429-437.

Trehu, A. M., Asudeh, T. M., Brocher, T. M., Luetgert, J. H., Mooney, J. L., Nabelek, J. L. and Nakamura, Y., 1994, Crustal structure of the Cascadia forearc: Science, v. 266, p. 237 – 243.

Trench, D., 2008, The Termination of the Basin and Range Province into a Clockwise Rotating Region of Transtension and Volcanism, Central Oregon: Oregon State University MS thesis, 71 p.

Valley, J. W., Kitchen, N., Kohn, M. J., Neindorf, C. R. and Spicuzza, M. J., 1995, UWG-2, a garnet standard for oxygen isotope ratios: Strategies for high precision and accuracy with laser heating: Geochemica et Cosmochemica Acta, v. 59, p. 5223-5231.

Vervoort, J. D., Patchett, P. J., Blichert-Toft, J. and Albarede, F., 1999, Relationships between Lu-Hf and Sm-Nd isotopic systems in the global sedimentary system: Earth and Planetary Science Letters, v. 168, p. 79-99.

Vigil, J. F., Pike, R. J. and Howell, D. G., 2000, A tapestry of time and terrain: U.S. Geological Survey Geologic Investigations Series 2720, scale 1:3,500,000.

Wacaster, S., Streck, M. J., Belkin, H. E., and Bodnar, R. J., 2011, Compositional zoning of the Devine Canyon Tuff, Oregon: American Geophysical Union Fall 2011 Meeting abstract V21C-2517.

Walker, G. W., 1974, Some implications of Late Cenozoic volcanism to geothermal potential in the High Lava Plains of south-central Oregon: Ore Bin, v. 36, p. 109-119.

Walker, G. W., 1979, Revisions to the Cenozoic stratigraphy of Harney Basin, southeastern Oregon: U.S. Geological Survey Bulletin 1475, 35 p.

Walker, G. W., 1981, Uranium, thorium, and other metal associations in silicic volcanic complexes of the northern Basin and Range, a preliminary report: U.S. Geological Survey Open File Report no 81-1290, 45 p.

Walker, G. W. and Swanson, D.A., 1968, Laminar flowage in a Pliocene soda rhyolite ash-flow tuff, Lake and Harney Counties, Oregon: U.S. Geological Survey Professional Paper 600-B, p. B37-B47.

Walker, G.W., and MacLeod, N.S., 1991, Geologic map of Oregon: U. S. Geological Survey, scale 1:500,000.

Walker, G. W. and Robinson, P. T., 1990, Paleocene (?), Eocene and Oligocene (?) rocks of the Blue Mountains region , in Walker, G. W., ed., Geology of the Blue Mountains Region of Oregon, Idaho, and Washington: US Geological Survey Professional Paper 1437, p 13-27.

Walker, G. W. and Robinson, P. T., 1990, Cenozoic tectonism and volcanism of the Blue Mountains region, in Walker, G. W., ed., Geology of the Blue Mountains Region of Oregon, Idaho, and Washington: US Geological Survey Professional Paper 1437, p. 119-135.

Watson, D. F. and Philip, G. M., 1985, A refinement of inverse distance weighted interpolation: Geo-Processing, v. 2, p. 315-327.

Wells, R. E., 1975, Geology of the Drake Peak rhyolite complex and the surrounding area, Lake County, Oregon: University of Oregon MS thesis, 130p.

Wells, R. E., 1979, Drake Peak – A structurally complex rhyolite center in southeastern Oregon: US Geological Survey Professional Paper 1124, p. E1-E16.

Wells, R. E. and Heller, P. L., 1988, The relative contribution of accretion, shear, and extension to Cenozoic tectonic rotation in the Pacific Northwest: Geological Society of American Bulletin, v. 100, p. 325-338

Wells, R. E., Weaver, C. S. and Blakely, R. J., 1998, Fore arc migration in Cascadia and its neotectonic significance: Geology, v. 26, p. 759-762.

Whitaker, M. L., Nekvasil, H., Lindsley, D. H., McCurry, M., 2008, Can crystallization of olivine tholeiite give rise to potassic rhyolites? – an experimental investigation: Bulletin of Volcanology, v. 70, p. 417-434.

Wilson, C. J. N., Blake, S., Charlier, B. L. A. and Sutton, A.N., 2006, The 26.5 ka Oruanui eruption, Taupo Volcano, New Zealand: development, characteristics and evacuation of a large rhyolitic magma body: J. of Petrology, v. 47, p. 35–69.

Wyld, S. J. and Wright, J. E., 2001, New evidence for Cretaceous strike-slip faulting in the United States Cordillera and implications for terrane-displacement, deformation patterns, and plutonism, American Journal of Science, v. 301, p. 150-181.

Wyld, S. J., Umhoefer, P. J. and Wright, J. E., 2006, Reconstructing northern Cordilleran terranes along known Cretaceous and Cenozoic strike-slip faults: Implications for the Baja British Columbia hypothesis and other models, in Haggart, J.E., Enkin, R. J. and Monger, J. w. H., eds., Paleogeography of the North American Cordillera: Evidence for and against large-scale displacements: Geological Association of Canada Special Paper 46, p. 277-298.

Xue, M. and Allen, R. M., 2006, Origin of the Newberry Hotspot Track: Evidence from shear-wave splitting: Earth and Planetary Science Letters, v. 244, p. 315-322.

APPENDICES

Appendix 1: Table of New Major and Trace Element Compositional Data

This table gives the new major and trace element compositional data of 118 previously unpublished whole rock samples from the HLP and NWBR. Date key and values as described in Table 1 (Chapter 2). Latitude and longitude (NAD 1927) given to appropriate significant digits except that JN samples are ± 0.3º. Five sets or errors analyses are provided and should be applied as follows. Standard error at the 95% confidence interval are calculated from t-distributions, compiled from duplicate analyses and given in either weight percent or ppm (XRF, n = 4 and ICP, n = 7 except Y and REE, n = 6). These errors are preferred over the WSU laboratory standard (see below) because they are from fairly uniform compositions (generally calculated from rhyolites and rhyodacite) whereas WSU calculates its standard errors from a very wide range of compositions (pers comm, R. Conrey). The standard errors from this work are generally applicable to "silicic" samples analyzed by the same methods (See Appendix 2). Due to the lower number of samples from which these errors were determined for this study, many of the errors are similar.

The "Largest" error is the highest percent error returned for a replicate sample. While it might not capture the entire range of error for all analytes (e.g. Ba and Sr), it does show that some samples with low concentrations have a greater percent error. Ba and Sr cover a very wide range of values, and percent errors on these values may be higher than this "largest" error, even though the standard errors are likely smaller on these low concentration samples than the stated standard error. The "applicable percent error" is the percent error that should be used for most concentrations. When concentrations are below those listed in the "applied to" column, then the error is larger than the applicable error but not necessarily as large as the "largest" error. This "applicable percent error" covers most of the compositional variability in the dataset. The applicable errors for W, Sb, As and Co are from INAA and are from similar samples (HLP basalts through rhyolites) from MacLean (1994).

The LOD – WSU – XRF are the limits of determination, comparable to our 95% confidence interval from > 250 replicates of various standards run on XRF at WSU (pers comm, R. Conrey). Values in italics are for analytes that are often reported from ICP-MS data but some samples in this set have used XRF for some of these trace elements (see Appendix 2). The LOD – WSU – ICP-MS is the similar limit of determination for ICP-MS from WSU for 50 trials of standard BCR-P run as an unknown (pers. Comm, C. Knaack). Additional analytical uncertainties for INAA for similar silicic samples (RST) are given in Streck and Grunder (1997). See the Electronic Data Supplement for more information including pre-normalized measurements and alternate results (e.g. INAA results for some analytes where the reported result was measured with XRF).

Sample No	MTF-07-02	MTF-07-04	MTF-07-05	MTF-07-06	MTF-07-08	MTF-07-09	MTF-07-10	MTF-07-11
age	*6.25*	*5.79*	*6.49*	**6.35**	**7.68**		*9.63*	9.48
error	*0.02*	*0.02*	*0.03*	**0.03**	**0.04**		*0.03*	0.3 *
Lat	43.7915	43.5515	43.5572	43.4777	43.5731	43.6588	43.4538	43.3414
Long	120.9407	120.0645	119.9335	119.3101	119.1303	119.2781	118.1844	118.4290
SiO2	72.36	77.42	77.30	73.49	74.51	74.93	76.54	76.01
TiO2	0.294	0.070	0.055	0.205	0.207	0.200	0.198	0.131
Al2O3	14.77	12.75	12.79	14.26	13.46	13.25	10.85	13.09
FeO*	2.55	0.73	0.62	1.77	1.53	1.47	2.80	1.01
MnO	0.064	0.041	0.058	0.054	0.043	0.042	0.056	0.048
MgO	0.48	0.05	0.03	0.41	0.15	0.14	0.08	0.22
CaO	3.06	0.52	0.41	1.73	0.66	0.62	0.26	1.04
Na2O	3.57	4.21	4.24	3.47	4.32	4.26	3.71	2.74
K2O	2.75	4.20	4.48	4.55	5.09	5.06	5.49	5.67
P2O5	0.097	0.012	0.008	0.059	0.026	0.024	0.013	0.029
PNT	98.95	98.50	98.85	96.31	99.17	99.22	96.32	96.63
Rb	68.4	81.8	123	114	115	119	134	179
Ba	1010	1160	36.1	1240	630	560	36.5	289
Sr	250	23.9	2.1	207	26.9	23.9	6.1	85
Zr	137	85	74	148	255	241	1160	95
Nb	4.3	10.2	13.3	13.0	26.7	27.3	80.5	12.9
Y	15.2	49.7	71.1	24.0	41.3	42.2	144	22.8
Pb	10.7	14.9	17.7	16.8	15.8	16.1	31.0	23.5
Zn	39	30	39	34	40	40	234	27
V	37	1	1	19	3	3	2	6
Cu	10	0	0	8	3	4	6	1
Ni	1	0	0	0	0	0	0	0
Cr	9	1	1	4	2	1	2	1
Sc	5.7	3.5	7.0	3.6	4.1	4.3	1.1	2.8
Ga	14.6	14.2	16.8	15.5	16.5	16.7	27.3	14.3
Cs	1.87	2.62	5.13	3.86	3.23	3.34	4.42	8.14
U	2.46	3.45	6.8	3.62	4.08	4.21	5.7	8.6
Th	6.8	7.7	12.6	8.7	10.5	10.8	14.0	17.2
Hf	3.91	4.06	4.34	4.52	7.9	7.6	25.6	3.57
Ta	0.44	0.89	1.15	1.27	1.98	2.02	4.97	1.79
La	20.6	25.3	14.7	27.3	40	41	90	22.3
Ce	37.7	54	37.0	49	77	78	188	39.8
Pr	4.2	6.7	5.2	5.3	8.7	8.9	23.8	4.8
Nd	15.2	25.6	22.2	18.7	31.0	31.0	93	16.9
Sm	3.03	6.4	7.6	3.86	6.3	6.4	22.5	3.64
Eu	0.77	0.63	0.20	0.68	0.47	0.41	0.72	0.46
Gd	2.77	6.7	8.9	3.50	5.9	5.9	23.1	3.42
Tb	0.44	1.28	1.77	0.63	1.07	1.09	4.1	0.57
Dy	2.67	8.4	11.9	4.15	7.1	7.1	26.7	3.68
Ho	0.55	1.80	2.58	0.86	1.50	1.53	5.6	0.78
Er	1.56	5.3	7.6	2.58	4.5	4.5	16.0	2.27
Tm	0.24	0.84	1.19	0.41	0.71	0.73	2.37	0.36
Yb	1.56	5.6	7.8	2.77	4.7	4.9	15.2	2.43
Lu	0.25	0.89	1.24	0.45	0.77	0.78	2.39	0.40
W								
Sb								
As								
Co								

Sample No	MTF- 07-12	MTF-07-14	MTF-07-15	MTF-07-16	MTF-07-18	MTF-07-20	MTF-07-25o	MTF-07-26
age	4	*5.67*		*4.34*		7.61	7.90	*17.30*
error	0.4 *	*0.08*		*0.03*		0.19 *	0.09 *	*0.05*
Lat	43.6198	43.0103	42.9866	43.3987	43.0048	42.6024	42.5852	42.4583
Long	120.4635	121.0304	121.0490	120.8844	120.7994	120.4281	120.6226	120.6550
SiO2	68.24	66.19	51.03	77.08	71.91	76.63	76.49	76.29
TiO2	0.760	0.93	1.34	0.061	0.345	0.049	0.053	0.147
Al2O3	14.65	15.17	19.37	12.75	14.68	13.22	13.36	12.92
FeO*	4.55	5.31	9.9	1.07	2.40	0.60	0.52	1.25
MnO	0.103	0.130	0.159	0.040	0.060	0.067	0.062	0.037
MgO	1.29	1.04	4.6	0.02	0.51	0.04	0.05	0.02
CaO	3.31	2.93	8.76	0.66	2.32	0.81	0.91	0.31
Na2O	4.19	4.57	3.67	4.49	3.77	3.72	3.92	4.01
K2O	2.71	3.41	0.72	3.82	3.86	4.84	4.63	5.01
P2O5	0.19	0.33	0.39	0.007	0.140	0.020	0.008	0.011
PNT	99.51	99.12	98.15	98.87	98.61	96.98	99.02	98.95
Rb	66.1	102	6.8	91.5	81.5	97.2	91.5	151
Ba	890	1020	356	1260	1410	290	339	145
Sr	193	239	720	35.1	315	48.4	67	16.0
Zr	233	291	71	120	149	63	58	183
Nb	10.5	11.1	3.6	10.7	6.7	10.1	9.7	25.4
Y	45.5	39.0	32.3	53.2	13.5	22.6	20.3	22.7
Pb	9.9	12.3	3.5	16.3	13.9	24.1	25.9	18.1
Zn	64	79	95	63	38	27	24	33
V	60	59	220	2	29	2	3	3
Cu	13	15	111	1	19	0	1	4
Ni	1	0	75	0	2	0	0	0
Cr	9	4	73	1	7	1	2	2
Sc	13	14	22	4.1	4.2	2.3	2.2	2.2
Ga	16.8	18.8	18.1	17.8	14.8	14.4	15.4	18.5
Cs	2.57	2.07	0.10	3.55	1.37	4.22	4.07	2.90
U	2.84	5.2	0.55	3.01	2.42	3.93	3.94	6.4
Th	6.9	12.9	0.71	7.3	6.7	8.2	6.6	19.5
Hf	6.5	7.7	2.03	5.2	4.09	3.10	2.96	6.3
Ta	0.83	0.79	0.21	0.87	0.61	1.04	1.12	2.34
La	26.0	26.6	16.4	18.5	27.4	13.5	8.7	39.2
Ce	50	58	25.4	42	47	24.6	17.3	63
Pr	7.3	7.3	5.3	5.7	5.3	3.16	2.15	8.2
Nd	30.5	30.5	25.0	24.3	18.7	11.8	8.4	26.6
Sm	7.5	7.2	6.0	6.9	3.43	3.05	2.39	5.0
Eu	1.79	1.92	2.13	0.85	0.89	0.39	0.39	0.21
Gd	7.7	7.1	6.5	7.5	2.80	3.04	2.49	3.94
Tb	1.34	1.18	1.02	1.42	0.43	0.57	0.48	0.68
Dy	8.4	7.3	6.1	9.3	2.52	3.75	3.14	4.28
Ho	1.74	1.54	1.23	1.97	0.51	0.80	0.70	0.85
Er	4.9	4.3	3.20	5.7	1.40	2.35	2.08	2.44
Tm	0.72	0.64	0.45	0.87	0.21	0.37	0.34	0.40
Yb	4.6	4.1	2.62	5.6	1.39	2.56	2.33	2.59
Lu	0.73	0.67	0.41	0.88	0.23	0.42	0.39	0.39
W								
Sb								
As								
Co								

Sample No	MTF-07-27a	MTF-07-28	MTF-07-29	MTF-07-30	MTF-07-32	MTF-07-33	MTF-07-34	MTF-07-37
age	7.38	*8.1*	*8.05*	*6.87*	1.13		*17.53*	*5.77*
error	0.33 *	*0.2* **	*0.02*	*0.04*	0.05 *		*0.04*	*0.04*
Lat	42.3969	42.3681	42.3242	42.3072	43.6153	42.6570	42.6230	42.5932
Long	120.5998	120.5992	120.5787	120.6293	120.9302	120.8126	120.7729	121.2682
SiO2	77.17	76.70	76.71	75.60	75.51	76.18	75.77	68.93
TiO2	0.055	0.057	0.061	0.187	0.103	0.151	0.167	0.692
Al2O3	12.91	13.47	13.46	13.27	13.39	11.03	10.37	15.36
FeO*	0.56	0.44	0.49	1.36	1.45	3.50	4.21	3.35
MnO	0.082	0.075	0.070	0.032	0.038	0.062	0.077	0.128
MgO	0.02	0.04	0.05	0.16	0.05	0.02	0.01	0.66
CaO	0.51	0.85	0.84	1.09	0.89	0.11	0.10	2.01
Na2O	4.28	3.89	3.57	3.67	4.49	4.66	4.91	5.30
K2O	4.40	4.48	4.75	4.58	4.07	4.28	4.36	3.37
P2O5	0.007	0.007	0.008	0.058	0.013	0.015	0.011	0.20
PNT	98.82	96.84	97.08	99.04	99.12	98.96	98.58	99.68
Rb	204	134	142	107	129	207	289	79.0
Ba	8.9	19.0	46.6	870	920	14.2	23.4	990
Sr	4.3	21.3	27.3	145	60	5.2	3.4	263
Zr	71	54	59	108	173	1170	1830	232
Nb	23.7	11.3	10.9	8.2	8.1	80.4	136	14.7
Y	38.1	15.3	15.7	14.7	40.6	49.6	7.9	39.4
Pb	33.5	27.0	26.9	19.2	18.0	15.6	26.3	16.1
Zn	31	21	23	34	56	183	169	79
V	0	1	0	13	1	2	1	30
Cu	0	0	0	6	2	2	2	3
Ni	0	0	0	0	0	0	0	0
Cr	2	1	1	3	0	0	1	1
Sc	4.7	2.9	3.0	2.7	3.8	1.5	1.8	11
Ga	18.1	17.2	16.9	14.2	21.0	29.4	29.7	18.8
Cs	8.21	5.20	5.24	3.64	5.85	1.69	1.03	1.49
U	8.3	5.1	5.0	4.20	4.60	4.05	3.58	4.17
Th	15.8	8.5	8.6	10.9	12.0	26.8	44	10.8
Hf	4.12	3.06	3.20	3.55	5.7	27.2	43.1	6.4
Ta	2.83	1.21	1.23	0.87	0.90	6.5	10.1	1.10
La	10.5	7.0	9.8	29.0	27.9	49	9.8	32.8
Ce	22.3	13.4	17.8	50	55	39.8	69	66
Pr	2.87	1.62	2.07	5.3	6.5	11.4	2.94	8.4
Nd	11.0	5.7	7.3	17.9	24.9	39.7	9.9	33.5
Sm	3.52	1.46	1.71	3.15	5.8	8.3	2.18	7.5
Eu	0.10	0.18	0.20	0.49	0.77	0.41	0.08	1.93
Gd	4.03	1.50	1.69	2.59	5.8	7.3	1.69	7.1
Tb	0.84	0.29	0.31	0.41	1.06	1.45	0.31	1.17
Dy	5.7	2.02	2.08	2.47	6.8	9.8	2.07	7.3
Ho	1.26	0.48	0.47	0.52	1.49	2.11	0.44	1.51
Er	3.84	1.51	1.51	1.52	4.3	6.3	1.45	4.2
Tm	0.64	0.27	0.27	0.25	0.67	1.02	0.31	0.63
Yb	4.5	1.97	2.00	1.67	4.4	6.9	2.57	4.1
Lu	0.74	0.35	0.35	0.28	0.70	1.13	0.50	0.63
W								
Sb								
As								
Co								

Sample No	MTF-07-38	MTF-07-39	MTF-07-40	MTF-07-41	MTF-07-42	MTF-07-47	MTF-07-48	MTF-07-49
age	*5.59*		5	4.79	5.15		*5.2*	*5.17*
error	*0.03*		0.7 *	0.17 *	0.21 *		*0.2* **	*0.05*
Lat	43.2921	43.4746	43.2745	42.9590	42.9103	42.3616	42.4382	42.4307
Long	121.0367	120.8616	121.3542	121.2483	121.2021	121.4058	121.3668	121.3598
SiO2	69.77	69.03	72.40	67.98	73.30	70.90	70.34	70.84
TiO2	0.174	0.495	0.258	0.643	0.315	0.507	0.530	0.468
Al2O3	16.05	15.32	15.03	16.02	14.41	15.67	15.20	15.46
FeO*	3.01	3.85	1.92	3.45	1.97	2.43	2.56	2.31
MnO	0.112	0.099	0.092	0.132	0.105	0.068	0.075	0.065
MgO	0.07	0.43	0.19	0.74	0.09	0.14	0.53	0.26
CaO	1.45	1.96	1.11	2.62	0.47	1.13	1.64	1.36
Na2O	5.56	5.14	5.22	5.35	5.53	5.76	5.76	5.95
K2O	3.72	3.58	3.72	2.88	3.78	3.32	3.19	3.18
P2O5	0.091	0.103	0.063	0.18	0.023	0.076	0.17	0.123
PNT	99.21	99.62	99.18	99.48	98.63	99.07	99.59	99.53
Rb	82.6	75.2	101	66.1	88.2	52.1	47.7	47.1
Ba	1240	1170	1100	900	1170	1040	1000	1010
Sr	194	174	151	358	77	164	213	191
Zr	306	358	236	208	355	250	237	241
Nb	16.3	13.2	12.9	7.7	17.6	9.2	8.6	8.8
Y	34.7	47.5	31.5	34.4	48.8	34.1	32.4	26.5
Pb	14.7	10.9	14.7	10.7	16.0	13.7	10.6	11.7
Zn	65	65	71	78	68	58	58	47
V	1	10	3	56	5	26	26	21
Cu	3	14	1	25	0	6	6	3
Ni	0	0	0	0	0	0	0	0
Cr	1	1	0	2	1	2	1	2
Sc	3.0	9.7	4.3	9.1	9.9	8.6	8.1	6.2
Ga	20.1	18.9	17.4	17.7	19.9	19.4	18.4	19.4
Cs	2.23	0.98	2.21	2.73	2.14	0.87	0.81	0.71
U	2.38	2.32	3.11	2.89	3.71	2.05	1.74	1.69
Th	8.7	7.5	9.7	7.1	10.1	4.6	4.3	4.3
Hf	8.3	9.6	6.7	5.7	9.4	7.0	6.6	6.7
Ta	1.19	0.90	0.98	0.61	1.16	0.60	0.56	0.57
La	35.3	29.6	30.8	22.9	41	29.7	24.1	22.2
Ce	70	67	62	47	77	64	49	45
Pr	8.5	8.3	7.5	6.0	11.0	9.2	6.8	6.0
Nd	31.8	34.1	28.9	24.9	43	37.0	27.4	23.5
Sm	6.4	8.1	6.0	5.6	9.6	8.1	6.1	5.1
Eu	1.48	1.75	1.25	1.38	2.18	1.45	1.41	1.17
Gd	5.7	7.8	5.3	5.5	8.6	6.8	5.5	4.42
Tb	0.97	1.38	0.91	0.92	1.48	1.14	0.92	0.74
Dy	6.0	8.7	5.6	5.6	9.2	6.8	5.7	4.71
Ho	1.28	1.85	1.18	1.21	1.90	1.35	1.18	1.00
Er	3.75	5.3	3.36	3.42	5.3	3.75	3.36	2.92
Tm	0.59	0.82	0.53	0.52	0.80	0.57	0.52	0.47
Yb	3.99	5.4	3.45	3.29	5.1	3.71	3.45	3.12
Lu	0.68	0.87	0.57	0.55	0.81	0.60	0.56	0.50
W								
Sb								
As								
Co								

Sample No	MTF-07-50	MTF-07-51	MTF-07-52	MTF-07-53	MTF-07-56	MTF-07-57	MTF-07-58	MTF-91-11
age			*6.79*	*6.16*		*15.03*	*8.96*	**6.90**
error			*0.02*	*0.02*		*0.04*	*0.03*	**0.02**
Lat	42.4139	42.2737	42.3308	42.4820	41.9822	42.0225	42.3013	43.2575
Long	121.2065	120.6941	120.8703	121.1820	120.2820	119.9969	120.1561	120.1659
SiO2	71.24	77.85	74.25	71.98	77.61	72.85	72.12	74.70
TiO2	0.491	0.059	0.223	0.397	0.142	0.209	0.305	0.151
Al2O3	14.71	12.56	13.88	14.75	12.35	14.23	14.81	13.85
FeO*	2.16	0.47	1.60	1.92	0.92	2.41	2.29	1.34
MnO	0.126	0.014	0.061	0.121	0.036	0.031	0.064	0.048
MgO	0.56	0.01	0.43	0.30	0.07	0.01	0.21	0.40
CaO	1.42	0.43	1.44	0.57	0.38	0.33	1.69	1.79
Na2O	6.03	3.84	3.41	6.73	3.53	4.66	3.86	3.16
K2O	3.13	4.73	4.66	3.17	4.94	5.24	4.54	4.46
P2O5	0.135	0.008	0.051	0.061	0.016	0.019	0.121	0.094
PNT	98.64	99.18	96.36	99.63	99.31	98.93	98.53	96.75
Rb	46.7	117	109	46.8	145	125	61.7	98.5
Ba	1070	32.1	1100	1180	318	311	1720	1310
Sr	167	7.2	201	56.2	41.3	18.4	251	228
Zr	258	82	116	250	109	388	154	102
Nb	9.7	11.0	7.6	9.2	12.1	24.1	6.5	6.2
Y	51.9	17.0	15.3	46.3	21.2	64.8	15.9	9.9
Pb	11.2	19.9	19.2	8.8	17.8	16.3	16.1	14.4
Zn	65	18	31	70	25	68	44	24
V	14	0	19	5	3	3	25	15
Cu	3	1	9	0	2	9	12	9
Ni	0	0	0	0	0	0	0	0
Cr	3	1	4	2	1	2	3	3
Sc	7.3	3.0	3.0	8.3	2.2	6.2	4.1	2.8
Ga	19.5	14.9	14.1	19.7	14.2	22.1	15.6	12.8
Cs	0.80	2.88	3.65	0.43	2.06	1.70	0.98	3.06
U	1.98	4.44	3.81	1.08	7.3	5.0	1.30	3.39
Th	5.1	11.2	9.0	5.4	18.4	12.6	4.1	7.1
Hf	7.3	3.65	3.60	7.4	4.20	11.5	4.18	3.12
Ta	0.62	0.99	0.83	0.59	1.33	1.60	0.54	0.82
La	30.6	20.9	28.2	28.0	28.5	55	33.8	21.2
Ce	60	39.8	46	57	53	83	56	35.1
Pr	8.5	4.9	5.2	8.3	5.6	14.3	5.9	3.63
Nd	35.3	17.2	18.1	34.9	18.6	53	20.0	12.0
Sm	7.9	3.55	3.35	8.2	3.57	11.2	3.55	2.16
Eu	1.84	0.17	0.57	1.97	0.26	0.77	0.91	0.46
Gd	7.8	2.94	2.73	7.6	3.07	10.0	2.93	1.74
Tb	1.32	0.50	0.44	1.34	0.53	1.75	0.46	0.28
Dy	8.4	3.12	2.67	8.4	3.45	11.2	2.81	1.66
Ho	1.85	0.64	0.54	1.77	0.75	2.39	0.58	0.35
Er	5.4	1.87	1.58	5.1	2.22	7.0	1.67	0.97
Tm	0.83	0.29	0.26	0.78	0.37	1.08	0.26	0.16
Yb	5.4	1.98	1.74	5.2	2.55	7.0	1.78	1.08
Lu	0.89	0.31	0.29	0.84	0.43	1.15	0.30	0.18
W								
Sb								
As								
Co								

Sample No	MTF-91-14	KCS-05-45	KCS-05-17	KCS-05-27	KCS-05-29	KCS-05-28	KCS-05-30	HP-91-1
age	**15.63**							
error	**0.03**							
Lat	43.1594	42.4158	42.3011	42.4803	42.4756	42.4767	42.4292	43.5813
Long	119.7533	119.2311	119.4117	120.8611	120.8633	120.8522	120.9308	119.1398
SiO2	68.57	52.89	49.36	59.69	64.79	64.24	48.03	59.41
TiO2	0.501	2.67	1.07	0.95	0.625	0.633	0.97	0.97
Al2O3	15.01	13.80	17.95	17.72	17.34	17.56	17.52	16.86
FeO*	4.27	12.1	10.0	6.4	4.03	4.08	9.2	6.7
MnO	0.109	0.223	0.171	0.140	0.143	0.165	0.169	0.128
MgO	0.64	3.9	7.5	2.64	1.10	1.22	9.4	3.08
CaO	2.53	8.30	10.4	5.52	3.01	3.05	11.9	6.11
Na2O	3.85	2.35	2.90	4.67	5.93	5.56	2.56	4.01
K2O	4.34	1.68	0.49	1.96	2.72	3.21	0.18	2.30
P2O5	0.20	2.09	0.17	0.27	0.30	0.29	0.090	0.48
PNT	96.98	92.86	98.64	99.03	98.22	98.15	99.22	
Rb	97.4	38.1	9.8	28.8	40.8	41.1	1.67	35.6
Ba	1320	3330	650	770	1000	1000	117	780
Sr	206	377	299	600	510	510	317	431
Zr	253	140	55	127	224	230	39	204
Nb	20.9	7.6	9.2	6.3	11.1	11.5	1.6	14.8
Y	39.1	72.1	24.3	19.5	29.5	28.8	22.3	24.4
Pb	13.7	8.0	3.7	5.7	10.6	10.5	0.6	11.0
Zn	86	118	70	76	91	91	66	83
V	17	297	253	160	14	14	256	157
Cu	12	28	41	42	2	2	102	43
Ni	0	20	113	12	6	5	168	19
Cr	2	12	72	3	3	1	208	13
Sc	8.5	34	33	15	7.1	7.2	47	17
Ga	19.0	16.4	16.3	19.0	20.0	19.9	17.9	17.3
Cs	4.01		0.06	0.36	0.62	1.14	0.04	0.7
U	3.78		0.24	0.80	1.30	1.31	0.04	1.2
Th	8.9	3.4	0.88	2.37	3.68	3.80	0.16	3.5
Hf	7.1		1.74	3.36	6.0	6.0	1.23	4.7
Ta	1.55		0.58	0.44	0.73	0.75	0.09	0.72
La	30.3	38.3	7.8	17.7	28.7	29.0	3.0	27.3
Ce	60	57	14.3	31.7	55	56	7.2	56
Pr	7.5		1.97	3.91	6.7	6.8	1.15	
Nd	29.7	53	9.4	16.6	28.0	27.7	6.3	24.4
Sm	7.0		2.97	3.89	6.2	6.1	2.44	5.1
Eu	1.69		1.18	1.26	1.76	1.77	1.01	1.51
Gd	6.8		3.58	3.66	5.4	5.2	3.09	
Tb	1.19		0.66	0.57	0.84	0.82	0.58	0.72
Dy	7.3		4.19	3.37	5.0	5.0	3.86	
Ho	1.49		0.91	0.69	1.03	1.03	0.84	
Er	4.2		2.54	1.94	2.93	2.86	2.35	
Tm	0.62		0.36	0.28	0.44	0.43	0.35	
Yb	3.96		2.21	1.73	2.82	2.82	2.20	2.31
Lu	0.64		0.36	0.29	0.47	0.46	0.35	0.32
W								
Sb								
As								
Co								20

Sample No	HP-91-2	HP-91-3	HP-91-4	HP-91-5	HP-91-6	HP-91-7	HP-91-10	HP-91-12
age	**7.68**		**6.35**	**2.89**		**15.65**	**7.096**	**7.093**
error	**0.04**		**0.03**	**0.08**		**0.04**	**0.015**	**0.015**
Lat	43.5697	43.4772	43.4896	43.2703	43.1298	43.1613	43.1776	43.3
Long	119.1373	119.3098	119.3042	119.4518	119.5844	119.8574	120.1190	119.5
SiO2	74.45	73.46	73.42	74.34	47.62	66.77	76.49	75.38
TiO2	0.217	0.212	0.212	0.161	2.03	0.570	0.202	0.162
Al2O3	13.52	14.36	13.96	13.95	16.40	16.24	10.43	12.14
FeO*	1.52	1.73	1.70	1.34	11.4	5.23	3.25	1.89
MnO	0.040	0.050	0.051	0.050	0.204	0.131	0.101	0.091
MgO	0.16	0.44	0.50	0.44	8.2	0.15	0.00	0.10
CaO	0.68	1.74	1.96	1.78	9.99	2.58	0.18	0.69
Na2O	4.32	3.42	3.39	3.31	2.96	4.52	4.83	2.85
K2O	5.05	4.53	4.75	4.58	0.59	3.57	4.50	6.64
P2O5	0.035	0.061	0.061	0.050	0.58	0.25	0.020	0.061
PNT								
Rb	115	110	111	114	6.1	86.6	123	70.2
Ba	498	1110	1150	990	510	1260	175	1820
Sr	27.2	201	202	209	387	248	0.5	25.4
Zr	293	170	162	108	131	312	733	444
Nb	31.8	14.6	14.6	9.7	9.5	24.8	40.7	26.8
Y	41.4	23.1	23.7	10.8	30	32.4	108	73.7
Pb	16.8	18.8	17.3	16.8	5.8	15.9	28.5	15.9
Zn	40	37	36	25	97	79	191	116
V	3	22	18	21	258	14	0	4
Cu	5	9	8	11	87	8	5	4
Ni	7	5	7	5	165	6	14	10
Cr	1	3	3	4	244	2	2	0
Sc	3.8	3.5	3.6	2.7	33	9.6	0.8	
Ga	15.7	14.3	14.5	12.6	18.3	20.8	22.6	17.5
Cs	3.3	3.8	3.8	5.2		1.8	5.8	
U	3.9	4.6	3.5	4.4	0.7	3.9	4.6	2.4
Th	11.2	8.6	9.2	11.3	0.3	8.8	13.3	6.4
Hf	8	4.5	4.6	3.1	3.2	7.9	17.1	
Ta	1.9	1.2	1.2	1.0	0.48	1.6	2.3	
La	41	26.4	26.6	20.4	12.6	32.0	62	
Ce	81	46	47	34.9	29.6	68	139	
Pr								
Nd	33.7	20.6	19.3	13.5	20.4	33.1	68	
Sm	6.3	3.68	3.77	2.19	5.2	7.0	16.2	
Eu	0.44	0.59	0.63	0.41	2.06	1.90	1.37	
Gd								
Tb	1.0	0.48	0.63	0.21	0.97	0.95	2.86	
Dy								
Ho								
Er								
Tm								
Yb	4.5	2.73	2.97	1.36	2.92	3.28	11	
Lu	0.7	0.45	0.44	0.21	0.38	0.46	1.58	
W			4				3	
Sb	1	0.5	0.5	0.8		0.5	2.5	
As	4	2.1	2.3	3.3			14.6	
Co	1.1	2.8	2.8	2.4	49	6.1	0.2	

Sample No	HP-91-13	HP-92-1	HP-92-2	HP-92-3	HP-92-4	HP-92-6	HP-92-7	HP-92-8B
age	**5.739**			11.3	11.3		11.3	
error	**0.016**			0.5 *	0.5 *		0.5 *	
Lat	43.5091	43.2647	43.2917	43.2928	43.2914	43.2896	43.2928	43.2965
Long	119.7401	118.0881	118.0171	118.0143	117.9972	117.9906	117.9942	117.9985
SiO2	77.60	60.84	54.29	76.79	76.80	48.46	76.69	68.06
TiO2	0.086	0.96	2.29	0.14	0.12	2.56	0.16	0.94
Al2O3	12.19	16.54	15.16	12.57	12.31	15.21	12.66	13.26
FeO*	1.10	6.1	11.2	0.82	1.36	13.0	1.04	4.65
MnO	0.030	0.12	0.19	0.04	0.05	0.21	0.04	0.09
MgO	0.02	2.88	3.41	0.11	0.07	6.3	0.14	2.08
CaO	0.37	6.13	6.75	0.57	0.38	9.86	0.62	3.44
Na2O	4.04	3.52	3.40	3.25	3.25	2.74	2.97	2.84
K2O	4.56	2.54	2.50	5.69	5.65	0.91	5.66	4.39
P2O5	0.015	0.33	0.76	0.02	0.02	0.68	0.03	0.24
PNT		97.97	97.63	97.02	95.84	98.64	95.59	97.26
Rb	99.1	39	49	185	174	23	176	145
Ba	750	1130	1290	500	137	640	620	550
Sr	8.6	550	405	40	10	304	65	155
Zr	245	195	245	129	329	176	127	141
Nb	22.0	24	28	25	62	33	28	40
Y	93.6	31	34	28	76	15	24	27
Pb	17.1							
Zn	112							
V	1							
Cu	0							
Ni	11							
Cr	2	56	39	22	44	152	28	73
Sc								
Ga	20.1							
Cs								
U	4							
Th	8							
Hf								
Ta								
La								
Ce								
Pr								
Nd								
Sm								
Eu								
Gd								
Tb								
Dy								
Ho								
Er								
Tm								
Yb								
Lu								
W								
Sb								
As								
Co								

Sample No	HP-92-9	HP-92-10	HP-93-2	HP-93-3	HP-93-4	HP-93-5	HP-93-6	HP-93-8
age	11.3	11.3	**7.177**		**7.126**			
error	0.5 *	0.5 *	**0.014**		**0.015**			
Lat	43.3144	43.3236	43.4328	43.4464	43.3942	43.3922	43.3839	43.3939
Long	118.0253	118.0426	119.8533	119.8803	119.8264	119.8256	119.8703	119.8653
SiO2	77.46	77.14	77.67	77.55	75.95	75.39	70.52	70.98
TiO2	0.15	0.13	0.12	0.11	0.13	0.16	0.55	0.53
Al2O3	12.17	12.44	12.15	12.20	13.12	13.40	15.15	14.84
FeO*	0.83	0.96	0.68	0.69	1.00	1.14	2.58	2.39
MnO	0.04	0.04	0.08	0.07	0.05	0.05	0.05	0.06
MgO	0.15	0.15	0.00	0.00	0.00	0.00	0.20	0.36
CaO	0.78	0.56	0.30	0.24	0.64	0.72	1.71	1.66
Na2O	2.98	3.40	4.03	4.42	4.48	4.62	5.26	4.66
K2O	5.40	5.16	4.96	4.69	4.61	4.50	3.85	4.41
P2O5	0.03	0.03	0.01	0.02	0.01	0.02	0.12	0.11
PNT	96.95	98.91	99.47	99.90	98.56	98.79	101.03	98.51
Rb	183	169	128	131	105	103	87	89
Ba	570	428	83		1360	1420		900
Sr	84	42	3	4	42	55	185	160
Zr	108	108	133	133	140	175	295	301
Nb	24	28	42	41	18.6	18.1	24	23.9
Y	31	19	101	101	41	43	31	33
Pb			22	20	17	18	12	12
Zn			90	75	45	44	49	55
V			0	0	0	0	20	22
Cu			4	1	13	11	7	14
Ni			15	16	11	10	8	11
Cr	49	35	2		2	1		3
Sc			4.1		3.9	4.4		6.4
Ga			19	19	15	15	19	18
Cs			4.5		4.8	4.7		3.1
U			4.32		2.56	3.06		3.74
Th			9.7		7.4	7.2		9.3
Hf			6.8		5.4	6.3		8.2
Ta			2.17		1.01	1.06		1.39
La			17.7		32.5	31.9		33.9
Ce			50		69	71		73
Pr								
Nd			29.1		31.5	32.7		31.6
Sm			8.2		6.2	6.1		6.2
Eu			0.57		0.7	0.83		1.2
Gd								
Tb			2.06		1.03	1.05		0.9
Dy								
Ho								
Er								
Tm								
Yb			10.2		4.4	4.3		3.34
Lu			1.6		0.67	0.67		0.52
W			1.2		1.2	0.8		1.6
Sb			1.48		2.67	2.57		0.64
As			4.6		18.1	17.3		3.3
Co			0.1		0.5	0.6		2.3

Sample No	HP-93-10	HP-93-11	HP-93-12	HP-93-13C	HP-93-14C	HP-93-15	HP-93-16	HP-93-18
age				**7.171**			**7.28**	
error				**0.018**			**0.016**	
Lat	43.4006	43.4311	43.3447	43.3528	43.2325	43.2278	43.2236	43.1378
Long	119.8758	119.9064	119.8589	119.8506	120.0944	120.1081	120.1081	120.1547
SiO2	77.25	76.93	73.69	77.56	85.52	76.28	77.93	76.66
TiO2	0.12	0.12	0.30	0.11	0.12	0.16	0.15	0.17
Al2O3	12.51	12.08	13.89	12.08	7.33	11.59	10.76	10.83
FeO*	0.75	0.66	1.78	0.69	1.56	2.32	1.98	2.57
MnO	0.09	0.08	0.05	0.08	0.05	0.06	0.06	0.07
MgO	0.00	0.00	0.13	0.00	0.00	0.00	0.14	0.00
CaO	0.33	1.17	1.12	0.30	0.28	0.34	0.24	0.22
Na2O	4.10	4.36	4.22	3.86	1.78	4.26	4.23	4.95
K2O	4.84	4.58	4.76	5.31	3.36	4.96	4.46	4.52
P2O5	0.01	0.02	0.05	0.00	0.01	0.01	0.05	0.00
PNT	98.78	99.46	98.85	99.75	96.85	98.76	99.50	99.17
Rb	128	125	101	134	83	118	111	121
Ba	62		950	62	207		161	105
Sr	4	11	100	1	6	49	6	1
Zr	137	132	264	138	305	548	500	551
Nb	42	41	21.7	42	21.5	36	32.2	37
Y	99	104	33	101	58	104	81	103
Pb	20	18	12	22	13	25	36	20
Zn	88	83	45	88	96	161	158	171
V	0	0	5	0	0	0	0	0
Cu	13	14	8	7	27	7	14	11
Ni	16	19	12	15	11	14	13	14
Cr	4		2	2	3		2	2
Sc	4.2		5.3	4.2	0.6		0.7	0.6
Ga	19	20	15	19	21	23	20	23
Cs	4.3		3.4	4.6	2.9		2.0	5.6
U	4.70		3.81	4.43	3.91		3.50	5.0
Th	9.7		8.8	10.2	6.5		10.9	11.9
Hf	6.8		7.7	7.2	8.6		15.1	16.7
Ta	2.16		1.32	2.23	1.01		1.81	2.07
La	18.7		30.0	19.4	30.1		55	59
Ce	50		63	56	70		125	141
Pr								
Nd	31.1		28	31.4	38		60	71
Sm	9.0		5.5	9.1	8.1		13	15.3
Eu	0.6		0.8	0.62	0.68		1.12	1.2
Gd								
Tb	2.13		0.81	2.27	1.47		2.35	2.72
Dy								
Ho								
Er								
Tm								
Yb	10.7		3.38	10.8	5.8		9.5	10.9
Lu	1.64		0.5	1.69	0.9		1.39	1.67
W	2.0		1.6	1.8	0.7		0.7	1.9
Sb	1.49		1.1	1.49	2.03		1.9	2.45
As	4.5		5.2	4.6	5.6		7.1	14.1
Co	0.2		1.5	0.2	0.1		0.3	0.2

Sample No	HP-93-19	HP-93-20	HP-93-21	HP-93-23	HP-93-25	HP-93-26	HP-93-27	HP-93-28
age					**7.176**			
error					**0.014**			
Lat	43.1389	43.1103	43.1167	43.1264	43.2517	43.3429	43.5220	43.4924
Long	120.1472	120.1528	120.1550	120.0764	120.0397	119.6603	119.5104	119.9433
SiO2	75.12	76.77	71.72	48.44	76.16	53.72	53.95	76.29
TiO2	0.17	0.17	0.41	1.06	0.18	1.80	1.34	0.07
Al2O3	10.85	10.85	13.89	16.93	11.03	16.22	16.98	13.41
FeO*	2.61	2.48	3.02	9.7	2.76	9.3	8.7	0.57
MnO	0.07	0.07	0.18	0.18	0.08	0.17	0.16	0.06
MgO	0.16	0.00	0.19	9.7	0.00	5.1	5.1	0.00
CaO	1.04	0.22	0.49	11.2	0.30	7.96	8.49	0.81
Na2O	3.94	4.94	6.64	2.58	4.69	3.80	3.63	4.02
K2O	5.91	4.50	3.37	0.16	4.77	1.39	1.19	4.77
P2O5	0.11	0.00	0.09	0.09	0.03	0.59	0.44	0.01
PNT	97.62	99.73	100.22	98.98	98.82	100.03	98.78	99.09
Rb	126	123	59	2	111	21	17	131
Ba		90		213	123	680	610	332
Sr	53	2	45	214	9	372	447	31
Zr	541	552	305	63	504	201	160	67
Nb	37	38	20.3	3.6	34.6	18.6	12.4	12.8
Y	105	104	76	23	90	37	26	35
Pb	22	24	10	0	22	7	2	17
Zn	183	170	116	74	143	100	86	21
V	0	0	0	243	0	207	205	0
Cu	13	8	8	149	7	38	69	4
Ni	15	12	13	207	13	47	48	11
Cr		2		319	3	71	80	2
Sc		0.5		38	1.1	27	26	3.7
Ga	23	25	21	14	25	19	16	16
Cs		5.5		0.4	4.5	0.6	0.3	5.4
U		4.58		1	4.47	0.83	0.62	4.75
Th		11.7		0.55	10.1	1.81	1.24	10.4
Hf		16.3		1.58	14.6	5.3	4.01	3.23
Ta		2.04		0.08	1.81	0.88	0.51	1.03
La		60		2.4	52	23.3	18.5	17.1
Ce		139		7.4	117	50	39.1	36.6
Pr								
Nd		74		7	56	25.3	20.4	17
Sm		15.1		2.21	12.8	6.7	4.9	3.98
Eu		1.13		0.93	1.03	2.14	1.66	0.43
Gd								
Tb		2.68		0.53	2.25	1.09	0.77	0.74
Dy								
Ho								
Er								
Tm								
Yb		10.7		2.17	9.3	3.46	2.52	3.63
Lu		1.63		0.33	1.4	0.54	0.39	0.58
W		1.5		3.7	4	3.5	6	2.5
Sb		2.51		0.15	2	0.2	0.17	0.33
As		13.8		1.8	11.8	7	5	3
Co		0.2		48	0.4	29.3	28.9	0.4

Sample No	HP-93-29	HP-93-30	HP-93-31	HP-93-32	HP-93-33	HP-93-34	HP-93-37A	HP-93-39
age	**2.09**							
error	**0.18**							
Lat	43.4944	43.62	43.6554	43.13	43.0931	43.0931	43.1556	43.1569
Long	119.9325	120.46	120.2510	119.94	119.9361	119.9361	118.4917	118.4944
SiO2	50.53	67.40	52.31	75.67	47.76	75.13	70.76	64.87
TiO2	1.81	0.77	1.24	0.14	0.77	0.23	0.48	0.96
Al2O3	16.30	14.93	16.67	11.93	17.78	12.79	14.95	15.79
FeO*	10.0	4.54	9.1	1.53	9.4	1.88	2.40	4.80
MnO	0.18	0.10	0.16	0.09	0.21	0.08	0.10	0.12
MgO	6.9	1.23	6.4	0.24	10.4	0.21	0.37	1.53
CaO	9.80	3.45	9.60	1.32	11.4	0.91	1.80	4.02
Na2O	3.41	4.58	3.40	3.37	1.95	3.22	4.47	3.99
K2O	0.69	2.78	0.77	5.64	0.20	5.53	4.58	3.58
P2O5	0.38	0.23	0.35	0.06	0.09	0.03	0.09	0.34
PNT	99.61	99.53	99.03	96.04	100.03	99.07	98.58	99.33
Rb	10	62	11	80	2	123	85	67
Ba	358			930	163			1250
Sr	262	198	462	56	197	59	219	371
Zr	164	219	115	317	47	250	271	219
Nb	18.6	12.6	8.6	28.1	2.1	37	21.4	13.9
Y	35	45	23	80	22	88	40	30
Pb	2	10	1	12	1	18	10	9
Zn	84	80	77	112	55	107	67	75
V	219	54	228	0	238	1	12	67
Cu	45	55	67	12	120	31	16	25
Ni	87	12	68	12	196	16	11	9
Cr	163			2	220			9
Sc	35			3.9	40			11
Ga	15	17	19	18	14	20	16	15
Cs	0.5			2.5	0.4			1.3
U	3			2.67	2			1.59
Th	1.41			6.3	0.44			3.5
Hf	4.44			9.8	1.13			5.9
Ta	1.00			1.39	0.07			0.76
La	15.3			45	2.1			27.4
Ce	34.2			110	5.7			61
Pr								
Nd	20.3			55	5.6			28.8
Sm	5.2			13.1	1.76			5.9
Eu	1.75			1.7	0.75			1.64
Gd								
Tb	1.01			2.12	0.45			0.87
Dy								
Ho								
Er								
Tm								
Yb	3.24			8.0	2.26			2.67
Lu	0.46			1.24	0.34			0.39
W	2.6			2.9	3.8			1.9
Sb	0.21			1.17	0			0.2
As	3			5.0	1.1			3.4
Co	36.9			0.8	43			10.6

Sample No	HP-93-40	HP-93-42	HP-93-43	HP-93-44	HP-93-45	DO-93-4	DO-93-7	DO-93-8
age			10.6	10.6	9.48			
error			0.7 *	0.7 *	0.3 *			
Lat	43.1575	43.1435	43.2208	43.2336	43.3441	43.2319	43.2689	43.2767
Long	118.4936	118.5612	118.5461	118.5811	118.4360	119.3581	119.3064	119.3189
SiO2	70.23	66.15	76.15	74.51	76.27	71.58	71.67	71.69
TiO2	0.58	1.27	0.10	0.14	0.10	0.42	0.39	0.39
Al2O3	15.27	14.61	12.69	12.99	13.06	14.37	14.48	14.45
FeO*	2.45	8.4	1.09	2.03	0.84	2.28	2.03	2.08
MnO	0.03	0.06	0.03	0.06	0.05	0.05	0.05	0.05
MgO	0.31	0.47	0.00	0.00	0.00	0.21	0.29	0.34
CaO	2.06	4.83	0.79	0.32	0.97	1.37	1.35	1.39
Na2O	4.65	2.68	3.37	4.83	3.14	4.60	4.47	4.33
K2O	4.24	1.32	5.75	5.07	5.51	5.03	5.20	5.21
P2O5	0.18	0.22	0.03	0.06	0.06	0.08	0.07	0.07
PNT	100.43	98.16	98.83	100.09	98.05	99.14	98.67	98.74
Rb	97	28	111	134	190	138	106	105
Ba		461		154	238	964	1020	1020
Sr	263	317	41	8	78	75	88	89
Zr	232	90	124	416	92	286	280	280
Nb	18.1	8.4	20.5	55	15.6	18.7	21.3	21.1
Y	40	27	28	64	23	37	30	31
Pb	9	4	15	32	21	12	11	21
Zn	34	81	36	102	23	37	33	33
V	22	168	0	2	2	0	11	7
Cu	6	150	9	6	6	15	6	8
Ni	7	29	10	12	12	12	8	10
Cr		137		2	1	2	2	5
Sc		35		3.3	2.0	5.5	1	3
Ga	16	18	12	22	15	16	16	14
Cs		15.8		1.4	8.8	4.8		
U		3		4.07	9.3	5.8		
Th		1.13		10.9	17.2	15.1	10	11
Hf		2.55		13.3	3.51	9.1		
Ta		0.52		2.85	1.67	1.21		
La		9.1		66	19.8	26.9		
Ce		19.4		139	37.9	55		
Pr								
Nd		10.8		63	17.6	24		
Sm		3.38		11.9	3.63	5.3		
Eu		1.04		0.54	0.37	0.87		
Gd								
Tb		0.67		1.88	0.53	0.88		
Dy								
Ho								
Er								
Tm								
Yb		2.74		3.79	2.44	4.1		
Lu		0.4		1.04	0.37	0.63		
W		4.7		2.3	1.3	2.3		
Sb		8.75		1.67	0.46	0.84		
As		100		7.5	2.2	3.2		
Co		21.6		0.6	0.6	2.8		

Sample No	DO-93-12	DO-93-13	DO-93-15	DO-93-16	DO-93-18	DO-93-19	DO-93-22	ER-93-1
age		**8.28**						
error		**0.05**						
Lat	43.2608	43.2508	43.2619	43.2539	43.2611	43.2564	43.2564	43.3711
Long	119.2789	119.2611	119.2847	119.2792	119.3383	119.3433	119.3737	119.7883
SiO2	76.75	71.88	76.78	76.52	71.67	70.16	48.55	75.10
TiO2	0.13	0.39	0.13	0.13	0.40	0.51	1.22	0.17
Al2O3	11.39	14.53	11.40	11.39	14.32	14.28	16.99	13.25
FeO*	2.13	1.91	2.11	2.15	2.24	2.63	10.2	1.64
MnO	0.04	0.05	0.05	0.05	0.05	0.06	0.18	0.07
MgO	0.00	0.25	0.06	0.00	0.24	0.63	8.7	0.00
CaO	0.17	1.36	0.29	0.23	1.34	2.44	11.0	0.60
Na2O	4.89	4.74	4.39	5.10	4.64	4.58	2.66	4.51
K2O	4.47	4.82	4.77	4.43	5.01	4.56	0.30	4.64
P2O5	0.03	0.07	0.02	0.00	0.76	0.17	0.24	0.02
PNT	100.75	98.68	98.33	100.13	99.97	98.13	100.55	98.80
Rb	106	105	107	105	138	124	3	95
Ba		1010	29		920	980	184	1480
Sr	3	87	9	1	71	106	258	26
Zr	473	275	493	474	276	284	77	282
Nb	50	20.9	52	52	19.9	19	4.8	22.2
Y	36	30	82	82	37	37	24	60
Pb	12	11	13	21	12	10		20
Zn	123	35	114	114	38	40	74	70
V	0	21	0	0	5	24	247	0
Cu	7	10	11	7	6	19	75	10
Ni	9	9	13	12	8	11	156	13
Cr	0	3	3	1	6	4	176	3
Sc	3	4.7	0.7	8	8	6.6	36	7.6
Ga	23	16	25	26	16	17	16	18
Cs		3.2	2.9			3.5	0.5	5.1
U		3.68	3.37			5.6	2	3.17
Th	8	9.3	9.6	9	14	12.9	0.32	7
Hf		8.2	14.3			8.6	1.98	8.5
Ta		1.31	2.63			1.23	0.19	1.06
La		27.1	62			26.9	6.2	38
Ce		51	126			54	14.2	76
Pr								
Nd		21.3	56			24.1	10.3	42
Sm		4.4	11.9			5.5	2.94	9.0
Eu		0.77	0.28			0.99	1.18	1.08
Gd								
Tb		0.74	2.02			0.88	0.62	1.45
Dy								
Ho								
Er								
Tm								
Yb		3.36	8.5			4.3	2.38	6.2
Lu		0.54	1.33			0.61	0.37	0.95
W		2.6	3.2			3.2	4	3.1
Sb		0.67	0.61			0.58	0.28	2.36
As		2.6	2.4			2.8	3.1	17.7
Co		2.6	0.5			3.6	47	0.4

Sample No	ER-93-6	JN-94-4	JN-94-5	JN-94-9	JN-94-11	JN-94-16
age						
error						
Lat	43.3558	43.2	43.2	43.2	43.2	43.2
Long	119.7282	118.3	118.3	118.3	118.3	118.3
SiO2	74.26	70.79	64.52	64.45	69.92	75.03
TiO2	0.19	0.34	0.84	0.84	0.48	0.06
Al2O3	13.64	15.38	14.77	14.59	13.66	13.98
FeO*	1.68	2.52	5.65	5.56	3.19	0.85
MnO	0.06	0.08	0.12	0.12	0.09	0.07
MgO	0.00	0.46	2.86	3.04	1.76	0.00
CaO	0.77	2.27	4.33	4.37	3.13	1.10
Na2O	4.98	4.48	3.36	3.59	3.57	4.34
K2O	4.39	3.57	3.36	3.21	4.09	4.55
P2O5	0.02	0.12	0.20	0.18	0.13	0.02
PNT	99.50	101.77	100.40	100.83	99.80	101.49
Rb	100	59	132	132	143	141
Ba	1490	1900	197	154	107	510
Sr	38	305	135	132	89	84
Zr	292	169	94	93	92	83
Nb	22.9	12.7	24.1	26.3	25.7	17.0
Y	54	20	37	37	32	27
Pb	16	16	15	17	18	23
Zn	57	48	62	64	46	36
V	2	20	128	119	51	4
Cu	6	9	21	16	5	5
Ni	13	7	39	42	28	9
Cr	1	2	33	36	26	1
Sc	9	14	25	20	12	6
Ga	18	15	19	19	16	19
Cs						
U						
Th	7	3	9	9	13	4
Hf						
Ta						
La		28	12	6	17	14
Ce		32	12	42	44	24
Pr						
Nd						
Sm						
Eu						
Gd						
Tb						
Dy						
Ho						
Er						
Tm						
Yb						
Lu						
W						
Sb						
As						
Co						

Errors	Standard error	"Largest"	applicable	applied to	LOD - WSU	LOD - WSU
	95 % confidence	error on	percent error	concentrations	XRF	ICP-MS
	interval	replicates		above	(at 2 - sigma)	(at 2 - sigma)
	w t % or ppm	(%)	(%)	w t % or ppm	w t % or ppm	w t % or ppm
SiO2	0.06	0.10	0.10	all	0.19	
TiO2	0.003	1.4	0.7	0.25	0.012	
Al2O3	< 0.03	0.25	0.25	all	0.082	
FeO*	0.07	10	3.0	2.0	0.18	
MnO	0.005	8	5.0	all	0.002	
MgO	0.02	30	2.5	0.5	0.073	
CaO	< 0.02	5	1.0	1.25	0.043	
Na2O	< 0.02	0.4	0.4	all	0.036	
K2O	< 0.01	0.3	0.25	all	0.015	
P2O5	< 0.01	10	3.0	0.03	0.003	
PNT						
Rb	0.35	5	1.0	35	*1.7*	0.67
Ba	12.7	7	3.0	300	*11.7*	12.7
Sr	1.0	3.0	< 1.0	100	*4.6*	7.0
Zr	1.3	1.7	< 1.0	100	*3.3*	1.9
Nb	0.15	4.0	< 1.0	10.0	*1.2*	0.29
Y	0.2	1.0	1.0	all	*1.2*	0.29
Pb	0.15	3.4	< 2.0	10.0	*2.6*	0.29
Zn	1.7	2.3	2.5	all	3.3	
V	1	100	10	10	5.0	
Cu	1.5	100	20	5	7.4	
Ni					3.5	
Cr	0.5	100	10	10	3.0	
Sc	0.4	30	5.0	5	*1.6*	3.6
Ga	0.5	2.6	2.5	all	2.7	
Cs	0.02	13	< 1.0	1.0	*5.1*	0.03
U	0.02	4.0	< 2.0	2.0	*2.7*	0.11
Th	0.08	11	< 2.0	5.0	*1.6*	0.49
Hf	0.06	2.8	< 1.0	5.0		0.07
Ta	0.01	6	< 2.0	0.5		0.02
La	0.42	2.5	< 2.0	all	*5.7*	0.49
Ce	0.60	2.4	< 2.0	all	*7.9*	0.62
Pr	0.09	1.7	< 2.0	all		0.06
Nd	0.37	2.0	< 2.0	all	*4.3*	0.48
Sm	0.09	2.4	< 2.0	all		0.15
Eu	0.01	1.4	< 2.0	all		0.04
Gd	0.06	2.0	< 2.0	all		0.08
Tb	0.02	4.1	< 2.0	all		0.01
Dy	0.08	3.0	< 2.0	all		0.10
Ho	0.01	1.5	< 2.0	all		0.02
Er	0.05	2.9	< 2.0	all		0.06
Tm	0.01	1.7	< 2.0	all		0.01
Yb	0.05	3.0	< 2.0	all		0.03
Lu	0.01	2.5	< 2.0	all		0.01
W			< 10			
Sb			< 20			
As			< 20			
Co			< 5			

Appendix 2: Summary Table for Geochemical Methods for This Study:

This table shows the methods for major and trace element geochemistry for previously unpublished samples. See Chapter 2 for method details for XRF and ICP-MS.

Sample Prefix	Approximate geographic location	Major Elements	Trace Elements	Exceptions
MTF	HLP and NWBR – province wide	XRF (WSU)	XRF, ICPMS+	none
KCS	Gearhart Mt and Beatys Butte (eastern NWBR)	XRF (WSU)	XRF, ICPMS+	none
HP 91-xx	RST area (central HLP)	XRF (WSU)	XRF, INAA#	11, 12, 13, 14: Ba by XRF
HP 92-xx	Stockade Butte area (HLP)	XRAL	XRAL	none
HP 93-xx	RST area (central HLP)	XRF (WSU)	XRF, INAA##	none
DO-xx	Western Harney Basin (HLP)	XRF (WSU)	XRF, INAA###	7, 8, 12, 16, 18: Cr, Sc, Th by XRF
ER-xx	Egli Ridge (south of Juniper Ridge) (HLP)	XRF (WSU)	XRF, INAA###	3, 6: Cr, Sc, Th by XRF
JN-xx	Malheur Cave area (eastern HLP)	XRF (WSU)	XRF, INAA###	none

\+ XRF: Zn, V, Cu, Ni, Ga
ICP-MS: Rb, Ba, Sr, Zr, Nb, Y, Pb, Sc, Cs, U, Th, Hf, Ta, La, Ce, Pr, Nd, Sm, Eu, Gd, Tb, Dy, Ho, Er, Tm, Yb, Lu

\# XRF: Rb, Sr, Zr, Nb, Y, Pb, Zn, V, Cu, Ni, Cr, Ga, U, Th
INAA: Ba, Sc, Cs, Hf, Ta, W, Sb, As, Co, La, Ce, Nd, Sm, Eu, Tb, Yb, Lu

XRF: Rb, Sr, Zr, Nb, Y, Pb, Zn, V, Cu, Ni, Ga
INAA: Ba, Cr, Sc, Cs, U, Th, Hf, Ta, W, Sb, As, Co, La, Ce, Nd, Sm, Eu, Tb, Yb, Lu

XRF: Rb, Ba, Sr, Zr, Nb, Y, Pb, Zn, V, Cu, Ni, Ga
INAA: Cr, Sc, Cs, U, Th, Hf, Ta, W, Sb, As, Co, La, Ce, Nd, Sm, Eu, Tb, Yb, Lu

Appendix 3: Database References

This table gives the sources and general locations for most data from the literature used in the major and trace element geochemistry for this work.

General area	References	notes
HLP and NWBR – province wide	Walker, 1981	Reconnaissance-style sampling
Central HLP, Rattlesnake Tuff	Streck and Grunder, 1997 Streck and Grunder, 1999 Streck and Grunder, 2008	Includes a few local basalts, rhyolites and inclusions within the RST
Central HLP, northern margin	Iademarco, 2009	Hampton Butte and surrounding area
Eastern HLP	Johnson and Grunder, 2000 Johnson, 1995	Duck Creek Butte and surrounding area
Eastern HLP,	Green, 1973	Devine Canyon Tuff
Mostly HLP, province wide	Jordan, et al., 2004 Jordan, 2001	Basalt focus with some from the NWBR, some rhyolites
Western HLP	Johnson, 1998	Frederick Butte
Central HLP,	MacLean, 1994	Juniper Ridge; Burns Butte
Central HLP	Berri, 1982 Roche, 1987	Glass Buttes, mostly rhyolites, some altered
Eastern NWBR	Wells, 1979 Wells, 1975	Drake's Peak
Eastern NWBR	Scarberry, 2007	Lake Abert area, Beatys Butte, some basalts and rhyolites
Central NWBR	Brikowski, 1983	Gearhart Mountain
Eastern NWBR	Hering, 1981	Yamsay Mountain
Newberry Volcano	MacLeod et al., 1995 Linneman, 1990 Higgins, 1973	
K-Ar dates	Fiebelkorn, et al., 1983 and sources therein	Updated ages (new constants applied) from previous workers

Additional references from this appendix only that are not cited in the chapters:

Linneman, S. R., 1990, The petrologic evolution of the Holocene magmatic system of Newberry volcano, central Oregon: University of Wyoming PhD thesis, 293 p.

Wells, R. E., 1975, Geology of the Drake Peak rhyolite complex and the surrounding area, Lake County, Oregon: University of Oregon MS thesis, 130p.

Appendix 4: Phenocryst Assemblages from the Literature

This table gives a generalized account of the major phenocryst assemblage details from the literature for samples used this work (see Table4, Chapter 2). SiO_2 content is given to help cross reference samples in Table 1 (Ford, Chapter 2) or Appendix 1. Aph = aphyric, with an asterisk (*) indicating very few phenocrysts are present; diseq. texture indicates if disequilibrium textures are either X = limited but present, XX = prevalent, or XXX = pervasive; ref. = the literature reference for the data (see below). For phases, qtz = quartz, alk feld = alkali feldspar (Na or K), plag = plagioclase (generally andesine or more calcic), cpx = clinopyroxene, opx = orthopyroxene, fa = fayalite, amph = amphibole, bt = biotite, op = opaque minerals where X = very uncommon or not present in all samples from that location, XX = sparse, but generally present, XXX = commonplace. Where left blank, phase was not observed. Disequilibrium textures for Drake's Peak samples with asterisk (*) are not noted for individual samples, but plagioclase is commonly resorbed and biotite commonly is "strongly resorbed and rimmed or replaced by granular iron oxides" (Wells, 1979). Disequilibrium textures for Gearhart Mountain samples with double asterisk (**) are not noted for individual samples, but most amphibole is replaced by opacite and where amphibole and clinopyroxene coexist, the pyroxene is corroded (Brikowski, 1983). Both authors indicate that disequilibrium textures are common in samples from their study.

Sources for data are as follows (all listed in the reference section):

1. Berri, 1982
2. Roche, 1987
3. Johnson, 1998
4, MacLeod et al., 1995
5. Johnson and Grunder, 2000
6. Johnson, 1995
7. MacLean, 1994
8. Wells, 1975
9. Wells, 1979
10. Brikowski, 1983
11. Hering, 1981

Samples from the HLP from the literature													
	SiO2	aph*	diseq.	ref	qtz	alk	plag	cpx	opx	fa	amph	bt	op
			texture			feld				(ol)			
Berri 1	74.87			1			XX	XX					XX
Berri 2	74.00			1			XX	XX					XX
Berri 3	75.83			1			XX	XX					XX
Berri 4	75.61	X		1									
Berri 5	77.07			1	XX	XX	XX	XX					
Berri 6	77.37			1	XX	XX	XX	XX					
Berri 7	77.46			1	XX	XX	XX	XX					
Berri 8	77.51			1	XX	XX	XX	XX					
Berri 9	77.85			1	XX	XX	XX	XX					
Berri 10	78.71			1	XX	XX	XX	XX					
EGB-1	78.51	X		2									
RB-1	75.10			2			XX	XX					XX
GB-7	78.43	X		2									
GB-44A	78.73	X		2									
GB-67	78.77	X		2									
GB-82	78.61			2	XX	XX	XX					XX	
GB-85	77.59			2	XX	XX	XX					XX	
GB-131	78.71			2	XX	XX	XX					XX	
GB-151	78.45	X		2									
FB-94-10	77.06			3	XX	XX							
FB 94-12	74.59			3			XX	XX		XX			XX
FB-94-15	66.28		XX	3			XX	XX	XX				XX
FB-94-19	74.44			3		XX	XX			XX			XX
FB-94-24	67.74			3			XX	XX	X	XX			XX
GW 4A	73.88			4			XX	*XX*	XX	XX			
GW 5A	74.83			4			XX	*XX*	XX	XX			
GW 6A	75.23	X		4									
GW 29A	72.31			4			XX	*XX*	XX	XX			
GW 30A	75.04			4			XX	*XX*	XX	XX			
GW 31A	74.50			4			XX	*XX*	XX	XX			
JJ 92-1	70.19		X	5, 6			XX	*XX*	XX		X	XX	XX
JJ 92-4	76.35		X	5, 6	XX	XX	XX				XX		
JJ 92-5	76.00			5, 6	XX	XX	XX				XX		
JJ 92-7	70.26		X	5, 6			XX	XX	XX		X	XX	XX
JJ 92-88	70.08		X	5, 6			XX	XX	XX		X	XX	XX
JJ 92-90	76.52			5, 6	XX	XX					X		
JJ 92-101	69.47		X	5, 6			XX	XX	XX		X	XX	XX
JJ 92-102	66.27		XX	5, 6	XX		XX	XX	XX		X		XX
JJ 93-158	76.04	X		5, 6									
JN 94-16	75.03	X		5, 6									

	SiO2	aph*	diseq. texture	ref	qtz	alk feld	plag	cpx	opx	fa (ol)	amph	bt	op
JR-91-2	77.52		XX	7	XX	XX	x	XX	X	X			X
JR-91-4	77.46	X		7									
JR-91-5	75.24			7			X	X	X				X
JR-91-13	77.19		X	7	XX	XX	X	XX	X	XX			X
JR-91-18	77.06		X	7	XX	XX	X	XX	XX	X			X
JR-91-19	73.75		XX	7	X	X	XX	X		X?			XX
JR-91-20	77.48	X		7									
JR-91-25	77.40	X		7									
JR-91-34	75.31			7			X	X	X				X
JR-91-35	75.47			7			X	X	X				X
JR-91-44	67.84		X	7		XX	XX	XX		X?			XX
JR-92-48	72.74			7		XX	XXX		XX				XX
JR-92-50	63.60		X	7		XX	XX	XX		X?			XX
JR-92-51	72.44			7		XX	XX		XX				XX
JR-92-54	72.75			7		XX	XX		XX				XX
JR-92-56	73.92	X		7									
JR-92-62	75.24			7			X	X	X				X
JR-92-63	65.14		X	7		XX	XX	XX					XX
JR-92-65	76.71	X		7									
JR-92-71	63.53		XX	7	X	X	XX	X		X?			XX
JR-92-72	75.16			7			X	X	X				X
HP-91-13	77.60		XX	7	XX	XX	X	XX	X	X			X

Samples from the NWBR from the literature													
	SiO2	aph*	diseq. texture	ref	qtz	alk feld	plag	cpx	opx	fa	amph	bt	op
Drake 83	71.01		*	8,9	X		XXX	X	XX		X	XXX	X
Drake 103	71.61		*	8,9	X		XXX	X	XX		X	XXX	X
Drake 103A	71.83		*	8,9	X		XXX	X	XX		X	XXX	X
Drake 109	70.98		*	8,9	X		XXX	X	XX		X	XXX	X
Drake 112	71.14		*	8,9	X		XXX	X	XX		X	XXX	X
Drake 122	71.59		*	8,9	X		XXX	X	XX		X	XXX	X
Drake 125	70.93		*	8,9	X		XXX	X	XX		X	XXX	X
Drake 131	72.38		*	8,9	X		XXX	X	XX		X	XXX	X
Drake 134	74.62		*	8,9	X		XXX				X	XXX	
Drake 139	74.01		*	8,9	X		XXX				X	XXX	
Drake 141	72.57		*	8,9	X		XXX	X	XX		X	XXX	X
Drake 144	76.16	X		8,9									
Drake 149	76.35	X		8,9									
GW 10C	76.32	X		8,9									
81-36	69.12		**	10			XXX					XXX	XX
81-58	66.84		**	10			XXX					XXX	XX
80-84	63.57		**	10			XXX	XXX	XXX		XXX		XX
81-113	63.65		**	10			XXX		XXX				XX
80-220	63.29		**	10			XXX	XXX	XXX		XXX		XX
80-284	64.06		**	10			XXX	XXX	XXX				XX
80-379	65.01		**	10			XXX	XXX	XXX		XXX		XX

	SiO2	aph*	diseq. texture	ref	qtz	alk feld	plag	cpx	opx	fa	amph	bt	op
YM-27	67.64		XXX	11			XXX	XXX	XXX		X		XX
YM-32	71.94		XXX	11			XXX		XXX				XX
YM-37	66.32		X	11			XXX	XXX	XXX		XXX		XX
YM-56	67.71		X	11			XXX	XXX	XXX		XXX		XX
YM-58	67.82		X	11			XXX	XXX	XXX		XXX		XX
YM-73	67.87		X	11			XXX	XXX	XXX		XXX		XX
YM-74a	68.12		XX	11			XXX	XXX	XXX		XXX		XX
YM-77	68.77		XXX	11			XXX	XXX	XXX		XXX		XX
YM-82	70.38		XX	11			XXX	XXX	XXX		X		XX
YM-83	68.75		X	11			XXX	XXX	XXX		X		XX
YM-92	65.36			11			XXX	XXX	XXX		X		XX
YM-103	67.89		XXX	11			XXX	XXX	XXX		XXX		XX
YM-109	69.12		XXX	11			XXX	XXX	XXX				XX
YM-110	66.67			11			XXX	XXX	XXX		XXX		XX
YM-125	68.87		XX	11			XXX	XXX	XXX		XXX		XX
YM-131	74.79	X*		11			X						
YM-150	73.42			11			XXX						XX
YM-156	68.59		XXX	11			XXX	XXX	XXX				XX
YM-159	69.96	X*		11			X						XX
YM-161	74.48	X		11									
YM-163	66.73			11			XXX	XXX	XXX		XXX		XX
YM-274	73.43			11			XXX						XX

Appendix 5: Petrogenetic Summaries of Comparison Suites:

Below we provide petrogenetic summaries of comparison suites including the Snake River Plain, Iceland and the Cascades.

Data presented for Iceland and the Cascades are from the GEOROC database which contains published whole rock geochemical data on more than 3,100 samples from Iceland and more than 1,950 samples from the Washington, Oregon and California Cascades, including Medicine Lake. The SRP data come from a database that largely duplicates the data compilation of Christiansen and McCurry (2008) and totals more than 1,950 samples with whole rock geochemical data, including many unpublished analyses. While data from the above sets are of variable quality, the large number of analyses minimizes the effect any outliers, poor analyses, or the occasional duplicate analyses have on the overall trends. In all cases, data are normalized to 100% totals, anhydrous with all iron reported as FeO*. Some of the analyses only contain major element data but most contain some sub-set of trace elements.

The SRP provides a regional comparison. It is strongly basalt-rhyolite bimodal and the basalts are of a similar character to those of the HLP, namely thin flows of diktytaxitic low-potassium olivine tholeiites with some evolved compositions (Leeman, 1982a; Kuntz, 1992; Hughes et al., 2002). The large, voluminous time-transgressive rhyolitic ignimbrite eruptions of the eastern SRP are thought to be partial melts of a hybrid zone of recently emplaced tholeiitic basalts and silicic upper crust. These melts, coupled with fractional crystallization, form a range from low to high silica rhyolite. Variable but small degrees of upper crustal assimilation or ingestion (re-melting) of earlier caldera complexes complete the large ignimbrite forming rhyolite petrogenesis (McCurry and Rodgers, 2009). Radiogenic isotopic compositions range from being similar to the basalts to having elevated $^{87}Sr/^{86}Sr_i$ ratios and low $\delta^{18}O$ indicating substantial mantle-derived component in the rhyolites (Leeman, 1982c; Frost and Frost, 1997; Bindeman, et al., 2008; Christiansen and McCurry, 2008). The primary tenets of the eastern SRP model are similar to those proposed for the RST from the HLP by Streck and Grunder (2008); namely, partial melts of a more mafic parent form a low silica rhyolite followed by crystal fractionation to form the higher silica rhyolitic trend. There are alternative models to explain the formation of rhyolites in the central and western SRP. These rhyolites form by partial melting of young (Eocene) crust, the calc-alkaline,

Idaho batholith rocks (Boroughs et al., 2005; Bonnichsen et al., 2008) or from contributions of both crustal melt and differentiated or remelted juvenile mafic component (Leeman et al., 2008).

One difference between the two similar mafic partial melt models given above is that the formation of the eastern SRP rhyolites requires melting of hybridized diorite, consisting of recently emplaced basaltic magmas that have a direct genetic link to the mantle and old silicic cratonic upper crustal rocks. The crustal rocks that underlie the eastern SRP are Archean to early Proterozoic with highly elevated (radiogenic) $^{87}Sr/^{86}Sr$ ratios and very low $^{143}Nd/^{144}Nd$ ratios (Leeman et al., 1985; O'Brien et al., 1995) compared to the tholeiitic basalts and thus partial melts of this old, isotopically evolved crust cannot be the sole parent to the eastern SRP rhyolites, although minor assimilation of this old crust is not precluded. In the HLP and NWBR, however, the crust is made up principally of young (Mesozoic and younger) accreted terranes that are more mafic than the old upper crust provinces that lie east of the 0.706 line (Figure 2) (Kistler and Peterson, 1978). These young, mafic crustal rocks are relatively isotopically unevolved and thus they could be a source of the partial melt that form the rhyolites (as per the model of Streck and Grunder, 2008). In any case, the HLP is made up of partial melts of a mafic protolith, not a diorite protolith as hypothesized for the SRP (McCurry and Rodgers, 2009).

Iceland presents another extensively studied, largely tholeiitic province that provides a useful comparison. Like the HLP and NWBR, the crust under Iceland is undeniably mafic, although potentially containing small slivers of Mesozoic continental crust (cf. Paquette et al., 2006), and thus such mafic crust might provide a better analog to eastern Oregon crust compared to the more silicic crust of the North American craton underlying the SRP. While three distinct types of basalts are present in Iceland, approximately 80%, by volume, are olivine tholeiites with the remainder roughly split between transitional (±olivine) basalt and alkali (±olivine) basalt (Jakobsson et al., 2008). While there are at least three mantle components required to create the major and trace element and isotopic variability of the basalts of Iceland, including a "MORB-type" source, a mantle plume, and recycled ocean crust (see review by Sigmarsson and

Steinthorsson, 2007, and sources therein), many of the basalts have a composition that lies between N-MORB and E-MORB, similar to the basalts of the HLP and NWBR (Hart et al., 1984; Jordan, 2001).

Icelandic volcanism is also strongly bimodal. Basalts make up about 85% of the volume and 80% of the analyses of volcanic rocks while intermediate and silica-rich compositions are approximately ten percent each (Jonasson, 2007; Jakobsson et al., 2008; database for this study). The large majority of the intermediate rocks are mingled or mixed magmas, containing disequilibrium phenocrysts and thus represent two end-member compositions and are not "true magmatic" compositions (e.g. Askja: Sigurdsson and Sparks, 1981, Krafla volcano: Jonasson, 1994; Katla: Lacasse et al., 2007). The petrogenesis of some other intermediate compositions is magma hybridization of two parental end-member compositions (e.g. Hekla: Sigmarsson et al., 1992; Schuessler, et al., 2009). Many workers ascribe the petrogenesis of the rhyolites to partial melting of basaltic crust, which may or may not have been hydrothermally altered (e.g. Jonasson, 1994; Jonasson, 2007; Lacasse et al., 2007; Martin and Sigmarsson, 2007). In the case of Torfajokull volcano the partial melt of an amphibolitic crust produces a dacite to low silica rhyolite and fractional crystallization of this parent produces higher silica rhyolite (Martin and Sigmarsson, 2007), a model similar to that for the RST (Streck and Grunder, 2008).

While the consensus is that partial melting of mafic to dioritic hybridized crust produces the majority of rhyolites or silicic rhyolite parental compositions in both the eastern SRP and Icelandic systems, some rhyolites from both systems show evidence of petrogenesis by protracted fractional crystallization of parental basaltic magmas. In Iceland, such cases include Ljosufjoll and Snaefellsjokull volcanoes (Martin and Sigmarsson, 2007), Oraefajokull volcano (Selbekk and Tronnes, 2007) and Austurhorn (Furman et al., 1992). A very few intermediate composition rocks may be "true liquids", lying along a liquid line of descent (Jonasson, 2005). In the eastern SRP, rhyolite domes not associated with the time-transgressive hot spot magmatism (e.g. Big Southern Butte, Cedar Butte, East Butte) have isotopic ratios (Sr, Nd, O) that are consanguineous to local basalts (McCurry et al., 1999; McCurry et al., 2008; Savov et al., 2009). This fact,

coupled with intermediate compositions that follow a liquid line of decent from basalt to rhyolite at COM and Cedar Butte lava fields and experimental fractionation studies indicate that these rhyolites were produced by extensive fractional crystallization of basaltic parent magmas (McCurry et al., 2008; Whitaker et al., 2008; Nekvasil et al., 2000). Similarly, topaz rhyolites of the bimodal Blackfoot Volcanic Field in eastern Idaho are produced by extensive fractional crystallization, coupled with low degrees of Archean crustal assimilation (Ford, 2005). There is still open debate on the origin of rhyolites in these systems and fractionation of a low silica parental rhyolite to a higher silica rhyolite can obscure the true lineage of rhyolites in these systems (Streck and Grunder, 2008; Frost et al., 2001).

Another regional comparison is the Cascades Arc of the western US and Canada (see summary by Hildreth, 2007, and sources therein). Unlike the study area, SRP or Iceland, the Cascades province is not bimodal, with a continuum of compositions ranging from basalts to rhyolites, although high silica rhyolites (> 75 wt. % SiO_2) are rare. A number of primitive basalts are recognized within the Cascades including 1) voluminous low-K olivine tholeiite, especially in the Oregon Cascades, analogous to HAOT, 2) appreciable amounts of an ocean island basalt (OIB), 3) lesser but still substantial quantities of calc-alkaline basalt (CAB) and lesser volumes of 4) absarokite and 5) high-Mg basaltic andesite (cf. Conrey et al., 1997). Unlike the nearly equal volume of basalts and rhyolites within the HLP and NWBR, and unlike other predominantly andesite arcs, the High Cascades (less than 8 Ma) volcanics are predominantly mafic. Quaternary volcanic volumes are up to 85% basalt and basaltic andesite (McBirney, 1978; Hildreth, 2007, and sources therein), and the proportion of mafic volcanics is still greater than 50% for 8 – 2 Ma volcanics (McBirney, 1978, Sherrod and Smith, 2000). Production of evolved basalts, andesites and more silicic rocks requires varying amounts and perhaps multiple polybaric episodes of magma recharge, crustal assimilation and fractional crystallization (RAFC) processes (Bohrson and Spera, 2001; Spera and Bohrson, 2001). Where the flux basaltic magma transfers enough energy into the crust, melting, assimilation, storage and homogenization (MASH process) result in andesite to dacite eruption and accumulation (stratovolcanoes) (Hildreth and Moorbath, 1988). Rhyolites

are formed from these hybrid magmas by a myriad of processes, such as fractionation of the intermediate magma, expulsion of silicic fluid from a mush, etc. but derivation by extensive fractional crystallization of a mantle-derived parent is precluded (Hildreth, 2007, and sources therein).

Additional references from this appendices only that are not cited in the chapters:

Bindeman, I. N., Fu, B., Kita, N. T., Valley, J. W., 2008, Origin and evolution of silicic magmatism at Yellowstone based on ion microprobe analysis of isotopically zoned zircons: J. of Petrology, v. 49, p. 163-193.

Boroughs, S. Wolff, J., Bonnichsen, B., Godchaux, M., Larson, P., 2005, Large volume, low $-\delta^{18}O$ rhyolites of the central Snake River Plain, Idaho, USA: Geology, v. 33, p. 821-824.

Ford, M. T., 2005, The petrogenesis of Quaternay rhyolite domes in the bimodal Blackfoot Volcanic Field, southeastern Idaho: Idaho State University MS thesis, 133p.

Jakobsson, S. P., Jonasson, K., Sigurdsson, I. A., 2008, The three igneous rock series of Iceland: Jokull, v. 58, p. 117-138.

Jonasson, K., 2005, Magmatic evolution of the Heidarsporour Ridge, NE-Iceland: J. of Volcanology and Geothermal Research, v. 147, p. 109-124.

Kuntz, M. A., Covington, H. R., and Schorr, L. J., 1992, An overview of basaltic volcanism of the eastern Snake River Plain, Idaho. In Link, P. K., Kuntz, M. A., and Platt, L. eds., Regional Geology of eastern Idaho and western Wyoming: Geological Society of America Memoir 179, p. 227-267.

Leeman, W. P., 1982, Rhyolites of the Snake River Plain – Yellowstone Plateau province, Idaho and Wyoming: A summary of petrogenetic models, in Bonnichsen, W and Brekenridge, R. M., eds., Cenozoic Geology of Idaho: Bureau of Mines and Geology Bulletin 26, p. 203-212.

Leeman, W. P., Menzies, M. A., Matty, D. J., and Embree, G. F., 1985, Strontium, neodymium and lead isotopic compositions of deep crustal xenoliths from the Snake River Plain: evidence for Archean basement: Earth and Planetary Science Letters, v. 75, p. 354-368

McCurry, M., Hackett, W. R. and Hayden, K. P., 1999, Cedar Butte and cogenetic quaternary rhyolite domes of the eastern Snake River Plain, Idaho, in Hughes, S. S. and Thackray, G. D., eds., Guidebook to the Geology of Eastern Idaho: Idaho Museum of Natural History, p. 169-179.

O'Brien, P. A., Irving, A. J., McCallum, I. S., and Thirlwall, M. F., 1995, Strontium, neodymium, and lead isotope evidence for the interaction of post-subduction asthenospheric potassic mafic magmas of the Highwood Mountains, Montana, USA, with ancient Wyoming craton lithospheric mantle: Geochimica et Cosmochimica Acta, v. 59, p. 4539-4556.

Paquette, J., Sigmarsson, O. and Tiepolo, M., 2006, Continental basement under Iceland revealed by old zircons: EOS transactions, American Geophysical Union, v. 52 abstract # V33A-0642.

Appendix 6: Regional Analogs for Accreted Terranes and Isotopic Ranges Used in Mixing Models

We give a brief discussion of the likely analogs for the cryptic (hidden) crust under the HLP- NWBR, using regionally exposed accreted terranes and their related, exposed plutonic sections. We then give a table that contains the isotopic ranges from many regional rocks and sediments that we used in our mixing models.

Here we detail the three regional analogs, related to accreted terranes, for the cryptic crust that likely underlies the area or may have made up the crust before magmatic modification: 1) the Devonian – Cretaceous accreted supra-subduction zone formed terranes and associated later plutons of the Klamath Mountains province in southwestern Oregon and northwestern California (Irwin and Wooden, 1999; review by Allen and Barnes, 2006 and sources therein), 2) the Devonian – Cretaceous accreted terranes and plutons of the Blue Mountains province of northeastern Oregon (Wyld et al., 2006; Schwartz et al., 2010) and 3) Cretaceous-age plutons in the Pine Forrest and Pueblo Mountains of northwestern Nevada and southeastern Oregon (Figure 2, Chapter 3), which might have genetic connections to the Blue Mountains and Klamath plutons, respectively (Wyld and Wright, 2001).

Of the above terranes, only the Klamath Mountains have received in-depth study (e.g. Snoke and Barnes, 2006) and petrogenesis of the associated silicic plutons is important for two reasons. First, the petrogenesis of some of these plutons includes partial melts of crust and a similar crust could underlie the HLP and NWBR, and secondly, these plutons themselves might also underlie the study region and contribute parental material for partial melting. The Klamath Mountains province generally ranges in age from the early Paleozoic to the early Cretaceous but does contain remnants of late Neoproterozoic marine sedimentary rocks and metasedimentary rocks (Lindsley-Griffen et al., 2006). Older plutons (older than ~160 Ma) are generally attributed to proto-arc settings, subduction-related volcanism or fractionation of arc-derived magmas (e.g. Ironside Mountain Batholith, some Bear Mountain units) (Snoke and Barnes, 2006; Barnes et al., 2006A; Bushey et al., 2006).

Formation of Middle Jurassic to Early Cretaceous plutons, especially those of the tonalite-trondhjemite-granodiotite (TTG) suite and granodiorite suite (see Figure 1 of Allen and Barnes, 2006; Irwin and Wooden, 1999) is ascribed to crustal melts of metabasic crustal rocks (e.g. ophiolites, excluding metasediments or flysch) coupled with mantle-derived magma (Barnes et al., 1996**;** Allen and Barnes, 2006). Detailed petrogenetic work is lacking on the youngest plutons, the granodiorite suite (e.g. Yellow

Butte, Shasta Bally, Grants Pass) but their origin is ascribed to crustal melting combined with magma mixing (Allen and Barnes, 2006) and some of these plutons may contain a metasedimentary signature as evidenced by inherited zircons (e.g. Grants Pass; Harper et al., 1994). It should be noted however that Allen and Barnes (2006) did not find evidence of old, metasedimentary zircon inheritance in the Yellow Butte pluton. Also, crustal zircons do not necessarily indicate that the plutons were derived by partial melting of the crust, just that the crust makes up a component of the melt, perhaps by assimilation or stoping of the crust.

Silicic units (tonalite or granodiorite) in the slightly older western Klamath plutonic suite (e.g. Bear Mountain Intrusive Complex; Pony Peak Pluton) show evidence of inherited zircons, with an age distribution similar to that of the detrital Galice Formation (Allen and Barnes, 2006; Barnes et al., 2006B). Allen and Barnes (2006) give multiple lines of evidence as to why anatectic melts of the Galice Formation, or indeed any high-Al metasedimentary rock, could not produce the compositions of silicic rocks in the Klamath Mountains. Wholesale assimilation of metasedimentary rocks into a mafic parent could however produce the tonalite or granodiorite in question, contribute inherited zircons, and explain the REE patterns within the magmatic zircons.

Finally, dioritic to granitic compositions of the Wooley Creek suite also show evidence of zircon inheritance, though this inheritance is not directly attributed to any exposed rocks within the Klamath Mountains. Metasedimentary crustal influence on these samples is evident from evolved Nd and Sr isotopic signatures, perhaps the most evolved of any plutonic rocks in the Klamath Mountains, and by elevated $\delta^{18}O$ signatures (over 12 ‰) (Allen and Barnes, 2006, Barnes et al., 1992).

Additional references from this appendices only that are not cited in the chapters:

Barnes, C. G., Petersen, S. W., Kistler, R. W., Prestvik, T. and Sundvoll, B., 1992, Tectonic implications of isotopic variation among Jurassic and Early Cretaceous plutons, Klamath Mountains: Geological Society of America Bulletin, v. 104, p. 117-126.

Barnes, C. G., Petersen, S. W., Kistler, R. W., Murray, R. and Kays, M. A., 1996, Source and tectonic implications of the tonalite-trondhjemite magmatism in the Klamath Mountains: Contributions to Mineralogy and Petrology, v. 123, p. 40-60.

Barnes, C. G., Mars, E. V., Swapp, S. and Frost, C. D., 2006A, Petrology and geochemistry of the Middle Jurassic Ironside Mountain Batholith; evolution of potassic magmas in a primitive arc setting, in Snoke, A. W. and Barnes, C. G., eds., Geological studies in the Klamath Mountains province, California and Oregon; a volume in honor of William P. Irwin: Geological Society of America Special Paper 410, p. 199-221.

Barnes, C. G., Snoke, A. W., Harper, G. D., Frost, C. D., McFadden, R. R., Bushey, J. C. and Barnes, M. A. W., 2006B, Arc plutonism following regional thrusting; petrology and geochemistry of syn- and post-Nevadan plutons in the Siskiyou Mountains, Klamath Mountains province, California, in Snoke, A. W. and Barnes, C. G., eds., Geological studies in the Klamath Mountains province, California and Oregon; a volume in honor of William P. Irwin: Geological Society of America Special Paper 410, p. 357-376.

Bushey, J. C., Snoke, A. W., Barnes, C. G. and Frost, C. D., 2006, Geology of the Bear Mountain intrusive complex, Klamath Mountains, California, in Snoke, A. W. and Barnes, C. G., eds., Geological studies in the Klamath Mountains province, California and Oregon; a volume in honor of William P. Irwin: Geological Society of America Special Paper 410, p. 287-315.

Harper, G. D., Saleeby, J. B. and Heizler, M., 1994, Formation and emplacement of the Josephine ophiolite and the Nevadan orogeny in the Klamath Mountains, California-Oregon: U/Pb zircon and $^{40}Ar/^{39}Ar$ geochronology: J. of Geophysical Research, v. 99, issue B3, p. 4293-4321.

Lindsley-Griffin, N., Griffin, J. R., Farmer, J. D., Sivers, E. A., Bruckno, B. and Tozer, M. K., 2006, Ediacaran cyclomedusoids and the paleogeographic setting of the Neoproterozoic-early Paleozoic Yreka and Trinity Terranes, eastern Klamath Mountains, California, in Snoke, A. W. and Barnes, C. G., eds., Geological studies in the Klamath Mountains province, California and Oregon; a volume in honor of William P. Irwin: Geological Society of America Special Paper 410, p. 411-431.

Location		Moses Lake, WA	Columbia River	Columbia River	Astoria Fan	Astoria Fan	HLP - NWBR
Sample type		Eolian deposits	Columbia River sediments	Columba River disolved load	Proxy for Columbia River	Older sediments - site 174	Mid-Miocene silicics
ref		1	2	3	4	4	Table 1 and 3 of Chapter 3
approx. age	Ma	0	0	0	0	<1	15.6 - 17.5
$^{87}Sr/^{86}Sr$	measured (m)	0.70732	0.71161	0.7121			.70387 - .74469
$^{143}Nd/^{144}Nd$	measured (m)	0.512329	0.511617	0.511693	0.512455	.511861 - .512373	.512893 - .512948
$e_{Nd}(0)$		-6.0	-19.9	-18.4	-3.5	-5.2 - -15.2	5 - 6.1
$^{206}Pb/^{204}Pb$	measured (m)					18.92 - 19.34	18.89 - 18.96
$^{207}Pb/^{204}Pb$	measured (m)					15.653 - 15.715	15.59 - 15.61
$^{208}Pb/^{204}Pb$	measured (m)					39 - 39.41	38.52 - 38.62
$^{176}Hf/^{177}Hf$	measured (m)				0.282832	.282206 - .282793	.283006 - .283057
$\delta\ ^{18}O$	of the melt						5.74 - 6.93

Location		HLP - NWBR	HLP - NWBR	Cenral Oregon	Cenral Oregon	Cenral Oregon	Cenral Oregon	Klamath Mts.
Sample type		Mid-Miocene mafics (Steens)	John Day silicics	John Day mafics	Clarno silicics	Clarno mafics	Eastern Clarno (primative mafic)	Galice argillites
ref		5	6, Table 1 and 3 of Chapter 3	23	8	8	23	7
approx. age	Ma	15.5 - 16.6	20.3 - 30.4	32.9 - 34.2	47 +/- 5	47 +/- 5	38 - 41	153
$^{87}Sr/^{86}Sr$	(m)	.70370 - .70386	.70364 - .71099	.70414 - .70495	.70416 - .70640	.70366 - .70393	.70357 - .70399	.70908 - .71575
$^{143}Nd/^{144}Nd$	(m)	.512851 - .512951	.512868 - .512935	.512856 - .512865			.512809 - .512931	.512201 - .512511
$e_{Nd}(0)$		4.2 - 6.1	4.5 - 5.8	4.3 - 4.5			3.4 - 5.8	-8.5 - 2.4
$^{206}Pb/^{204}Pb$	(m)	18.84 - 19.00	18.81 - 19.15	19.17 - 19.18			18.89 - 18.96	
$^{207}Pb/^{204}Pb$	(m)	15.58 - 15.6	15.59 - 15.62	15.63			15.57 - 15.59	
$^{208}Pb/^{204}Pb$	(m)	38.48 - 38.62	38.41 - 38.75	38.85 - 38.87			38.53 - 38.63	
$^{176}Hf/^{177}Hf$	(m)		.28293 - .283108				.28299 - .28308	
$\delta\ ^{18}O$	melt		6.66 - 6.99					

Location		Klamath Mts.	Klamath Mts.	Klamath Mts.	Klamath Mts.	Klamath Mts.	Blue Mts.	Blue Mts.
Sample type		Rattlesnake Creek argillites	Jospehine Ophiolite	Bear Mt intrusive (mafic)	Grano-diorite (e.g. Grants Pass)	Granite (e.g. Wooley Creek)	Bourn meta-plutonic	Bourn argillite
ref		7	9,10	11,12	11	11, 13	22	22
approx. age	Ma	210	157	148	137	161	220	220
$^{87}Sr/^{86}Sr$	(m)	.70733 - .72131	0.70365	.70311 - .70382	.70343 - .7039	~.705 - .71	.70325 - .70376	.71804 - .72053
$^{143}Nd/^{144}Nd$	(m)	.512093 - .512563		.512718 - .512998		.51264 - .51274	.512926 - .513023	.512127 - .512283
$e_{Nd}(0)$		-10.4 - 1.4					5.7 - 7.5	~ - 10 - 7
$^{206}Pb/^{204}Pb$	(m)							
$^{207}Pb/^{204}Pb$	(m)							
$^{208}Pb/^{204}Pb$	(m)							
$^{176}Hf/^{177}Hf$	(m)							
$\delta\ ^{18}O$	melt		~6 - 12	6.8 - 9.9	6.5-7.9	8 - 12.2		

Location		CRB	CRB	CRB	CRB	CRB	Pacific Ocean	Pacific Ocean
Sample type		Picture Gorge (B - BA)	Imnaha (Basalts)	Grande Ronde (B - BA)	Wanapum (B - BA)	Saddle Mountain (B - BA)	Pacific MORB	Juan de Fuca MORB
ref		14, 15, 21	14	14, 21	14, 21	14, 21	16, 17	18, 19, 20
approx. age	Ma	16.5 - 17	17 - 17.5	16.5 - 17	15.5	10 - 13	0	0
$^{87}Sr/^{86}Sr$	(m)	.7034 - .70383	.70377 - .70448	.70412 - .70575	.70508 - .70520	.706 - .715	.7023 - .7028	.70244 - .70258
$^{143}Nd/^{144}Nd$	(m)	.51290 - .51303	.51283 - .51292	.51261- .51284	.51262 - .51269	.5117 - .5125	.5129 - .51325	.513097 - .513193
$e_{Nd}(0)$		5.2 - 7.7						
$^{206}Pb/^{204}Pb$	(m)	18.53 - 18.85	18.98 - 19.08	18.74 - 19.03	18.75	18.16 - 18.69	17.75 - 19.25	18.45 - 18.77
$^{207}Pb/^{204}Pb$	(m)	15.561- 15.595	15.555 - 15.653	15.56 - 15.65	15.61	15.59 - 15.71	15.40 - 15.58	15.46 - 15.56
$^{208}Pb/^{204}Pb$	(m)	38.268 - 38.489	38.495 - 38.839	38.60 - 38.95	38.88	39.09 - 39.70	37 - 38.6	37.8 - 38.6
$^{176}Hf/^{177}Hf$	(m)	.283159 - .283181						
$\delta\ ^{18}O$	melt	6.4		5.8	6.8	6.5, 6.7, 8.3		5.46 - 6.04

Location		Cascades	Cascades	Cascades	Cascades
Sample type		MCT (basalts - andesites)	MCT (dacites - rhyolites)	JHA (basalts - andesites)	JHA (dacites - rhyolites)
ref		24, 25, 27, 28, 29, 31	24	20, 26, 30, 32	20, 26
approx. age	Ma	<5	<5	<5	<5
$^{87}Sr/^{86}Sr$	(m)	.07324 - .70388	.07324 - .70388	.70281 - .70369	.70281 - .70369
$^{143}Nd/^{144}Nd$	(m)	.51283 - .51301	.51283 - .51301	.51273 - .51304	.51273 - .51304
$e_{Nd}(0)$					
$^{206}Pb/^{204}Pb$	(m)	18.69 - 18.97	18.69 - 18.97	18.59 - 19.04	18.59 - 19.04
$^{207}Pb/^{204}Pb$	(m)	15.538 - 15.627	15.538 - 15.627	15..51 - 15.607	15..51 - 15.607
$^{208}Pb/^{204}Pb$	(m)	38.38 - 38.62	38.38 - 38.62	38.10 - 38.63	38.10 - 38.63
$^{176}Hf/^{177}Hf$	(m)			.283031 - .283092	.283052 - .283071
$\delta\ ^{18}O$	melt	5.2 - 6.9	4.4 - 7.0	5.1 - 6.7	5.1 - 7.6

References for Appendix 6 Table:

1. Nakai, S., Halliday, A. N., and Rea, D. K., 1993, Provenance of dust in the Pacific Ocean: Earth and Planetary Science Letters, v. 119, p. 143-157.

2. Goldstein, S. J. and Jacobsen, S. B., 1988, Nd and Sr isotopic systematics of river water suspended material: implications for crustal evolution: Earth and Planetary Science Letters, v. 87, p. 249-265.

3. Goldstein, S. J. and Jacobsen, S. B., 1987, The Nd and Sr isotopic systematics of river-water dissolved material: implications for the sources of Nd and Sr in seawater: Chemical Geology, v. 66, p. 245-272.

4. Prytulak, J., Vervoort, J. D., Plank, T., and Yu, C., 2006, Astoria Fan sediments, DSDP site 174, Cascadia Basin: Hf-Nd-Pb constraints on province and outburst flooding: Chemical Geology, v. 233, p. 276-292.

5. Carlson, R. W. and Hart, W. K., 1987, Crustal genesis on the Oregon Plateau: J. of Geophysical Research, v. 92, no. B7, p. 6191-6206.

6. Scarberry, K. C., 2007, Extension and volcanism: Tectonic Development of the northwestern margin of the Basin and Range Province in Southern Oregon: Oregon State University PhD thesis, 168 p.

7. Frost, C. D., Barnes, C. G, and Snoke, A. W., 2006, Nd and Sr isotopic data from argillaceous rocks of the Galice Fromation and Rattlesnake Creek terrane, Klamath Mountains: Evidence for the input of Precambrian sources, in Snoke, A. W. and Barnes, C. G., eds., Geological studies in the Klamath Mountains province, California and Oregon; a volume in honor of William P. Irwin: Geological Society of America Special Paper 410, p. 103-120.

8. Suayah, I. B., and Rogers, J. J. W., 1991, Petrology of the lower Tertiary Clarno Formation in north central Oregon: The importance of magma mixing: J. of Geophyisical Research, v. 96, p. 13357-13371.

9. Shaw, H. F. and Wasserburg, G. J., 1984, Isotopic constraints on the origin of Appalachian mafic complexes: American Journal of Science, v. 284, p. 319-349.

10. Harper, G. D., Bowman, J. R., and Kuhns, R., 1988, A field, chemical, and stable isotope study of subseafloor metamorphism of the Josephine Ophiolite, California - Oregon: J. of Geophysical Research, v. 93, p. 4625-4656.

11. Allen, C. M and Barnes, C. G, 2006, Ages and some cryptic sources of Mesozoic plutonic rocks in the Klamath Mountains, California and Oregon, in Snoke, A. W. and Barnes, C. G., eds., Geological studies in the Klamath Mountains province, California and Oregon; a volume in honor of William P. Irwin: Geological Society of America Special Paper 410, p. 223-245.

12. Barnes, C. G., Snoke, A. W., Harper, G. D., Frost, C. D., McFadden, R. R., Bushey, J. C. and Barnes, M. A. W., 2006B, Arc plutonism following regional thrusting; petrology and geochemistry of syn- and post-Nevadan plutons in the Siskiyou Mountains, Klamath Mountains province, California, in Snoke, A. W. and Barnes, C. G., eds., Geological studies in the Klamath Mountains province, California and Oregon; a volume in honor of William P. Irwin: Geological Society of America Special Paper 410, p. 357-376.

13. Barnes, C. G., Petersen, S. W., Kistler, R. W., Prestvik, T. and Sundvoll, B., 1992, Tectonic implications of isotopic variation among Jurassic and Early Cretaceous plutons, Klamath Mountains: Geological Society of America Bulletin, v. 104, p. 117-126.

14. Hooper, P.R. and Hawkesworth, C.J., 1993, Isotopic and geochemical constraints on the origin and evolution of the Columbia River basalt: J. of Petrology, v. 34, p. 1203-1246.

15. Stefano, C. J., 2010, Volatiles, major oxide, trace element and isotope geochemistry in the Snake River Plain and Columbia River Flood Basalts: Implications for the evolution of a continental hotspot: University of Michigan PhD thesis, 191 p.

16. Hanan, B. B. and Graham, D. W., 1996, Lead and Helium isotope evidence from oceanic basalts for a common deep source of mantle plumes: Science, v. 272, p. 991-995.

17. Hanan, B. B., Shervais, J. W. and Vetter, S. K., 2008, Yellowstone plume-continental lithosphere interaction beneath the Snake River Plain: Geology, v. 36, p. 51-54.

18. Hegner, E. and Tatsumoto, M., 1987, Pb, Sr, and Nd isotopes in basalts and sulfides from the Juan de Fuca Ridge: J. of Geophysical Research, v. 92, p. 11380-11386.

19. Ito, E., White, W. M. and Gopel, C., 1987, The O, Sr, Nd and Pb isotope geochemistry of MORB, Chemical Geology, v. 62, p. 157-176.

20. Jicha, B. R., Hart, G. L., Johnson, C. M., Hildreth, W., Beard, B. L., Shirey, S. B. and Valley, J. W., 2009, Isotopic and trace element constraints on the petrogenesis of lavas from the Mount Adams volcanic field, Washington: Contributions to Mineralogy and Petrology, v. 157, p. 189-207.

21. Carlson, R. W., Lugmair, G.W., and Macdougall, J. D., 1981, Columbia River volcanism: the question of mantle heterogeneity or crustal contamination: Geochimica et Cosmochimica Acta, v. 45, p. 2483-2499.

22. Schwartz, J. J., Snoke, A. W., Frost, C. D., Barnes, C. G., Gromet, L. P. and Johnson, K., 2010, Analysis of the Wallowa-Baker terrane boundary: Implications for tectonic accretion in the Blue Mountains province, northeastern Oregon: Geological Society of America Bulletin, v. 122, p. 517-536.

23. Bromley, S. A., 2011, Evolution and inheritance of Cascadia sub-arc mantle reservoirs: Oregon State University MS Thesis, 192 p.

24. Bacon, C. R., Gunn, S. H., Lanphere, M. A and Wooden, J. L., 1994, Multiple isotopic components in Quaternary volcanic rocks of the Cascades Arc near Crater Lake, Oregon: J. of Petrology, v. 35, p. 1521-1556.

25. Schmidt, M. E., Grunder, A. L. and Rowe, M. C., 2008, Segmentation of the Cascade Arc as indicated by Sr and Nd isotopic variations among diverse primitive basalts: Earth and Planetary Science Letters, v. 266, p. 166-181.

26. Conrey,R. M., Hooper, P. R., Larson, P. B., Chesley, J. and Ruiz, J., 2001, Trace element and isotopic evidence for two types of crustal melting beneath a High Cascade volcanic center, Mt. Jefferson, Oregon: Contributions to Mineralogy and Petrology, v. 141, p. 710-732.

27. Grove, T. L., Donnelly-Nolan, J. M. and Housh, T., 1997, Magmatic processes that generated the rhyolite of Glass Mountain, Medicine Lake volcano, N. California: Contributions to Mineralogy and Petrology, v. 127, p. 205-223.

28. Kinzler, R. J., Donnelly-Nolan, J. M. and Grove, T. L., 2000, Late Holocene hydrous mafic magmatism at the Paint Pot Crater and Callahan flow, Medicine Lake Volcano, N. California and the influence of H2O in the generation of silicic magmas: Contributions to Mineralogy and Petrology, v. 138, p. 1-16.

29. Bacon, C. R., Bruggman, P. E., Christiansen, R. L., Clynne, M. A., Donnelly-Nolan, J. M. and Hildreth, W., 1997, Primitive magmas at five Cascade volcanic fields: Melts from hot, heterogeneous sub-arc mantle: The Canadian Mineralogist, v. 35, p. 397-423.

30. Leeman, W. P., Smith, D. R., Hildreth, W., Palacz, Z. and Rogers, N., 1990, Compositional diversity of late Cenozoic basalts in a transect across the southern Washington Cascades: Implications for subduction zone magmatism: J. of Geophysical Research, v. 95, p. 19561-19582.

31. Donnelly-Nolan, J. M., 1998, Abrupt shift in $\delta^{18}O$ values at Medicine Lake Volcano (California, USA): Bulletin of Volcanology, v. 59, p. 529-536.

32. Alison Koleszar, pers com., 2011.